Water Technology and Sciences

Included in Thomson Reuters Science Citation Index® (ISI) • Expanded Thomson Reuters Research Alert® (ISI) • EBSCO • ProQuest • Elsevier • Redalyc

Vol. V, No. 5, September-October, 2014

Water Technology and Sciences

Edit Board

Editorial coordination and careful editing: Helena Rivas-López • **Editorial assistance and editorial layout:** Luisa Guadalupe Ramírez-Martínez • **Figures design:** Luisa Guadalupe Ramírez-Martínez and Rosario Castro-Rivera • **Coordination arbitration:** Elizabeth Peña and Bibiana Bahena • **Proofreading English:** Ellen Weiss • **Logo design and cover:** Oscar Alonso-Barrón • **Design format:** Gema Alín Martínez-Ocampo • **Marketing:** Marco Antonio Bonilla-Rincón.

Editorial Committee

©***Water Technology and Sciences.*** Vol. V, No. 5, September-October, 2014, is a bimonthly publication edited by the Instituto Mexicano de Tecnología del Agua, Paseo Cuauhnáhuac 8532, Colonia Progreso, Jiutepec, Morelos, C.P. 62550, telephone +52 (777) 3 29 36 00, extension 474, www.imta.gob.mx/tyca, fsalinas@tlaloc.imta.mx. Responsible editor, Nahún Hamed García Villanueva; Copyright No. 04-2013-121014514100-203, granted by the Instituto Nacional de Derechos de Autor. ISSN pending. Responsible for the latest update of this issue: Sub-Department of Dissemination and Circulation, Francisco José Salinas Estrada, Paseo Cuauhnáhuac 8532, Colonia Progreso, Jiutepec, Morelos, C.P. 62550.

Water Technology and Sciences is the traslation of *Tecnología y Ciencias del Agua*, which is the continuation of the following journals: *Irrigación en México* (1930-1946); *Ingeniería hidráulica en México* (1947-1971); *Recursos hidráulicos* (1972-1978), and *Ingeniería hidráulica en México*, second period (1985-2009).

For subscriptions, click here

Coordination for editorial comments, click here give

Water Technology and Sciences

Vol. V, No. 5, September-October, 2014

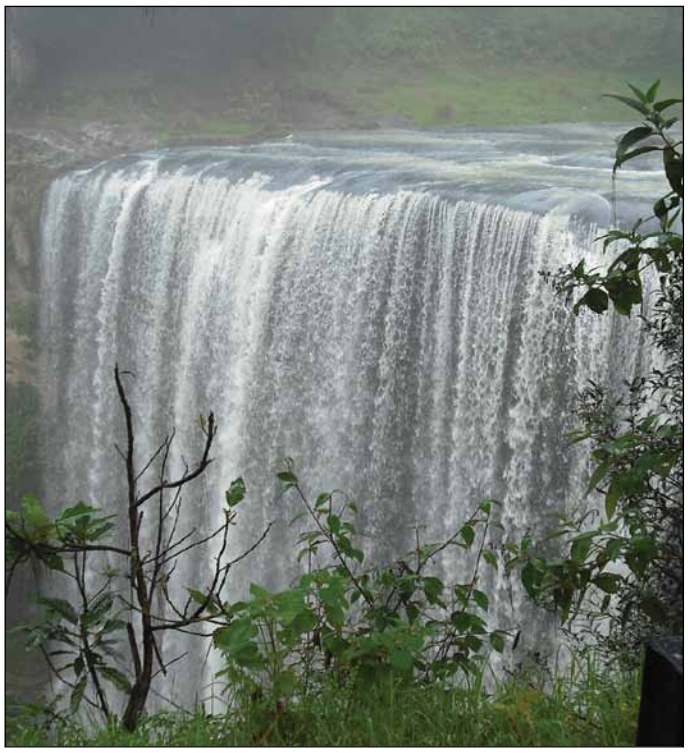

Cover: Sampling station, San Pedro Falls, San Pedro Amatla, Puebla, Mexico. The majority of the surface water in the state of Puebla is found in the Sierra Norte, where it is primarily used for farming, followed by industry, aquaculture and therapy. The wastewater from industries and the various towns in the region discharges into the river channels. Since surface water is available all year long, farmers use it as a direct source to irrigate their main crops, that is, without prior treatment. Given this background, it is suggested that the geological materials in the region and wastewater discharges qualitatively and quantitatively change the ions in solution, that is, the water quality. Considering that the surface water used for farming comes from different sources and has different concentrations, this study determined its chemical composition and total electrolytic concentrations in order to evaluate its quality for agricultural use. See article "Irrigation Water Quality in the Sierra Norte in Puebla, México by Álvaro Can-Chulim *et al*. (pp. 77-96).

Photo: Álvaro Can Chulim.

Lake Louise, Alberta, Canada.

Photo: Rebeca González Villela.

Contents

Technical articles

Contenido

Artículos técnicos

Effects of Increased Sea Levels from Climate Change on the Celestún Estuary Morphology

• Rogelio Torres-Mota* • Paulo Salles-Afonso-de-Almeida •
• José López-González •
Universidad Nacional Autónoma de México
*Corresponding Author

Abstract

Torres-Mota, R., Salles-Afonso-de-Almeida, P., & López-González, J. (September-October, 2014). Effects of Increased Sea Levels from Climate Change on the Celestún Estuary Morphology. *Water Technology and Sciences* (in Spanish), 5(5), 5-19.

This work evaluates the effect of potential increases in mean sea levels on the morphology of a lagoon system using a stability analysis of the lagoon's inlet with the sea. To this end, the study was divided into two phases: a) obtaining the maritime climate through a time-series resulting from a historical retro-analysis to identify the main oceanographic parameters, complemented with an analysis of data measured in situ to characterize the current hydrodynamics of the lagoon system and b) modeling the hydrodynamic response of the estuary for two scenarios for increased sea levels (25 and 50 cm) based on studies by the Intergovernmental Panel on Climate Change, with an emphasis on changes in flow systems, currents and tides, sediment transport capacity and tidal distortion. The results of the present work show that maximum flow velocities through the lagoon inlet increased 18 and 29% over the current condition for each scenario modeled. In addition to variations in flow and ebb duration, this suggested that the Celestún coastal system has the adaptive capacity to maintain a certain degree of morphological equilibrium for a given mean increase in sea levels. Net sediment transport does not only depend on the direction of the residual current but also on the distortion in velocity fields and in maximum flow and ebb velocity values.

Keywords: Increase in mean sea level, lagoon coast, lagoon inlet stability, sea flow and ebb, tidal distortion.

Resumen

Torres-Mota, R., Salles-Afonso-de-Almeida, P., & López-González, J. (septiembre-octubre, 2014). Efectos del aumento del nivel del mar por cambio climático en la morfología de la ría de Celestún, Yucatán. Tecnología y Ciencias del Agua, *5(5), 5-19.*

Se evaluaron los efectos de un potencial incremento del nivel medio del mar sobre la morfología de un sistema lagunar por medio del análisis de estabilidad de la boca de comunicación con el mar. Para llevar a cabo lo anterior, el estudio se dividió en dos fases: a) obtención del clima marítimo a través de series de tiempo obtenidas como resultados de retroanálisis históricos para conocer los principales parámetros oceanográficos, complementado con el análisis de datos medidos in situ para una caracterización hidrodinámica actual del sistema lagunar; b) modelación de la respuesta hidrodinámica de la ría a dos escenarios de aumento del nivel del mar (25 y 50 cm) con base en los estudios del Grupo Intergubernamental del Cambio Climático, haciendo énfasis en cambios en el sistema de flujos, corrientes y prisma de marea, capacidad de transporte de sedimento y distorsión de la marea. Los resultados del presente trabajo muestran que las velocidades máximas del flujo a través de la boca lagunar aumentaron en un 18 y 29%, en relación con la condición actual para cada escenario modelado, lo cual, aunado a variaciones de las duraciones del flujo y el reflujo, sugiere que el sistema costero de Celestún presenta una capacidad adaptativa para mantener cierto nivel de equilibrio morfológico ante un aumento del nivel medio del mar. El transporte de sedimento neto no depende sólo de la dirección de la corriente residual, sino también de la distorsión de los campos de velocidades y de los valores de velocidad máxima de flujo y reflujo.

Palabras clave: *aumento del nivel medio del mar, laguna costera, estabilidad de boca lagunar, flujo y reflujo de marea, distorsión de marea.*

Received: 26/09/12
Accepted: 24/01/14

Introduction

The coastal zone is a sea-land spatial strip varying in width and constitution with different sea and land components interacting. It contains the greatest diversity of environments and resources. This creates ecosystems with environmental, climatic, geomorphological

and hydrological characteristics that are unique to the planet (Botello, Villanueva, Gutiérrez, & Rojas, 2010). As a result, interest has arisen in evaluating the repercussions of an intensification in the maritime climate on the coast's morphology (for example, beach erosion, destabilization of the inlets of coastal lagoons and estuaries).

The gradual increase in mean sea level (msl) along with the sinking of land have made some coastal regions particularly vulnerable to erosion and flooding, resulting in increased studies of the land's climate system and the development of new models (Battjes, 2006). For example, an increase in the msl for the current century has been estimated to be of the order of 0.4 m (IPCC, 2007), and more recent calculations have indicated an increase of 0.15 m from the year 2010 to 2100, which when adding acceleration —for example, of 0.10 mm/year^2— would increase to 79 cm (Houston & Dean, 2011).

In Mexico, coastal areas exist with little geomorphic elevation and made up of fine non-cohesive material, giving them a character similar to plains that are susceptible to fluvial flooding, or marine flooding in the case of substantial over-height. When treated in a sustainable manner, the marine riches of the Mexican coasts provide inexhaustible resources and serve as a key part of scientific and technological development. The Yucatan Peninsula is one of the regions in the Gulf of Mexico's geological basin which is vulnerable to an increase in mean sea level (Ortiz-Pérez & Méndez-Linares, 1999; Yañez-Arancibia, 2010). A particular case study involves the lagoon in the Celestun estuary, located in the western portion of the peninsula. This coastal lagoon constitutes a biosphere reserve because of the amount and type of ecosystems found there, which serve as a habitat for different species and as a source of resources for fishing by the communities situated on its banks (Conanp, 2000). Therefore, it has the characteristic of a coastal unit which is highly vulnerable to both natural and manmade alterations. Alterations in its natural equilibrium greatly impact both humans and flora and fauna species.

For these reasons the possible and probable effects of an increase in sea levels on the morphology of the coastal area are studied, particularly erosion and flooding. In the case of coastal lagoons, such changes in sea level can cause significant changes in hydrodynamics, which in turn affect the morphodynamics and stability of these systems. This work analyzed the effect of an increase in msl on currents and flows. Special attention was placed on the coastal body's inlet connecting it to the sea. Repercussions on potential sediment transport were also studied. Finally, the future vulnerability of and physical implications for the Celestun estuary were evaluated. The main hypothesis of this study was that the lagoon dynamics of a coastal body such as the Celestun estuary, with a permanent connection to the sea, may be altered by an intensification in the maritime climate due to the modification of tidal flow conditions at the inlet of the lagoon.

Study Area

The Celestun estuary is located on the northwest coast of the Yucatan peninsula, Mexico, between the coordinates 20° 42', 21'' N and 90° 18', 90° 33'W, and is part of the Chicxulub hydrological basin, whose functional boundary is the Ring of Cenotes (Batllori, Gonzáles, Díaz & Febles, 2005). The hydrology of the region is regulated by a rocky phreatic surface, which is composed of two layers —an exterior layer called the calcareous shell (known locally as *caliche*), which is impermeable and hard, and an interior layer made up of porous sedimentary limestone through which groundwater flows from the upper basin to the coast. The existence of cracks in the *caliche* allows for groundwater to well up in the form of *petenes* and bogs. The estuary is a semi-closed water body with a permanent connection to the sea through a lagoon inlet. It measures 24 km at its longest axis and its width ranges from 140 m to 2.3 km. Its volume is estimated to be between 12.59 x

10^6 m^3 and 38.25 x 10^6 m^3 during the dry and rainy season, respectively (Batllori *et al.*, 1987).

The depth of the estuary body ranges from 3 m in the area near the inlet to over 1.7 m in the middle and 0.50 m in the northern portion of the system (Figure 1). A set of saltwater pools exist on the sandbar separating the estuary from the sea, with a mean depth of 0.30 m. The intertidal zone is located in the east (with an average width of 7 km), and extends from the mangrove strip marking the eastern boundary of the lagoon to the maximum flood limit (1 m above sea level).

The salinity of the lagoon ranges from 2.6 ups in April to 15.3 ups in July. The climate of the region is hot-semi-dry and the mean annual temperatures are 27.4°C for the water and 26.5°C for the region. Mean annual precipitation is 767 mm and mean annual evaporation is 1 400 mm. Because of its location, during winter the estuary receives northern winds which generate the greatest atmospheric and oceanographic energies of the year (Duch, 1988).

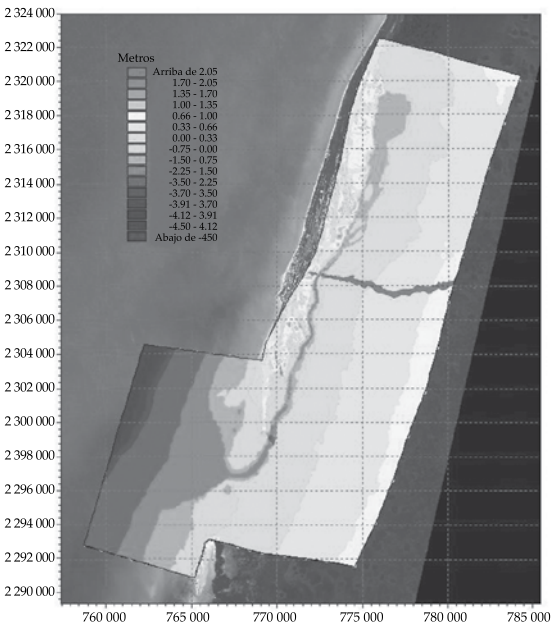

Figure 1. Bathymetry of the coastal lagoon in the Celestun Estuary and sampling areas.

Methdology

To evaluate the effects of climate change on the coastal morphology, the possible repercussions of this on the maritime climate (mean sea level, waves and currents) must first be identified. Then, the changes in these variables that most greatly affect the morphology of the system can be determined (Torres-Mota, Salles, Mariño, & López, 2012). Once the study variables are determined, their historical records must be researched and the current conditions evaluated, to later determine future conditions. To estimate the present and future conditions of the physics of the lagoon, a hydrodynamic numerical model was used to study the present system of currents and sea levels, based on two scenarios of increased msl issued by the IPCC (2007). The last phase consisted of analyzing the ebb and flow conditions in the inlet connecting the estuary with the sea, their implications on potential sediment transport rates through it and repercussions on the stability of the lagoon system.

Historical Data

For the purpose of identifying the historical maritime conditions at the site of interest, an analysis was conducted of winds and normal and extreme waves based on a historical 30-year time series, which was taken from a retro-analysis by the Engineering Institute of the National Autonomous University of Mexico (Appendini *et al.*, 2012) for an area consisting of the Gulf of Mexico and the Caribbean sea (the time series was extracted from the coordinates 90.60° W and 20.74° N). The analysis and the characterization of the study variables were divided into (1) a statistical analysis of wave data and (2) an analysis of extreme wind and wave data. The 30-year time series was divided into four parts: a) spring (S), from March 21 to June 20, b) summer (S), from June 21 to September 20, c) autumn (A), from September 21 to December 20, and d) winter (W), from December 21 to March 20. Thus each year of

the series was divided into four seasons, the seasons for each year were grouped together (for example, all S seasons) and the results for each were obtained.

Sampling and Methods of Analysis of Environmental Variables

A field campaign was conducted in the study area in order to obtain data pertaining to the environmental variables of interest, to characterize the Celestun estuary and generate input data for numerical simulations. These included the lagoon and two adjacent areas —the sandy zone and the intertidal zone (floodable zone), corresponding to the west and east portions of the lagoon, respectively. The environmental variables observed in the maritime zone were sea surface elevation, currents and waves. In the central portion changes in water surface, salinity and temperature at the sensor were registered. Surface elevation, temperature and salinity were measured in the north. On land, elevations were obtained in order to determine the configuration of the land adjacent to the lagoon and to define, with the help of satellite images, the floodable zones at high tide when live tides and extraordinary over-heights were present.

Description and Calibration of the Numerical Model

The MIKE21 model was used to determine the hydrodynamics of the lagoon, which numerically solves the Navier-Stokes equations for two-dimensional and uncompressible flow. The implementation of the model consisted of generating a calculation grid (encompassing the lagoon, the sand bar and the intertidal zone in the east), which was discretized into triangular elements with variable resolution, based on which primitive continuity and momentum equations were solved using finite volumes. The configuration of the bottom of the lagoon and the type of materials of which it is composed (sand, organic matter, vegetation) generate different frictional environments, which produce changes in the amplitude and phase of sea waves due to dissipation and transference of energy. The horizontal continuity and momentum equations on the x and y axes integrated into the vertical are, respectively:

$$\frac{\partial h}{\partial t}+\frac{\partial h\bar{u}}{\partial x}+\frac{\partial h\bar{v}}{\partial y}=hS \tag{1}$$

$$\frac{\partial h\bar{u}}{\partial t}+\frac{\partial h\bar{u}^2}{\partial x}+\frac{\partial h\bar{v}\bar{u}}{\partial y}=f\bar{v}h-gh\frac{\partial \eta}{\partial x}-\frac{h}{\rho_0}\frac{\partial p_a}{\partial x}$$
$$-\frac{gh^2}{2\rho_0}\frac{\partial \rho}{\partial x}+\frac{\partial \tau_{sx}}{\partial \rho_0}-\frac{\partial \tau_{bx}}{\partial \rho_0}-\frac{1}{\rho_0}\left(\frac{\partial s_{xx}}{\partial x}+\frac{\partial s_{xy}}{\partial y}\right)$$
$$+\frac{\partial}{\partial x}\left(hT_{xx}\right)+\frac{\partial}{\partial y}\left(hT_{xy}\right)+hu_sS \tag{2}$$

$$\frac{\partial h\bar{v}}{\partial t}+\frac{\partial h\bar{v}^2}{\partial y}+\frac{\partial h\bar{u}\bar{v}}{\partial x}=f\bar{v}h-gh\frac{\partial \eta}{\partial y}-\frac{h}{\rho_0}\frac{\partial p_a}{\partial y}$$
$$-\frac{gh^2}{2\rho_0}\frac{\partial \rho}{\partial y}+\frac{\partial \tau_{sy}}{\partial \rho_0}-\frac{\partial \tau_{by}}{\partial \rho_0}-\frac{1}{\rho_0}\left(\frac{\partial s_{yx}}{\partial x}+\frac{\partial s_{yy}}{\partial y}\right)$$
$$+\frac{\partial}{\partial x}\left(hT_{xy}\right)+\frac{\partial}{\partial y}\left(hT_{yy}\right)+hv_sS \tag{3}$$

The lateral tension T_{ij} includes viscosity, turbulent friction and differential advection, calculated using the eddy viscosity formula based on averaged velocity gradients at depth. Table 1 defines the variables in the governing equations.

The main calibration parameter was bottom roughness, which was included in the model by zoning the environments, assigning a determined roughness to them depending on the zone involved —ocean, lagoon or adjacent areas.

The physical parameters and primary conditions included in the hydrodynamic model are:

Table 1. Definition of the variables in the governing equations.

Variable/symbol	Definition	Variable/symbol	Definition
x, y	Cartesian coordinates	h	Depth
η	Elevation of the sea surface	t	TIme
ρ	Water density	ρ_0	Water density reference
P_a	Air pressure	g	Aceleración de la gravedad
S	Discharge	f	Acceleration of gravity
$\bar{u}, \bar{v}$	Velocities in directions x and y averaged on the vertical	τ_{bx}, τ_{by}	Coriolis parameter
$T_{xx}, T_{xy}, T_{yx}, T_{yy}$	Lateral tension components	τ_{bx}, τ_{by}	Components of surface tension from wind
$S_{xx}, S_xy, S_{yx}, S_{yy}$	Radiation tensor components	u_s, v_s	Velocity of discharge from the source

- Domain and time parameters:
  - Computational and bathymetry grid; drying and wetting of areas.
  - Length of simulation and increase in time.
- Calibration factors:
  - Dispersion of momentum.
  - Bottom forces.
  - Tensions forces from wind.
- Coriolis Force.
- Initial conditions:
  - Level of sea surface.
  - Components of current velocity.
- Barometric pressure gradients.
- Tide potential.
- Precipitation/evaporarion.
- Boundary conditions:
  - Closed.
  - Sea level.
  - Discharge.
- Other stress elements:
  - Wind speed and direction.
  - Tide.
  - Radiation tensor of waves.
  - Sources and sinks.

Some of the limitations and conditions of the model are: 1) the need to simplify the topo-bathymetric configuration of the space to be studied, even though the topo-bathymetric surveys in the zones of greatest interest are obtained with high resolution; 2) a need for detailed boundary conditions requires flow or sea level measurements that may be located in zones that are difficult to access or identify (for example, diffuse discharges of freshwater from the aquifer to the lagoon); 3) wetting and drying of some areas can generate two-directional flows and internal waves not pertaining to the system; 4) need for recalibration when updating the bathymetry; 5) the model is vertically integrated, thereby preventing the identification of processes that occur in the water column.

Figure 2 shows the computational calculation grid, in which the sizes of the triangular elements can be seen, which vary from 200 m (ocean zone) to 30 m (central channel).

IPCC Intensification Scenarios

Scenarios of increases in sea level established by IPCC (Intergovernmental Panel on Climate Change) were used, which present a range of probable values for the increase in sea level for different scenarios (Nakičenovič & Swart,2000). Among these, a rate of 0.425 cm/year was estimated for the period 2009-2099 (based on maintaining the same use of fossil fuels to obtain energy). This is equivalent to an increase of 21.25 cm in msl over 50 years and

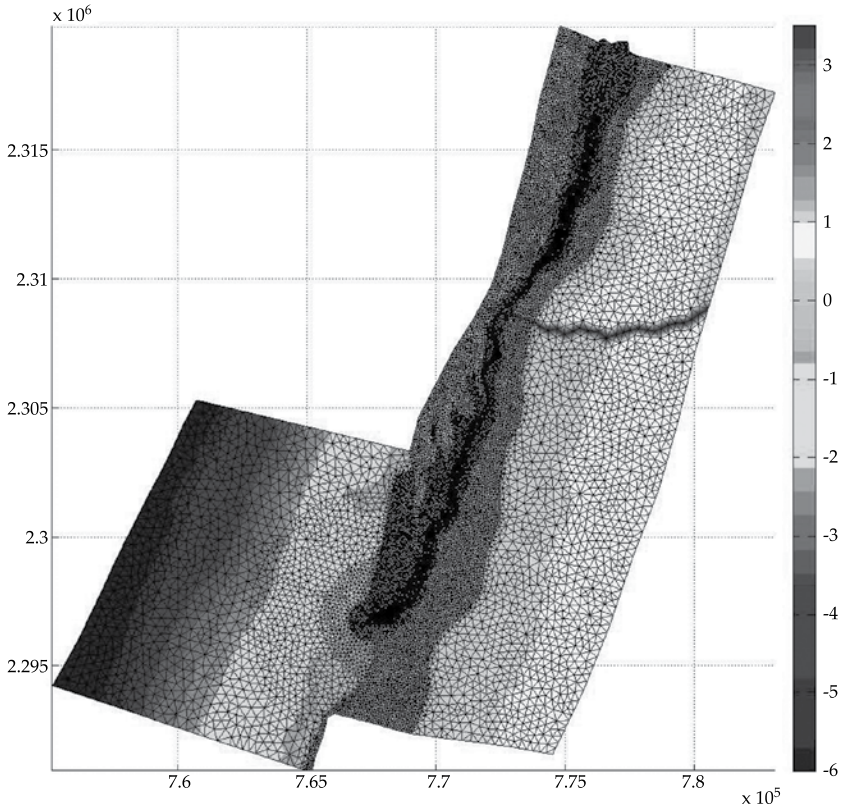

Figure 2. Computational calculation grid for the Celestun estuary (UTM coordinates).

42.5 cm over 100 years (IPCC, 2007). The IPCC indicated that the effect of the flow of ice in the poles should be added to these estimates, resulting in final values of 25 and 50 cm for 50 and 100 years, respectively. In addition, a study performed by Zavala-Hidalgo, De Buen-Kalman, Romero- Centeno and Hernández-Maguey (2010), which analyzed the trends in sea level changes on Mexican coasts, indicated trends of 3.4 ± 1 mm year^{-1} and 2.5 ± 1.2 mm year^{-1}, respectively, for sites closest to the study area (Ciudad del Carmen, Campeche, and Progreso, Yucatán). For scenarios corresponding to 50 and 100 years, this results in changes of 17 and 34 cm for the Ciudad del Carmen and 123. 5 and 25 cm for Progresso. Tests obtained significant changes in flow and ebb behavior for the first 50 cm, and local over-heights (between 12.5 and 34 cm) provided incomplete results. Therefore, and in order to analyze changes in hydrodynamic regimes, 25 and 50 cm scenarios were established for 50 and 100 years, respectively.

Analysis of Flows and Currents

The analysis of flows and currents in the lagoon inlet consisted of determining the changes in flow and ebb by evaluating the two scenarios for increased msl, with an emphasis on the tidal prism and the duration of the two components of the tidal cycle (ebb and flow) (Salles, Voulgaris, & Aubrey, 2005). Changes were also evaluated in the maximum velocities of the current and in flows in the inlet. The type of regime was also analyzed based on the distortion of the ocean wave in the Celstun estuary. Lastly, the results from the simulations were compared with the current conditions (Torres-Mota *et al*., 2012).

Results

In situ records and historical time series

The following sections describe the statistical analyses of waves and the extreme analyses of winds based on the historical time series.

Waves

- Statistical analysis. The waves with the most energy ($Hs > 2.35$ m) occurred during autumn and winter from September to March. A low energy mean climate (mean height of 0.50 m) was observed for the maritime zone outside of the estuary, with a mean period of 5 s and an approximate predominant NNW direction (Table 2).
- Extreme analysis. The data for each of the seasons were fitted to the Weibull maximum probability distribution function and their probabilistic roles were graphed. For example, Figure 3 presents the results corresponding to autumn, which is the hurricane season. These results suggest a return period of 24 years for the peak wave height (2.37 m) during autumn, according to the 30-year time series. With regard to the 50- and 100-year scenarios evaluated by the present study, the graph indicates wave heights of 2.39 and 2.43 m, and a probability of occurrence of less than 2 and 1%, respectively. To fit the Weibull probability distribution, as shown in Figure 3, higher wave heights corresponding to autumn were used for each year (30 data for each probabilistic role). As a first approximation, the data was shown to behave according to two data subsets (statistically different), which could be fit to two different trend lines, with an approximate threshold value of 2.2 m. The literature indicates that when this occurs, the data can be divided into two probabilistic roles, which reflect a correct fit (Abernethy, 2000).

Table 2. Wave statistics for the four seasons from the 1979-2008 time series obtained from the retro-analysis.

Season	H_s (m)	Hrms (m)	T_p (s)	θ (°)
Spring				
Maximum	2.28	1.61	13.29	360.00
Average	0.58	0.41	4.89	338.06
Minimum	0.11	0.08	1.85	0.01
Standard Deviation	0.23	0.16	1.56	129.06
Summer				
Maximum	2.21	1.56	16.05	360.00
Average	0.42	0.29	4.14	354.23
Minimum	0.07	0.05	1.85	0.00
Standard Deviation	0.19	0.12	1.30	106.35
Autumn				
Maximum	2.37	1.67	14.38	360.00
Average	0.64	0.45	5.92	346.90
Minimum	0.07	0.05	1.85	0.00
Standard Deviation	0.33	0.23	1.92	155.54
Winter				
Maximum	2.36	1.67	14.02	360.00
Average	0.69	0.49	6.10	341.40
Minimum	0.13	0.09	1.85	0.00
Standard Deviation	0.36	0.25	1.99	153.70

Characterization of Current Conditions

Tide

To determine the changes in the tidal waves throughout the lagoon, pressure was measured at three points. These were later transformed to the free surface level of the water referenced to the same level bank (Figure 4): a) in the maritime zone outside the estuary (10 km northwest of the lagoon inlet, data from 05/03/2009 to 28/10/2009); b) in the central portion of the lagoon (at the center of its longest axis, data from 16/10/2008 to 17/01/2009), and c) in the northern zone, or "head" of the estuary (data from 10/10/2008 to 17/11/2008).

Tidal measurements included the astronomical tide expressed in terms of harmonic components and the meteorological tide re-

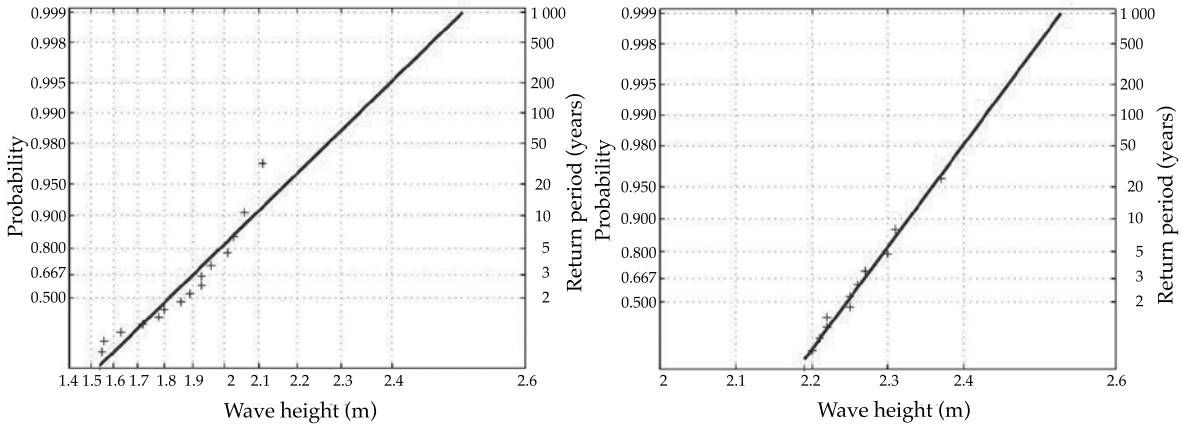

Figure 3. Fitted Weibull maximum for autumn.

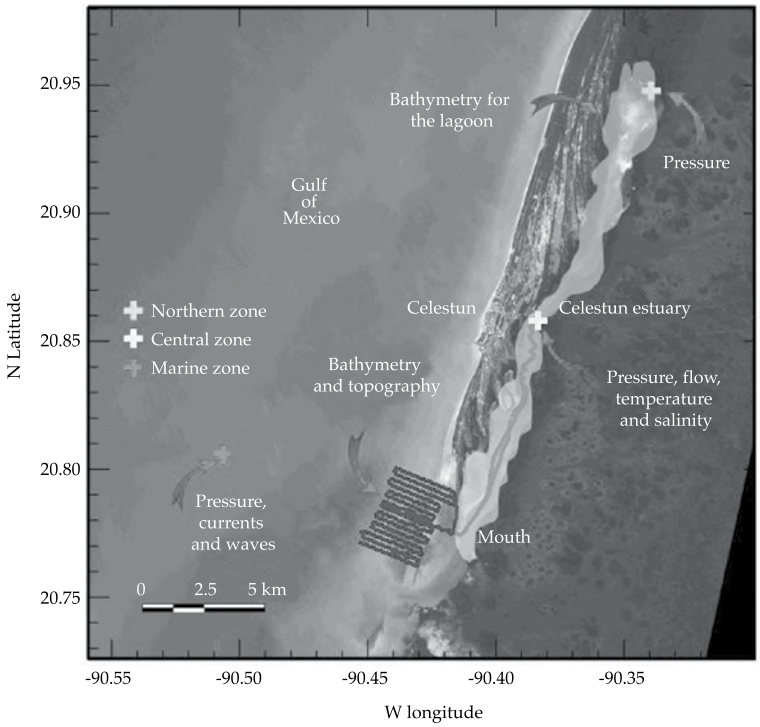

Figure 4. Celestun estuary study area, indicating points at which instruments were located, the variables measured at each of those and the zone where the bathymetry was performed.

sulting from the effect of climate processes (breezes, northerly winds, storms) on water bodies (sea coast and lagoon), translated into oscillations having different spatial-temporal scales (for example, seiches and storm tides). Table 3 shows the harmonic components corresponding to compound tides and overtides, 17 of which are significant (13 are of astronomical

origins and 4 are non-linear (MN_4, M_4, MKS_2, $2MS_6$)). The daytime frequency band is primarily represented by components K_1 and O_1, and the semi-daytime by components M_2 and S_2. To determine the type of sea in the Celestun estuary and verify whether significant changes in its advance exist, the form factor (Pugh, 1987) was calculated, defined as the result of dividing the sum of the amplitudes of the main daytime tide components (K_1 and O_1) by the sum of the amplitudes of the semi-daytime components (M_2 and S_2), thereby assigning the type of regime according to the value obtained. Since the prevalent tide regime throughout the estuary is mixed, with daytime being predominant, this factor was greater than 1.5 in the three zones in the system (with the value increasing from the marine zone to the north zone, the semi-daytime component decreasing with a trend towards daytime tide in the northern portion of the system).

Waves and Currents

The recorded wave data is from October 13, 2008 to October 28 2009. This series was divided into three periods: hurricanes (01/06-30/11), northerly winds (01/12 – last day of February) and a calm period (1/03-31/05). The predominant direction for the three periods was N-ESE (Figure 5), representing 43% of the waves during the hurricane period and 47% during the northerly wind period.

Table 3. Harmonic components of the tide recorded in the marine zone of the Celstun estuary during March 5 to October 28, 2009.

Harmonic constant	Period (h)	Amplitude (m)	*Phase* (°)
Q_1	26.868	0.04	*296.76*
O_1	**25.92**	**0.16**	***306.95***
TAU_1	25.67	0.02	*160.48*
NO_1	24.83	0.02	*287.80*
P_1	24.07	0.07	*324.98*
K_1	**23.93**	**0.18**	***313.31***
PHI_1	23.80	0.02	*325.94*
J_1	23.10	0.01	*293.26*
OO_1	22.31	0.008	*306.71*
N_2	12.66	0.007	*93.30*
M_2	**12.42**	**0.11**	***111.56***
MKS_2	12.38	0.02	*137.90*
S_2	**12.00**	**0.03**	***97.62***
K_2	11.97	0.01	*102.87*
MN_4	6.27	0.005	*269.71*
M_4	6.21	0.007	*285.27*
$2MS_6$	*4.09*	*0.003*	*216.83*

The mean significant wave height (by direction) for the hurricane period ranged from 0.24 to 0.44 m, and the significant peak height was 0.99 m (NNW direction). For the northerly period, the mean heights ranged from 0.38 m (SW-WSW) to 0.54 m (NW), and the peak was 1.15 m (WNW). The mean of the peak periods recorded for each direction ranged from 2.72 to 8.2 s during the hurricane period, and from 4.79 to 16.41 s during the northerly period. The maximum peak period recorded was 25.6 s during the hurricane period.

The currents were measured at the same time as the tide in the marine zone, with a sampling interval of 30 minutes, in 50 cm thick layers throughout the water column. The behavior of the current was uniform throughout the water column. The direction was sensitively parallel to the coastline of the Celestun estuary, NNE during tidal flow and SSW during tidal ebbs. The greatest velocities were associated with tidal ebbs, with a SSW direction, an average value of 0.09 $m.s^{-1}$, and maximum of 0.37 $m.s^{-1}$.

Hydrodynamic simulations

The numerical modeling of the hydrodynamics of the lagoon consisted first of test implementation and simulations (conservation of mass with monochromatic tide) as well as simulations using field measurements for calibration and validation, as described in the section "Description and Calibration of the Numeric Model." Then, hydrodynamic simulations were performed with a monochromatic tide in order to isolate dissipation and distortion processes resulting from the physical characteristics of the system (geometry, bathymetry, intertidal zones, etc.), to avoid contamination or overshadowing from

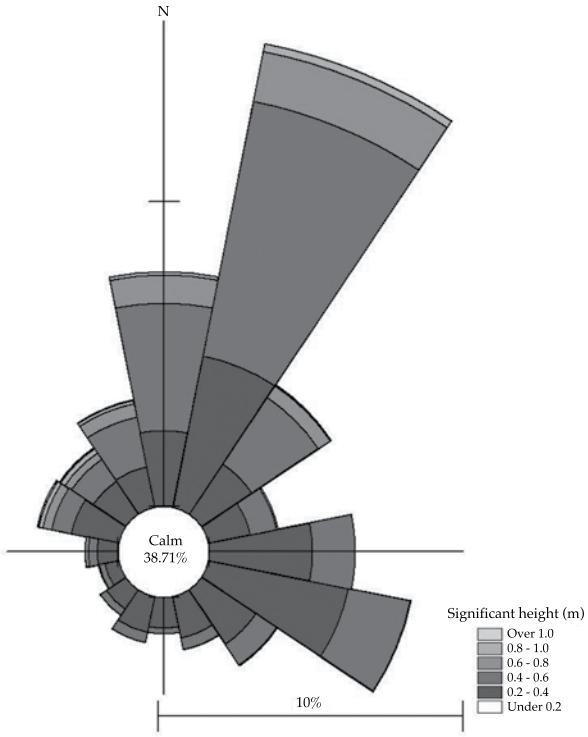

Figure 5. Wave rose from the series measured in the marine zone of the estuary (13/10/2008-28/10/2009).

the forcing of the real tide, which inherently presents a distorted signal. The amplitude of this tide was determined based on a statistical analysis of the live tide present in the signal measured in Celstun (0.76 m) and was adjusted to a 24-h daytime period. The three primary simulations correspond to the current condition and scenarios for increases in sea levels of 0.25 and 0.50 m (scenarios I and II, respectively).

Volumes and durations of flow and ebb for increased mean sea level scenarios

Flow and ebb conditions were analyzed based on the hydrodynamic simulations of current conditions and increased sea level scenarios, calculating the tidal prism, flow and ebb durations and the respective maximum velocities in the inlet (Table 4). For a 25 cm increase in msl, the flow and ebb capacity increases 53%, and for an increase of 50 cm it increases 114% (Table 4). In this latter case, the increase in msl corresponds to approximately 1.3 times the amplitude of the tide considered.

The maximum current velocities of the tidal wave propagated for the present scenario were roughly 60 $cm.s^{-1}$ at the inlet for both flow and ebb conditions. These increased 18% for scenario I and 29% for scenario II. Figure 6 shows the durations of flows and ebbs for each of the increased mean sea level scenarios.

Based on the results presented in the table and the previous figures, the following can be deduced:

- The Celestun estuary has a hydrodynamic regime in which the duration of the ebb is always greater than that of the flow, and the maximum velocities in the inlet are always greater for ebb.
- As the mean sea level increases, the tidal prism also increases, first at a relatively constant rate of 0.61 x 10^6 m^3 between scenarios 0 and I (25 cm increase in msl),

Table 4. Maximum velocities, durations and volumes of flow and ebb, for current conditions and scenarios for increasing mean sea level.

Condition	Flow Volume	Flow		Ebb		Differences		
	Prism P (10^6 m^3)	V_{max} (m/s)	Duration (h)	V_{max} (m/s)	Duration (h)	ΔP (10^6 m^3/cm)	ΔV (cm/s)	ΔD (h)
Scenario 0 (actual)	28.42	0.608	10.29	0.630	13.71	-	2.2	3.42
Scenario 0b (12.5 cm)	36.02	0.684	10.15	0.691	13.85	0.61	0.7	3.70
Scenario 0c ((16.67 cm)	38.54	0.706	10.09	0.712	13.89	0.60	0.6	3.80
Scenario 0d (20.83 cm)	41.11	0.727	10.03	0.734	13.97	0.62	0.7	3.94
Scenario I (25 cm)	43.65	0.746	9.93	0.756	14.07	0.61	1.0	4.14
Scenario Ib (35 cm)	50.19	0.787	9.86	0.812	14.14	0.65	2.5	4.28
Scenario Ic (43 cm)	55.74	0.813	9.89	0.859	14.11	0.69	4.6	4.22
Scenario II (50 cm)	60.84	0.831	9.97	0.901	14.03	0.73	7.0	4.06

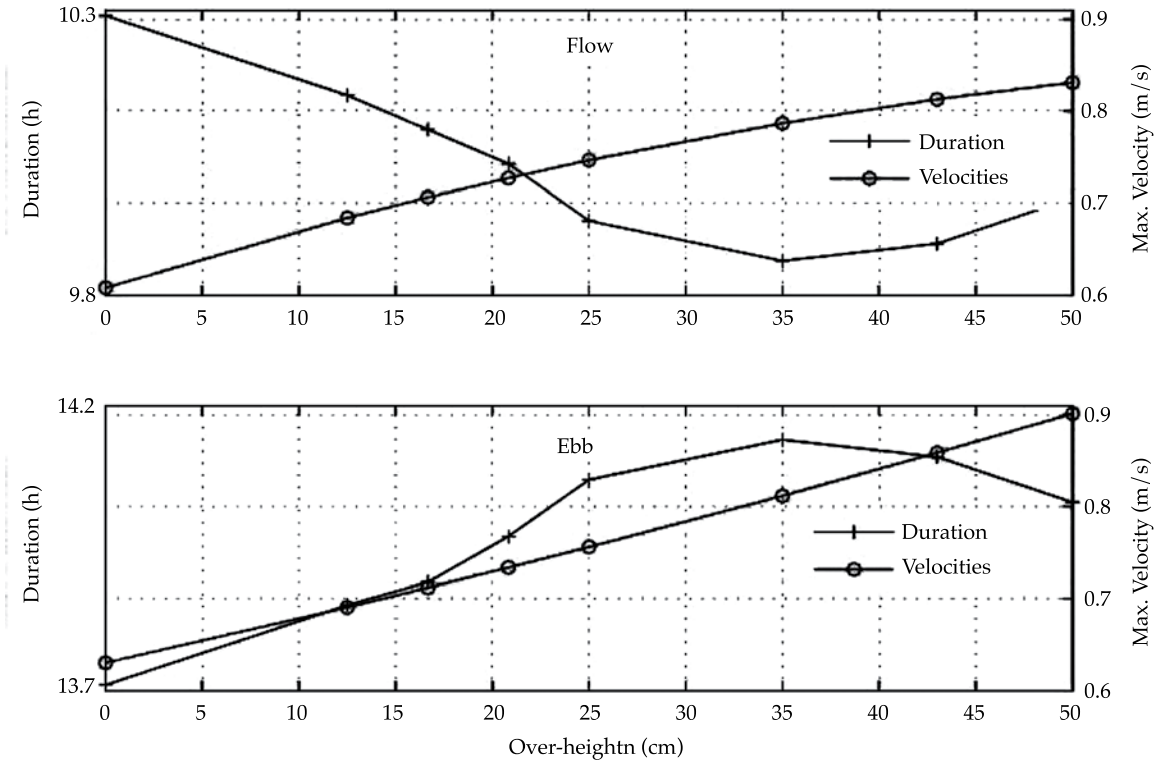

Figure 6. Durations of ebbs and flows in the Celestun estuary and maximum velocities at the inlet for each of the scenarios for increased mean sea level.

then 0.65, 0.69 and 0.73 x 10^6 m^3 for scenarios IB (35cm), Ic and II (50cm), respectively. This is essentially because in the zone with a low slope, in the eastern portion of the lagoon, flooding accelerates more quickly beginning at a 35 cm increase in msl. Therefore, the volume collected in that area results in the prism increasing more rapidly than for scenarios with smaller increases in mean sea level.

- In addition, a decreasing trend (increase) in the duration of flow (ebb) can be seen between the present condition and Scenario 0d (35 cm, see Table 4). This is because as the flood areas increase the ebb or "emptying" of those areas slows down due to the high friction in those areas. Nevertheless, that trend reverses in the scenarios that follow. That is, the duration of the ebb gradually decreases with an increase of 35 cm and above.
- In this case, what likely occurs is that after reaching a certain free surface level in the flooded zone, the ebb becomes more efficient because of the low height of the vegetation in that zone (especially for marine grass).
- Nevertheless, the difference in maximum velocities at the inlet for ebb and flow from scenario 0 to scenario 0c decreases (ΔV decreases from 2.2 to 0.6 cm/s) and then significantly increases in the scenarios that follow, reaching a maximum difference of 7 cm/s in scenario II (50 cm).

Given what has been described above, in terms of the maximum velocity in the inlet and the associated transport of sediments, the results suggest the following. First, the difference in maximum velocities between flow and ebb decrease to practically 0, up to a certain value of increase in msl (scenario 0c, 16.7 cm). This can translate into a lower capacity by the system to export sediments. Nonetheless, gradual increases in msl indicate a change in that behavior, in which the ebb velocity increases in relation to the flow velocity and, therefore, the capacity of the system to export sediments to the sea (during ebb) is greater than the capacity to import them (during flow). This can be seen as the capacity of the system to maintain equilibrium and to keep the inlet open.

In order to explain this phenomenon, Figure 7a presents a simplified model to determine the velocity induced by the tide, which is composed of the superposition of two monochromatic signals (M^2 and its subharmonic M_4) and a null phase (2M2 - M4 =0), such that the resulting tide is shorter and more intense during flow. That is, is the flow is dominant (for example, see Speer & Aubrey, 1985). The maximum velocities during flow are also observed to be 1.8 times greater than those of ebb. Figure 7b shows an approximation of the bottom transport, calculated as a simplification of the transport equations by Meyer-Peter and Müller (Speer & Aubrey, 1985) taken as the cube of the magnitude of the current velocity. An arbitrary value (V_c) for critical velocity at initiation of transport is also presented and the shaded areas represent the magnitude of sediment transport. Positive values (potential for importing sediments) can be seen to be much higher than negative values (potential for exporting sediments) and a small difference in velocity represents a significant change in transport. For this regime, the transport carried into the system is shown to be 19.5 times greater than the sediment carried outside the system, which can result in potential depositing in the system over the long term.

The behavior is similar for the case pertaining to the study herein, the Celestun estuary, only in this case the higher velocities occur during ebb. Figure 8 shows the approximation (V^3) of the sediment transport rates calculated for the three experiments: the present conditions and scenarios I and II. An increase in the msl generates an increase in the tidal prism, which leads to an increase in the magnitudes of the velocities as well as an increase in the sediment transport capacity of both flow and ebb, to nearly three times the present transport. This graph suggests that an increase in the mean sea level will produce an increase in the velocities and sediments transported in the inlet (up to three times the present amount), with a significantly greater sediment transport capacity during ebb than during flow for these scenarios.

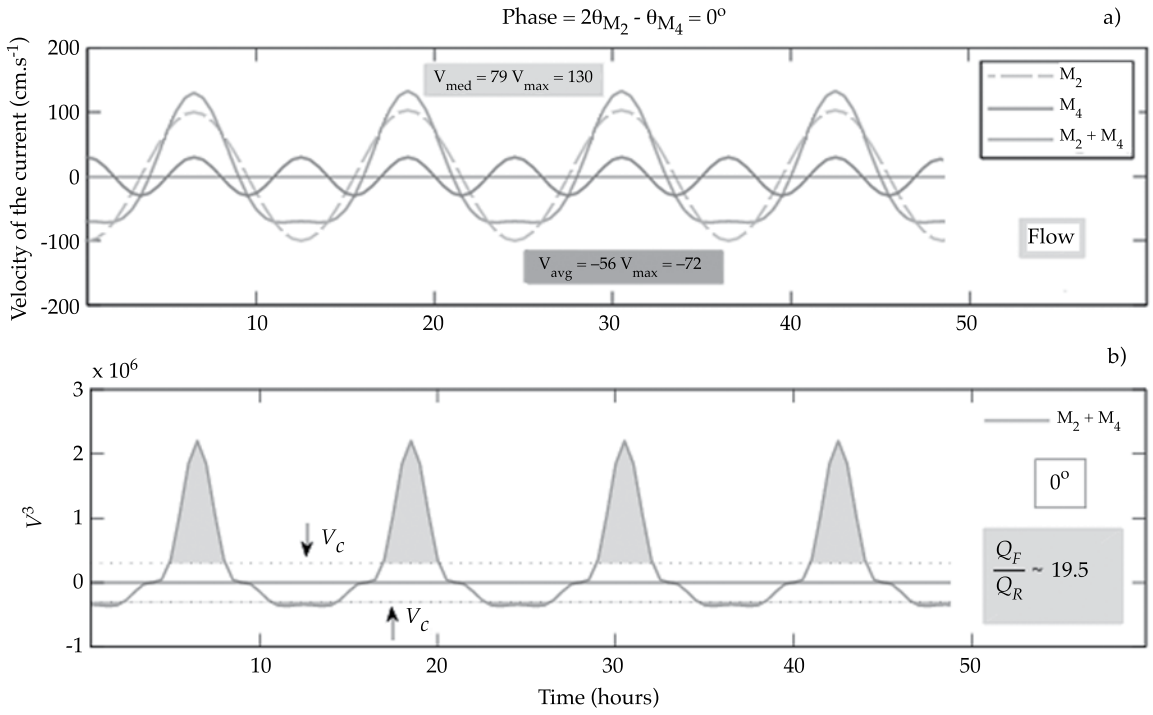

Figure 7. Example of the asymmetry of the velocity of the tidal wave for a regime where flow is dominant: a) principal harmonic, M_2, secondary component, M_4, and difference between them; b) qualitative sediment trasnport parameter, proportional to the velocity cubed (obtained by simplifying the Meyer-Peter & Muller equation).

Conclusions

This work consists of studying the effect of an increase in mean sea level on the hydrodynamics of a coastal lagoon, particularly the inlet connecting it with the sea, and the possible implications on the morphology over the medium and long term. Even though this simplified model of the analysis of flows and qualitative estimate of possible sediment transport does not take into account the availability of sediment and coastal transport, it has been proven as a useful tool to calculate equilibrium conditions for coastal water bodies. The most relevant conclusions are presented below:

- The net sediment transport depends not only on the direction of the residual current but also on the distortion of the velocity fields as well as maximum flow and ebb velocities.
- Intertidal areas should not be underestimated because of their involvement in the propagation and asymmetry of the tide. The present morphological characteristics that determine the reach of the present tide strongly affect the flows in the inlet. An increase in sea level results in new areas being covered by the tidal wave and in their active involvement in the lagoon's dynamics, with physical as well as biological implications at different spatial and temporal levels and scales.
- From the perspective of tidal asymmetry, the Celestun coastal system has the capacity to adapt to an increase in mean sea level and is able to transport sediment through the inlet.

- During the first stage of a probable increase in mean sea level, the stability of the system is at risk from a relative decrease in the capacity to export sediment during ebb. Nevertheless, if the system can remain open after that stage, the results suggest that the changes in the distortion of the tide due to the flooding of adjacent areas would produce a decrease in the duration of the ebb, accompanied by an increase in maximum velocities in the inlet during that tidal period.
- The above translates into a greater capacity to transport sediment outside the system; that is, a better capacity to export sediment, which is important during the flow phase.
- The information generated by the present study is intended for use as part of the scientific basis for managing coasts and can be used by decision-makers and environmental policy-makers to manage the coastal area based on changes that could be generated in the future which, although uncertain, can be roughly approximated using scenarios based on probabilities.
- Thus, knowing the future conditions of the coastal system and its physical components, a basis is established to prevent and/or mitigate changes to natural spaces such as lagoons, in order to foster natural development, in space and time, that is sustainable for the humans, flora and fauna that inhabit the coast and use its resources.

Acknowledgements

The authors thank the financial support provided by the Postgraduate Department of the National Autonomous University of Mexico (Coordinación de Estudios de Posgrado de la UNAM), project *PAPIIT IN 120708* and *OMIXYUC106400*.

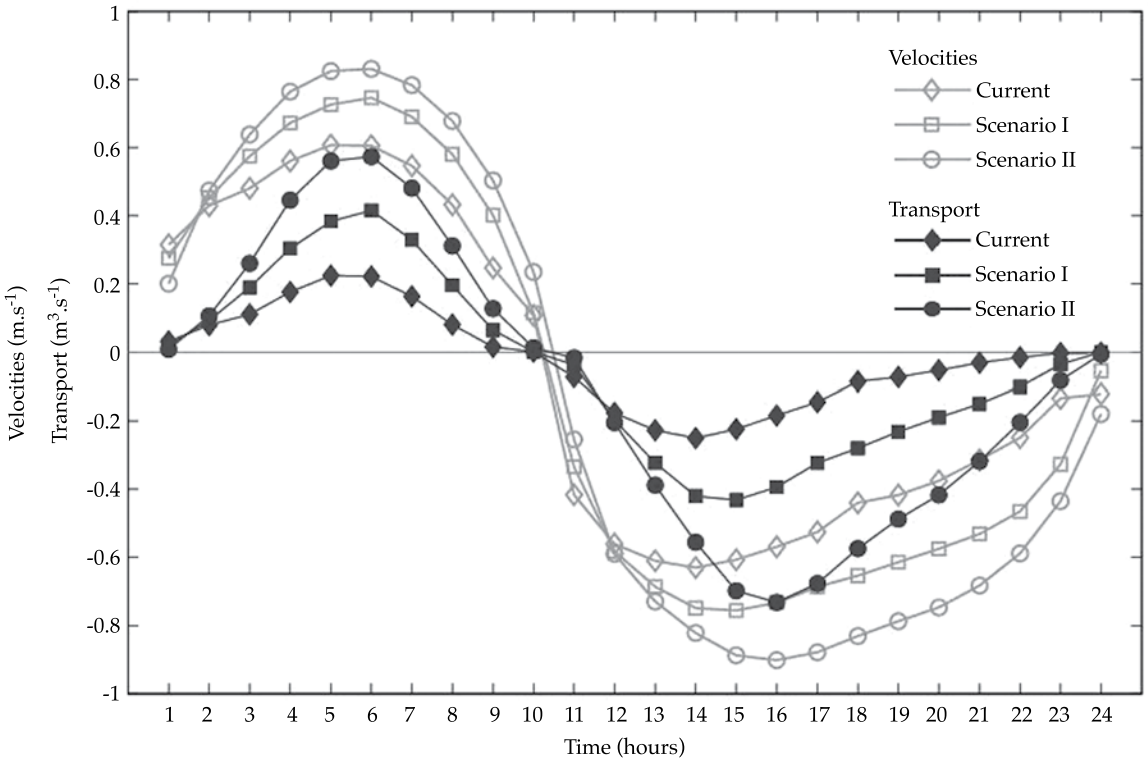

Figure 8. Velocities and approximation (V^3), sediment transport in the lagoon inlet during flow and ebb in one tide cycle in the Celstun estuary for three primary scenarios: current, I and II. Negative values correspond to ebb.

References

Abernethy, R. B. (2000). The New Weibull Handbook. Fourth Edition. North Palm Beach, Florida: Published by the author.

Appendini, C. M., A. Torres-Freyermuth, F. Oropeza, P. Salles, J. López, & E. T. Mendoza (2013). Wave modeling performance in the Gulf of Mexico and Western Caribbean: wind reanalyses assessment, *Applied Ocean Research*, *39*, 20-30.

Batllori, E., Chávez, E., Díaz de León, A., Herrera-Silveira, J., Garduño, M., González, A., & Torruco D. (1987). *Caracterización estructural de la laguna de Celestún*. Simposio Internacional del Mar, La Habana, Cuba.

Batllori, E., Gonzáles, J., Díaz, J., & Febles, J. (2005). Caracterización hidrológica de la región costera noroccidental del estado de Yucatán, México. *Investigaciones Geográficas, Boletín del Instituto de Geografía, 59*, 74-92.

Battjes, J. A. (2006). Developments in Coastal Engineering Research. *Coast. Eng.*, *53*(11), 121-132.

Botello, A., Villanueva, S., Gutiérrez, J., & Rojas, J. (Eds). (2010). *Vulnerabilidad de las zonas costeras mexicanas ante el cambio climático* (514 pp.). Campeche, México: Gobierno del Estado de Tabasco, Semarnat-IINE, UNAM-ICMYL, Universidad Autónoma de Campeche.

Duch, J. (1988). *La conformación territorial del estado de Yucatán. Los componentes del medio físico*. México, DF: Universidad Autónoma Chapingo, Centro Regional de la Península de Yucatán.

Houston, J. R., & Dean, R. G. (2011). Sea-Level Acceleration Based on U.S. Tide Gauges and Extensions of Previous Global-Gauge Analyses. *Journal of Coastal Research*, *27*(3), 409-417.

IPCC (2007). *Cambio climático 2007: Informe de síntesis. Contribución de los Grupos de trabajo I, II y III al Cuarto Informe de evaluación del Grupo Intergubernamental de Expertos sobre el Cambio Climático* (104 pp.). Equipo de 1.7 Bibliografía 14 redacción principal: R. K. Pachauri & A. Reisinger (directores de la publicación). Ginebra: IPCC.

Meyer-Peter, E. y Müller, R. (1948) Formulae for bedload transport. *Proceedings of 3rd Congress, International Association of Hydraulic Research*, Sweden, 39-64.

Nakičenovič, N., & Swart R. (Eds.) (2000). *Emissions Scenarios. Special Report of the Intergovernmental Panel on Climate Change* (599 pp.). Cambridge: Cambridge University Press.

Ortiz-Pérez, M. A., & Méndez-Linares, A. P. (1999). Escenarios de vulnerabilidad por ascenso del nivel del mar en la costa mexicana del golfo de México y el mar Caribe. *Investigaciones Geográficas (Mx)*, *39*, 68-81.

Pugh, D., & Tides, T. (1987). *Surges and Mean Sea Level, a Handbook for Engineers and Scientists*. Chichester, UK: John Wiley & Sons.

Salles, P., Voulgaris, G., & Aubrey, D. (2005). Contribution of Nonlinear Mechanisms in the Persistence of Multiple Tidal Inlet Systems. *Estuarine, Coastal and Shelf Science*, *65*, 475-491.

Secretaría de Medio Ambiente y Recursos Naturales. 2000. *Programa de manejo Reserva de la Biosfera Ría Celestún*. Comisión Nacional de Áreas Naturales Protegidas. México, D.F. 191 pp.

Speer, P. E., & Aubrey, D. G. (1985). A Study of Non-Linear Tidal Propagation in Shallow Inlet/Estuarine Systems. Part II: Theory. *Estuarine, Coastal and Shelf Science*, *21*, 207-224.

Torres-Mota, R., Salles, P., Mariño, I., & López, J. (July, 2012). Effects of Ocean Climate Change on the Celestún Estuary Morphology. *Proceedings*. 33rd International Conference on Coastal Engineering (ICCE2012), ASCE, Spain.

Yañez-Arancibia, A. (Ed.) (2010). *Impactos del cambio climático sobre la zona costera*. México, DF: Instituto de Ecología A.C. (INECOL), Texas Sea Grant Program, Instituto Nacional de Ecología (INE-Semarnat).

Zavala-Hidalgo, J., De Buen-Kalman, R., Romero-Centeno, R., & Hernández-Maguey, F. (2010). Tendencias del nivel del mar en las costas mexicanas. En A. V. Botello, S. Villanueva-Fragoso, J. Gutiérrez, & J. L. Rojas-Galaviz (Eds.). *Vulnerabilidad de las zonas costeras mexicanas ante el cambio climático* (pp. 249-268). Campeche, México: Semarnat-INE, UNAM-ICMYL, Universidad Autónoma de Campeche.

Institutional Address of the Authors

Dr. Rogelio Torres Mota
Dr. Paulo Salles Alfonso de Almeida
Dr. José López González

Laboratorio de Ingeniería y Procesos Costeros
Unidad Académica Sisal del Instituto de Ingeniería
de la UNAM
Puerto de Abrigo S/N, Sisal
97355, Yucatán, México
Teléfono +(52) (988) 9120 147 al 49, extensión 7403 y
(55) 5622 6710 al 17, extensión 7403
rogelio.torres03@cfe.gob.mx
psallesa@iingen.unam.mx
jlopezgo@ii.unam.mx

Click here to write the autor

Remains from the storm "Simon," San Quintin Bay, Baja California, Mexico.

Photo provided by Fabiola Arellano Lara.

Sediment Transfer from a Microwatershed to an Urban Drainage Network

• Guillermo José Mendez* • Carlos Alberto Depettris • Jorge Víctor Pilar •
• Oscar Orfeo • Alejandro Ricardo Ruberto •
Universidad Nacional del Nordeste, Argentina
*Corresponding Author

Abstract

Mendez, G. J., Depettris, C. A., Pilar, J. V., Orfeo, O., & Ruberto, A. R. (September-October, 2014). Sediment Transfer from a Microbasin to an Urban Drainage Network. *Water Technology and Sciences* (in Spanish), 5(5), 21-36.

Little data exists on sediment generation and transport rates in urban areas. This is due to the complexity of the phenomenon and, in particular, its variability. Three factors are investigated in this article: (1) annual sediment rate generated in a micro-basin over three years, (2) determination of the precipitations resulting in the highest values and (3) how prior hydrological conditions in the basin affect the sediment load in runoff. A basin in the city of Resistencia, in Chaco, Argentina, was monitored (4.76 ha with residential use) from September 2009 to March 2010. A hydrological model was calibrated with the SWMM program 5.0 and the primary sediment curves were drawn. With this and daily precipitation data for the years 2007/2008, 2008/2009 and 2009/2010 the annual sediment load transported by urban runoff was obtained for the analysis period. These ranged from 0.8 to 1.40 t/ha. The highest values documented occurred from September to December of each year, during which 60% of the load was trasnported. It is concluded that there is a strong incidence of volume runoff of sediment loads, where the most impermeable areas generate large flows and, therefore, higher sediment loads than permeable areas. The results obtained were consistent with the measurements and, therefore, quantification of sediments in pluvial drainage in urban basins is feasible.

Keywords: Sediments, urban drainage, plain basins.

Resumen

Mendez, G. J., Depettris, C. A., Pilar, J. V., Orfeo, O., & Ruberto, A. R. (septiembre-octubre, 2014). Transferencia de sedimentos de una microcuenca a la red de drenaje urbano. Tecnología y Ciencias del Agua, *5(5), 21-36.*

Los datos referentes a las tasas de generación y movilización de sedimentos en áreas urbanas son exiguos. Esto se debe a la complejidad del fenómeno y, especialmente, a su variabilidad. En este artículo se abordan tres aspectos: (1) la tasa anual de sedimento que genera una microcuenca durante tres años; (2) qué precipitaciones provocan mayores valores, y (3) cómo afectan las condiciones hidrológicas antecedentes de la cuenca en la carga de lavado de la escorrentía. Se monitoreó un microcuenca de la ciudad de Resistencia, Chaco, Argentina, de 4.76 ha y uso residencial, desde septiembre de 2009 hasta marzo de 2010. Se calibró un modelo hidrológico bajo el programa SWMM 5.0 y se trazaron curvas claves de sedimentos. Con esto y con las precipitaciones diarias de los años 2007/08; 2008/09 y 2009/10 se pudo obtener la carga anual de sedimentos trasportados por la escorrentía urbana durante el periodo de análisis. Las cargas anuales de sedimentos transportadas oscilaron entre 0.8 y 1.40 t/ha. Los mayores valores se registraron en el periodo de septiembre a diciembre de cada año, en el que se transporta el 60% del total anual. Se concluye que existe una fuerte incidencia de los volúmenes de escurrimiento en las cargas de sedimentos, donde las áreas más impermeables son capaces de generar importantes caudales líquidos y, por tanto, mayores cargas de sedimentos que las zonas permeables. Los resultados obtenidos fueron coherentes con las mediciones, por tanto es factible cuantificar el aporte de sedimentos de cuencas urbanas al drenaje pluvial.

Palabras clave: *sedimentos, drenaje urbano, cuencas de llanura.*

Received: 19/12/11
Approved: 23/01/14

Introduction

The quality of water in urban areas, and rainwater drainage in particular, is a subject that has become important over recent years. There are two reasons for this: a) cities house 50% of the population worldwide, and this is expected to increase to 70% by the middle of the 21st century

(Niemcynowicz, 1996, *apud* Maksimovic, 2001); b) human activities generate a large amount of pollution which is deposited on the surface of streets, sidewalks and the roofs of buildings, and is washed off by urban runoff. Therefore, rainwater drainage contains high concentrations of pollutants.

Consequently, an increasingly higher portion of the population is regularly exposed to water with a negative visual impact, to the degradation of receptor bodies, accumulative toxic effects in plants and animals and the growth of undesirable microorganisms.

In Argentina, the development of the metropolitan area of the city of Buenos Aires in the Matanza-Riachuelo watershed can be cited as a paradigmatic case. Throughout its history settlements have been established in areas that are naturally floodable, with the uncontrolled growth of impermeable surfaces and a lack of space to efficiently manage rainwater. Today's problems reflect multiple factors, such as the effect on the health of the population, frequent flooding and the loss of a rich and diversified environment, among others. With the transformation of a rural environment into an urban one, this type of problem becomes increasingly worse (Subsecretaría de Recursos Hídricos de la Nación Argentina, 2009). In the watershed and its surrounding area, where roughly five million persons live, current water problems can be classified simply as those associated with the quality of runoff and the quantity of both surface water and groundwater.

To achieve sustainable development, the purpose of urban drainage has changed worldwide and, now, in addition to providing protection from floods it must also make it possible to control pollutants and provide rainwater drainage characteristics that contribute to a livable urban environment.

The pollutants present in the urban runoff include: sediments, substances demanding oxygen, nutrients (nitrates and phosphates), heavy metals, pesticides, fats and oils, bacteria and viruses, acids and bases, humic substances that are precursors of trihalomethanes, foul-smelling gases, chlorides and sodium, etc. (Jiménez-Gallardo, 1999).

Sediments represent one of the most significant pollutants. Transported by urban drainage, these create deposits that obstruct piping in the main system, increase the turbidity of water, change the beds of receptor bodies, reduce flow capacity and affect aquatic life. In addition, the finest fraction of sediments is able to transport adsorbed pollutants such as heavy metals, ammonium, fertilizers, pesticides and polychlorobiphenyls (PCBs), among others (Porto, 2001). That is, the problems generated by sediments not only impact the quality of water but also involve losses of soil and affect the drainage system. Therefore, addressing this problem requires a combined approach involving sedimentology and hydrology, among other disciplines.

Given the complexity of the urban erosion process, it is difficult to identify the sources that generate sediments. In effect, the urban environment creates a large and complex mixture of sediments that could come from the vicinity or be imported from nearby areas, or even those far away. In addition, the materials used in construction represent significant sources of urban sediments. Studies have shown that high concentrations of calcium in lakes are due to this type of sediment (Poleto, 2008). Runoff generates forces that can cause accumulated sediments to be dragged into streets and areas with unprotected soil and transport them to conduits in secondary urban drainage systems.

There are little data regarding rates of generation and mobilization of sediments in urban areas. This is due not only to the complexity of the phenomena but also to its variability, in particular (Ramos, 1995). Sediment loads are usually related to runoff volume, which directly depends on impermeability. Studies performed in the United States, in urban regions with 1 016 mm of yearly precipitation, indicate the annual sediment load of commercial watersheds is 2.28

times higher than a residential watershed. This is because commercial areas in that country have more impermeable areas than residential areas (EPA, 1983).

The city of Resistencia is located in northeastern Argentina. It is the capital of the province of Chaco and has a population of 386 391 inhabitants (INDEC, 2010). The Gran Resistencia Metropolitan Area (GRMA) is composed of the cities of Resistencia, Puerto Vilelas, Barranqueras and Fontana. The GRMA is located in the floodplains of the Parana River, downstream from the confluence with the Paraguay River (Figure 1). It is in the Negro River watershed in the north and the Araza in the south, both tributaries on the right banks of the Parana River (Figure 2).

The GRMA is located in a zone affected by overflowing and spills from the Parana River, determining the presence of abundant fluvial sediments on the surface and in the subsoil. The surface sediments (up to 2 m) are composed primarily of alternating silt and clay, partially worn away, with subordinate sands and high levels of plasticity. Underneath, silty sands and sandy silt are found to a depth of 5 m. These are disaggregated, saturated with moisture and very fluid (Mendez, 2013). These

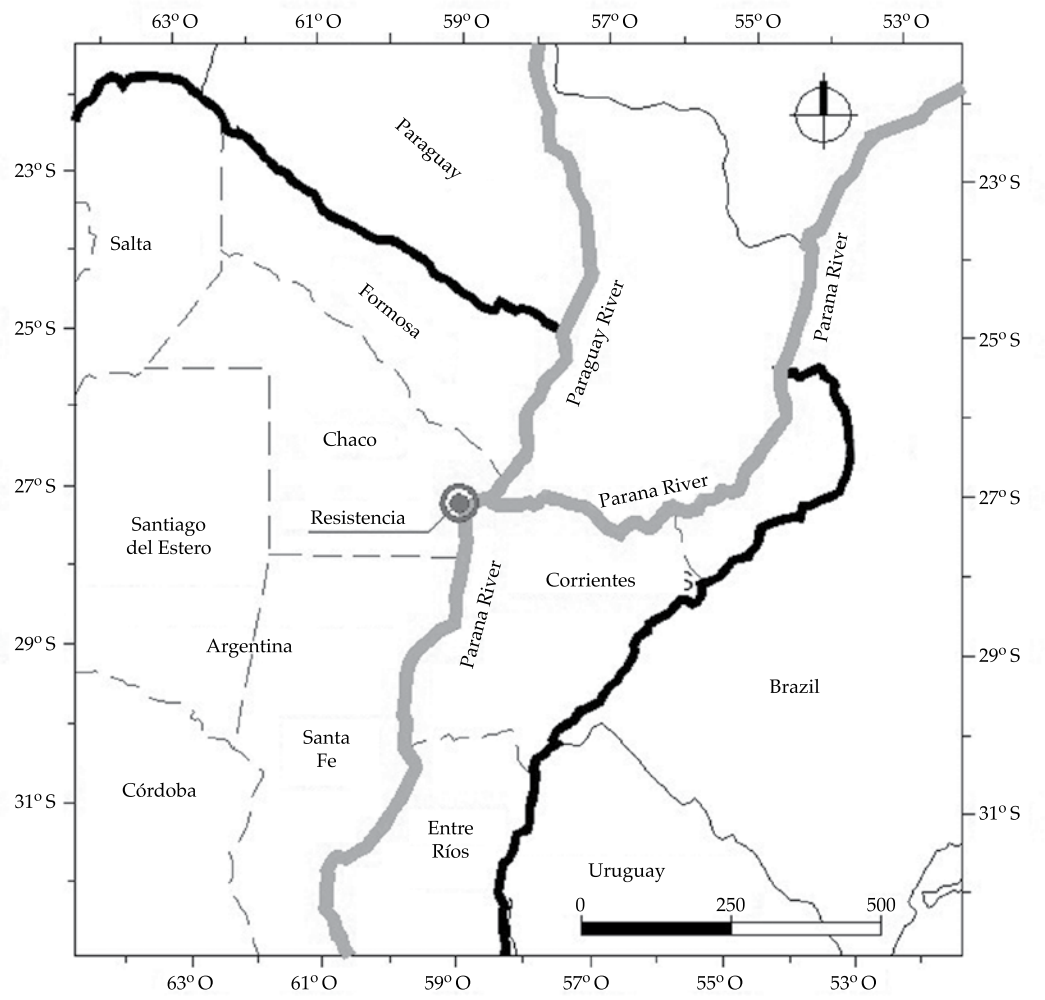

Figure 1. Location of the city of Resistencia in northeastern Argentina.

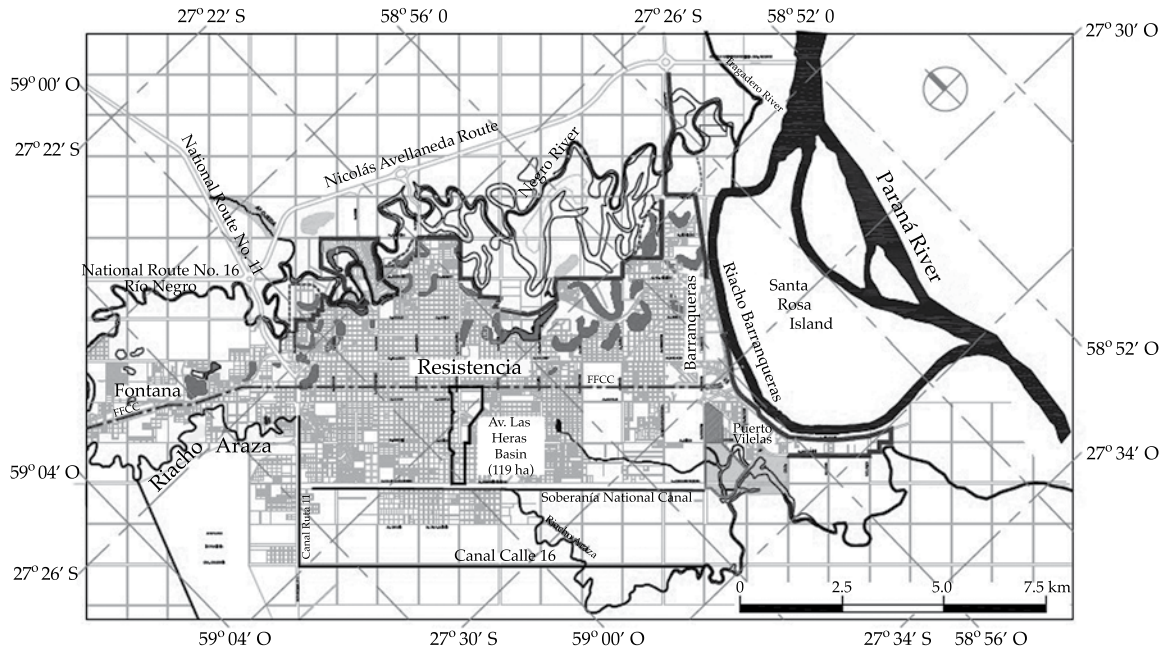

Figure 2. Location of the Avenida Las Heras basin.

sedimentary materials are generally known as alluvial deposits. The surrounding area also contains silts and sandy silts of eolian origin (Segemar, 1997). From the edaphological perspective, the development of argiudolls on top of alluvial deposits has been observed, as well as natracualf soils in the region dominated by eolian deposits (INTA, 1990).

Dispersion is another characteristic of soils that influences the way in which they contribute to urban runoff. This is a process through which soil spontaneously deflocculates when exposed to water with little or no hydraulic velocity. Dispersion is thought to be generally caused by electrostatic repulsion between clay particles, resulting in the formation of a stable colloidal suspension of the soil (Garay-Porteros & Alva-Hurtado,1999). Orfeo (1997) found an important disaggregation trend with the presence of water, which reveals a potential risk factor for the mobilization of particles and a low sustenance capacity which must be taken into account.

This article addresses three important aspects: (1) the annual sediment rate generated in a micro-watershed in the southern portion of the city of Resistencia for the three years during which the present study was conducted, (2) which precipitations generate higher sediment loads and (3) how the antecedent hydrological conditions of the watershed affect the wash-load in rainwater drainage.

A better understanding of these aspects will help to identify the quality of urban runoff and provide a better design of drainage systems and plains areas.

This study was conducted by the research group at the Hydraulics Department of the National Northeastern University's Engineering School (Departamento de Hidráulica de la Facultad de Ingeniería de la Universidad Nacional del Nordeste (UNNE)), in collaboration with researchers at the Coastal Ecology Center (Centro de Ecología del Litoral (Cecoal)), Conicet, as part of the Project "Urban Hydrology in Northeastern Argentina,"

financed by the National Agency for Scientific and Technological Promotion (ANPCyT, Spanish acronym) of the Republic of Argentina.

Study Area

The study area adopted is the micro-watershed that discharges into the drains located in San Lorenzo street, in the city of Resistencia, Chaco, upstream from the intersection with Avenida Castelli (Figures 2 and 3). The selection of the study area depended on a series of factors (Depettris, Depettris, Kutnich, & Ruberto, 2009): a) easy access and monitoring; b) closed supply area; c) ability to measure the flow on the street; d) few parked vehicles on the zone to be measured and 3) having storm drains which are representative of those used in the region and located on straight sections.

This mirco-watershed is categorized by residential usage and belongs to the Avenida de Las Heras watershed. The latter has a total area of 119 ha and a very small slope (less than 0.1%). It discharges through closed and open conduits into the Avenida Soberania Nacional canal (Figure 2), the receptor and transporter sewage pipe for all discharges in that section of the city (CFI-AFIN, 1995).

The drains supplied by the watershed studied are located on the right and left shoulders of San Lorenzo street. Taking the center of this street as the divider of the water, it can be presumed that two different watersheds discharge into these drains. The watershed on the left shoulder, where three towers were built during the stage to collect the field data (Figure 3) has a lower percentage of impermeable area than the opposite size (Table 1; Depettris *et al.*, 2009).

Figure 3. Micro-watershed containing sinks in San Lorenzo Street and Castelli Avenue. References: 1) exposed soil, 2) construction tower, 3) sampling sites (upstream from the drain entrances).

Table 1. Distirbution of areas of the micro-watershed studied.

Area type	Right side		Left side		Total	
	(ha)	(%)	(ha)	(%)	(ha)	(%)
Permeable	0.293	14	0.464	17	0.757	16
Impermeable	1.7290	86	2.2780	83	4.007	84
Total	2.02	100	2.74	100	4.764	100

Materials and Methods

Period of Analysis

The period of analysis corresponds to hydrological years 2007/2008, 2008/09 and 2009/10. The hydrological years in the region begin during the month of September and end in August of the following calendar year (Bruniard, 1981). The city of Resistencia has a mean annual precipitation of 1 350 mm (APAAFIN, 2001), and the maximum annual daily precipitation is 116.8 mm (Mendez, Ruberto, & Pilar, 2009). The first two years of analysis coincided with a dry period, with annual precipitations below the mean (Table 2), a situation which reversed itself in the last year, as of November 2010 when 351 mm fell over seven days, an event with an estimated recurrence of 20 years (Mendez, Ruberto, Pilar, & Depettris, 2011).

Determination of Liquid Flows

Liquid flows were determined using a rainfall-runoff transformation model with the SWMM (*Stormwater Management Model*) program, version 5.0, by the United States Environmental Protection Agency.

The SWMM can be used for a unique precipitation event or to perform continuous simulation during an extended period. The program makes it possible to simulate the quantity as well as quality of evacuated water, particularly urban drainage (Huber & Dickinson, 1988).

Continuous modeling was performed over the three hydrological years of the analysis period. Precipitaiton data recorded every 15 minutes were used, as well as daily evaporation. The precipitation data for the year 2009/10 were registered by rain gauges belonging to the Provincial Water Administration (Administración Provincial del Agua (Chaco-Argentina)) installed in the vicinity of the "Los Lirios" lagoon located 2 km east of the micro-watershed studied. The records from the "Los Lirios" station are incomplete for the years 2007/08 and 2008/09, and therefore data were used from the rain gauge from the National Institute for Farming Technology, in Colonia Benitez located 15 km north of the micro-watershed (Instituto Nacional de Tecnología Agropecuaria (INTA, Spanish acronym)). The evaporation data were recorded in the tank at the Training Weather Station of the UNNE Engineering School located 300 m from the micro-watershed.

Table 2. Annual and annual maximum daily precipitations for the analysis period and their corresponding times of recurrence of exceedance.

Year	*P* annual (mm)	Recurrence (years)	*P*max (mm)	Date	Recurrence (years)
2007/2008	870	0.9	82.5	27/12/2007	1.2
2008/2009	935	0.9	86.5	05/02/2009	1.3
2009/2010	1 347.3	2.3	155	19/01/2010	6.6

The study area was divided into 18 sub-watersheds which supply the respective streets, considered irregular conduit sections (Figure 4). Since the watersheds on the left and right shoulders were analyzed separately, San Lorenzo street was treated as two conduits divided along its center.

Five gauges were used to calibrate the parameters, corresponding to precipitations on days 14/10/2009, 06/11/2009, 20/11/2009, 08/02/2010 and 22/02/2010, as described in detail by Mendez, Depettris, Orfeo, Ruberto, & Pilar (2010). To perform the flow gauging, hydrometric scales placed on the roads for the purpose of this study were used (Depettris *et al*., 2009). The wet width in the control section was converted to flows using the Manning formula, adopting 0.013 as the value for the roughness of the concrete (Chow, 1983).

Both the flow gauging and the collection of samples, described further below, were performed on the left and right shoulders of San Lorenzo street (Figure 5). This enabled studying the behavior of both supply areas separately and performing a comparative analysis.

An adequate adjustment of the model for extreme flows was achieved, as in the case of the precipitation on 20/11/2009. The adjustment for that event (Figure 6) was performed considering both watersheds working together, taking into account that during that event water depths exceeded the divide in San Lorenzo street.

For low flows, the model showed lower values than those from the gauges, as is the case

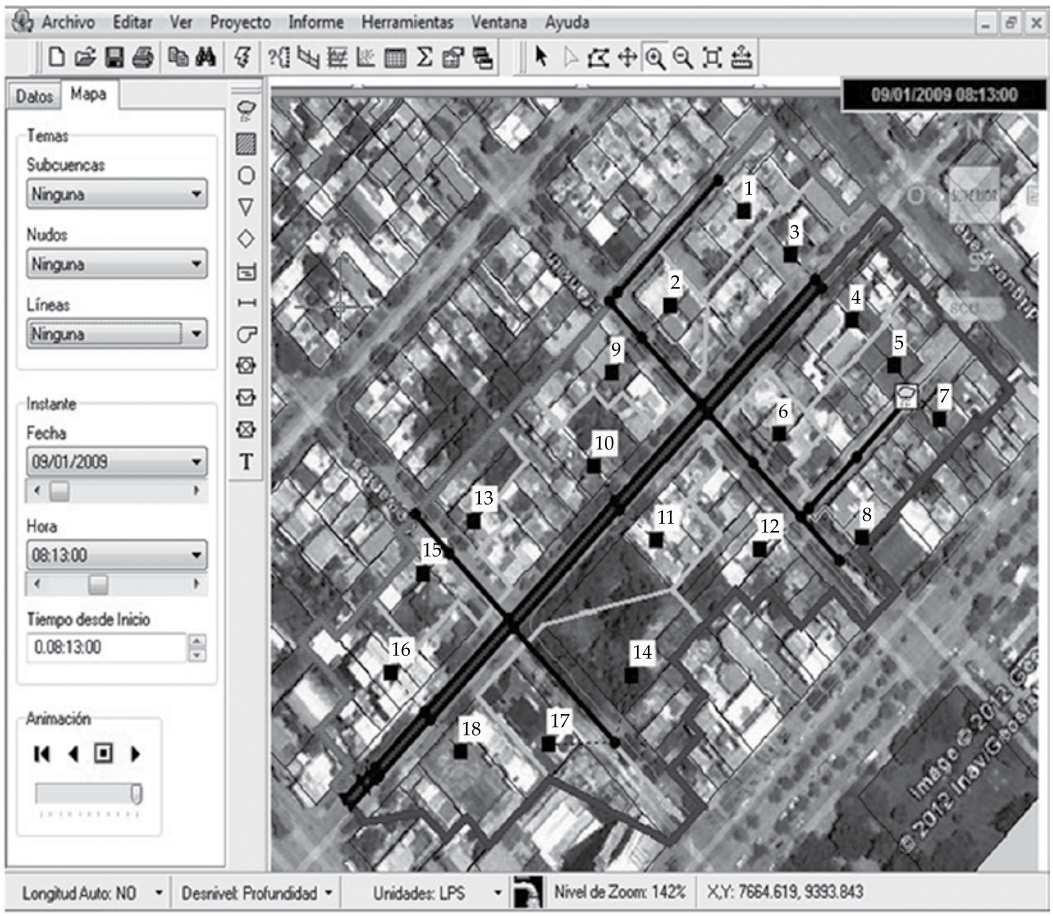

Figure 4. Model used to analyze the San Lorenzo street micro-watershed.

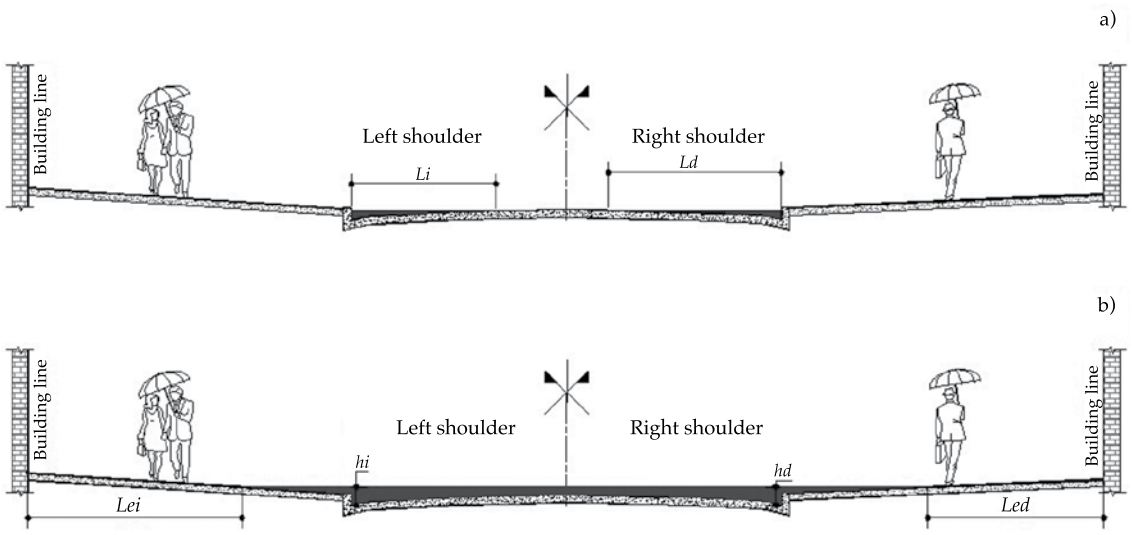

Figure 5. Measurments performed on San Lorenzo street: a) when the runoff remains in the gutter, b) when the runoff overflows the gutters.

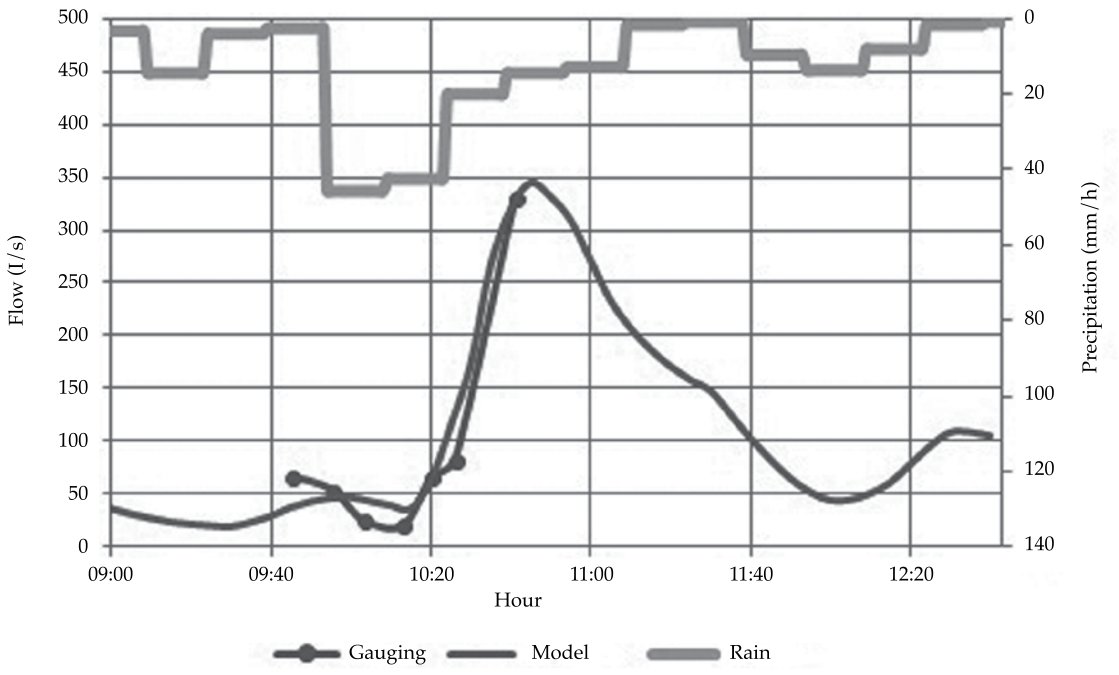

Figure 6. Hyetograph and hydrograph of the event on 20/11/2009.

for precipitation on 08/02/2010 (Figures 7 and 8). It is important to mention that liquid flow is imprecise for flows under 10 l/s, especially because of the variability in the width of the runoff in a section with very shallow water depth and notably sub-critical flow.

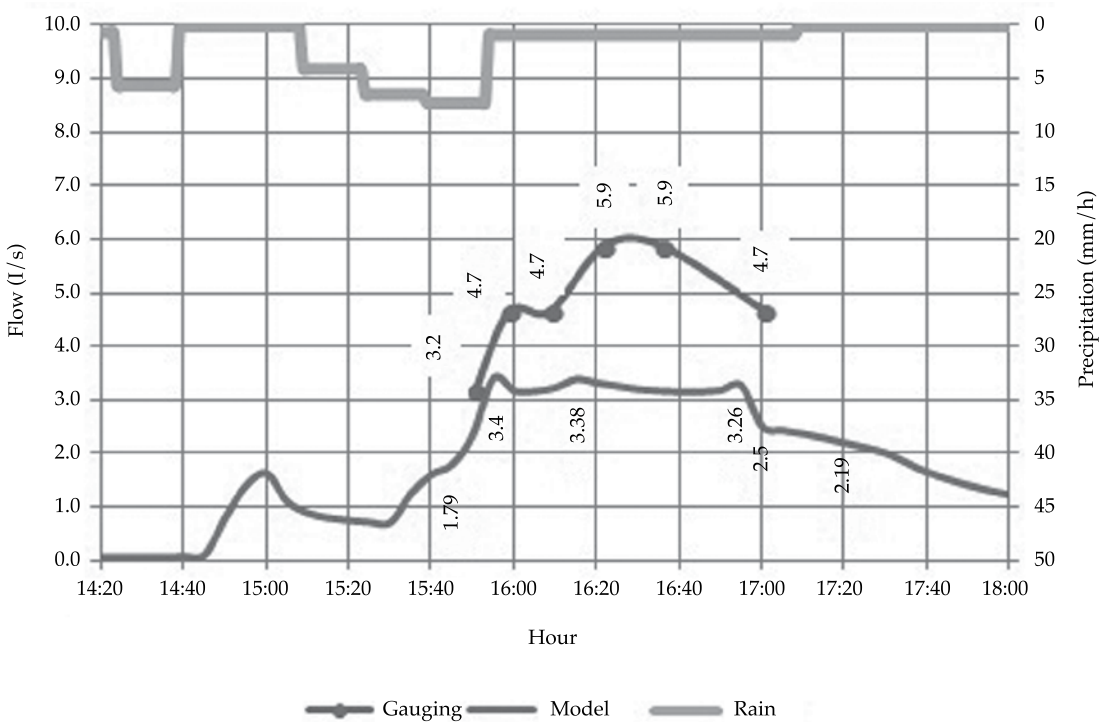

Figure 7. Hyetograph and hydrograph of the right shoulder of the watershed for the event on 08/02/2010.

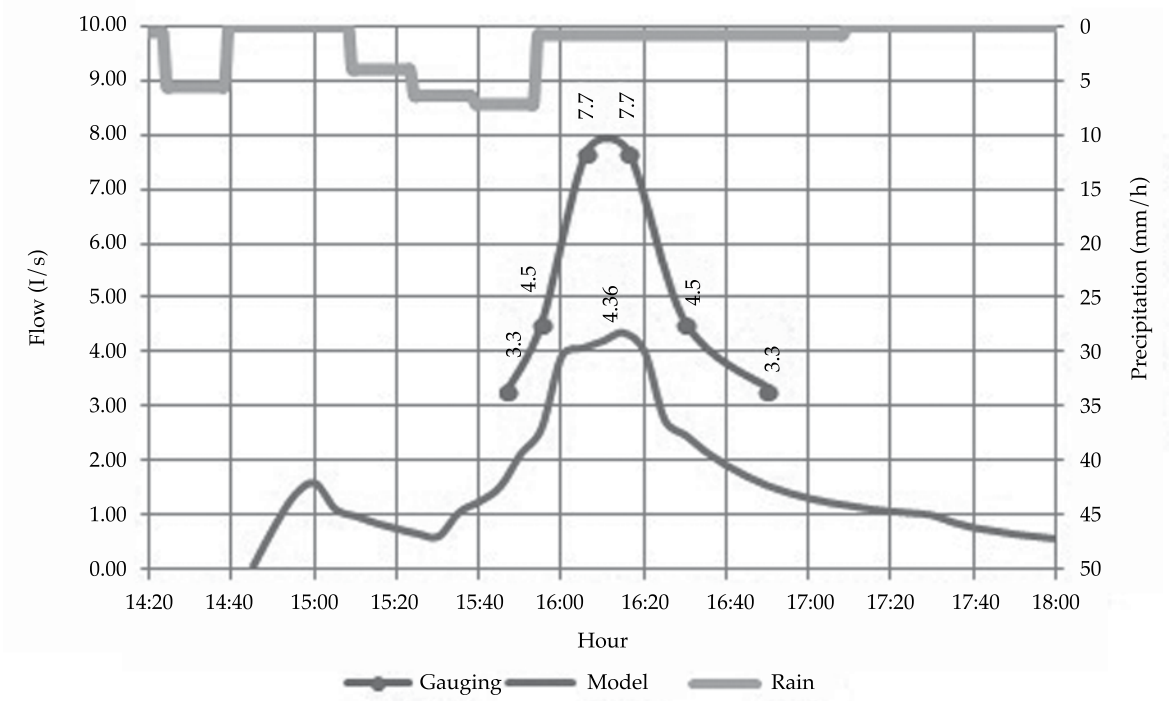

Figure 8. Hyetograph and hydrograph of the left shoulder of the watershed for the event on 08/02/2010.

Determination of Sediment Loads

The sediment load transported for each precipitation was obtained using two regression curves: one corresponding to the watershed on the left shoulder and the other to the one on the right shoulder. The predictive values used were liquid flow from runoff and 42-days antecedent precipitation.

The use of these variables is justified because the removal of pollutants in an urban watershed depends on the direct runoff volume, that is, effective precipitation. Therefore, the amount of possible pollutants transported during a rainfall depends on the runoff generated previously. Given the difficulty of obtaining effective precipitation and considering that the predictive variables must be easily measurable, total antecedent precipitation was used, which is directly related with the former.

In addition, for the micro-watershed studied, a good correlation was found between 42-days antecedent precipitation and the MCE of the events measured (Figure 9).

The mean concentration of the event can be obtained using equation (1) (Novotny, 1992):

$$MCE = \frac{\Sigma Qi \cdot Ci}{\sum Qi} \qquad (1)$$

where:

MCE: mean concentration of the event.
Qi: liquid flow.
Ci: concentration of suspended solids.

The linear relationship between the liquid flow and the solid is considered to reasonably represent the correlation of values, which coincides with Vanoni, 1975 (*apud* Huber y Dickinson, 1988).

The regression curves were fitted based on 89 samples of runoff water from the street, which were analyzed in the laboratory to determine the concentration of suspended solids.

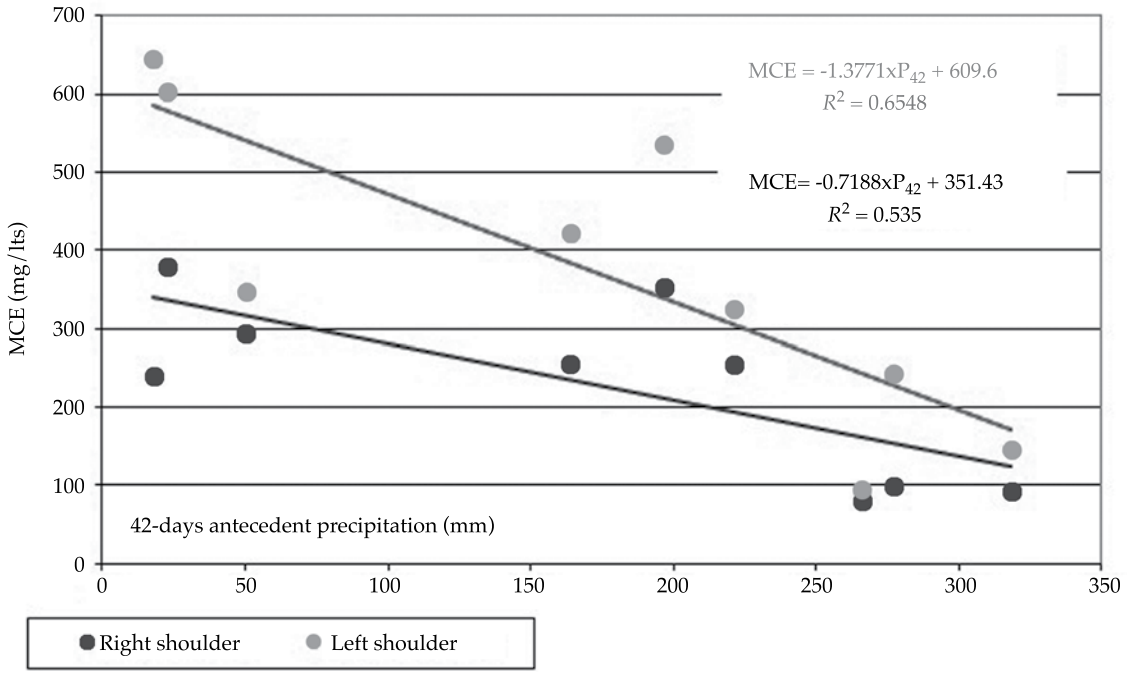

Figure 9. Variation in MCE with respect to 42-days antecedent precipitation.

The samples were collected manually using a DH3 collector developed by the UNNE Engineering School's Hydraulics Department Research Group specifically for monitoring urban rainwater. The collector was placed in position with the valves open so that neither the device nor the operator would interfere with the flow. At the appropriate moment, the valves closed instantaneously and the contents were put in plastic containers (Figure 10).

The field samples were processed in the laboratory to determine the total concentration of suspended sediments. To this end, 50 ml of each sample were filtered with dehydrated and pre-weighed 0.45 μm porous discs made of cellulose acetate using a vacuum pump. After filtering, the discs were placed in a stove at 105°C for one hour and dried until reaching constant weight. Lastly, the filters were weighed with a analytical precision scale (± 1 × 10^{-4} g). The amount of material retained was determined by the difference in weight and the calculation of the concentration was based on 1 liter.

The solid discharge was obtained according to the relationship between the liquid flows and the concentration of suspended solids (Mendez *et al.*, 2010). The regression curves were drawn for the watersheds on the left and right shoulders (equations (2) and (3), respectively):

$$Qs = 2.62 + 0.325 \cdot Q - 0.0163 \cdot P_{A42d} \quad (2)$$

$$Qs = 1.53 + 0.277 \cdot Q - 0.00758 \cdot P_{A42d} \quad (3)$$

where:

Qs: sediment load (g/l).
Q: liquid flow (l/s).
P_{A42d}: 42-days antecedent precipitation (mm).

Figure 10. Collection of samples with a DHL collector.

The fit shown by equations (2) and (3) was acceptable (R^2 equal to 95.5% and 99.1%, respectively) and the *p*-value of the different explanatory values indicates significance with a confidence interval of 95%, according to the available data.

Figures 11 and 12 show the regression curves (solid line) for different 42-days antecedent precipitations for the right and left watersheds, respectively, and the dots indicate the values obtained from the events measured.

The equations presented are considered valid for liquid flow volumes over 1 l/s. For lesser flows, the sediment load is virtually negligible.

Results

Annual Sediment Rate

With the precipitation and evaporation data, the liquid flows generated by the micro-watershed were obtained for the years 2007/08, 2008/09 and 2009/10. Later, based on regression curves (equations (2) and (3)), the sediment load (solid flow) transported by the urban runoff was determined for the entire analysis period (Figures 13, 14 and 15).

The results of the modeling indicate that the annual sediment loads transported by surface runoff in the left watershed were higher than those in the right. Nevertheless, the annual sediment rates, which relate the sediment load with the supply area, indicate slightly higher values for the right shoulder than for the left for the three years of analysis (Table 3). Therefore, it was concluded that runoff volumes strongly influence annual sediment loads, and the most impermeable areas can generate significant liquid flows, and therefore, higher sediment loads than permeable areas.

Antecedent Conditions

Figures 13, 14 and 15 show that the highest sediment loads are registered from September

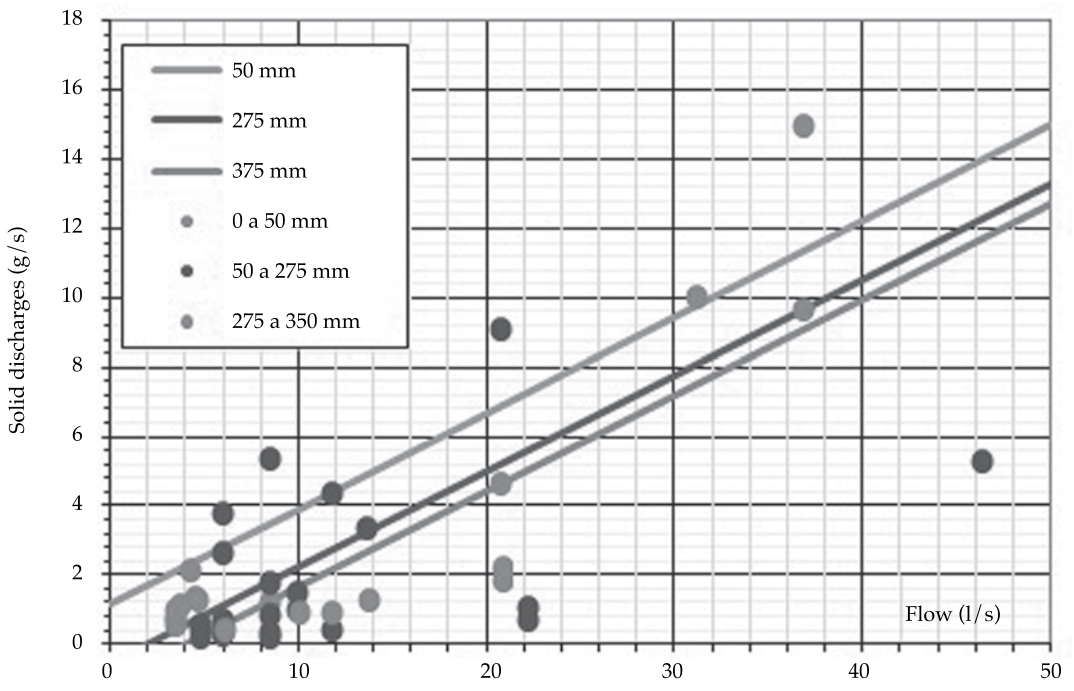

Figure 11. Regression curves for the right shoulder.

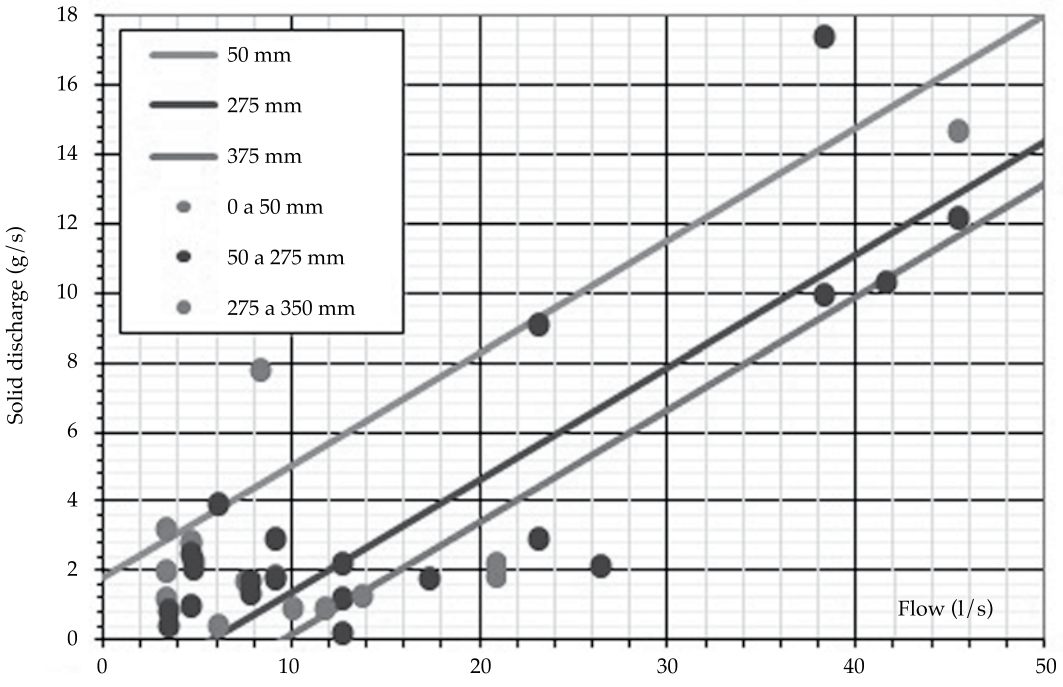

Figure 12. Regression curves for the left shoulder.

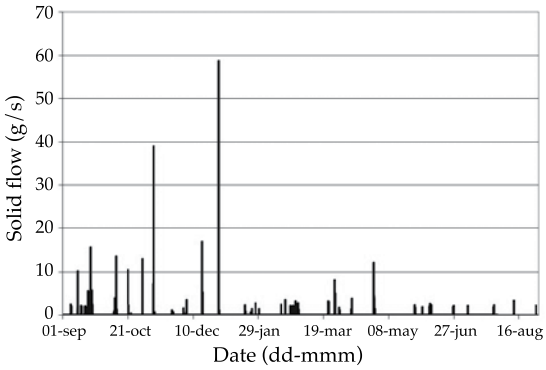

Figure 13a. Solid flows, right shoulder, 2007/08.

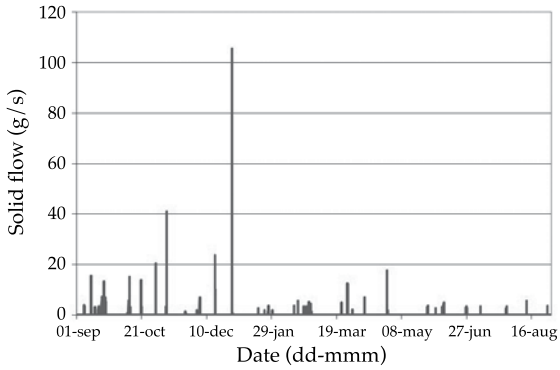

Figure 13b. Solid flows, left shoulder, 2007/08.

to December of each year. In effect, the rainy period is beginning during these months and, therefore, two conditions favoring the generation and transport of sediments exist —high liquid flow runoff and scarce antecedent precipitation. Figure 16 indicates the accumulated precipitation per four-month period during the analysis.

Thus, from September to December a wash of the watershed occurs, generating 60% of the sediment transported during the year (Table 4).

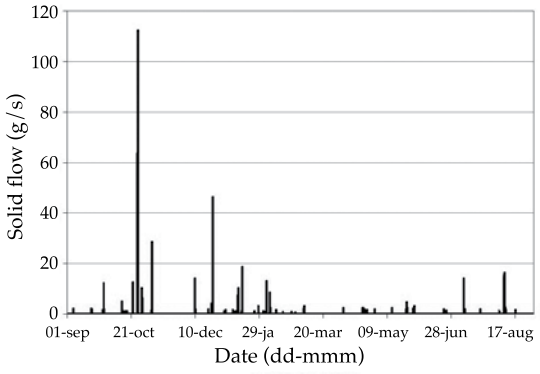

Figure 14a. Solid flows, right shoulder, 2008/09.

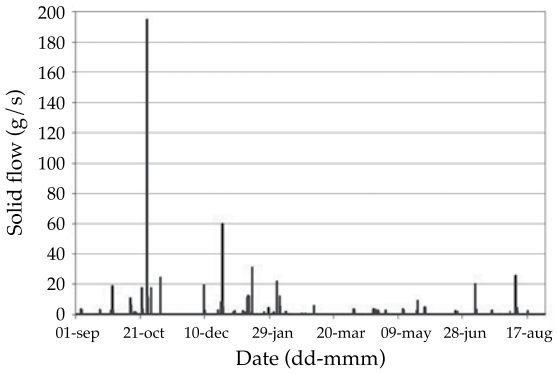

Figure 14b. Solid flows, left shoulder, 2008/09.

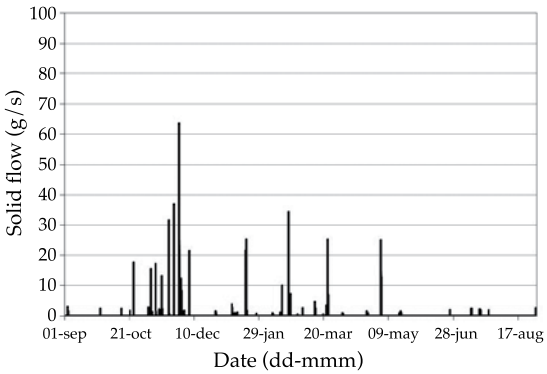

Figure 15a. Solid flows, right shoulder, 2009/10.

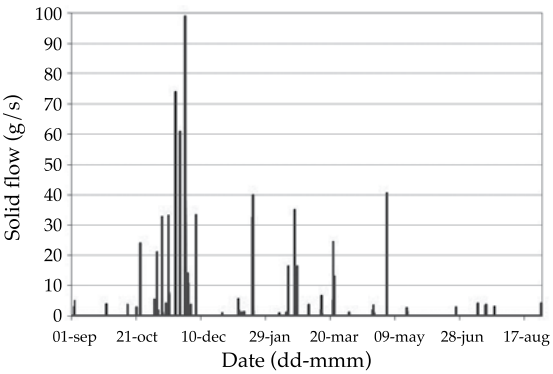

Figure 15b. Solid flows, left shoulder, 2009/10.

Table 3. Annual sediment load.

Shoulder	Area (ha)	Permeable area (%)	Annual sediment load			Sediment rates		
			2007/08 (t)	2008/09 (t)	2009/10 (t)	2007/08 (t/ha)	2008/09 (t/ha)	2009/10 (t/ha)
Right	2.02	**14**	1.75	2.26	2.98	0.86	1.12	1.47
Left	2.74	**17**	2.16	2.98	4.17	0.73	1.01	1.41
Total	4.76	**16**	3.91	5.24	7.16	0.78	1.05	1.43

Conclusions and Recommendations

Results from the solid sediment load were obtained for hydrological years 2007/08, 2008/09 and 2009/10 for a micro-watershed in the southern area of the city of Resistencia, using the SWMM model and regression curves of the relationship between liquid and solid discharge. Given the deficiencies of the hydrological model in predicting flows from low-intensity precipitation (less than 7.5 mm/h), differences are observed between the

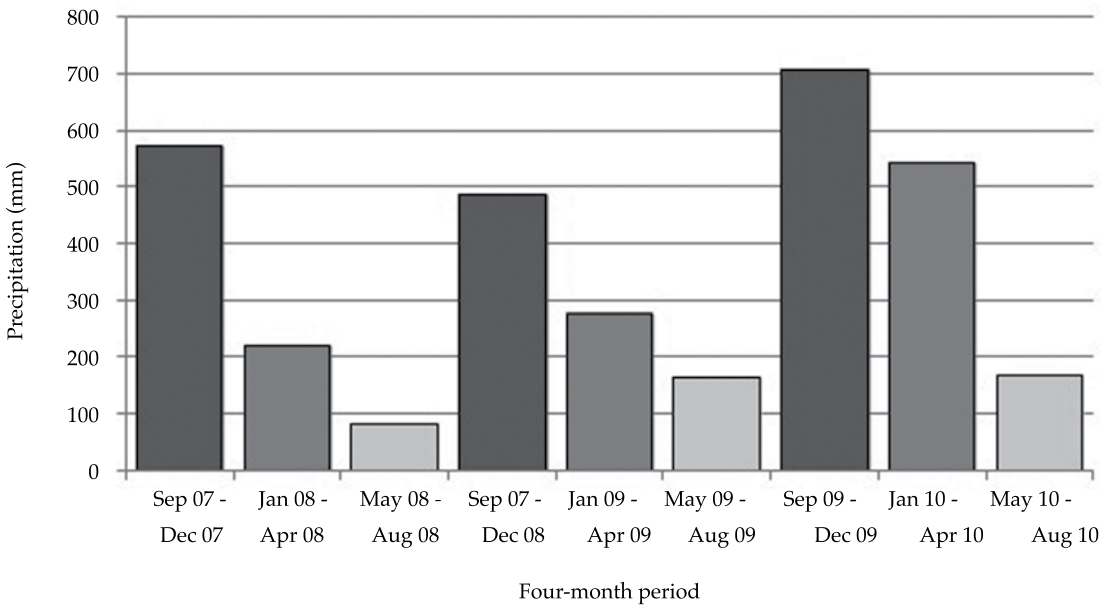

Figure 16. Accumulated Precipitation per four-month period.

Table 4. Percentage of sediment transported from September to December.

Year	Right	Left
2007/08	62%	66%
2008/09	58%	60%
2009/10	58%	55%

solid flow obtained using the methodology described and the data measured from the events. Although they are frequent, the latter do not affect the results pertaining to annual sediment loads. In effect, of the results of the modeling presented, the sediment loads generated by low-intensity rains represented 14 to 5% of the annual load. This indicates that the imprecision of these events is not relevant.

It is worth mentioning that the methodology presented was adjusted to conditions for residential use of the micro-watershed, without considering changes in land use produced by the construction of public works.

The annual sediment transport loads from surface runoff in the right watershed ranged from 1.75 for 2.26 t, and for the left from 2.16 to 4.17 tons. The annual sediment rates for both watersheds, which related the sediment load with the supply area, are similar for the three years of analysis, presenting values from 0.8 to 1.40 t/ha.

It is concluded that runoff volumes could affect annual sediment loads, and more impermeable areas can generate significant liquid flows and, therefore, higher sediment loads than permeable areas.

The largest sediment loads are registered from September to December of each year, a period during which 60% of the annual total is transported. It is worth highlighting that through runoff, one single event can transport more than 20% of the sediment transported for the entire year.

References

APA-AFIN (2001). *Línea de ribera de lagunas ubicadas en el sistema Hídrico del río Negro*. Informe final. Administración Provincial del Agua (APA)-Asociación de Apoyo a la Facultad de Ingeniería UNNE (AFIN). Resistencia (Chaco), Argentina.

Bruniard, E. D. (1981). *El clima de las planicies del norte argentino (Ensayo metodológico de geografía de los climas)*. Tesis de Doctorado en Geografía. Facultad de Humanidades de la Universidad Nacional del Nordeste. Resistencia (Chaco), Argentina.

Chow, V. T. (1983). *Hidráulica de canales abiertos* (584 pp.). México, DF: Editorial Diana.

CFI-AFIN (1995). *Estudio de los desagües pluviales del sector sur de Resistencia.* Argentina: Consejo Federal de Inversiones, Asociación de Apoyo a la Facultad de Ingeniería de la UNNE. Resistencia (Chaco), Argentina.

Depettris, C. A., Kutnich, E. J., & Ruberto, A. R. (2009). *Hidrología urbana: instrumentación y evaluación del escurrimiento superficial en una microcuenca de Resistencia*. Congreso Nacional del Agua, Trelew (Chubut), Argentina.

EPA (1983). *Results of the Nationwide Urban Runoff Program* (pp. 6-64). Vol. I. Enviromental Protection Agency. Washington D.C.

Garay-Porteros, H., & Alva-Hurtado, J. E. (1999). *Identificación y ensayo de suelos dispersivos*. XII Congreso Nacional de Ingeniería Civil, Lima, Perú.

Huber, W. C., & Dickinson, R. E. (1988). *Stormwater management model Version 4. User's Manual*. (313 pp.). Athens (GA), USA: EPA-600/3-88-001a.

INTA (1990). *Atlas de suelos de la República Argentina*. Buenos Aires: Instituto Nacional de Tecnología Agropecuaria, Secretaría de Industria, Ganadería y Producción.

Jiménez-Gallardo, B. R. (1999). *Contaminación por escorrentía urbana* (435 pp.). Madrid, España: Colegio de Caminos, Canales y Puertos.

Maksimovic, C. (2001). Urban drainage in specific climates, Francia: UNESCO – Technical Documents in Hydrology, Vol. I, N°40, 277 pp.

Mendez, G. J., Depettris, C. A., Orfeo, O., Ruberto A. R., & Pilar, J. V. (2010). *Curva clave de sedimentos de una microcuenca en Resistencia, Chaco, Argentina*. XXIV Congreso Latinoamericano de Hidráulica. Punta del Este, Uruguay.

Mendez, G. J., Ruberto, A. R., & Pilar, J. V. (2009). *Regionalización de precipitaciones para las provincias de Chaco, Formosa y Santiago del Estero*. XXII Congreso Nacional del Agua, Argentina. Trelew (Chubut), Argentina.

Mendez, G. J., Ruberto, A. R., Pilar, J. V., & Depettris, C. A. (mayo de 2011). Regionalización de Precipitaciones Máximas Acumuladas de 7, 15 y 30 días para las Provincias de Chaco y Formosa. *Revista ASAGAI, (26)*, 71-78.

Mendez, G. J. (2013). *Sedimentos en el drenaje urbano*. Tesis de Maestría en Ciencias la Ingeniería, Facultad de Ingeniería, Universidad Nacional del Nordeste. Resistencia (Chaco), Argentina.

Niemczynowicz, J. (1996). Challenges and Interactions in Water Future. *Environmental Research Forum Transtec Publications*, *34*, 1-10.

Novotny, V. (1991). *Urban diffuse pollution: Sources and abatement*. Water Environment & Technology. 3 (12), 60-65.

Orfeo, O. (1997). *Comparación sedimentológica y geomorfológica de los ríos Paraná y Paraguay en su área de confluencia*. Primer Congreso Latinoamericano de Sedimentología-VIII Congreso Geológico Venezolano, Sociedad Venezolana de Geólogos-International Association of Sedimentologists. Porlamar (Islta Margarita).

Poleto, C. (2008). *Ambiente sedimentos*. Porto Alegre, Brasil: Associacao Brasileira de Recursos Hídricos.

Porto, M. F. A. (2001). Urban Drainage in Specific Climates. In *Technical Documents in Hydrology* (pp. 103-124). Vol. I, No. 40, Cap 4. Paris, Francia: UNESCO.

Ramos, C. (1995). *Drenagem Urbana* (pp. 249-250). Cap. 6. Porto Alegre, Brasil: Editora de la UFRGS.

Segemar (1997). *Mapa geológico de la República Argentina*. Buenos Aires: Instituto de Geología y Recursos Minerales, Servicio Geológico Minero Argentino.

Subsecretaría de Recursos Hídricos de la Nación Argentina (2009). *Criterios conceptuales propuestos para la integración, articulación y actualización tendientes al completamiento y desarrollo del Plan Director Básico de Drenaje Pluvial de La Cuenca del Río Matanza-Riachuelo* (78 pp.). Ciudad Autónoma de Buenos Aires, Argentina: Ministerio De Planificación Federal, Inversión Pública y Servicios de la Nación - Secretaría de Obras Públicas.

Vanoni, V. A. (1975). *Sedimentation Engineering* (418 pp.). New York, Estados Unidos: ASCE.

Institutional Address of the Authors

Mg. Ing. Guillermo José Mendez
Mg. Ing. Carlos Alberto Depettris
Dr. Jorge Víctor Pilar
Ing. Alejandro Ricardo Ruberto

Grupo de Investigación del Departamento de Hidráulica
Facultad de Ingeniería
Universidad Nacional del Nordeste
Av. Las Heras 727 (CPA H3500COI)
Resistencia, Argentina
Teléfono +37 (22) 427 006, interno 142
guillermojosemendez@hotmail.com
cdepettris@ing.unne.edu.ar
aruberto@ing.unne.edu.ar
jpilar@ing.unne.edu.ar

Dr. Oscar Orfeo

Vicedirector
Centro de Ecología Aplicada del Litoral
Ruta Provincial núm. 5, km 2.5
3400, Corrientes, Argentina
Teléfono: +54 (379) 4454 417
oscar_orfeo@hotmail.com

Click here to write the autor

Estimation of Storm Potential by Combining Satellite Images and Meteorological Data: A Case Study in Northwestern Mexico

• Fabiola Arellano-Lara* • Carlos Escalante-Sandoval •
Universidad Nacional Autónoma de México
*Corresponding Author

Abstract

Arellano-Lara, F., & Escalante-Sandoval, C. (September-October, 2014). Estimation of Storm Potential by Combining Satellite Images and Meteorological Data: A Case Study in Northwestern Mexico. *Water Technology and Sciences* (in Spanish), 5(5), 37-58.

Mexico frequently experiences floods due to storms generated by Mesoscale convective systems. It is therefore very important to determine their characteristics in order to estimate in advance the amount of rain they will produce. This work presents a methodology to estimate potential storms based on their previous patterns by combining measured surface data and information interpreted from satellite images. This study was conducted in a region in northwestern Mexico. The results showed that meteorological information can be effectively used in isolation to estimate potential storms 12 hours in advance.

Keywords: Convective storms, satellite images, estimate of storm potentiality.

Resumen

Arellano-Lara, F., & Escalante-Sandoval, C. (septiembre-octubre, 2014). Estimación del potencial de tormentas vía la combinación de imágenes satelitales e información meteorológica: caso de estudio al noroeste de México. Tecnología y Ciencias del Agua, *5(5), 37-58.*

México sufre frecuentes inundaciones provocadas por tormentas generadas por los sistemas convectivos de mesoescala, por lo que es importante realizar su caracterización, a fin de estimar con cierto tiempo de antelación la cantidad de lluvia que producirán. Este trabajo presenta una metodología para la estimación del potencial de tormentas basada en el empleo de patrones antecedentes de éstas, obtenidos al acoplar datos medidos en superficie e información interpretada de imágenes de satélite, la cual fue aplicada a una región del noroeste de México. Los resultados mostraron que la información meteorológica puede ser empleada de manera aislada y eficiente en la estimación del potencial de tormentas con una anticipación de 12 horas.

Palabras clave: *tormentas convectivas, imágenes de satélite, estimación potencial de tormentas.*

Received: 19/10/12
Accepted: 13/02/14

Introduction

A large variety of climates and hydrometeorological conditions exist in Mexico, which often lead to extreme storms and flooding with resulting damages to the population. In general, coastal regions are most affected by this type of phenomenon.

Most of the highly dangerous storms in Mexico are caused by mesoscale convective systems (MCS), defined as a special type of cloud structure with large spatial coverage (100 km or more in just one direction).

For the purpose of preventive and mitigation measures against the effects of these extreme rains, the phenomenon needs to be characterized in order to estimate, in advance, the amount of rain that could be generated.

To effectively estimate rainfall for the prediction of runoff, the spatial and temporal distribution of the rainfall must be accurately measured. The use of rainfall data recorded

by rain gauge networks or meteorological radars alone cannot completely observe the evolution and magnitude of convective storms because of the spatial coverage of the phenomenon. Alternatives used to address this condition have included the use of satellite images or a combination of data from radar, land measurements and atmospheric models (Moses & Barret, 1986; Clark & Morris, 1986; Creutin, Lacomba, & Obled, 1986; Milford, Dugdale, & McDougall, 1994; Carn, 1994; Hubert & Toma, 1994; Laurent, 1994; Touré & N'Diaye, 1994; Ravelo & Santa, 2000; Rojas & Eche, 2005; Feidas *et al*., 2005; Feidas *et al*., 2008; Sawunyama & Hughes, 2008).

This work presents a methodology to estimate storm potential based on the use of patterns prior to its occurrence, obtained from coupling measured surface data and information interpreted from satellite images.

Study Zone

The analysis was performed in northwestern Mexico, which includes the states of Chihuahua, Durango, Sonora and Sinaloa. This area is characterized by its large hydrological spatial-temporal variability (Figure 1).

The state of Chihuahua is located in the center of northern Mexico covering an area of 247 455 km^2. It is distributed across 67 municipalities and has a population of 3 640 000 inhabitants. The territory of Chihuahua belongs to two large physiographical provinces which divide the state in half —basins and mountains in the east and the Sierra Madre Occidental in the west. The hydrological resources in Chihuahua are supplied by a mean annual precipitation of 470 mm. The hydrological potential of the state includes the tributaries of the Yaqui, Mayo, Fuerte and Sinaloa rivers, which feed

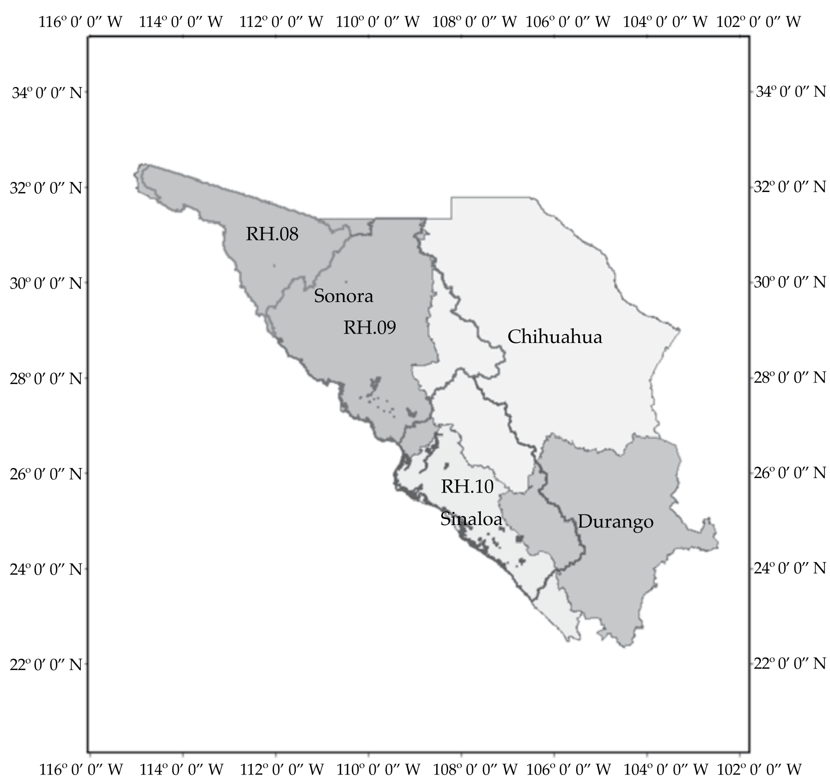

Figure 1. Location of study area.

the watersheds, providing Sonora and Sinaloa with their agricultural richness. Nevertheless, the velocity and entrenchment of the river prevent local use. Water is also usable from the Conchos River (which begins in the foothills of the Sierra Tarahumara) and from the interior watershed —including Casas Grandes, Santa Maria and Carmen, which flow into a lagoon with little storage because of leakage and rapid evaporation. The predominant climates in the state are very dry-temperate (26%), semi-dry temperate (16%) and very dry semi-warm (15%). While the presence of extreme hydrometeorological events can contribute to increasing storage in dams and lakes, they can also cause harm to the population and damage infrastructure, services and productive systems. Flooding in 1990 in the state caused the death of 200 persons and resulted in 2.5 million dollars in economic damages. Hurricane Iris in 2001 caused losses valued at 14.9 million dollars, and extreme events in 2006 resulted in losses of 163.8 million (Cenapred, 2013).

The state of Durango borders two of the states in the study region —Chihuahua and Sinaloa. The area measures 123 181 km^2 and it is divided into 39 municipalities with a population of 1 730 000 inhabitants. The average altitude is 1 775 masl and the physical features of the state are defined according to four physiographic provinces: Sierra Madre Occidental, mountains and plains in the north, Sierra Madre Oriental and the central plateau. The hydrography is represented by the main rivers: Nazas, Aguanaval, Baluarte, Mezquital, Acaponeta, Tepehuanes, Ojo Caliente and Tamazula. Several dams are located on these rivers, which are all used for irrigation and fishing, including Francisco Zarco, Lázaro Cárdenas (El Palmito), Peña de Águila, San Bartoleo and Guadalupe Victoria. The climates in Durango can range from semitropical, with generally high temperatures, to very dry in the eastern portion of the state. The occurrence of torrential rains in the state has resulted in loss of lives and economic damages which have increased over time. The event in September 2000 caused economic losses of roughly 620 000 dollars, and 800 000 dollars of losses resulted from the events of 2002, with 20 000 persons affected and 4 000 homes damaged. Although damages in 2006 were only 8 000 dollars, 12 people lost their lives. Finally, in August 2008, the rains caused losses of 32.1 million dollars (Cenapred, 2013).

The state of Sinaloa is located in the northwestern region of the Mexican republic. It is bordered on the north by the states of Sonora and Chihuahua, on the east by Durango, on the south by Nayarit, and on the west by the Pacific Ocean and the Gulf of California. It has an area of 58 092 km^2 and a population of 2 950 000 in 18 municipalities. The orographic system of Sinaloa consists of a set of mountain units that extend out from the Sierra Madre Occidental, entering the state through the municipalities bordering the states of Nayarit, Durango, Chihuahua and Sonora. Most of Sinaloa is made up of flat terrain, and the remaining is part of a small mountainous region. Roughly 80% of the land in the state is under 600 masl and over half of the territory is under 150 masl, resulting in a mean elevation of 344 masl. Less than 1% of the state exceeds an altitude of 1 820 meters. Eleven rivers supply water to the dams, which generate electric energy and make up the main irrigation infrastructure, leading to the development of the best technological agriculture in the country. The predominant climates in the state are warm sub-humid with summer rains (36%), very hot semi-dry (21%) and dry very warm (18%). Two very significant hydrometeorological events have occurred in the state. The first was in the year 2002 when flooding caused the loss of 20 000 ha of crops valued at over 5.5 million dollars. In 2006, the economic losses were estimated at 163.8 million dollars and six deaths occurred (Cenapred, 2013).

The state of Sonora is located in the northwest most portion of the country. It measures 184 934 km^2 and has a population of 2 850 000, as of the year 2013. It is divided into 72 municipalities. The orography is made up hills

and flat areas, and mountains to a lesser extent. The main rivers in the state are the Colorado, Concepción, San Ignacio, Sonora, Mátepe, Yaqui and the Mayo. There are also some large dams, such as Álvaro Obregón, Adolfo Ruiz Cortines, Plutarco Elías Calles, Abelardo Rodríguez and Lázaro Cárdenas. The climate is dry and semi-dry in 90% of the state and, in general, there is little water availability and overexploitation of the aquifers is common. Of the four states in the study area, Sonora is most adversely affected by extreme hydrometeorological phenomena. In October of 2000, the presence of hurricane Keith affected one-fifth of the area of the state and caused over 5.2 million dollars in damages. In the year 2001, hurricane Juliette caused the death of seven people and affected 16 365 inhabitants, with damage to 15 344 homes and 44 210 km of roads, for a total loss of 72.4 million dollars. In 2006, 14 people were killed and roughly 72 000 dollars in damage resulted. In 2008, tropical storms from September to October had an economic impact of 33.5 million dollars. Lastly, in the year 2009, hurricane Jimena caused losses of 78.8 million dollars (Cenapred, 2013).

Added to the social an economic affects resulting over the last 10 years are those which occurred in September 2013 from the simultaneous presence of hurricane Ingrid and tropical storm Manuel.

Damages associated with flooding have increased significantly due, in part, to precarious human settlements located near rivers which do not respect land planning and, primarily, due to the process of deforestation of the upper basins, whose effect is reflected in an increase in surface runoff and the transport of soil and sediment to the plains.

Structural and non-structural measures must be adopted to reduce damage from floods. This work addresses the latter for the purpose of providing a tool that, 12 hours prior to the event, can establish the magnitude of rainfall that is likely to occur at a certain site so that civil protection authorities can generate response mechanisms to protect the lives and property of the inhabitants.

Materials and Methods

The monsoon season in the study area is directly associated with the occurrence of severe storms produced by the combination of diverse factors, such as unstable atmospheric conditions, the topography of the orographic barrier created by the Sierra Madre Occidental, and different types of climates in the area.

Since the information available from the satellite images used for the study included the years 2004 to 2006, the two types of data were coupled based on this time period. Next, the different analyses performed and the coupling of storm data will be described.

Databases were created based on records from Automatic Weather Stations (AWS) in order to obtain the meteorological conditions prior to the occurrence of moderate ($10 < Hp$ (mm) < 20) and strong ($20 < Hp$ (mm) < 50) storms. Since the greatest accumulation of precipitation in the region occurs in July (Figure 2), only rainfalls available for this month during the period 1999-2006 were included.

The measuring stations used in the mountainous region of the state of Chihuahua are listed in Table 1 (Figure 3).

The information collected for each storm corresponds to the prevalent climate conditions 12 hours prior to the occurrence of the event and four hours after. The variables considered are: wind direction (Dir), direction of wind gusts (WSMDir), wind speed (WSK), speed of wind gusts (WSMK), temperature (Temp), relative humidity (HR), precipitation, barometric pressure (BP) and solar radiation (RS).

The information was processed according to hourly averages of the variables recorded, except for precipitation, for which the records were accumulated. With this information, the behavior curves over time were obtained for each variable associated with the ranges of the storms in question, the month and the study site. In turn, these evolution curves made it possible to identify the variables with the most significant patterns for the purpose of coupling with the information from satellite images. A

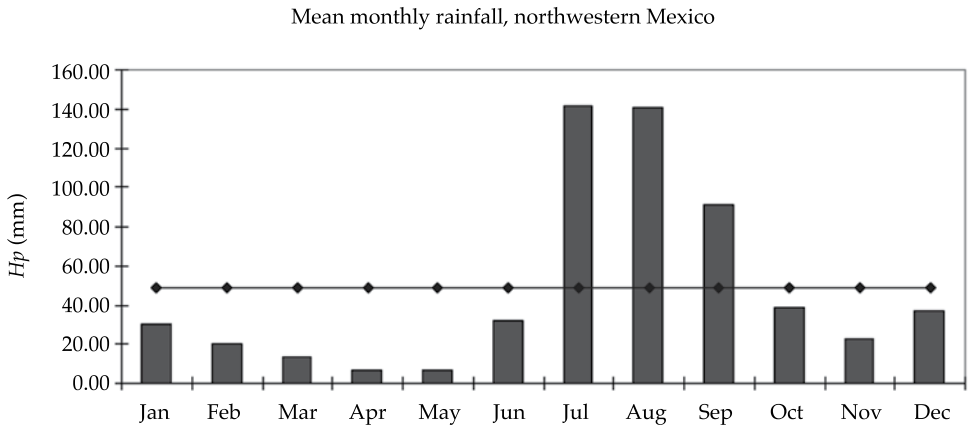

Figure 2. Distribution of monthly rainfall in the study area.

Table 1. General characteristics of the AWS in the study area.

Estate	Name	Starting data	Latitude	Longitude	Altitude (m)
Chihuahua	Basesachi	07-may-99	28° 11′ 57″	108° 12′ 32″	1 973
	Chinatú	04-jun-99	26° 13′ 46″	106° 46′ 14″	1 982
	Chinipas	24-may-99	27° 23′ 34″	108° 32′ 11″	431
	Guachochi	31-may-99	26° 48′ 49″	107° 04′ 23″	2 390
	Maguarichi	10-jun-99	27° 51′ 30″	107° 59′ 40″	1 663
	Urique	15-apr-99	27° 12′ 56″	107° 55′ 1″	577

total of 105 moderate storms and 44 strong storms were used, distributed according to Table 2.

Based on the collected and processed information, those variables were selected that presented the most observable average behaviors (mountainous region) over a time period of 12 hours prior to the occurrence of the rainfall. These variables are temperature and relative humidity. The correlation coefficients for all the variables mentioned were evaluated according to range of storm, and the highest values had a correlation between temperature and relative humidity of -0.996 and -0.988 for moderate and strong storms, respectively. This can be observed in Tables 3 and 4. Thus the average surface temperature was selected for coupling with temperatures interpreted from satellite images, so as to use the same type of variable to ensure the most certainty.

In addition, most of the variables presented sensitive differences between the ranges of storms (moderate and strong), except for barometric pressure which did not vary. Wind direction (Dir) did not present an evident pattern before the rainfall in the cases mentioned, which was contrary to the rest of the variables.

Given these results, the analysis proceeded to coupling the average surface temperatures with those obtained from satellite images in order to study the cases previously identified for this purpose.

To study the storms based on brightness temperatures obtained from satellite images, those registered on land during 2004-2006 were identified, a timeframe for which satellite images are available.

The satellite images were provided by the Mexico National Weather Service (NWS). The

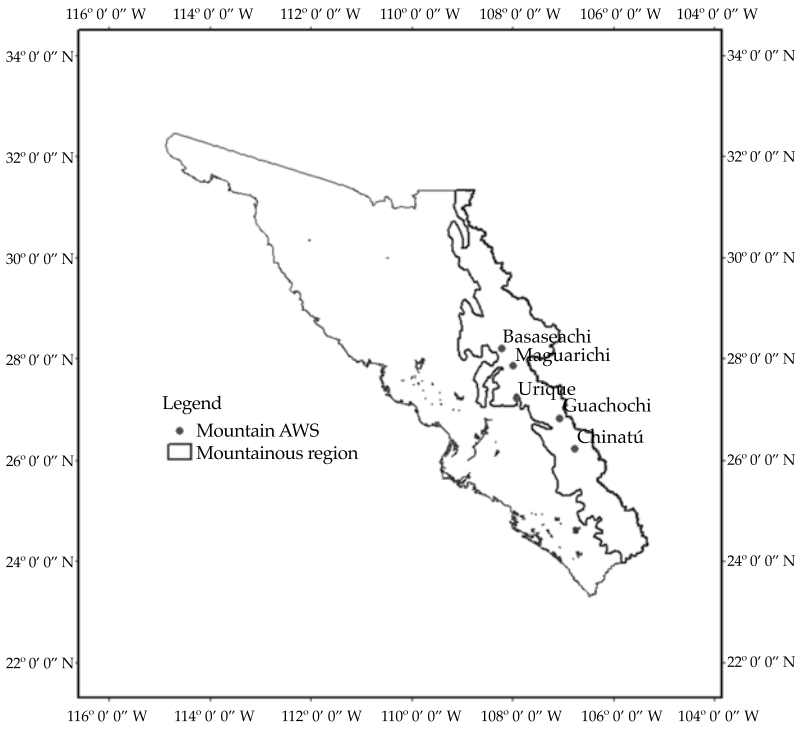

Figure 3. Location of the AWS in the mountainous region analyzed.

images used corresponded to the 10.7 μm band (channel 4) infrared (IR) spectrum, obtained from GOES-11 and GOES-12 satellites which observe the Mexican territory.

In general, the processing of the IR images consisted of transforming the pixel values of the images (0 to 255) into brightness temperatures in °C. The NOAA Standard Curve (NOAA, 1975; Weinreb *et al*., 1997) was used to estimate the temperature of cold clouds. This formula was developed specifically for IR images from GOES satellites, in 8-bit format (NASA, 2005).

The brightness temperatures obtained with this and other procedures are used to infer precipitation based on diverse indirect techniques involving infrared data. According to Barret and Martin (1981), the techniques to estimate rainfall based on infrared and visible data include cloud indexing, life history, bispectral methods and cloud modeling techniques. In addition, methods using infrared data and the combination of visible and infrared include Barret (1970); Arkin (1979); Dittberner and Vonder Haar (1973); Lovejoy and Austin (1979); Tsonis and Isaac (1985), Stout, Martin and Sikdar (1979); Griffith-Woodley Technique (Griffith *et al*., 1976); Gruber (1973); Wylie (1979); Técnica Convectiva-Estratiforme by Adler and Negri (1988), and Scofield and Oliver (1977).

The NOAA brightness temperature conversion equations consider -32°C as the

Table 2. Mountain storms used for the antecedent climate surface analysis.

AWS	Moderate storms	Strong storms
Basesachi	19	10
Chinatú	21	9
Guachochi	23	10
Maguarichi	22	6
Urique	20	9
Total	**105**	**44**

Table 3. Correlation coefficients among meteorological surface values maesured for moderate storms.

	Dir_10	WSK_10	Tmont_10	HR_10	BP_10	SR_10
Dir_10	1	0.156	-0.158	0.214	-0.081	-0.409
WSK_10		1	0.758	-0.729	-0.854	0.517
Tmont_10			1	**-0.996**	-0.82	0.929
RH_10				1	0.82	-0.941
BP_10					1	-0.6
SR_10						1

Table 4. Correlation coefficients among meteorological surface values maesured for strong storms.

	Dir_20	WSK_20	Tmont_20	RH_20	BP_20	SR_20
Dir_20	1	0.026	-0.143	0.192	-0.244	-0.454
WSK_20		1	0.7	-0.679	-0.836	0.493
Tmont_20			1	**-0.988**	-0.857	0.896
RH_20				1	0.839	-0.925
BP_20					1	-0.599
SR_20						1

initial temperature threshold for cold clouds. These conversions make clouds and other cold bodies in an image appear in shades of white, while warm bodies such as land are shown in dark shades. Thus, the images in IR channels are transformed into images in visible channels. The expressions for the transformation of the pixel value to brightness temperature are:

Cold clouds: if $B > 176$, then $T = 418 - B$

Warm clouds: if $B <= 176$, then $T = 330 - (B/2)$

Where B is the pixel value.

According to the literature, different thresholds have been established for the temperatures of cold clouds according to different latitudes and types of satellites. Therefore, equations for the transformation to brightness temperatures vary. The study area is located in North America, which enables applying the formulas mentioned without modifications. Sets of images every 15 minutes were used, consisting of 12-hours prior to and 4-hours after the occurrence of rainfall for the range of moderate and strong storms. Tables 5 and 6 list the moderate and strong storms, named by a code made up of the date and beginning and ending hour of the rainfall.

The area covered by all of the IR images analyzed corresponds to the mountainous region in particular. The data pertaining to the study area mentioned were extracted from each of the IR images. The compressed original format (brightness values of pixels in .PCX format) of the IR satellite images were processed into spatial raster format (thermal maps) with temperature values in °C. To facilitate the management of the images, each one was assigned NAD 27 system coordinates. The thermal maps which were originally in intervals of 15 minutes were converted into intervals of hours to enable coupling with surface information analyzed by hour.

The nature of the surface data, that is, the hourly temperature series, determined the discretization of the thermal maps into concrete statistical data, that is, a series of average, maximum and minimum hourly temperature values for the study area, referred to as satellite series. After unifying the surface and satellite temperature time series, they were compared based on the temporal evolution of the average patterns and the correlation

Table 5. List of moderate storms used in the analysis.

Number	Date and hour of storm	Rainfall (mm)
1	01/07/2004 23:10 - 23:50	10.66
2	07/07/2004 21:00 - 21:30	11.42
3	08/07/2005 21:30 - 22:00	18.04
4	08/07/2006 00:00 - 00:30	14.48
5	08/07/2006 20:50 - 21:20	12.2
6	14/07/2006 00:00 - 00:40	19.55
7	22/07/2005 17:50 - 18:30	15.49
8	24/07/2004 00:10 - 01:00	11.68
9	24/07/2005 01:20 - 02:10	19.3
10	28/07/2004 23:10 - 23:50	11.94

Table 6. List of strong storms used in the analysis.

Number	Date and hour of storm	Rainfall (mm)
1	02/07/2004 22:00 - 22:50	32.76
2	03/07/2005 21:00 - 21:40	20.07
3	04/07/2004 20:10 - 21:30	20.05
4	04/07/2006 22:20 - 23:20	23.11
5	05/07/2006 02:20 - 03:00	22.86
6	09/07/2006 01:20 - 02:00	26.66
7	20/07/2004 20:20 - 20:50	21.33
8	22/07/2004 04:00 - 04:40	20.58
9	22/07/2004 21:40 - 22:10	21.33
10	27/07/2005 22:10 - 22:50	22.11

between variables for the range of storms, from moderate to strong. The correlation coefficients between surface data and the satellite series for both ranges of storms were thereby obtained. The temporal evolution of the satellite and surface temperature series, for each range of storms analyzed, is shown in Figures 4 and 5, where PromT_Mont_10,20 = average surface temperature, moderate/strong storms Med_min/max/med = average minimum brightness, maximums and averages associated with moderate/strong storms.

The highest correlation coefficients for both types of storms corresponded to maximum satellite temperatures obtained from thermal maps. This is evident in the respective curves shown in Figures 4 and 5. The results of the correlation coefficients are presented in Table 7.

The differences in the patterns of the temperature classes among types of storm is barely noticeable due to the large spatial coverage of the analysis corresponding to the entire mountainous region. Nevertheless, the high correlation identified between surface and satellite temperatures over a 12-hour period prior to rainfall supported the later analysis of coupling temperatures from the regions of influence surrounding the automated weather stations located in the mountainous region, including Basesachi, Chinatú, Guachochi, Maguarichi and Urique.

Based on the above results, information was extracted from IR images for the same groups of storms in the study (moderate and strong), according to each one of the previously mentioned AWS's regions of influence. These are described herein as partial zones and were delimited according to the following criteria: eastern and western borders of each of the partial zones corresponding to the eastern and western boundaries of the mountainous region; transverse boundaries between each AWS are roughly perpendicular to the coast, at the midway point between the AWS. In the cases of the stations on the far ends (Baseseachi and Chinatú), the AWS are located at the halfway point inside the partial zone, between the outer boundaries and the inner

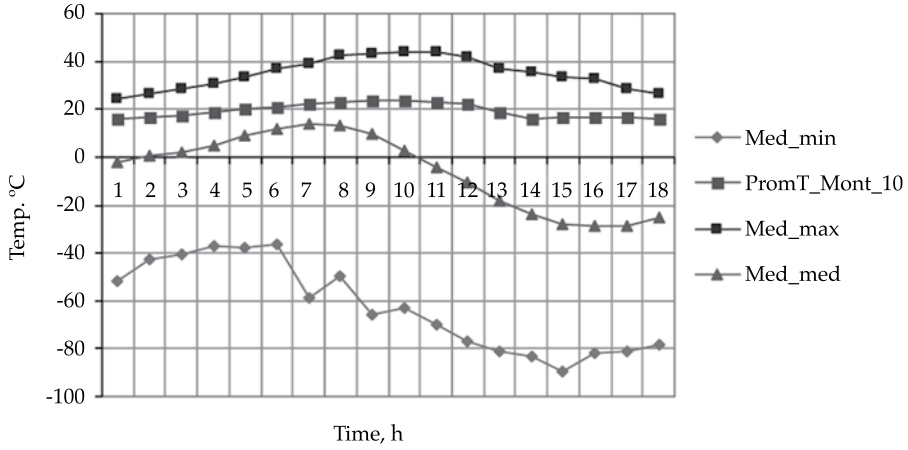

Figure 4. Average temperature curves, moderate storms.

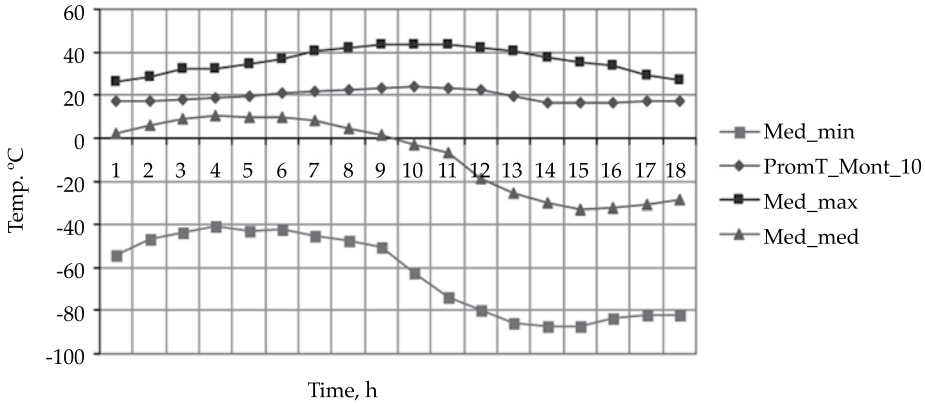

Figure 5. Average temperature curves, strong storms.

Table 7. Correlation coefficients between surface and satellite, 12 hours prior to precipitation.

Temperature	Moderate storms	Maximum storms
Minimum	-0.652	-0.53
Intermediate	0.178	-0.542
Maximum	0.984	0.989

boundaries transverse to the mountain zone. These conditions are indiscriminate, since the purpose of this second test was to obtain a better spread between temperature classes, subject to areas of influence associated with the land stations. The distribution of the regions is shown in Figure 6.

Strong storms (20-50 range), mountainous region

The analyses described were conducted in the mountainous regions to obtain a set of partial thermal maps associated with the storm cases measured on land. Surface conditions were also determined. The following was found by analyzing the correlation coefficients

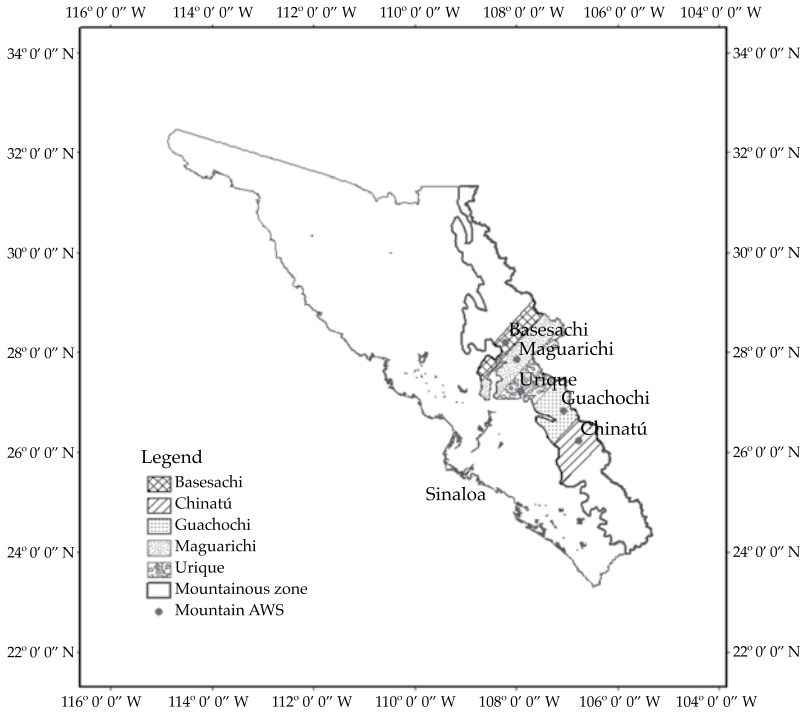

Figure 6. Coverge of partial regions in the mountainous region.

between the surface temperature series and the brightness temperature series (maximums, minimums and average) obtained from the infrared images, both associated with the samples of strong storms corresponding to 12 hours prior to rainfall in the mountainous region:

1. According to the coefficients for the correlation between minimum brightness temperatures (coldest) and average surface temperatures, only four of the storms presented values between ± 0.6 and 1.0, that is, there is a close relationship among these temperatures in only 40% of the samples, but not significant for the analysis, as observed in Figure 7a. The average correlation value for the four storms is -0.821.
2. In terms of the *r* coefficients for maximum brightness temperatures (warmest) and average surface temperature, 80% of the storms in the sample had values between ± 0.6 and 1. This behavior is very important and indicates a strong relationship between the values, as observed in Figure 7b. The average correlation value for the eight storms is 0.835.
3. Forty percent of the storms in the sample presented values ranging from ± 0.6 and 1 for mean brightness temperatures and average surface temperatures, indicating the lack of a good relationship between these variables, as observed in Figure 7c. The average correlation value for the four storms is -0.772.

From these observations, the relationship between average surface temperatures and the corresponding maximum brightness temperatures was found to be the most representative. Nevertheless, no notable difference was found between the correlation coefficients pertaining to the mountainous

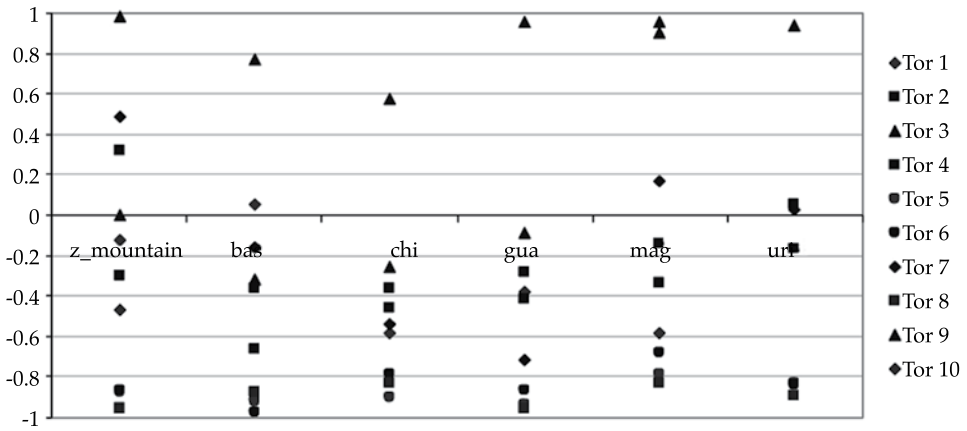

a) Surface T / Minimum brightness T

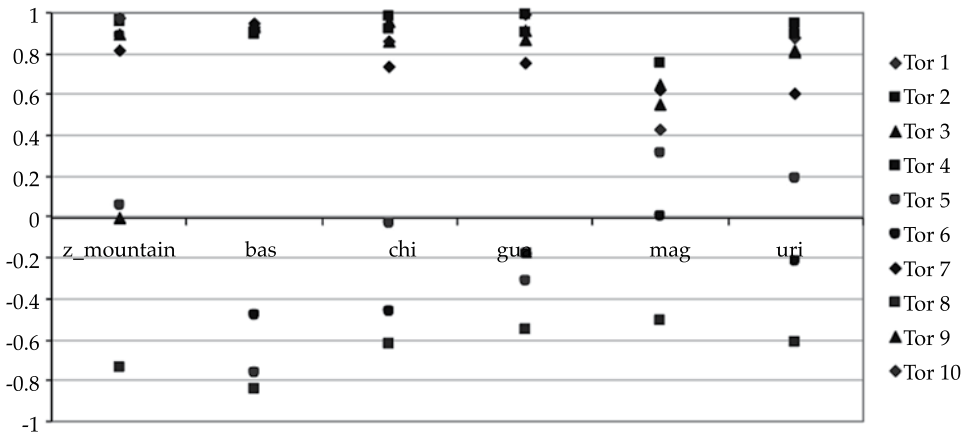

b) Surface T / Maximum brightness T

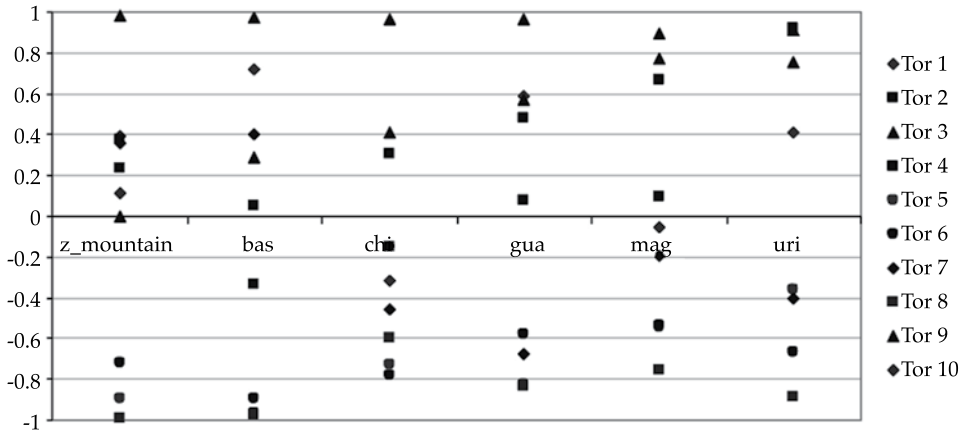

c) Surface T / Intermediate brightness T

Figure 7. Temperature correlation coefficients for sup-satellites in the mountainous region and partial mountain zone, storng storms.

region and those pertaining to the partial AWS zones.

In order to obtain a more detailed evaluation of the relationship between surface temperatures and maximum brightness temperatures, the following parameters were determined: differences between surface and satellite temperatures, Δ*ssi*, gradients of the evolution between these differences, δ*ssi*, internal gradient of the evolution between satellite temperatures, δ*sat_i*, and internal gradient of the evolution between surface temperatures, δ*sup_i*. These parameters were obtained according to the respective hourly series for the complete mountainous region as well as the areas of influence of the automated stations in the partial mountain zones, according to the corresponding maximum brightness temperature series.

The δ*ssi* for each partial zone in the study had smaller ordinates than those corresponding to the Δ*ssi* curve (Figure 8). That is, the decrease in areas of influence clearly intervene in reducing the differences between the two types of temperatures. This is demonstrated by the decrease from -15.14 °C average in the mountains to -6.92 °C average in the partial mountain zones. In addition, the δ*ssi* curves show the Δ*ssi* values (difference between sat and sup temperatures) to be insignificant for three hours prior to the rainfall. That is, the results between the Δ*ssi* curves and the δ*ssi* series were consistent. Together, the spread between both temperature measurements improved for the parameters evaluated, when considering the partial zones corresponding to each one of the stations instead of the complete mountainous region.

The spread of the measurements obtained for the complete mountainous region were based on the Δ*ssi* values (difference between maximum brightness temperatures and mean surface temperatures) measured for each of the partial zones in the mountainous region during a 12-hour period prior to rainfall. When spatially reducing the study areas, significant decreases were found for both types of temperatures. Nevertheless, the reductions were not constant over time, and began at instant 10 in roughly 20% of all the partial cases. The differences in the estimate of the hour of rainfall decreased 80% on average. That is, the temperatures were nearly identical during this period. It is therefore concluded that a large decrease in spreads between temperature classes is obtained by relating the measurement to the area of influence and, thus, the use of meteorological surface measurements is significantly more reliable.

Moderate Storms (range 10-20), mountainous region

The analyses was performed with the same pairs of surface and satellite temperatures, as described in the previous case, but in this case for the moderate storms. The findings are presented below.

1. According to the coefficients for the correlation between minimum brightness temperatures (coldest) and average surface temperature, only four storms presented values between ± 0.6 and 1.0, that is, only 40% of the sample was closely related to these temperatures, but this is not significant for the analysis, as shown in Figure 9a. The average correlation value for the four storms is -0.722.
2. In terms of the *r* coefficients for maximum brightness temperatures (warmest) and average surface temperature, 80% of the storms in the sample had values between ± 0.6 and 1. This behavior is very important and indicates a strong relationship between the values, which is shown in Figure 9b. The average correlation value for the eight storms is -0.812.
3. Forty percent of the storms from the sample presented values in the range of ± 0.6 and 1 for mean bright temperatures and average surface temperatures, indicating the lack of a good relationship between these variables, as observed in Figure 9c. The average correlation value for the four storms is 0.724.

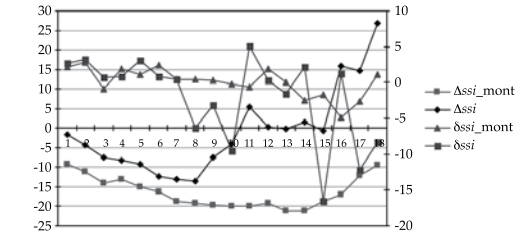

Basesachi Δ*ssi* y δ*ssi*

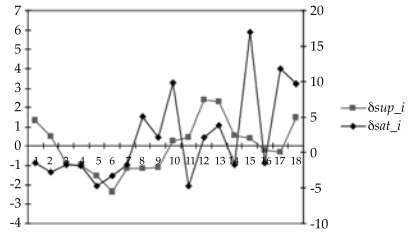

Basesachi δ*sup_i* y δ*sat_i*

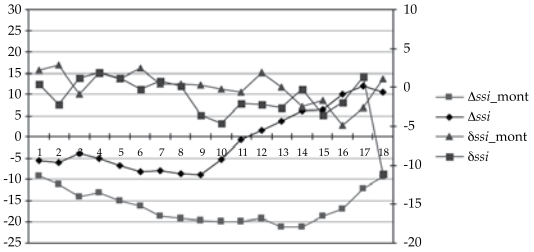

Chinatú Δ*ssi* y δ*ssi*

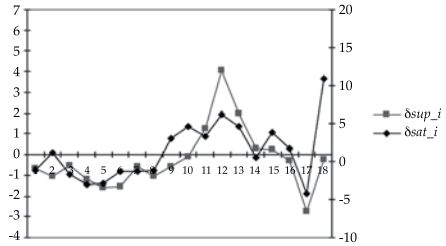

Chinatú δ*sup_i* y δ*sat_i*

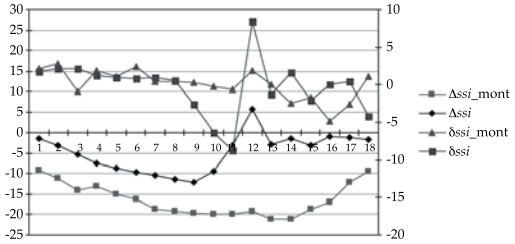

Guachochi Δ*ssi* y δ*ssi*

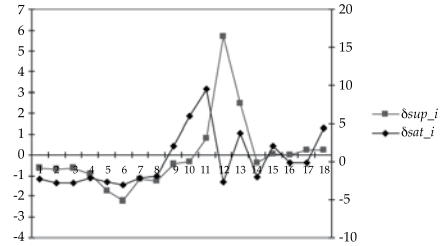

Guachochi δ*sup_i* y δ*sat_i*

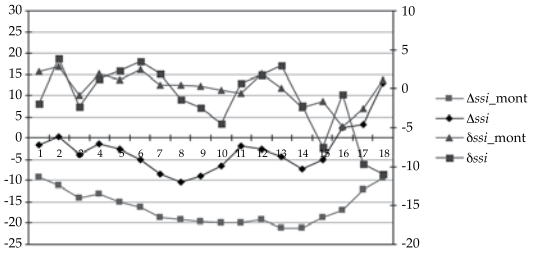

Maguarichi Δ*ssi* y δ*ssi*

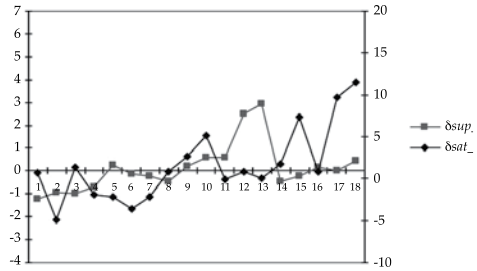

Maguarichi δ*sup_i* y δ*sat_i*i

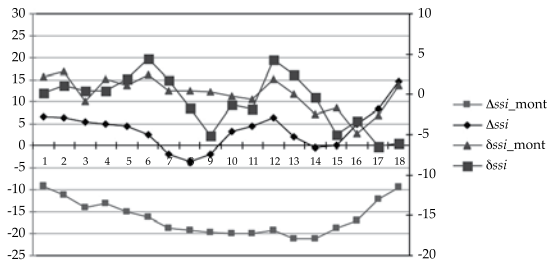

Urique Δ*ssi* y δ*ssi*

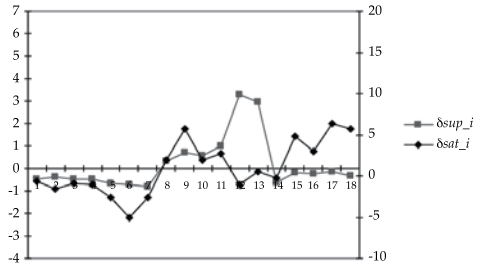

Urique δ*sup_i* y δ*sat_i*

Figure 8. Δ*ssi* curves (difference between sup and sat temp) and δ*ssi* (changes in difference over time), strong storms. δ*sat_i* curves (evolution of changes in sat temperatures) and INSERTAR SIMBOLO curves (evolution of changes in sup temperatures), mountainous region and partial zones, strong storms.

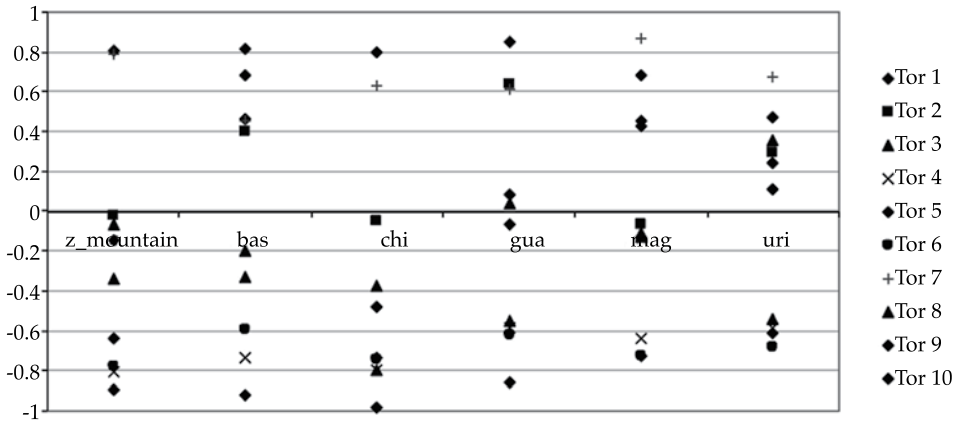

a) Surface T / Minimum brightness T

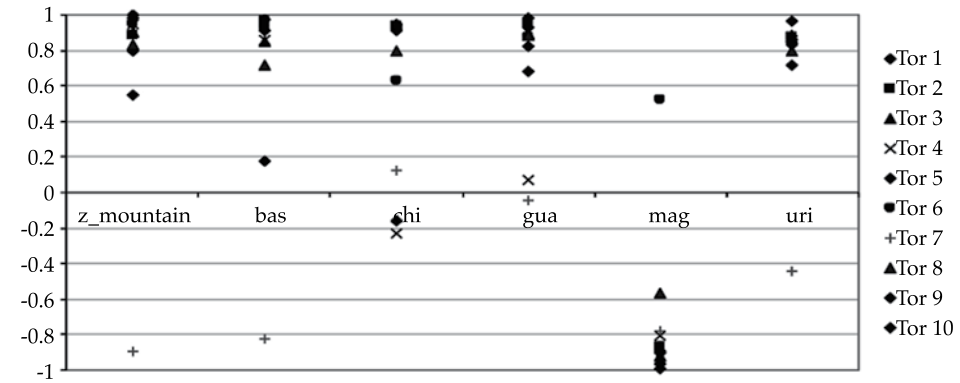

b) Surface T / Maximum brightness

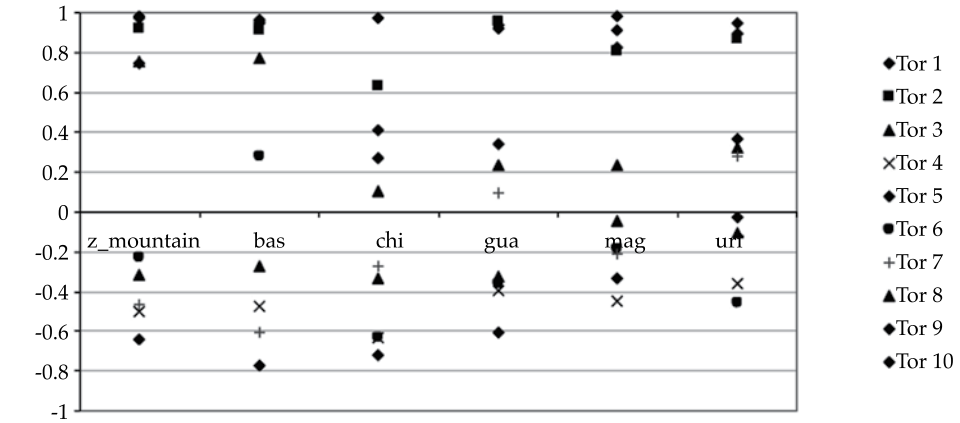

c) Surface T / Intermediate brightness

Figure 9. Correlation coefficients of sup-satellite temperatures in mountainous region and partial zones, moderate storms.

The best coefficient correlations were observed again among the groups of variables corresponding to the relationship between average surface temperatures and maximum brightness temperatures, which is consistent with the previous case study of strong storms. Therefore, the specific analysis of internal parameters in the group of series in question was conducted, as in the case of strong storms.

Based on the parameters obtained, an improvement in the estimates between the two types of temperatures is observed when reducing the study area to partial zones of influence related to each automated weather station, finding a decrease from an average -14.05 °C for the mountainous region to -5.82 °C average for the partial mountain zones. Nevertheless, unlike the case of the strong storms, the moderate storms present differences, of roughly 5 degrees, between surface temperatures and satellite temperatures during the first three hours prior to rainfall whereas for similar instants for strong storms the differences were virtually insignificant. With regard to the values of the Δ*ssi* curves (series of differences between sup and sat temperatures) for the mountainous region (Figure 10), those corresponding to partial zones improved an average of 70%. The greatest similarity occurred during the first 10 hours. It is important to clarify that the instant-to-instant decreases present variations over the 12 hours of the study. This behavior also shows slightly better patterns between the two measurements (surface and satellite) of the atmospheric conditions prior to rainfall for strong storms. The average improvement is roughly 10%.

An analysis was also performed of δ*sup_i* trends (changes in the surface data series over time) and δ*sat_i* trends (changes over time in the series of data obtained from satellites). With respect to strong storms, the δ*sup_i* and δ*sat_i* curves for each of the partial zones and the mountainous region were very similarly aligned, especially during the first nine hours of the series.

In the case of moderate storms, the greatest concordance occurred during the first 10 hours of the series. The *Cv* calculated for the surface and satellite time series of strong storms obtained in partial zones shows a difference of -0.066 units, on average, a deviation of 0.042 and a proportion factor between *Cv* of roughly 2 for both measurements.

With respect to the moderate storms, the calculated *Cv* values had an average difference of -0.078 units, a standard deviation of 0.064 and a proportion factor between *Cv* of approximately 1.76, values calculated for the partial zones.

The variations over time in δ*sup_i* and δ*sat_i* demonstrate very similar trends for the two types of storms analyzed, and the *Cv* between the series is shown to be very close. Nevertheless, the δ*sup_i* and δ*sat_i* curves for moderate storms are more similar to each other since the atmospheric conditions are more stable than the dynamic atmospheric state related to strong storms. In both cases, the values of the δ*sup_i* and δ*sat_i* curves are drastic around hour 10, unlike the gradual behavior during the previous hours, which is due to the closeness to the time of precipitation.

The high correlation coefficients between the temperature series measured on the surface and the maximum brightness series for the ranges of both strong and moderate storms located in the partial mountain zones, as well as the differences among the changes within the series (δ*sup_i* and δ*sat_i*) and those between both temperatures series (Δ*ssi*) altogether represent the sign of rainfall, through different measuring devices and with a very close margin between both types of data, as was shown. This special behavior enabled the use of one measuring system or another to observe and estimate the occurrence of the phenomenon, resulting in high certainty.

Given that meteorological surface measurements are more accessible than indirect measurements from real-time satellite images, tools that can be successfully used to estimate the occurrence of strong and moderate

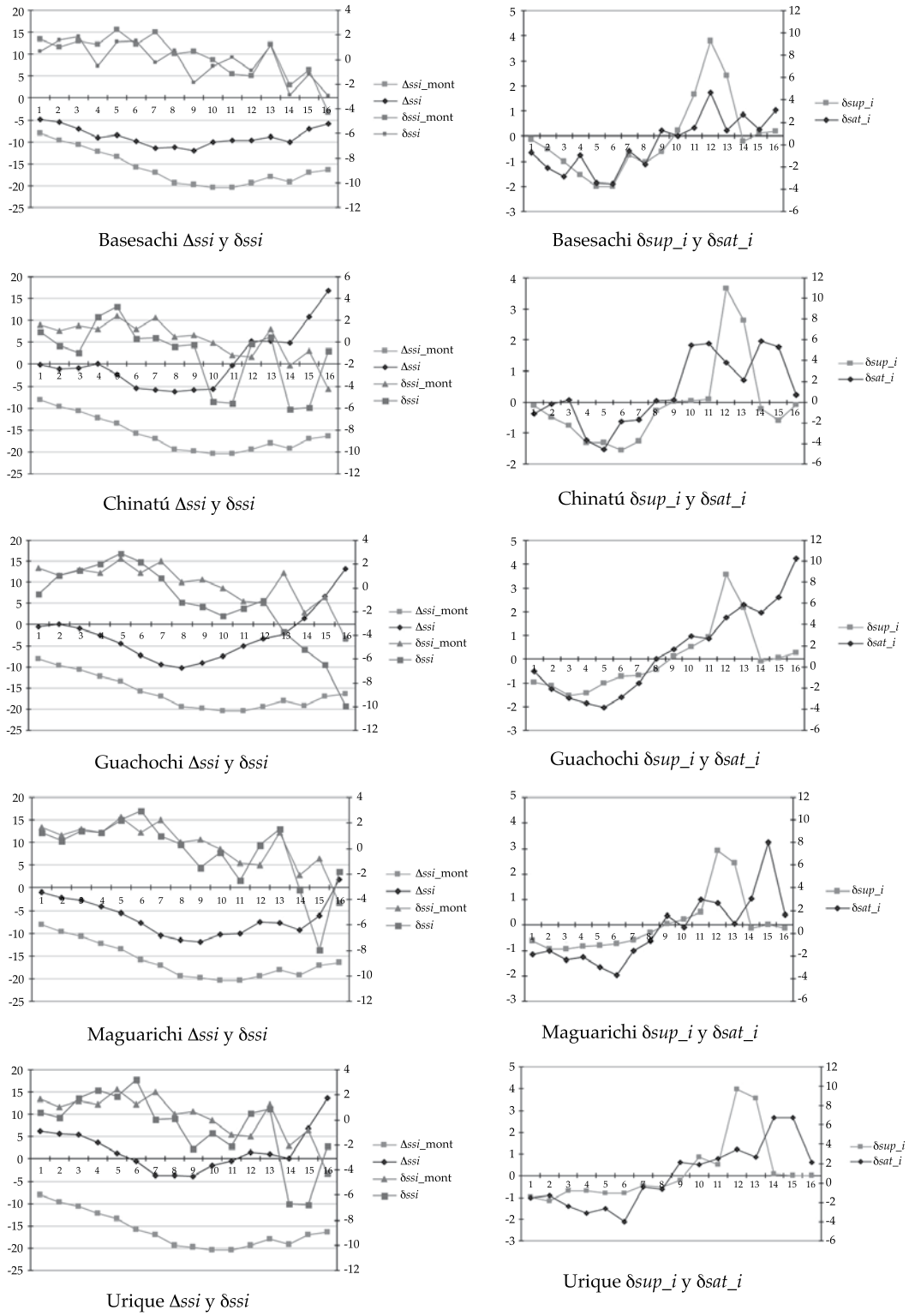

Figure 10. Δ*ssi* ssi curves (difference between sup and sat temp) and δ*ssi* ssi (changes in difference over time), strong storms. δ*sat_i* curves (evolution of changes in sat temperatures) and δ*sup_i* curves (evolution of changes in sup temperatures), mountainous region and partial zones, moderate storms.

storms in the partial mountain zones during July include average temperature patterns for 12-hours prior to the occurrence of rainfall, partial to complete cloud cover and equations for relative humidity trends corresponding to each of the AWS in this study. The correlation between temperatures and relative humidity is 0.996 and 0.989 for moderate and strong storms, respectively. These equations are presented in Figures 11 and 12.

Application of Temperature Patterns to Estimate the Range of Rainfall

In order to demonstrate the fit of the temperature and relative humidity patterns obtained to estimate the range of precipitation in the different study regions, storms not included in the analysis of the satellite images were selected, which formed within the sample of storms recorded by the AWS. Thus, the records of two storms registered by the Basesachi AWS were extracted (Table 8) and temperature values for the 12 hours prior to the rainfall events were graphed on calculated average trend and boundary curves of the Basesachi temperatures. The same procedure was performed with data for relative humidity (Figure 13). A 90% fit of the values to the antecedent trends in question was obtained for the 05/07/2000 storm. In the case of the 22/07/2001 storm, the fit was 85%.

The fits obtained are acceptable in terms of this first approximation of this study. These results indicate that the temperature and relative humidity values of these storms present patterns of behavior corresponding to rainfall events from 20 to 50 mm, in the range of strong storms. These results were obtained in a simple manner based on surface records with a coverage of 12 hours in advance. In addition, a third storm was selected in order to compare the estimate of precipitation based on IR images with an indirect estimate based on antecedent trends. This storm was named 04/07/2004. Its Temp and HR variables were graphed on trend curves and a 75% fit was observed.

Rainfall based on IR images for this same storm was estimated with the procedure described in Arellano *et al*., (2010), corresponding to an adjustment-simplification of the auto-estimator technique (Vicente, Scofield, & Menzel, 1998). Figure 14 shows the rainfall estimated for the mountainous region and the detail of the spatial distribution of the rainfall in the Basesachi section.

Conclusions

Significant topographical spatial variations exist in the broad study area. This behavior was reflected in the results from the comparison of the coupling of meteorological patterns prior to storms, obtained from average surface temperatures, and maximum temperatures of cold clouds obtained from satellite images for 10 strong storms and 10 moderate storms, respectively. The best *Cv* among the series mentioned were the most accurate (0.835 and -0.812 for strong and moderate events, respectively). The average surface temperatures series was used for the coupling because of its high correlation coefficient with relative humidity records, -0.996 and -0.989 for both moderate and strong storms, and also because temperature was the variable obtained from the satellite measurements.

As was mentioned, the *Cv* of the average variation between both types of time series was 0.835 for strong storms and -0.812 for moderate storms, disregarding surface areas. Nevertheless, the use of zones of influence of weather stations instead of the mountainous region notably decreased the spreads between these temperature trends, from 20% to 80% near hour 10 of the time series for strong storms, and to 70% for moderate storms. That is, the coupling of measurements applied to the zones of influence improved the relationships between the series. These results are observed in the Δssi and δssi curves for strong and moderate storms.

The values of the δsup_i and δsat_i curves were also used to evaluate the coupling of both

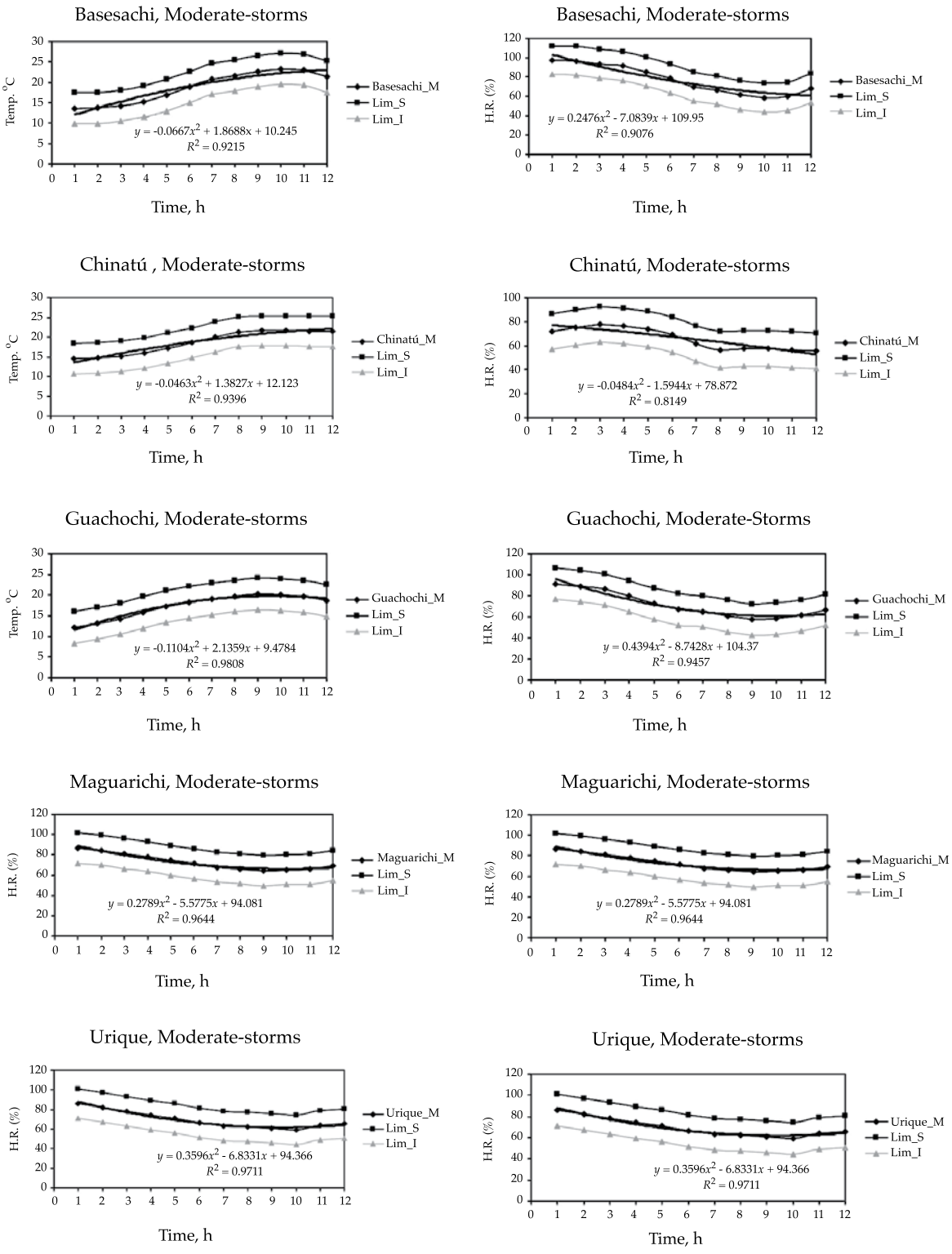

Figure 11. Equations for surface temperature and relative humidity patterns, 12 hours prior. Moderate storms.

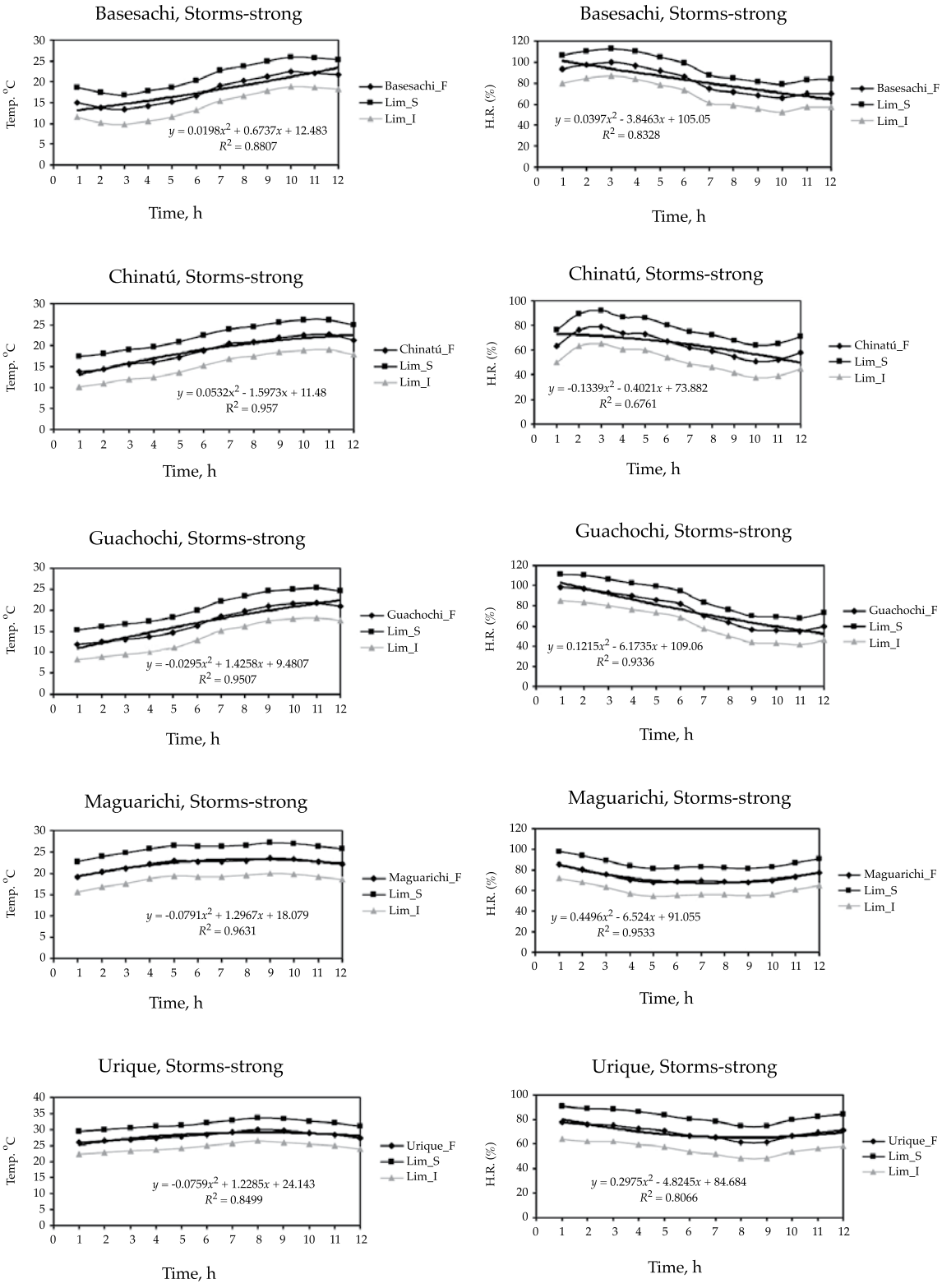

Figure 12. Equations for surface temperature and relative humidity patterns, 12 hours prior. Strong storms.

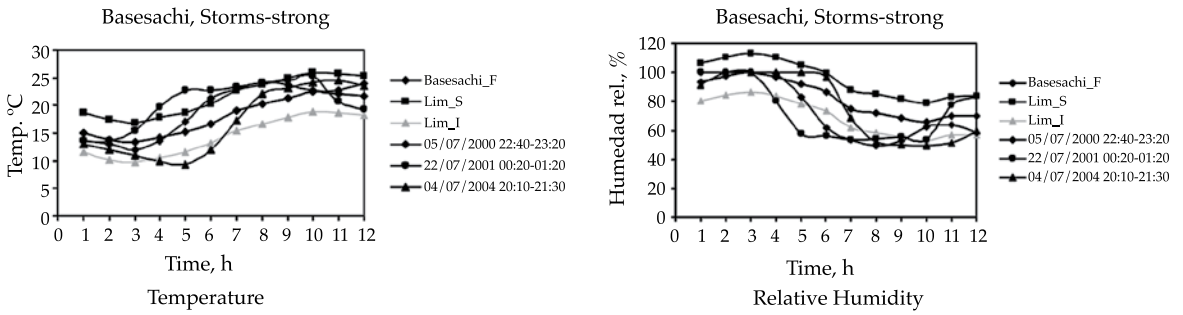

Figure 13. Curves for surface temperature and relative humidity patterns. Test storms.

Table 8. Storms to test antecedent trends.

Storm (day and hour)	Precipitation (mm)
05/07/2000 22:40 - 23:20	37.58
22/07/2001 00:20 - 01:20	27.92
04/07/2004 20:10 - 21:30	20.05

types of antecedent temperatures, in which the trends in temperature changes within each one of the series evolved very similarly during the first 9 hours of the series corresponding to strong storms and the first 10 hours of the series for moderate storms. Thus, the average difference between the *Cv* calculated for the average surface temperature series and the maximum satellite temperature series was 0.066 ± 0.04 for strong storms and -0.078 ± 0.064 for moderate storms.

This study demonstrated the close relationship between surface and satellite antecedent temperature series in terms of the occurrence of rainfall for strong and moderate events in the study area. As a result, trends in surface temperature over time coupled can be coupled with the respective relative humidity curves —both associated with the AWS zones of influence located in the site and with cloud cover— in order to estimate, 12 hours before a rainfall event, the potential amount of rainfall during the month of July. In addition, the formulas in question can be successfully included in a real-time storm warning alert systems.

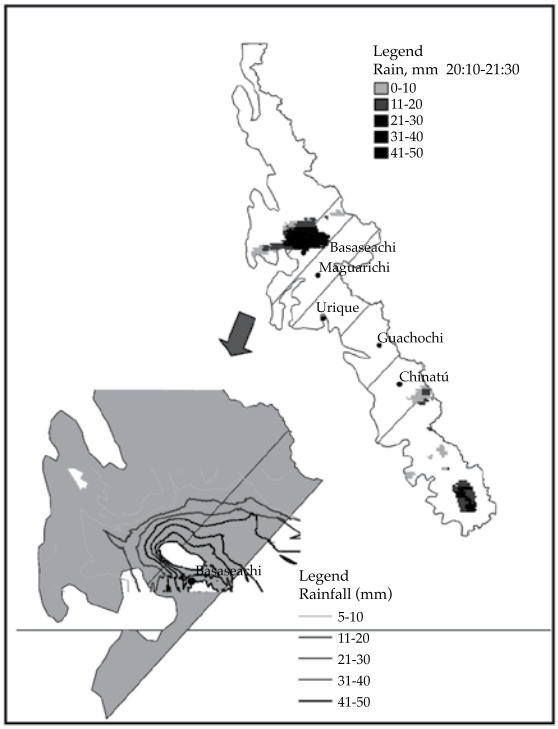

Figure 14. Spatial distribution of rainfall estimated for storm 04/07/2004.

Acknowledgements

Thank you to the National Weather Service (SMN, Spanish acronym) for supplying the satellite images used in the investigation, as well as to Dr. Michael Weinreb and Dr. Dejianh Han, researchers with the NOAA.

References

Adler, R. F., & Negri, A. J. (1988). A Satellite Infrared Technique to Estimate Tropical Convective and Stratiform Rainfall. *J. Appl. Meteor*., *27*(30), 30-51.

Arellano, L. F., Gutiérrez, L. A., & Arellano, L. H. (2010). Comportamiento de tormentas extremas de Querétaro en base a imágenes de satélite. Casos de estudio. *Extensión Nuevos Tiempos, Universidad Autónoma de Querétaro*, 17, 39-46.

Arkin, P. A. (1979). The Relationship between Fractional Coverage of High Cloud and Rainfall Accumulations during GATE over the B-Scale Array. *Mon. Wea. Rev*., *107*, 1382-1387.

Barret, E. C. (1970). The Estimation of Monthly Rainfall from Satellite Data. *Mon. Wea. Rev*., *98*, 322-327.

Barrett, E. C. & Martin, D. W. (1981). *The Use of Satellite Data in Rainfall Monitoring* (340 pp.). London: Academic Press.

Carn, M. (1994). *Apport de la Télédétection Satellitaire á la Pluviométrie de Bassin dún Flueve Sahélien: Le Sénegal. Validation Problems of Rainfall Estimation Methods by Satellite in Intertropical Africa*. Paris: B. Guillot (Ed.). Orstom Éditions, Collection Colloques et Séminaires.

Cenapred (2013). *Publicaciones. Características e impactos socioeconómicos de los principales desastres ocurridos en la República Mexicana*. Centro Nacional de Prevención de Desastres. Recuperado de www.cenapred.gob.mx.

Dittberner, G. J., & Vonder Haar, T. H. (1973). Large Scale Precipitation Estimates using Satellite Data; Application to the Indian Monsoon. *Arch. Met. Geoph. Biokl. Ser. B*., *21*, 317-334.

Feidas, H., Lagouvardos, K., Kotroni, V., & Cartalis, C. (2005). Application of Three Satellite Techniques in Support of Precipitation Forecasts of a NWP Model. *International Journal of Remote Sensing*, *26*(24), 5393-5417.

Feidas, H., Kokolatos, G., Negri, A., Manyin, M., Chrysoulakis, N., & Kamarianakis, Y. (2008). Validation of an Infrared-Based Satellite Algorithm to Estimate Accumulated Rainfall over the Mediterranean Basin. *Theo. Appl. Clim*., *95*, 91-109.

Griffith, C. G., Woodley, W. L., Browner, S., Teijeiro, J., Martin, M. D. W., Stout, J., & Sikdar, D. N. (1976). *Rainfall Estimation from Geosynchronous Satellite Imagery during Daylight Hours* (106 pp.). NOAA Tech. Rep. ERL 356-WMPO 7. Boulder, USA: NOAA.

Gruber, A. (1973). *An Examination of Tropical Cloud Clusters using Simultaneously Observed Brightness and High Resolution Infrared Data from Satellites* (22 pp.) NOAA Tech. Memo. Ness 50. Washington, DC: NOAA.

Hubert, P., & Toma, C. A. (1994). Étude des Cumulus de Pluie Sahéliens. Validation Problems of Rainfall Estimation Methods by Satellite in Intertropical Africa. Paris: B. Guillot (Ed.), Orstom Éditions, Collection Colloques et Séminaires.

Laurent, H. (1994). *Validation des Estimations de Précipitation á Grande Échelle. Validation Problems of Rainfall Estimation Methods by Satellite in Intertropical Africa*. Paris: B. Guillot (Ed.), Orstom Éditions, Collection Colloques et Séminaires.

Lovejoy, S., & Austin, G. L. (1979). The Delineation of Rain Areas from Visible and IR Satellite Data for GATE and Mid-Latitudes. *Atmosphere-Ocean*, *17*, 77-92.

Milford, J. R., Dugdale, G., & McDougall, V. D. (1994). *Rainfall Estimation from Cold Cloud Duration: Experience of the TAMSAT Group in West Africa. Validation Problems of Rainfall Estimation Methods by Satellite in Intertropical Africa*. Paris: B. Guillot (Ed.), Orstom Éditions, Collection Colloques et Séminaires.

Moses, J. F. & Barrett, E. C. (1986). Interactive Procedures for Estimating Precipitation from Satellite Imagery. In Hydrologie Application of Space Technology. Ed. Johnson, A. I. *Int. Assoc. Hydrol. Sci. Publ*., *160*, 25-40.

NASA (2005). *The Importance of Understanding Clouds*. National Aeronautics and Space Administration. Available Online at http://icp.giss.nasa.gov/education/cloudintro/.

NOAA (1975). *Central Processing and Analysis of Geostationary Satellite Data* (155 pp.). NOAA Tech. Memo. NESS 64, U.S. Washington, DC: Department Commerce, National Oceanic and Atmospheric Administration.

Ravelo, A. C. & Santa, J. A. (2000). Estimación de las precipitaciones utilizando información satelital y terrestre en la provincia de Córdoba (Argentina). *AgriScientia*, *17*, 21-27.

Sawunyama, T., & Hughes, D. A. (2008). Application of Satellite-Derived Rainfall Estimates to Extend Water Resource Simulation Modelling in South Africa. *Water SA*, *34*, 1-9.

Scofield, R. A., & Oliver, V. J. (1977). *A Scheme for Estimating Convective Rainfall from Satellite Imagery* (47 pp.). NOAA Tech. Memo. NESS 86. Washington, DC: NOAA.

Stout, J. E., Martin, D. W., & Sikdar, D. N. (1979). Estimating GATE Rainfall with Geosynchronous Satellite Images. *Mon. Wea. Rev., 107*, 585-598.

Touré, A., & N´Diaye, N. (1994). *Estimation des Pluies au Séneégal par Lápproche TAMSAT. Validation Problems of Rainfall Estimation Methods by Satellite in Intertropical Africa*. Paris: B. Guillot (Ed.). Orstom Éditions, Collection Colloques et Séminaires.

Tsonis, A. A., &. Isaac, G. A. (1985). On a New Approach for Instantaneous Rain Area Delineation in the Midlatitudes using GOES Data. *J. Climate Appl. Meteor*., *24*, 1208-1218.

Vicente, G. V., Scofield, R. A., & Menzel, W. P. (1998). The Operational GOES Infrared Rainfall Estimation Technique. *Bulletin of the American Meteorological Society*, *79*, 1883-1898.

Weinreb, M. P., Jamieson, M., Fulton, N., Chen, Y., Johnson, J. X., Bremer, J., Smith, C., & Baucom, J. (1997). Operational Calibration of Geostationary Operational Environmental Satellite-8 and -9 Imagers and Sounders. *Applied Optics*, *36*, 6895-6904.

Wylie, D. P. (1979). An Application of a Geostationary Satellite Rain Estimation Technique to an Extratropical Area. *J. Appl. Meteor.*, *18*, 1640-1648.

Institutional Address of the Authors

Dra. Fabiola Arellano-Lara
Dr. Carlos Escalante-Sandoval

Facultad de Ingeniería
Universidad Nacional Autónoma de México
Av. Universidad 3000, Delegación Coyoacán, Ciudad Universitaria
04510 México, D.F., México
fabi_arelara@yahoo.com.mx
caes@unam.mx

Click here to write the autor

Hydrodynamic Criteria to Design Water Recirculation Systems for Aquaculture

• Juan A. García-Aragón* • Humberto Salinas-Tapia • Víctor Díaz-Palomarez •
• Boris M. López-Rebollar • Javier Moreno-Guevara •
• Leonarda M. Flores-Gutiérrez •
Universidad Autónoma del Estado de México
*Corresponding Author

Abstract

García-Aragón, J. A., Salinas-Tapia, H., Díaz-Palomarez, V., López-Rebollar, B. M., Moreno-Guevara, J., & Flores-Gutiérrez, L. M. (September-October, 2014). Hydrodynamic Criteria to Design Water Recirculation Systems for Aquaculture. *Water Technology and Sciences* (in Spanish), 5(5), 59-71.

Closed water recirculation systems (WRS) have been developed for aquaculture in order to more efficiently use water. In terms of water quality and biological studies, the hydrodynamics of recirculation tanks is an aspect that has been least studied. The work herein describes an experimental investigation carried out with a reduced-scale plexiglass model of these tanks. Fish food was used in one tank in which the resulting flocs served as tracers to determine sedimentation characteristics. Using optical techniques —particle image velocimetry (PIV)— it was possible to determine the optimal distribution of diffusers to obtain different velocities in the tank in order to facilitate the flocculation and sedimentation processes. A design for a central settling basin is also proposed based on the characterization of the flocs and their hydrodynamic behavior, particularly the fall velocity. Particle trace velocimetry (PTV) was used to calculate the fall velocity of the flocs. The experimental results enabled calibrating a mathematical model for fall velocities of flocs.

Keywords: aquaculture, WRS, flocs, PIV, PTV, settling velocity.

Resumen

García-Aragón, J. A., Salinas-Tapia, H., Díaz-Palomarez, V., López-Rebollar, B. M., Moreno-Guevara, J., & Flores-Gutiérrez, L. M. (septiembre-octubre, 2014). Criterios hidrodinámicos para el diseño de sistemas de recirculación en acuicultura. Tecnología y Ciencias del Agua, *5(5), 59-71.*

Con el objetivo de hacer más eficiente el uso del agua se ha desarrollado la técnica de sistemas cerrados de recirculación de agua (SRA) para acuicultura. Un aspecto que se ha relegado, en cuanto a los estudios de calidad de agua y biológicos, es el relativo a la hidrodinámica de esos tanques de recirculación. En este trabajo se describe una investigación experimental llevada a cabo en un modelo en plexiglass a escala reducida de dichos tanques de recirculación. En un tanque circular se utilizó comida para peces; los flóculos resultantes sirvieron de trazadores para establecer las características de sedimentación. Por medio de técnicas ópticas, velocimetría por imágenes de partículas (PIV), se pudo determinar una distribución óptima de difusores para lograr diferentes velocidades en el tanque, a fin de facilitar los procesos de floculación y, a su vez, los de sedimentación. Igualmente se propone un diseño del sedimentador central en función de las características de los flóculos y de su comportamiento hidrodinámico, en especial su velocidad de caída. Para calcular las velocidades de caída de los flóculos se utilizó la técnica de velocimetría por rastreo de partículas (PTV). Los resultados experimentales permitieron calibrar un modelo matemático de velocidades de caída de flóculos.

Palabras clave: *acuicultura, SRA, flóculos, PIV, PTV, velocidades de caída.*

Received: 07/11/12
Accepted: 29/01/14

Introduction

Closed water recirculation systems (WRS) are used as an alternative for fish farming in regions with little water (Wheaton, 1977). The main characteristics of these systems are to reuse and conserve water. They are equipped with a series of water treatment modules to maintain the quality at levels adequate for reusing the water and for the survival of the fish (Wheaton, 1977;

Gallego-Alarcón, 2010). Although WRS have been able to reduce the use of large amounts of water, most of the studies have focused on the quality of the water and conditions for the survival of fish, from the biological point of view (Gallego-Alarcón, 2010). Meanwhile, the hydrodynamic study of the fish tanks (recirculation tanks) has been neglected. These tanks are the principal unit for the growth of the fish and where solids from fish excrement and unconsumed food settle, contaminating the water with high levels of nitrites and nitrates.

The main problem with aquaculture recirculation tanks is their poor efficiency in removing suspended solids, since they are under 70 microns and, therefore, are considered cohesive sediments (Droppo, 2001) and only settle when being added. For quick settling, cohesive sediments must form flocs, or aggregates, composed of water, inorganic particles and organic particles (Droppo & Ongley, 1994; Nicholas & Walling, 1996; Droppo, 2005). And this depends on the fall velocity. This field is open to investigation (García- Aragón, Droppo, Krishnappan, Trapp, & Jaskot, 2011) into the factors that affect the settling of flocs and their characterization. To this end, it is important to apply non-invasive methods that enable identifying criteria for designing tanks with self-cleaning characteristics. In addition, no agreement is found in the scientific literature regarding criteria for designs that provide the efficient removal of flocs in recirculation tanks used in aquaculture, and thus the importance of the present work.

Circular tanks are most commonly used (Watten & Beck 1987; Sommerfeld, Wilton, Roberts, Rimmer, & Fonkalrsrud, 2004). Water is fed to these tanks through diffusers attached to the outer wall, in order to control the mean velocities on the vertical and transversal to the tank. A suitable arrangement of the diffusers enables selecting the velocity that is comfortable to the fish while also obtaining appropriate particle settling conditions.

The importance of a hydrodynamic study of this type of system is its defining the hydraulic conditions —primarily the inflow and outflow— that affect the recirculation velocity of the water and the settling of particles, the latter being dependent on the vertical velocity. If these parameters are adequately controlled, a homogeneous distribution of fish can be obtained, thereby guaranteeing the optimal amount of water use (Duarte, Reig, Oca, & Flos, 2004) and the rapid settling of suspended solids. In addition, by determining the hydrodynamics, the natural removal (through settling) of solids can be optimized. Since it is complicated to experimentally determine these conditions with invasive methods, non-invasive techniques need to be applied that enable jointly determining the velocity of the fluid and the settling of particles, without affecting flow behavior.

The 2D study of the movement of fluids uses non-invasive optical particle image velocimetry (PIV) and particle tracking velocimetry (PTV) techniques (Adrian, 1991; Salinas, 2007; Salinas-Tapia & García-Aragón, 2011). These enable instantaneously determining the velocity fields of fluids by processing an optical image recorded at two very short successive times. The main characteristic of these techniques is the use of tracer particles to describe flow patterns, enabling a better understanding of hydrodynamic behavior. Appropriate hydrodynamics makes it possible to design recirculation tanks that are self-cleaning and result in the efficient settling of particles.

The present study determined the velocity field of the fluid and solid particles by applying PIV and PTV techniques. The experimental data obtained are scientifically valuable since this type of data is needed to study disperse phases, as mentioned by Sundaresan, Eaton, Koch and Ottino (2003). These data enable determining the diffuser and settler design characteristics that best facilitate the removal of solid particles. They also make it possible to propose a model to determine the fall velocity of flocs made up of cohesive sediments from the aquaculture tanks themselves.

PIV and PTV techniques have been used (Salinas-Tapia & García-Aragón, 2011) to determine the fall velocity (settling) of non-cohesive particles. Therefore, the present project used these techniques to determine the velocity fields of fluid based on different configurations of diffusers, and PTV to determine the settling velocities of the flocs.

Experimental Design

This work was performed using a reduced scale model of a circular recirculation tank. The hydrodynamic analysis was based on different diffuser configurations (inflow) as criteria to select the most suitable one, which would be highly efficient for removing solids from the tank. This criterion was used in combination with the analysis of the outflow device and the main settler. The settler consisted of two concentric tubes in the center of the tank which functioned according to the hydrocyclone principle (Timmons, Summerfeld, & Vinci, 1998). The outer tube had grooves on the bottom which allowed water and sediment to enter. The water entering rose through the outer tube until reaching the maximum height of the inner tube, which functioned as a weir to control the depth and was connected to the outlet system. In the space between the two tubes, a low velocity zone was generated to enable the flocs to settle.

The pilot fish farming system installed at the hydraulics model laboratory at the Inter-American Water Resources Network (CIRA, Spanish acronym) was used as the scale model. This system is a full-scale design for fish farming, measuring 3 m in diameter and 1.0 m high. It was built using a masonry construction, and with water depths of 0.90 cm and maximum velocities of 30 cm/s.

The main problem with this type of tank is its poor efficiency for the settling of particles (Gallego-Alarcón, 2010). The efficiency of the settler was 5.56%, much lower than that reported by previous investigators (García, 2008; Gallego-Alarcón, García, Díaz, & Fall, 2004; Gallego-Alarcón, 2004). This problem justifies the evaluation of the hydrodynamics of the system, an important factor in the settling of the particles, using the selection and configuration of inflow and outflow as the main criteria.

To evaluate and determine the correct inflow and outflow configurations, using PIV and PTV techniques, a full-scale system needed to be built by applying the laws of dynamic and kinematic similarity. The Reynolds number $\left(Re = uh/v\right)$ and the Froude number $\left(Fr = u/\sqrt{gh}\right)$ were the main criteria used to transfer the results from the hydrodynamic studies of the prototype model. Table 1 summarizes the geometric properties as well as the hydrodynamic parameters of the prototype and of the model used for this work.

Given the geometric similarity, the scales obtained were longitude, $l_e = 3.0$ and velocity $v_e = \sqrt{3.0} = 1.73$. That is, to obtain the velocities of the model, the velocities measured in the prototype needed to be divided by 1.73.

Methodology

After applying the dimensional analysis to the prototype installed at the CIRA, the experimental design used to conduct the present investigation consisted of a water recirculation tank 1.03 m in diameter and 40 cm high, with Plexiglas for adequate viewing. It was gravity fed through diffusers arranged according to three proposed configurations to evaluate the hydrodynamics of the flow. The diffusers were interchangeable in order to control the flow and direction and to analyze the behavior of the flow (Figure 1). For this work, three different diffuser configurations were considered as a hydrodynamic factor, corresponding to three different liquid flows. The mean flow velocity (u_{med}) was also determined using a digital current meter with a precision of 0.1 cm/s. The Reynolds $\left(Re = uh/v\right)$ and Froude $\left(Fr = u/\sqrt{gh}\right)$

Table 1. Parameters for the model and prototype recirculation tank.

Parameters	Prototype	Model
Construction material	Masonry, concrete	Acrylic
Fluid	Water	Water
Water temperature (°C)	13° - 17°	15° - 17°
Tank Diameter,, *D* (cm)	300	100
Tank height, *H* (cm)	100	35
Hydrocyclone Diameter (cm)	85	30
Raidal distnace (width of canal) from tank wall to hydrocyclone wall (cm)	93	35

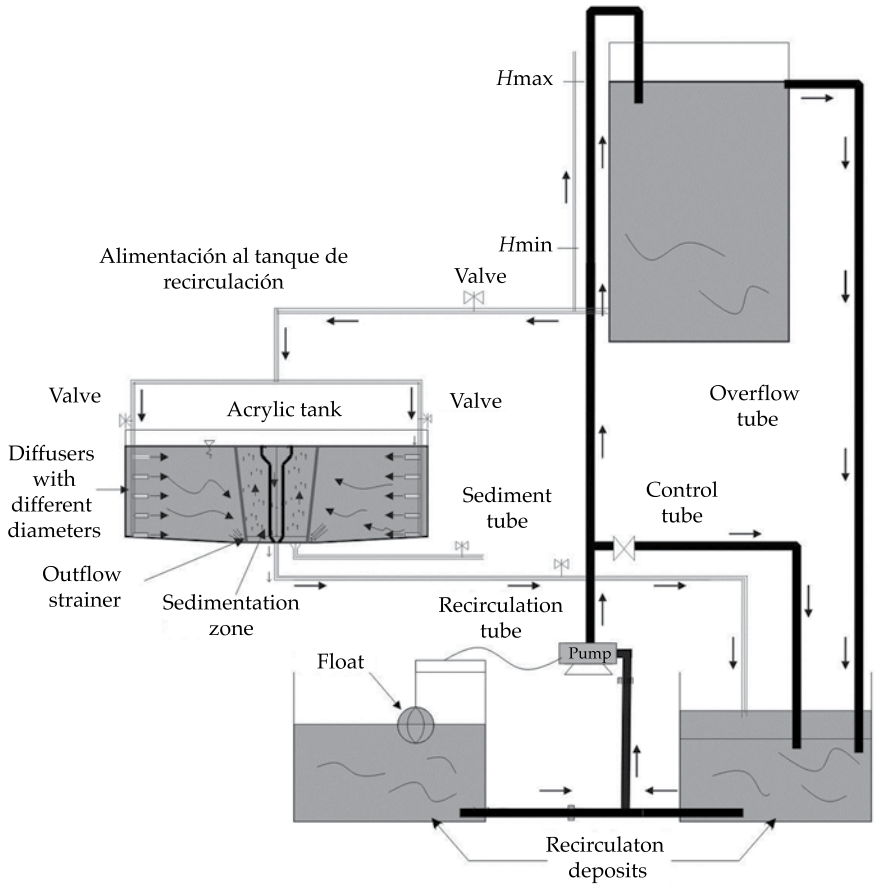

Figure 1. Experimental setup.

numbers were determined based on this data. Table 2 presents the hydraulic parameters used.

The selection of outflow devices was another factor considered for the hydrodynamics of the tank, which according to previous results is important in this type of system in order to design self-cleaning systems.

To obtain a constant velocity and uniform flow in the system, the water was fed through two diffuser trains having different diameters (Figure 2). These were installed in such a way as to be able to control the direction of the inflow. To determine the flow conditions, the direction of the diffusers was adjusted to create

Table 2. Distribution and size of diffusers.

Configuration	Diffuser diameter (mm)	Direction of diffuser (°)					Q (l/min)
		1	2	3	4	5	
A	4.37	45	135	45	45	90	14.62
B	3.18	45	30	45	90	135	9.00
C	3.18 y 1.08	45	45	135	90	135	10.91

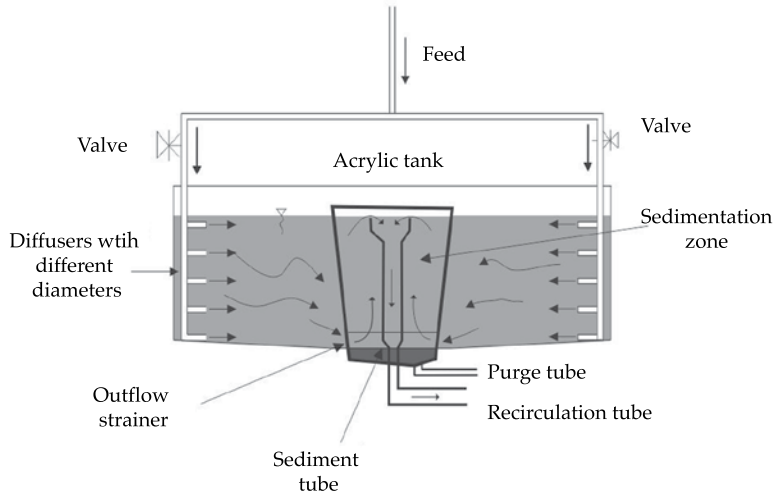

(a)

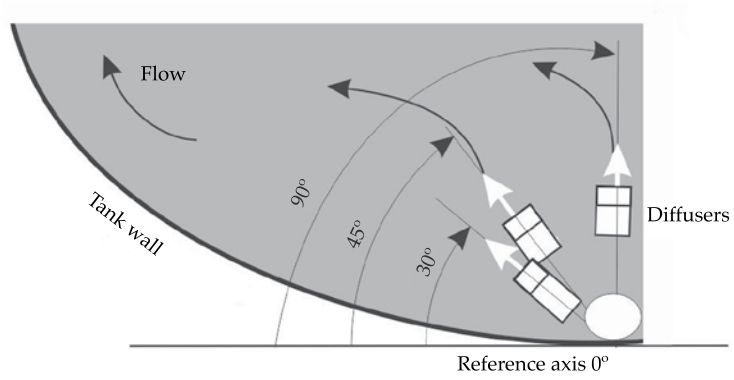

(b)

Figure 2. Location of feed diffusers: a) direction of diffusers, b) position of diffusers.

higher or lower velocity zones, depending on the need, in order to improve the solid removal efficiency. Three diffuser configurations were used by the present study. The configuration data are shown in Table 2. Each train consisted of five diffusers. The direction angles were measured beginning at the tangent with the tank wall, reference 0°, and moving in a clockwise direction (Figure 2). Figure 2b shows the distribution of the diffusers, which created a circular flow in the canal.

The hydrocyclone principle was used as an outflow device (Timmons *et al.*,1998), with a modification to enable the settling of particles.

This device consisted of two concentric tubes in the center of the tank. The outer tube was 30 cm in diameter and 35 cm high, with grooves along the bottom perimeter to enable water to enter. It ascended up to the inner tube, measuring 10 cm in diameter and 30 cm high. The latter was connected to an outlet tube for recirculation (Figure 2a).

To install the PIV system, a 15 mJ, Nd:YAG, double pulse laser light source was used. This equipment made it possible to illuminate the area of analysis (10 x 10 cm). To capture the images, a Lumenera (60 fps) camera with a CCD sensor and a JAI (250 fps) CCD camera with a sensor were used. They were equipped with a 50 mm Nikon lens and synchronized with the laser light source using a NI-PCIEE-1430 National Instruments synchronization card.

The experiment consisted of two stages. The first was to conduct the experiments to determine the hydrodynamic behavior of the tank, for which the different inflow and outflow configurations were evaluated. Three different flows were used, taking as a reference the range of velocities appropriate for the adequate growth of the fish (Gallego-Alarcón, 2010) and selecting those which presented better conditions for the settling of particles. The second stage involved determining the behavior of the sediments which, because of their origin, are considered cohesive. To this end, the sedimentation velocity was determined. During this stage, the fish food in the aquaculture tank was used as cohesive sediments and characterized to obtain its granulometry.

The velocity fields were obtained by applying the PIV and PTV techniques. Velocity profiles were also calculated to analyze flow behavior, applying the statistical analysis described in Salinas (2007). The experiments were conducted using uniform flow conditions with water as the fluid, at 15°C (kinematic viscosity of 1 x 10^{-6} m^2/s). To eliminate impurities, a filter was used which retained particles over 5 μm, which could interfere in the processing of the images given that 25 μm diameter PSP polyamide tracer particles were used, with a density of 1.03 g/cm^3. Fish food was used as the sediment, which was filtered to obtain particle sizes under 75 microns in order to stimulate the formation of flocs and determine their fall velocity.

To determine the velocity fields of the fluid as well as the sediments, an average of 100 images per run, with three repetitions per configuration, were obtained from the inflow and outflow systems (configurations A, B and C), in a zone illuminated by a laser light sheet.

In configurations A and B, the two diffuser trains were on opposite sides of the tank (Figure 2a) and had the same diameter. In configuration C, the two trains were on the same side of the tank and parallel; one had a diameter of 3.18 mm and the other 1.98 mm.

As can be seen in the configurations, the directions of the diffusers at the top of the tank were 45° or less, in order to obtain higher velocities in that zone of the tank and facilitate flocculation processes using differential velocity. The configurations at the bottom of the tank had angles of 90° or larger in order to reduce the velocity in that zone of the tank and accelerate settling processes.

The images were processed using PIV, with *SwPIV* software for the hydrodynamics of the tank. To determine the fall velocity of settled particles, the PTV technique was used with *PTVsed* V.1.0 software, developed to characterize non-spherical and non-uniform particles (Salinas-Tapia, García-Aragón, Moreno, & Barrientos, 2006).

Particle tracking velocimetry (PTV) was used to calculate the fall velocity of flocs, which is a suitable technique to determine the velocity of disperse particles in a biphasic system (Salinas, 2007). To obtain the velocity of the flocs and the fluid, the flow of the tracer particles, with different densities, needed to be added to the disperse phase. This made it challenging to determine the velocity for the different phases (Chetverikov, Nagy & Verestóy, 2000; Guasto, Haung, & Breuer, 2005; Udrea, Bryanston-Cross, Lee, & Funes-

Gallanzi, 1996). In addition, when dealing with a solid-liquid system (sediment transport), the problem is even greater since the particles do not have a uniform shape or diameter, creating a more complex behavior than conventional biphasic flow.

Results

The analysis of the results consisted of determining the fall velocities of the flocs and the hydrodynamic conditions for this to occur. In addition, the hydrodynamic conditions favoring the removal of solids were identified. To this end, the optimal physical characteristics of the settler were determined, for the purpose of generating concentrations of solids suitable to the growth of the fish.

As a result of applying the PIV technique, 2D velocity fields were obtained for each inflow configuration. Figure 3 shows only the velocity fields corresponding to configuration C, which presented the best hydrodynamic behavior since the distribution of the velocities was variable throughout the width and height of the tank. In this configuration, the maximum velocity of 11.05 cm/s was obtained at the wall of the tank at a height of 15 cm and the minimum velocity was 3.75 cm/s near the outer hydrocyclone tube at a height of 15 cm. This made it possible to accelerate contact among particles at the top of the tank and create suitable conditions for the settling of particles at the bottom. This behavior was not achieved with configurations A and B.

Figure 4 shows a comparison of the velocity profiles obtained with configurations A, B and C. The profiles shown indicate that the velocity in the tank was variable, which is not taken into account in the conventional design of a tank. This depends on the configuration of the inflow devices, primarily the direction of the flow injection. This 2D spatial analysis makes it possible to establish the criteria to be taken into account for the hydrodynamics of tanks, which are important for the particles to be able to efficiently settle and to create optimal conditions for the growth of fish. The key to success is the distribution and installation of the inflow and outflow devices. As seen in Figure 4, the direction and diameter of the diffusers must be established in order to guarantee conditions for a high settling rate while also addressing optimal conditions for the fish to adequately grow according to their size (Gallego-Alarcón, 2010).

The center outer tube is an important factor in the design of tanks, to allow for the settling of particles. The diameter of the center outer tube (D_{tc}) depends on the flow supplied, Q, and the characteristics of the sediments that need to be removed, particularly their fall velocity (W_s). The velocity at which they rise in the settler must be less than the fall velocity of the sediments. If the main settler is made up of an outer tube and an inner tube of radius $D_{tc}/3$, the following should be met:

$$V_{as} = \frac{Q}{\pi\frac{D_{tc}^2}{4} - \pi\frac{\left(\frac{D_{tc}}{3}\right)^2}{4}} \quad (1)$$

If $V_{as} < W_s$, then the following should be met:

$$D_{tc} > 1.19\sqrt{\frac{Q}{W_s}} \quad (2)$$

The greatest difficulty is related to defining the value of W_s, since that fall velocity is not constant, given the wide range of sediments, and that fall velocity not only depends on the diameter but also on the density of the cohesive sediments.

In this investigation, the definition of a suitable fall velocity was explored in depth. To this end, a formula was experimentally calibrated to relate the density of the flocs with their diameter, which was measured experimentally using the PTV technique. Figure 5a shows an image with settled particles (flocs), in which their variability can be seen. Figure 5b shows a velocity field of flocs, determined with PRV, in which variations can also be observed.

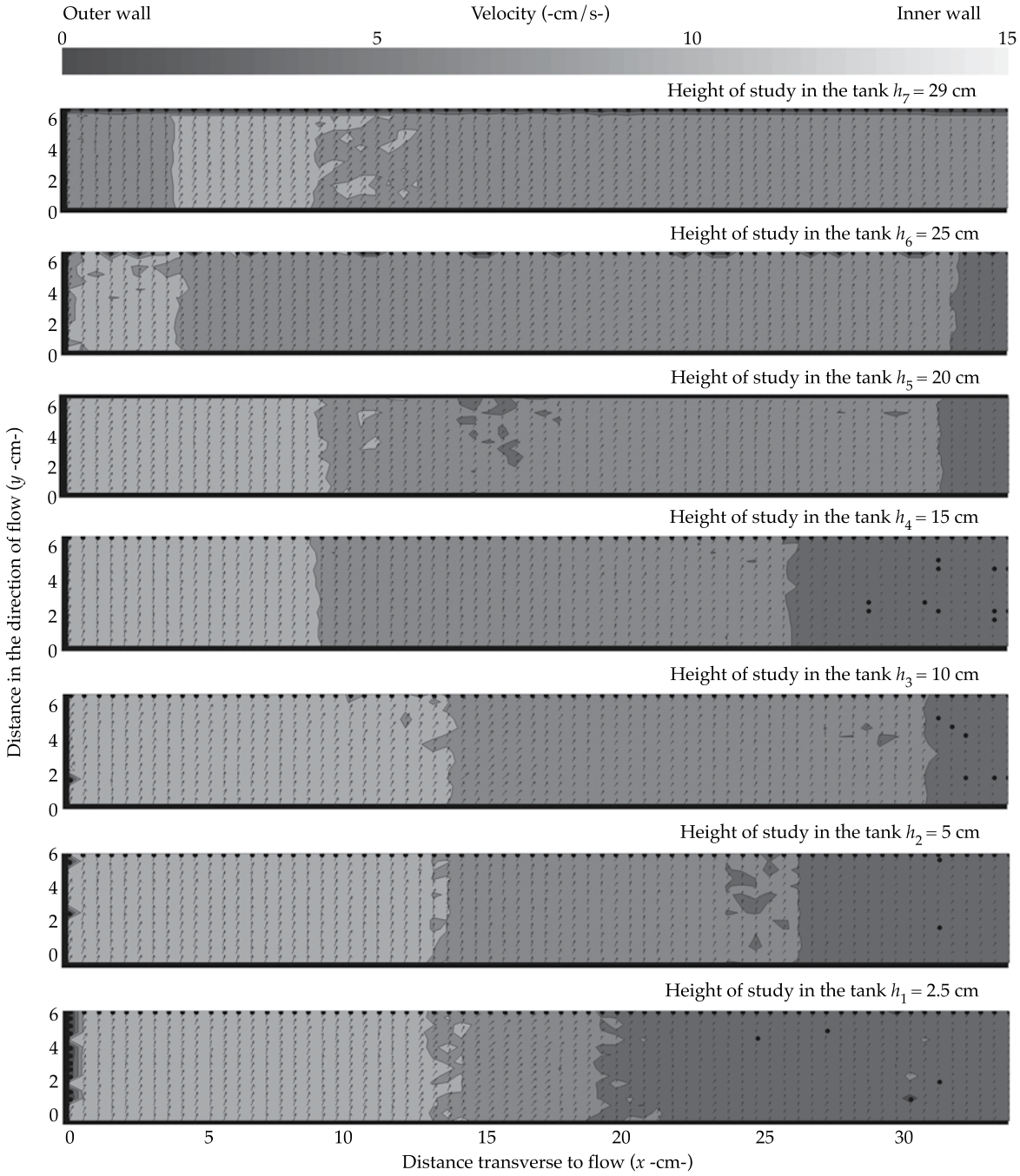

Figure 3. Velocity fields for configuration C.

Using the following formula proposed by Lau and Krishnappan (1997):

$$\rho_s - \rho_w = \left(\rho_p - \rho_w\right) \exp\left(-bD^c\right) \qquad (3)$$

Where ρ_s is the density of the sediment (flocs); ρ_p is the density of the main particles that constitute the aggregate; and b and c are two constants which depend on the type of flocs and shear rate.

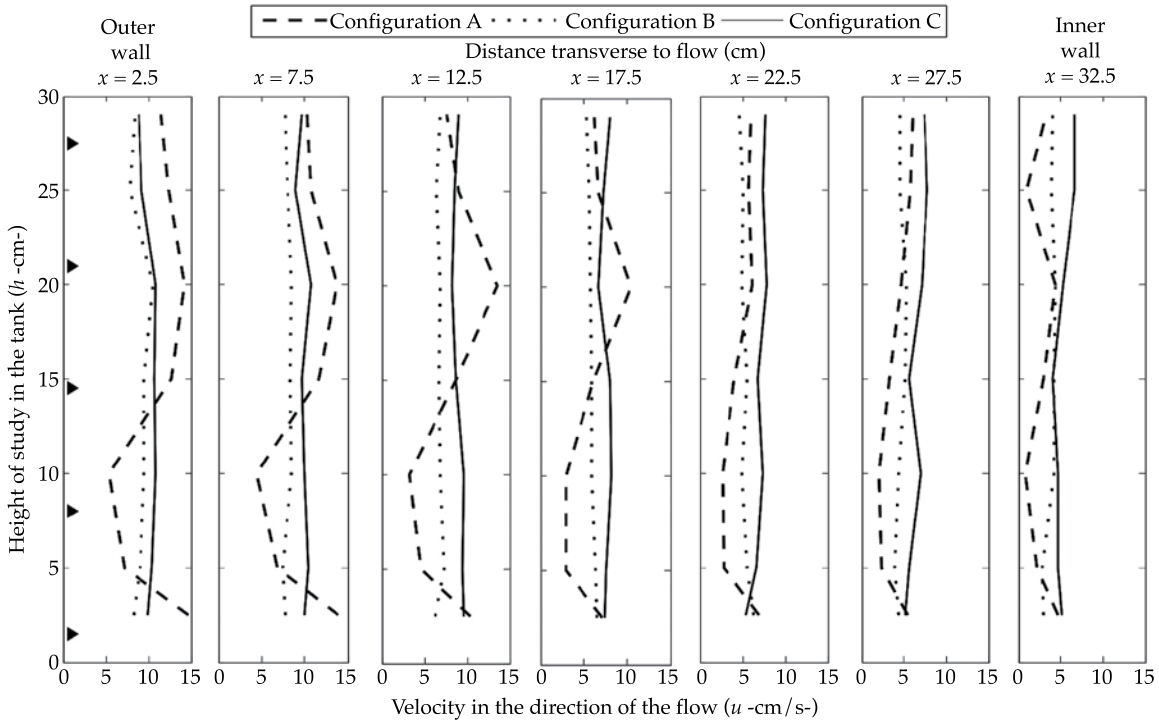

Figure 4. Comparison of velocity profiles for the different configurations (A, B and C) and at different distances in the direction transverse to the flow.

By balancing the lift and settling forces, the fall velocity obtained is:

$$Ws^2 = \frac{4(\rho_s - \rho_w)gD}{3C_d\rho_w} \qquad (4)$$

If equation (3) is replaced by (4) and the drag coefficient is defined as $Cd = 24/Rep$, where $Rep = \rho_w W_s D/\mu$ and μ is the dynamic viscosity of the water, then equation 4 is rewritten as:

$$Ws = \frac{(\rho_p - \rho_w)g\exp(-bD^c)D^2}{18\mu} \qquad (5)$$

Coefficients b and c are calibrated using the diameter of the flocs, in microns. Knowing that $\mu = \rho_w \nu$, where v is the kinematic viscosity of the water, which at 20°C is $1*10^{-6}$ m^2/s, and considering that D is in microns, equation (5) is written as:

$$Ws = 5.45*10^{-7}\left(\frac{\rho_p}{\rho_w} - 1\right)\exp(-bD^c)D^2 \qquad (6)$$

Where D is the diameter of the flocs, in microns, and the velocity is W_s in m/s.

With the experimental data, the values of b and c that best reproduced the fall velocities measured by PTV were determined.

Next, the experimental data from the flocs (product of fish food with diameters between 20 and 150 microns, and a mean density of 1 430 kg/m^3) that best fit equation (6) are presented.

Images were taken every five minutes for experiments lasting roughly one hour. Some of the data fitted to equation (6) are shown. Figures 6 and 7 show that the data for the fall velocity of flocs obtained experimentally using PTV were adequately fitted to equation (6), with values of $b = 0.0037$ and $c = 1.1$. In addition, a flocculation process can be observed, where the diameters of the main particles were less than

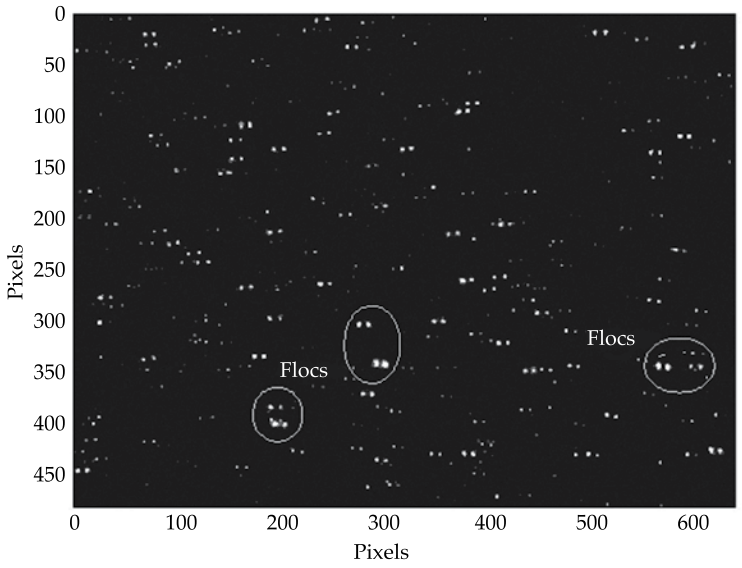

(a)

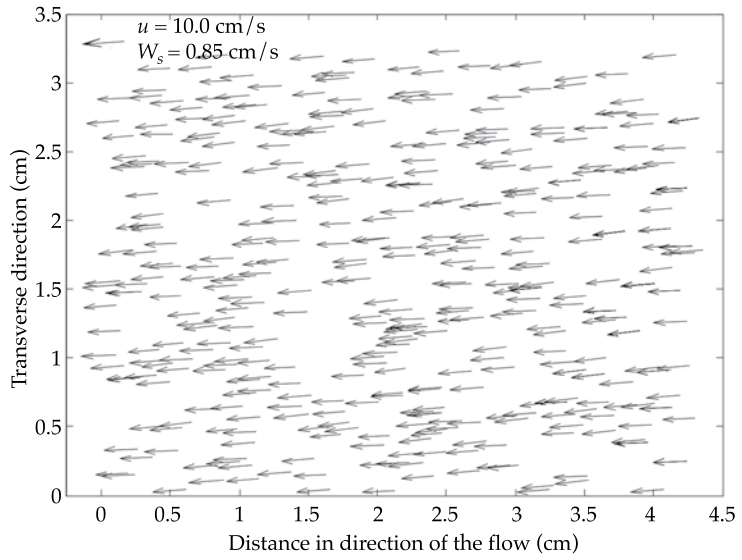

(b)

Figure 5. Application of the PTV technique: a) image of particles (flocs); b) velocity fields of sedimentary particles (flocs).

75 microns. Diameters over 300 microns were obtained from the result of the analysis of the images.

Therefore, equation (7) is the resulting equation to calculate the fall velocity of the sediments from the fish food. This can be used to design recirculation tanks with self-cleaning characteristics for use in aquaculture, without neglecting the selection of the inflow and outflow systems, considering main particles with a density of 2 650 kg/m^3.

$$Ws = 9 * 10^{-7} D^2 \exp\left(-0.0037 D^{1.1}\right) \qquad (7)$$

In which W_s is in m/s and D in microns.

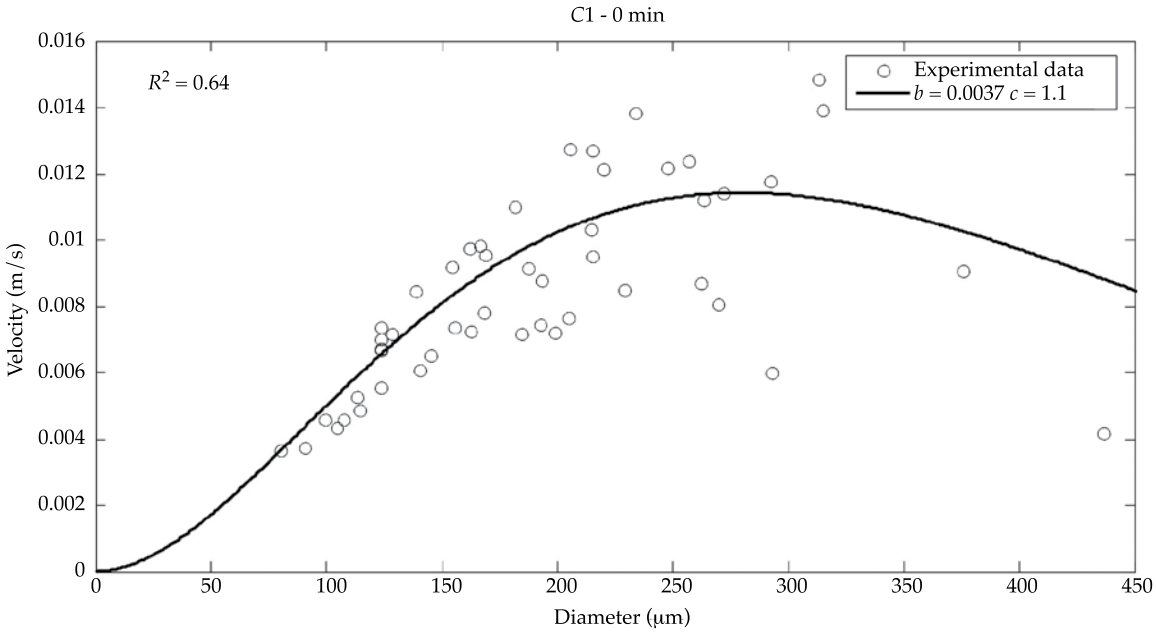

Figure 6. Experimental results for fall velocity of sediments, t = 5 minutes.

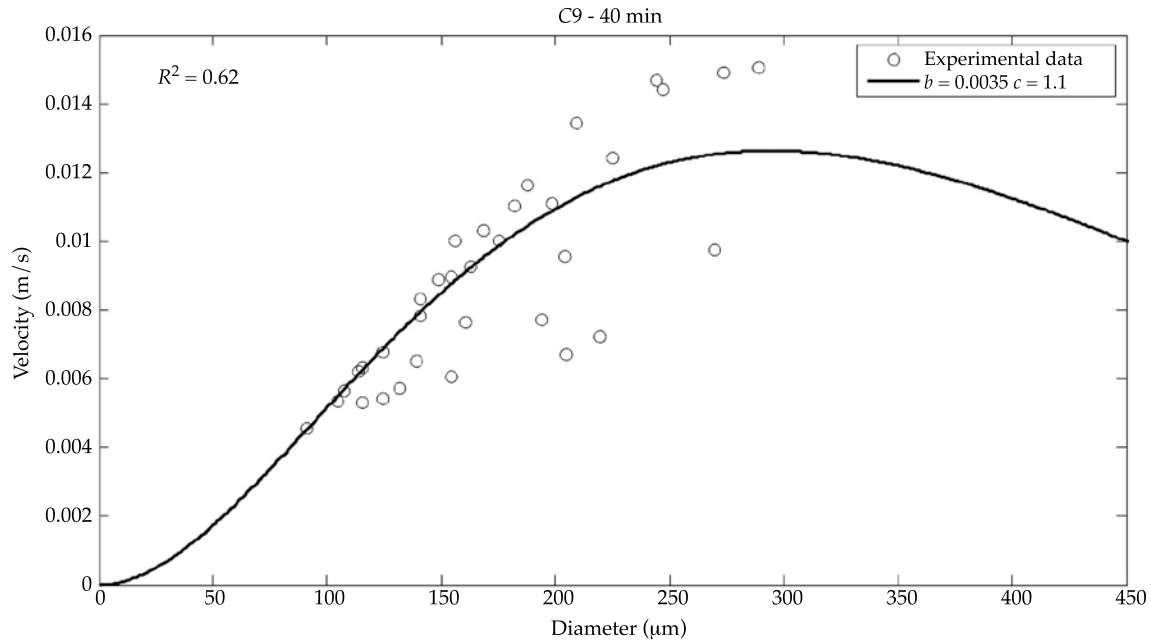

Figure 7. Experimental results for fall velocity of sediments, and fit for t = 40 minutes.

Conclusions

Using a full-scale model of an aquaculture recirculation tank and fish food, the variables governing the functioning of this type of tank were optimized. Using the PIV technique, the flow characteristics and distribution of diffusers producing adequate tank hydrodynamics were determined, enabling flocculation and sedimentation processes to occur. Using the PTV technique, a formula was proposed to determine the characteristics of the main settler that would produce the best removal of sediments.

It was possible to demonstrate that the optimal diameter of the settler depends on the fall velocity of the sediments present in the tank (equation (2)). The greatest difficulty was adequately estimating that fall velocity. This investigation used advanced optical techniques (PIV and PTV) which made it possible to calibrate a formula to estimate the fall velocity in function of the physical characteristics of the sediment and the hydrodynamics of the recirculation tank (equation (7)).

With the results obtained from the different inflow and outflow configurations and the application of the optical PTV and PIV techniques to determine velocity fields, it was possible to establish the hydrodynamic criteria to be considered in the design of this type of tanks. These criteria are inflow and outflow conditions, which affect the distribution of the flow velocity on the vertical and the sedimentation velocities of the flocs.

References

Adrian, R. J. (1991). Particle-Imaging Techniques for Experimental Fluid Mechanics. *Annu. Rev. Fluid Mech*., *23*, 261-304.

Chetverikov, D., Nagy, M., & Verestóy, J. (2000) Comparison of Tracking Techniques Applied to Digital PIV. *Proc. 15th ICPR*, Barcelona, Spain.

Droppo, I. G., & Ongley, E. D. (1994). Flocculation of Suspended Sediment in Rivers of Southeastern Canada. *Water Research*, *28*, 1799-1809.

Droppo, I. G. (2001). Rethinking what Constitutes Suspended Sediment. *Hydrological Processes*, *14*, 653-667.

Droppo, I. G. (2005). Suspended Sediment Transport-Flocculation and Particle Characteristics. *Encyclopedia of Hydrological Sciences*. M. G. Anderson (Ed.). New York: John Wiley & Sons, Ltd.

Duarte, S., Reig, L., Oca, J., & Flos, R. (October, 20-23, 2004). Computerised Imaging Techniques for Fish Tracking in Behavioural Studies. Biotechnologies for Quality. *Proceedings of the European Aquaculture Society* (pp. 310-311). Vol. 34. EAS Special Publication. Barcelona, Spain.

Gallego-Alarcón, I. (2010). *Evaluación y modelación de un tren de tratamiento de agua residual acuícola con recirculación y del cultivo de trucha arco-iris alimentado por cosecha pluvial*. Tesis de doctorado en Ciencias del Agua. Toluca, México: Universidad Autónoma del Estado de México.

Gallego-Alarcón, I. (2004). *Diseño y evaluación de un sistema prototipo para el tratamiento de agua residual acuícola con reúso de agua en el cultivo de* Oncorhynchus mykiss *en la fase alevín-juvenil*. Tesis de maestría. Toluca, México: CIRA, Facultad de Ingeniería, UAEM.

Gallego-Alarcón, I., García, D., Díaz, C., & Fall, C. (2004). Production of Juveniles of Oncorhynchus mykiss Using an Aquaculture Water Treatment Plant. En: Adams S. & J. Olafsen (Eds.). *Biotechnologies for Quality* (884 pp.). Bruselas: EAS.

García, P. D. (2008). *Evaluación de un sistema prototipo integral de cultivo de trucha con tratamiento y reciclado del efluente*. Tesis de Doctorado. Toluca, México: CIRA, Facultad de Ingeniería, UAEM.

García-Aragón, J., Droppo, I., Krishnappan, B., Trapp, B., & Jaskot, C. (2011). Experimental Assessment of Athabasca River Cohesive Sediment Deposition Dynamics. *Water Quality Research Journal of Canada*, *46*(1), 87-96.

Guasto, J. S., Haung, P., & Breuer, K. S. (November, 5-11, 2005). Statistical Particle Tracking Velocimetry Using Molecular and Quantum Dot Tracer Particles. *Proceedings of IMECE 2005-80051*, Orlando, Florida, USA.

Lau, Y. L., & Krishnappan, B. G. (1997). Measurement of Size Distribution of Settling Flocs. NWRI. Publication No. 97-223. Ontario: National Water Research Institute, Environment Canada, Burlington.

Nicholas, A. P., & Walling, D. E. (1996). The Significance of Particle Aggregation in the Overbank Deposition of Suspended Sediment on River Floodplains. *Journal of Hydrology*, *186*, 275-293.

Salinas-Tapia, H., García-Aragón, J. A., Moreno, D., & Barrientos, G. B. (2006). *Particle Tracking Velocimetry (PTV) Algorithm for Non-Uniform and Nonspherical Particles* (pp. 322-327). Vol. II. Cuernavaca, México: CERMA.

Salinas, T. (2007). *Determinación de parámetros para flujo bifásico (sólido-líquido) por medio de técnicas ópticas*. Tesis de doctorado en Ingeniería. Toluca, México: Centro Interamericano de Recursos del Agua, Facultad de Ingeniería, UAEM.

Salinas-Tapia, H. & García-Aragón, J. A. (2011). Fórmula experimental para determinar la velocidad de caída de sedimentos en flujo transversal. *Tecnología y Ciencias del Agua,* 2(2), 175-182.

Sundaresan, S., Eaton, J., Koch, D., & Ottino, J. (2003). Appendix 2: Report of Study Group on Disperse Flow. *International Journal of Multiphase Flow*, *29*, 1069-1087.

Timmons, M. B., Summerfeld, S. T., & Vinci, B. J. (1998). Review of Circular Tank Technology and Management. *Aquacultural Engineering*, *18*, 51-69.

Udrea, D. D., Bryanston-Cross, P. J., Lee, W. K., & Funes-Gallanzi, M. (1996). Two Sub-Pixel Processing Algorithms for High Accuracy Particle Centre Estimation in Low Seeding Density Particle Image Velocimetry. *Optics. & Laser Tech*, *28*, 389-396.

Sommerfelt, S. G., Wilton, G., Roberts, D., Rimmer, T., & Fonkalrsrud, K. (2004). Developments in Recirculating Systems for Artic Char Culture in North America. *Aquacultural Engineering*, *30*, 31-71.

Watten, B. J., & Beck, L. T. (1987). Comparative Hydraulics of Rectangular Cross Flow Rearing Unit. *Aquaculture Engineering*, *6*, 127-140.

Wheaton, F. W. (1977). *Aquaculture Engineering* (708 pp.). New York: Wiley-Interscience.

Institutional Address of the Authors

Dr. Juan A. García-Aragón
Dr. Humberto Salinas-Tapia
M.C.A. Víctor Díaz-Palomarez
Ing. Boris M. López-Rebollar
Ing. Javier Moreno-Guevara
Ing. Leonarda M. Flores-Gutiérrez

Centro Interamericano de Recursos del Agua
Facultad de Ingeniería
Universidad Autónoma del Estado de México (UAEM)
Cerro de Coatepec, CU
50130 Toluca, Estado de México
Teléfono: +52 (722) 2965 550
jagarciaa@uaemex.mx
hsalinast@uaemex.mx
palomarez64@hotmail.com

Click here to write the autor

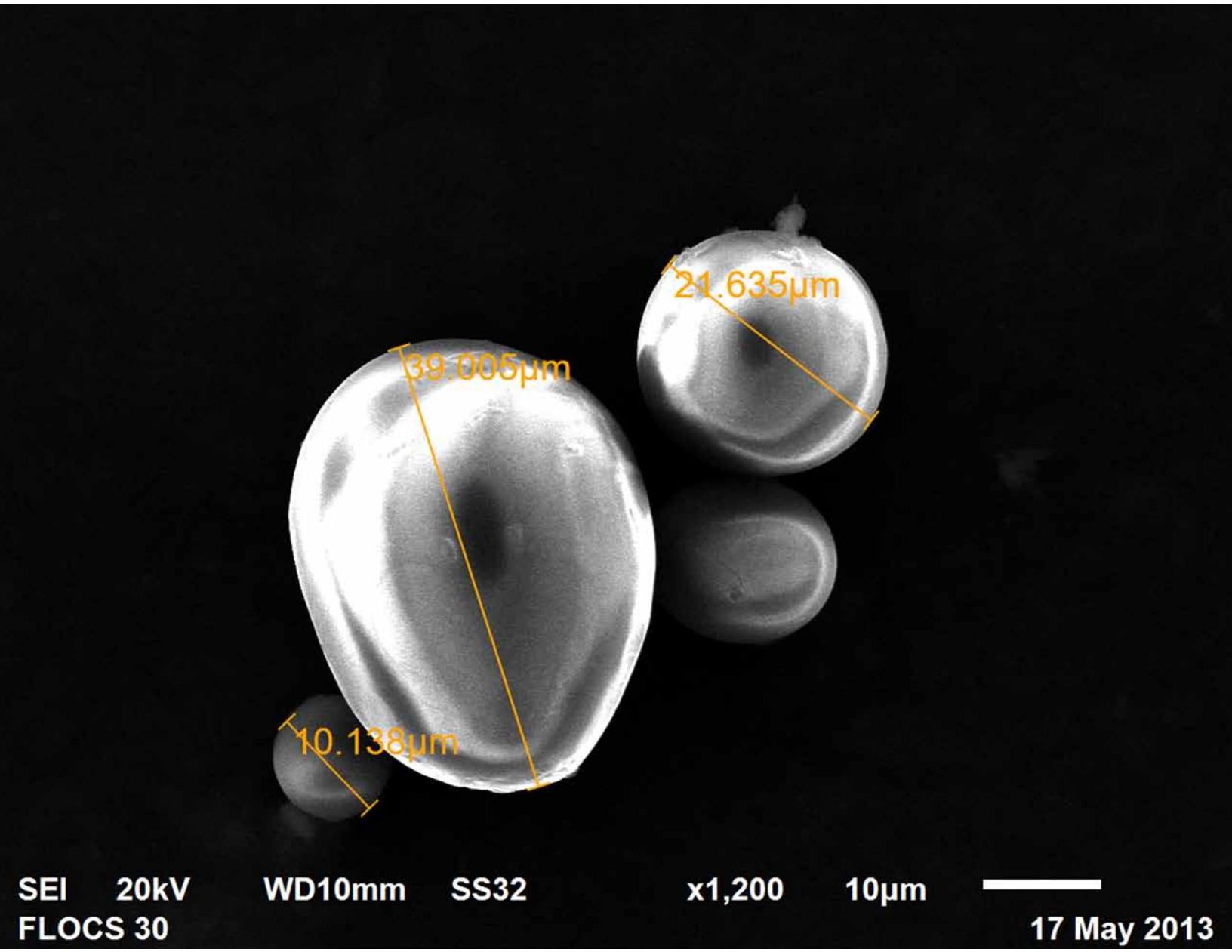

Flocs of fish food seen through an electronic sweep microscope (TEM).

Photo provided by Juan Antonio García Aragón.

Irrigation Water Quality in the Sierra Norte in Puebla, México

• Álvaro Can-Chulim* •
Universidad Autónoma de Nayarit, México
*Corresponding Author

• Héctor Manuel Ortega-Escobar •
Colegio de Postgraduados, México

• Edgar Iván Sánchez-Bernal •
Universidad del Mar, México

• Elia Cruz-Crespo •
Universidad Autónoma de Nayarit, México

Abstract

Can-Chulim, A., Ortega-Escobar, H. M., Sánchez-Bernal, E. I., & Cruz-Crespo, E. (September-October, 2014). Irrigation Water Quality in the Sierra Norte in Puebla, México. Water Technology and Sciences (in Spanish), 5(5), 73-91.

Water is crucial to the state of Puebla because of its importance to increasing economic development. Most of the surface water is found in the Sierra Norte, where it is primarily used for agriculture. Wastewater and water from thermal springs spill into the river channels, modifying the quality. Since different sources and concentrations of surface water are used in agriculture, its concentration and chemical compositions were determined in order to evaluate its quality for use in agriculture. The primary quality parameters and their values were: pH, mean of 7.7, minimum 6.1 and maximum 9.2; mean electric conductivity 346, minimum 61.0 and maximum 1913.0 µS cm^{-1}; sodium adsorption ratio (SAR) with SAR means RAS = 1.0, RASaj = 1.4 and RAS^{o} = 1.0; residual sodium carbonate, with positive values in the springtime and negative in autumn; and boron, mean of 0.7, minimum 0.0 and maximum 4.0 mg L^{-1}. Surface water in the Sierra Norte is suitable for irrigation. Its ionic concentration is low since it comes from runoff, with greater variations where it receives water from thermal springs and more moderate variations where it receives wastewater. The hydrogeochemistry indicates that the dominant chemical characteristics result from the physical and chemical processes of the water due to the regional geology. The water is bicarbonate, with variations in sodium and calcium. Sodium is predominant in the dry season and calcium predominates in the rainy season.

Keywords: Adjusted SAR, bicarbonate water, corrected SAR, dilution, precipitation.

Resumen

Can-Chulim, A., Ortega-Escobar, H. M., Sánchez-Bernal, E. I., & Cruz-Crespo, E. (septiembre-octubre, 2014). Calidad del agua para riego en la Sierra Norte de Puebla, México. Tecnología y Ciencias del Agua, 5(5), 73-91.

En el estado de Puebla, el agua es de gran importancia, ya que condiciona la posibilidad de incrementar el desarrollo económico. La mayor proporción de agua superficial se encuentra en la Sierra Norte, donde se emplea principalmente en la agricultura. A los cauces de los ríos se vierte agua de origen residual y de nacimientos termales, que modifican la calidad. Como el agua superficial de diferente origen y concentración se utiliza en la agricultura, se determinó su concentración y composición química, con el objetivo de evaluar su calidad para uso agrícola. Los principales parámetros de calidad y sus valores fueron: pH, media de 7.7, mínimo 6.1 y máximo 9.2; conductividad eléctrica, media de 346, mínimo 61.0 y máximo 1 913.0 µS cm^{-1}; relación de adsorción de sodio (RAS) con medias de RAS = 1.0, RASaj = 1.4 y RAS^{o} = 1.0; carbonato de sodio residual, con valores positivos en primavera y negativos en otoño; boro, media de 0.7, mínimo 0.0 y máximo 4.0 mg l^{-1}. El agua superficial de la Sierra Norte es apta para el riego, su concentración iónica es baja, debido a que proviene de los escurrimientos pluviales, teniendo variaciones mayores donde recibe agua de nacimientos termales y moderadamente donde recibe residuales. La hidrogeoquímica indica que el carácter químico dominante del agua es resultado de los procesos físico-químicos del agua con la geología regional. El agua es bicarbonatada, con variaciones en sodio y calcio. En temporada de estiaje, el sodio predomina, y en lluvias, el calcio.

***Palabras clave**: RAS ajustado, RAS corregido, agua bicarbonatada, precipitación, dilución.*

Received: 07/11/12
Accepted: 25/01/14

Introduction

The concept of water quality refers to the characteristics of the water that can affect its applicability for a specific use. Water quality is defined by physical, chemical and biological characteristics (Ayers & Westcot, 1987). For agricultural use, it is defined by the concentration of specific ions: Ca^{2+}, Mg^{2+}, Na^{+} and K^{+} as cations and CO_3^{2-}, HCO_3^{-}, Cl^{-} and SO_4^{2-} as anions; and others in lower proportions, such as B_3^{+} and P (Nishanthiny, Thushyanthy, Barathithasan, & Saravanan, 2010; Korzeniowska, 2008). In addition, Silva (2004) states that the most important characteristics for determining the quality of water for irrigation are total concentration of soluble salts, relative concentration of sodium with respect to other cations, the concentration of boron or other elements that can be toxic and, under certain conditions, the concentration of bicarbonates relative to the concentration of calcium plus magnesium. In other words, the quality of irrigation water is determined by the concentration and composition of the dissolved constituents it contains.

The importance of identifying the quality of irrigation water is to be able to predict its effect on soil and crops (Rashidi & Seilsepuor, 2011). To this end, the qualitative and quantitative concentrations of ions in solution must be determined, particularly the ions that cause toxicity and those that produce the formation of toxic salts.

The most common problems caused by poor quality irrigation water include the gradual salinization of the soil, which causes osmotic problems for plants, and the toxicity of some salts and ionic elements. The osmotic factor can be explained in terms of the saline concentration —the greater the concentration the less the osmotic potential and, therefore, less water will be available for the plants (Casierra & Rodríguez, 2006; Baccaro *et al.*, 2006). With respect to toxicity, a high concentration of salts or ions will cause toxic effects in plants. The degree of toxicity will depend on the type of salt or ion that is predominant. Toxicity is commonly reflected by physiological and morphological changes in leaves (Strogonov, 1964; Sánchez *et al.*, 2002). The defense mechanism used by plants in the presence of saline stress is osmotic adjustment, which consists of the accumulation of solutes in response to the a water deficit and a decrease in the total hydric potential of leaves, stems and roots. Although the plants can absorb water and maintain their physiological activity, this osmotic adjustment requires an expense of energy which translates into decreased vegetation growth and plant productivity, among other effects (Silva, Ortiz, & Acevedo, 2007).

The elements in water and soil result from the chemical weathering (hydrolysis, hydration, solution, oxidation and carbonatation) of rocks when coming into contact with water. Then, these elements form into salts in the soil and accumulate, as a result of many geochemical processes that occur in the surface layers of the earth's crust (Grattan, 2006). In the sedimentary rocks and soils —weathering layers— a large portion of the salts are found in crystalline form and, when moistened, some of them change into the liquid phase. As the temperature rises, the solubility of some of the salts increases. The sequence of the precipitation of the salts of a polycomponent solution depends on the degree of solubility. The process of precipitation has been widely studied in water with high saline contents. First, the silicon and iron hydroxides precipitate, then the calcium and magnesium carbonates, and the gypsum and magnesium sulfates, and lastly, sodium, potassium and magnesium chlorides (Szabolcs, 1989).

The main process involved in the salinization of agricultural soils is the application of irrigation water when its use is not in accordance with its quality. Most of the types of irrigation water considered to be dangerous have a relative salt content which is not very

harmful in itself. The problem is when that water interacts with the saline concentration in the soil (Rashidi & Seilsepuor, 2011). Evaporation and transpiration consume large amounts of water and decrease the moisture of the soil, but do not affect the dissolved salts. Therefore the solution of the soil becomes more saline as the soil becomes drier. For this reason, saline concentration levels that are initially acceptable in water can reach high values in the soil. In addition, other phenomena occur when salts become concentrated. For example, some can reach their solubility limit and precipitate, withdrawing certain cations from the soil solution and altering the initial proportions (Miyamoto & Pingitore, 1992). This commonly occurs with certain low solubility calcium salts ($CaCO_3$ and $CaSO_4$), resulting in an increase in the proportion of sodium in the soil solution and in the percent of exchangeable sodium (Silva, 2004).

In the state of Puebla, water is very important since it strongly influences the ability to increase economic development. Currently agriculture uses 48.97% of the total area of the state and 78% of the water is used for this activity (Guevara-Romero, 2011; López-Téllez, 2011). Most of the surface water in the state is located in the Sierra Norte, where it is primarily used in agriculture, followed by industry, aquaculture and therapy. Wastewater from industries and different towns in the region is discharged into rivers. Since surface water is available year-round, farmers use it directly, without prior treatment, to irrigate their main crops. Given this background, it is suggested that geological materials in the region and wastewater discharges modify the qualitative and quantitative concentration of ions in solution, that is, the quality of the water. Since surface water from different sources and with different concentrations is used in agriculture, this study determined the chemical composition and total electrolytic concentrations in order to evaluate its use in agriculture.

Methodology

Location and characteristic of the study area

Sierra Norte de Puebla is geologically located primarily in the Sierra Madre Oriental, with a small portion in the Neovolcanic Axis. It is part of the physiographic province of Sierra Madre Oriental, a physiographic subprovince of Carso Huasteco, which runs through the state of Puebla. It is located in the north-central portion of the state, between coordinates 19° 39′ north latitude and 97° 15′ west longitude.

Geological Background

This region is entirely mountainous and covers practically the whole northern mountain region, which is part of the Sierra Madre Oriental. Its topography is relatively modern and its rivers have many waterfalls and cascades. The altitude ranges between 1 000 and 3 000 m. The rocks that make up the Sierra Norte are primarily thick layers of limestone, intercalated slate and sedimentary lutites and sandstone. Nearly all the rocks are Mesozoic. The sedimentary rocks are found in layers of different thickness and are resistant to erosion processes and cortical forces. They form large structures that bend and twist in small angles (Capra, Lugo-Hubp, & Zamorano-Orozco, 2006).

The orogenic deformations are what mostly make up the original topography, on which erosion process have acted, controlled by systems of faults and fractures. The dissolving effect of water has contributed to generating a karstic morphology and deep canyons have been carved out, draining different rivers into the Gulf of Mexico.

Hydrology

The Tuxpan-Nautla hydrological region is located in the northern portion of the state of Puebla, represented by parts of the Tecolutla, Cazones and Tuxpan river watersheds,

which flow into the Gulf of Mexico. The main hydrography includes the northern watershed, where the main river is the Tecolutla River, in the Sierra Norte, which is composed of the Necaxa, San Marcos, Tenango, Laxaxalpan, Tecuantepec or Zempoala, Joloapan, Apulco and Chichicatzapa. The important Necaxa hydroelectric system was built with water from the upper portion of the three main rivers. The north-southwest area contains the Ajajalpa and the Marimba rivers, two of the main rivers, and lakes Cruz Colorada, Cuatelolulco, Ajolotla and Chignahuapan (Galván *et al*., 1999). Several of these rivers come from surface runoffs and springs in the area.

The river channels have been carved out through unconsolidated granular volcanic material deposited during volcanic events occurring after the compression stage, produced by tectonic movements and causing marine rocks to rise and become exposed (Cuanalo & Melgarejo, 2002).

The runoff patterns are dictated by the Sierra Madre Oriental. Runoff from the large rivers originates in its eastern watershed. The small streams are perennial because of high infiltration, and they are used for agriculture. There is a also a series of small reservoirs used for this purpose (Galván *et al*., 1999).

Climate

The climatic in the Sierra Norte de Puebla includes a series of northwest-southeast strips bands which generate a hot and semi-hot humid climatic gradient in the lower elevations and temperate humid in the higher elevations (Martínez, Evangelista, Basurto, Mendoza, & Cruz-Rivas, 2007). In the highest elevations, annual precipitation is roughly 3 000 mm (Murillo-Licea, López-Ramírez, Chávez-Hernández, Marañón- Pimentel, & Brie-Gowland, 2010).

Soil and crops

According to Vázquez-Martínez *et al*. (2009), the predominant soil in the Sierra Norte is andosol. The primary crop species in the Sierra Norte were identified during sampling in the month of April, 2010, and included peanuts, coffee, zucchini, cilantro, peaches, beans, fava beans, corn, oranges, potatoes, peppers, alfalfa, oats, barley, tomato, wheat, apples, pears and blackberries.

Water sampling and analytical methods

In accordance with the objectives of this study, two samplings were performed, one in spring and one in autumn of 2011, with 22 sampling stations. Water samples were taken throughout the entire area (southeast-northwest) in order to obtain the best representation of the surface waters in the area. To select the sampling sites, the main factors that contribute to altering the quality of water were considered, such as water springs from different sources and water containing wastewater. The samplings were conducted based on NMX-AA-034-SCFI-2001, with three samples per station. Figure 1 shows the location of the different sampling stations and Table 1 presents the parameters determined for each sample.

Water Quality Parameters

Given that surface water from different sources is used in agriculture, this study determined its chemical composition and total electrolytic concentrations. The values for sodium adsorption were determined —sodium adsorption ratio (SAR) and corrected sodium adsorption ratio (RAS°)— since this is an especially important parameter in the evaluation of the quality of water used to irrigate crops. This index directly affects the physiochemical properties of the soil and, thus, the plants. Boron and phosphate contents in the water samples were also determined.

Ionic Concentration

In order to prevent the salinization of soil, the quality of water for irrigation takes into account

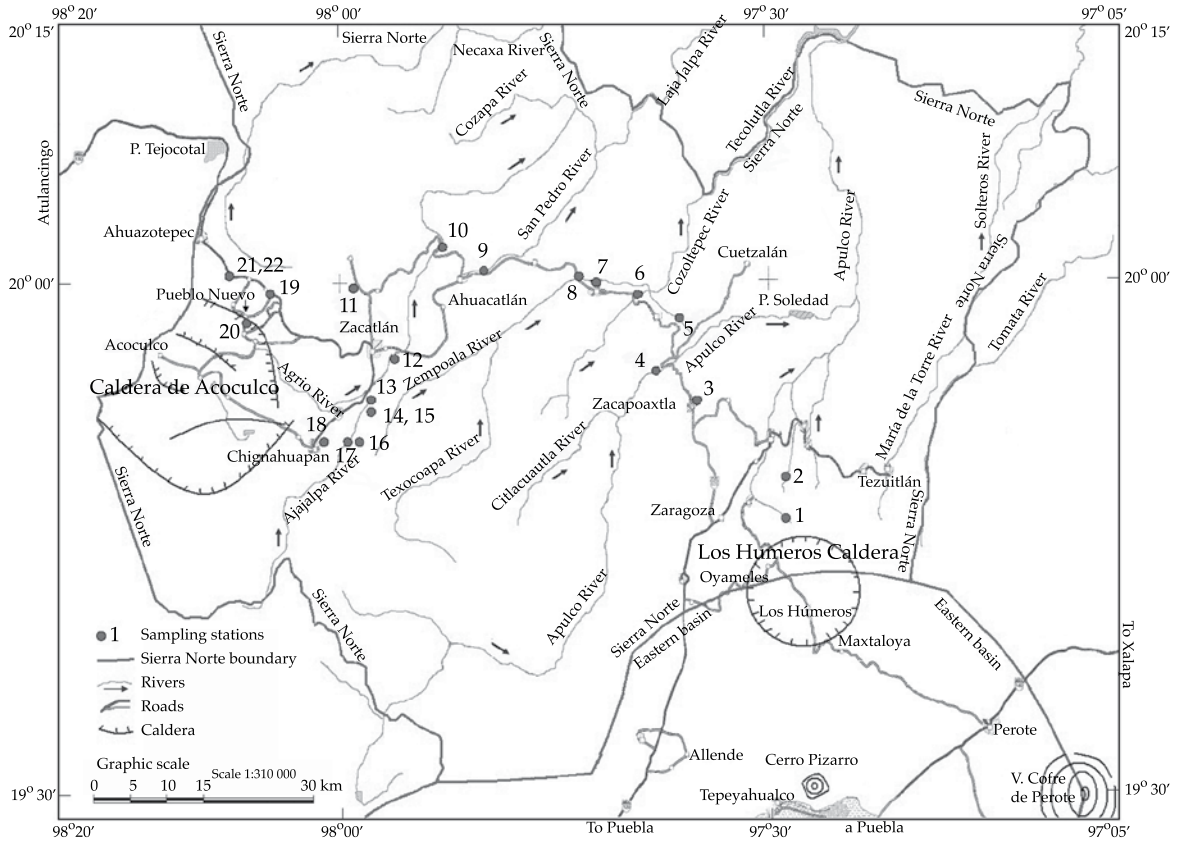

Figure 1. Location of the surface water sampling stations in the Sierra Norte de Puebla.

Table 1. Analytical marks used to determine the parameters in surface water in the Sierra Norte de Puebla.

Determination	Method	Reference
pH	Potentiometry	NMX-AA-008-SCFI-2000
Electrical conductivity	Conductometry	NMX-AA-093-SCFI-2000
Evaporated dry residue	Gravimetry	NMX-AA-034-SCFI-2001
Calcium and magnesium	Volumetry	Richards, 1990
Sodium and potassium	Flame photometry	NOM-021-SEMARNAT-2000
Carbonates and bicarbonates	Volumetry	NOM-021-SEMARNAT-2000
Chlorides	Volumetry	NMX-AA-073-SCFI-2001
Sulfates	Turbidimetry	NOM-021-SEMARNAT-2000
Boron	Colorimetry	NOM-021-SEMARNAT-2000
Orthophosphates	Colorimetry	Rodier, 1990

the concentration of total soluble salts. For diagnostic and classification purposes, it can be expressed in terms of electrical conductivity (EC) and is divided into four classes: low water salinity (C1: < 250 µS cm-1), medium (C2: 250 - 750 µS cm-1), high (C3: 750 - 2 250 µS cm-1) and very high water salinity (C4: > 2 250 µS cm-1) (Richards, 1990).

Sodium Content

With regard to the sodium content in irrigation water, this is classified using the SAR with respect to the ionic concentration (EC), according to the diagram proposed by Richards (1990). This classification is primarily based on the effect of adsorbed sodium ion on the physical conditions of the soil, that is, it predicts the effect of the sodium from irrigation water after it becomes part of the soil. Based on the SAR, irrigation water is classified according to four classes: water low in sodium (S1), medium in sodium (S2), high in sodium (S3) and water very high in sodium (S4).

By calculating the SAR for these different scenarios, the range of concentrations of Ca^{2+} ions can be predicted. Therefore, given a wide range of maximum and minimum SAR values for different solutions and considering the water that passes though the soil surface, it is possible to calculate the different levels of exchangeable sodium acquired by the soil when irrigating with water having different SAR values.

The SAR values are calculated using equations (1), the original SAR proposed by Gapon (cited by Richards, 1990); equation (2), a modification of the original or explicit SAR values for irrigation water, determined in 1968, Bower, Ogata and Tucker. These new SAR values are known as adjusted SAR (SAR_{adj}); and equation (3) a new procedure to calculate SAR, called the corrected SAR (SAR°), recommended in 1981 by Suarez, which along with the value of Ca° offers a better understanding of the changes in calcium in the soil solution:

$$SAR = \frac{C_{Na^+}}{\sqrt{\frac{C_{Ca^{2+}} + C_{Mg^{2+}}}{2}}} \quad (1)$$

$$SAR_{adj} = \frac{C_{Na^+}}{\sqrt{\frac{C_{Ca^{2+}} + C_{Mg^{2+}}}{2}}}\left[1+\left(8.4-pHc\right)\right] \quad (2)$$

The Langelier equation (1936) —pHc = (pK2´- pKc´) + *p*(Ca) + *p*(Alk)— is used to calculate pHc:

$$SAR^o = \frac{C_{Na^+}}{\sqrt{\frac{C_{Ca^o} + C_{Mg^{2+}}}{2}}} \quad (3)$$

In the above equations, Na^+, Ca^{2+} and Mg^{2+} refer to the concentration of soluble cations expressed in $mmol_c\ L^{-1}$; pHc is the theoretical pH that the water will reach in equilibrium with $CaCO_3$; pK_2 is the negative logarithm of the second disassociation constant for carbonic acid (H_2CO_3), with ionic strength correction; pK_c is the product of the solubility of $CaCO_3$ with ionic strength correction; pCa corresponds to the negative logarithm of the molar concentration of Ca; p(Alk) corresponds to the negative logarithm of the concentration equivalent to the titratable base (CO_3 + HCO_3); Ca° is the corrected calcium content in the irrigation water, in $mmol_c\ L^{-1}$; the value of Ca° represents the calcium contents in the irrigation water, corrected for the salinity of the water (EC), as well as for the bicarbonate ion content in relation to its own calcium content (HCO_3^-/Ca^{2+}) and for the partial pressure of carbon dioxide (CO_2) in the first millimeters of the soil (P = 0.0007 atm).

Residual Sodium Carbonate

Another consideration recommended by Richards (1990) when evaluating quality is the concentration of bicarbonates relative to that of calcium plus magnesium. Water with high concentrations of bicarbonate ions has a tendency for calcium and magnesium to precipitate in the form of carbonates, as the solution of the soil becomes more concentrated. Eaton (1950) refers to this action as residual sodium carbonate (RSC). This index is calculated using the following formula, where all the ionic constituents are expressed in $mmol_c\ L^{-1}$:

Residual sodium carbonate

$$(RSC) = (CO_3^{2-} + HCO_3^{-}) - (Ca^{2+} + Mg^{2+})$$

Water with a value under 1.25 is classified as good quality for agricultural use, between 1.25 and 2.5 as conditional and over 2.5 as not recommended (Nishanthiny *et al*., 2010). When the difference is negative, the problem does not exist and the RSC value can be presumed to be equal to zero. When the value is positive, this indicates that Ca and Mg precipitate as carbonates, where only sodium salts exist in the solution.

Boron

Boron is a micronutrient required by plants, for which the range between deficiency and toxicity is small (Goldberg, Corwin, Shouse, & Suarez, 2005). The contents of boron in irrigation water is expressed in mg l^{-1} and the tolerance value were established by Wilcox in 1948. For sensitive crops, under 0.33 is excellent, 0.33 – 0.67 is good, 0.67 – 1.00 is acceptable, 1.00 – 1.25 unsafe, and over 1.25 is not recommended. For semi-tolerant crops, under 0.67 is excellent, 0.67 - 1.33 is good, 1.33 - 2.00 is acceptable, 2.00 - 2.50 is unsafe, and over 2.50 is not recommended. For tolerant crops, under 1.00 is excellent, 1.00 - 2.00 is good, 2.00 – 3.00 is acceptable, 3.00 - 3.75 is unsafe and over 3.75 is not recommended.

Phosphorus

In the guidelines for interpreting the quality of irrigation water, Ayers and Westcot (1987) indicate that a phosphorus content of 2.0 mg l^{-1} is normally acceptable.

CHydrogeochemical Classification of Water

Hydrochemical or hydrogeochemical studies are used to determine the origin of the chemical composition of water and the relationship between the water and the chemical composition of the rocks. The most commonly used graphical methods for observing and classifying hydrochemical data is the trilinear Piper diagram (Ray & Mukherjee, 2008).

Statistical Analysis (association of variables) and evaluation of analytical data

Linear regression is the most suitable tool to identify the dependency or functional association among the variables obtained in a sample from a particular population (Méndez, Namihira-Guerrero, Moreno-Altamirano, & Sosa-De-Martínez, 1990). This investigation calculated a linear model with no ordinate, or fitted at the origin, using linear regression. The fit of the model was performed by relating the ionic concentration of the solutions, in mg l^{-1}, to the concentration in terms of electrical conductivity, in μS cm^{-1}, using the least squares method. The model has the structure:

$$Y = f\,a\,X$$

Where *Y* is the concentration of the solution in mg L^{-1} (total dissolved solids); *a* is the slope of the line, that is, the number of units *Y* increases for each unit of X; X is the electrical conductivity of the solution in μS cm^{-1}.

The accuracy of the analytical values was verified using the method recommended by Eaton, Clesceri and Greenberg (1995), defined as:

$$\%\ \text{difference} = 100\left[\frac{\sum \text{cations} - \sum \text{anions}}{\sum \text{cations} + \sum \text{anions}}\right]$$

Results

Ionic concentration of the water

The analytical data have a margin of error under 2%, an acceptable value for this type of water with low concentrations (Tables 2 and 3).

According to the characteristics of the electrical conductivity values established by Richards (1990) for the use of water in irrigation, the surface water from the Sierra Norte is classified as follows: spring sample, 16 samples classified as C1, 3 samples as C2 and 3 samples as C3; autumn, 14 samples classified as C1, 5 samples as C2 and 3 samples as C3.

It is also important to mention that for the functional relation mg $l^{-1} = fa$ EC, proportionally, the slope of the line depends on the type of salinity. Figure 2, presents the functional relationship between the concentrations of the soluble salts in the surface water from the Sierra Norte and their corresponding electrical conductivity values. The value of the slope, *a*, found for the spring sample was 0.7341 and 0.7062 in autumn. The value of *a* is over 0.700, which corresponds to water with considerable bicarbonate contents.

Sodium Content

Table 4 presents the classification of surface water in the Sierra Norte according to their SAR values and Table 5 shows the SAR values according to the different scenarios, taking into account variations in the concentrations of calcium (CA^{2+}) and magnesium (Mg^{2+}) ions during the process of precipitation or dissolution of calcite. The surface water in the Sierra Norte is classified generally as S1, indicating that the effect of sodium would not pose a problem for the soil properties. The SARadj indicates that two stations are classified as S2 —Barranca Chignahuapan thermal spring (number 16) in the spring sample and Agua Mineral spring (number 14) in spring and autumn.

Residual sodium carbonate

As seen in Table 6, the stations in the Sierra Norte that were sampled in spring contain considerable amounts of bicarbonates, given the positive RSC values. One station is classified as conditional due to a value of 2.29 $mmol_c$ l^{-1}, corresponding to the Agua Mineral River in Ejido Tuliman (number 15). In autumn, the values are negative, indicating that they are calcic-magnesic and magnesic-calcic. This is deduced from their negative (-) values and is corroborated with the analytical data corresponding to these elements.

Boron

Table 6 presents the boron contents for the Sierra Norte stations. Most of the stations contain acceptable amounts of boron. The water source that is not recommended is the Barranca Chignahuapan thermal spring (number 16), with a value over 4 mg B l^{-1}. This spring discharges into the Agua Mineral River (number 15), which is sampled downstream and contains 3.28 mg B l^{-1}. Another two points correspond to springs: Agua Mineral spring (number 14) with a concentration of 2.95 mg B l^{-1} and El Pinal thermal spring (number 11), with 1.61 mg l^{-1}, both in autumn.

Phosphorus

The phosphorus contents of the water in the samples was between 0.023 and 0.69 mg l^{-1}. All were considered suitable for irrigation (Table 6). A maximum of 0.28 mg l^{-1} was found in spring, corresponding to the Ajajalpa River in Barranca Chignahuapan (number 17) and the maximum of 0.69 mg l^{-1} was found in autumn, in the Cascada Quetzalapa (number 13).

Hydrogeochemical Classification

This classification indicates that the surface water sampled at the different stations in the Sierra Norte was mostly bicarbonate, with variations in sodium and calcium cations. The first sample was classified as sodium bicarbonate. The second sample was classified as calcium bicarbonate (Figure 4).

Table 2. Ionic concentration of surface water in Sierra Norte de Puebla. Spring sample.

Station	Source	pH	CE	Ca^{2}	Mg^{2+}	Na^{+}	K^{+}	Sum cat	CO_3^{2-}	HCO_3^{-}	Cl^{-}	SO_4^{2-}	Sum ani	Error	*TDS*
			$\mu S\ cm^{-1}$	$mmol_c\ L^{-1}$					$mmol_c\ L^{-1}$					%	$mg\ L^{-1}$
1	Springs in Gomez Tepetenco Communal Lands	8.7	83	0.12	0.18	0.44	0.08	0.82	0.02	0.57	0.15	0.05	0.79	1.86	63.37
2	River in Tlautitlaltepa	8.6	129	0.18	0.24	0.75	0.10	1.27	0.04	0.81	0.26	0.12	1.23	1.60	97.00
3	Texpilco River at the Zacapoaxtla Bridge	7.2	263	0.54	0.66	1.31	0.09	2.60	0.00	1.21	0.77	0.53	2.51	1.76	186.21
4	Apulco River in Cascada La Gloria	7.5	157	0.37	0.39	0.73	0.06	1.55	0.00	0.63	0.51	0.35	1.49	1.97	108.27
5	Cuetzalan River in Nauzontla	7.6	241	0.61	0.55	1.18	0.03	2.37	0.00	1.24	0.42	0.67	2.33	0.85	175.03
6	Tepeacan River in San Miguel	7.4	99	0.22	0.17	0.52	0.07	0.98	0.00	0.56	0.32	0.07	0.95	1.55	72.84
7	Escorial River in Zapotitlán	7.8	78	0.16	0.19	0.37	0.05	0.77	0.00	0.47	0.20	0.09	0.76	0.65	58.31
8	Escorial River at the Zacapoaxtla Bridge	8.1	186	0.48	0.50	0.67	0.16	1.81	0.00	1.21	0.40	0.18	1.79	0.56	137.35
9	San Pedro River in Ahuacatlán	8.0	225	0.60	0.34	1.19	0.09	2.22	0.00	1.15	0.73	0.31	2.19	0.68	162.70
10	Ajajalpa River at bridge at km 92	8.0	256	0.58	0.65	1.10	0.20	2.53	0.00	1.93	0.40	0.12	2.45	1.61	196.98
11	Thermal spring El Pinal in Jicolapan	7.3	897	2.40	2.60	3.57	0.29	8.86	0.00	5.61	2.60	0.39	8.60	1.49	651.30
12	Agrio River in Cascada San Pedro	8.0	132	0.24	0.30	0.72	0.04	1.30	0.00	0.67	0.48	0.12	1.27	1.17	93.84
13	Quetzalapan Cascada in Tuliman	8.9	161	0.20	0.26	1.04	0.08	1.58	0.06	1.01	0.35	0.12	1.54	1.28	120.43
14	Agua Mineral Spring in Tuliman Communal Lands	7.8	1332	2.50	3.05	7.18	0.42	13.15	0.00	7.84	4.62	0.35	12.81	1.31	964.65
15	Ajajalpa River in Ejido Tuliman	8.1	672	1.80	1.90	2.75	0.19	6.64	0.00	3.97	2.10	0.40	6.47	1.30	484.29
16	Thermal Spring Chignahuapan Ravine	7.5	1343	6.90	1.10	4.94	0.32	13.26	0.00	8.84	3.50	0.58	12.92	1.30	1007.70
17	Ajajalpa River in Barranca Chignahuapan	8.8	169	0.18	0.23	1.21	0.05	1.67	0.04	1.13	0.32	0.14	1.63	1.21	129.36
18	Manantial in Chignahuapan	9.2	149	0.25	0.32	0.84	0.06	1.47	0.02	0.98	0.28	0.15	1.43	1.38	112.40
19	Origin of Junction to Pueblo Nuevo	8.8	61	0.12	0.18	0.22	0.08	0.60	0.02	0.33	0.15	0.08	0.58	1.69	44.38
20	Jagüey in Pueblo Nuevo	6.7	107	0.20	0.32	0.37	0.17	1.06	0.00	0.65	0.25	0.12	1.02	1.92	80.42
21	Spring in Puente Atotonilco	9.1	77	0.18	0.20	0.29	0.09	0.76	0.02	0.49	0.20	0.03	0.74	1.33	57.46
22	Agrio River in Puente Atotonilco	8.3	156	0.38	0.45	0.62	0.09	1.54	0.00	1.05	0.38	0.07	1.50	1.32	116.21

Table 3. Ionic Concentration of Surface Water Sierra Norte in Puebla. Sampling in autumn.

Station	Altitude	pH	CE	Ca^{2+}	Mg^{2+}	Na^{+}	K^{+}	Sum cat	CO_3^{2-}	HCO_3^{-}	Cl^{-}	SO_4^{2-}	Sum ani	Error	*TDS*
	m		µS cm^{-1}	mmol$_c$ L^{-1}					mmol$_c$ L^{-1}					%	mg L^{-1}
1	2 616	8.0	93	0.40	0.32	0.15	0.05	0.92	0.00	0.60	0.21	0.08	0.89	1.66	67.48
2	2 576	8.4	149	0.60	0.46	0.34	0.07	1.47	0.03	1.05	0.23	0.11	1.42	1.73	110.29
3	1 725	7.0	321	2.04	0.56	0.42	0.08	3.10	0.00	1.75	0.80	0.62	3.17	1.12	233.25
4	1 734	7.7	221	1.67	0.32	0.15	0.04	2.18	0.00	1.10	0.62	0.40	2.12	1.40	156.69
5	1 434	7.8	263	2.08	0.24	0.22	0.06	2.60	0.00	1.12	0.55	0.86	2.53	1.36	188.37
6	598	7.7	121	0.77	0.21	0.18	0.04	1.20	0.00	0.57	0.55	0.05	1.17	1.27	83.17
7	696	7.3	89	0.41	0.25	0.19	0.03	0.88	0.00	0.55	0.25	0.06	0.86	1.15	64.26
8	710	8.1	288	1.91	0.35	0.52	0.06	2.84	0.00	1.88	0.75	0.12	2.75	1.61	211.00
9	1 278	8.0	354	2.76	0.38	0.24	0.12	3.50	0.00	2.28	0.92	0.22	3.42	1.16	258.71
10	1 248	8.0	295	1.65	0.72	0.46	0.08	2.91	0.00	1.96	0.70	0.17	2.83	1.39	216.38
11	2 232	6.1	1261	7.70	3.25	1.15	0.35	12.45	0.00	6.53	3.92	1.68	12.13	1.30	881.73
12	2 048	7.2	134	0.51	0.41	0.32	0.08	1.32	0.00	0.66	0.44	0.18	1.28	1.54	92.45
13	2 166	6.9	245	0.57	1.02	0.68	0.15	2.42	0.00	1.52	0.61	0.23	2.36	1.26	176.69
14	1 905	6.4	1913	7.71	6.00	4.76	0.42	18.89	0.00	9.77	8.30	0.33	18.40	1.31	1309.74
15	1 905	7.0	243	0.93	0.75	0.61	0.11	2.40	0.00	1.30	0.85	0.19	2.34	1.27	170.40
16	2 170	7.0	1471	7.19	3.05	3.97	0.28	14.49	0.00	10.13	3.55	0.47	14.15	1.19	1091.74
17	2 170	6.7	108	0.35	0.40	0.26	0.06	1.07	0.00	0.60	0.30	0.14	1.04	1.42	77.13
18	2 273	6.6	238	0.94	0.87	0.46	0.08	2.35	0.00	1.25	0.75	0.29	2.29	1.29	166.28
19	2 572	6.7	119	0.58	0.30	0.23	0.04	1.15	0.00	0.65	0.37	0.16	1.18	1.29	85.88
20	2 613	6.4	104	0.41	0.25	0.29	0.08	1.03	0.00	0.63	0.28	0.08	0.99	1.98	76.18
21	2 224	8.7	90	0.39	0.27	0.15	0.08	0.89	0.04	0.51	0.27	0.05	0.87	1.14	64.44
22	2 224	7.3	116	0.37	0.36	0.32	0.10	1.15	0.00	0.58	0.38	0.16	1.12	1.32	82.78

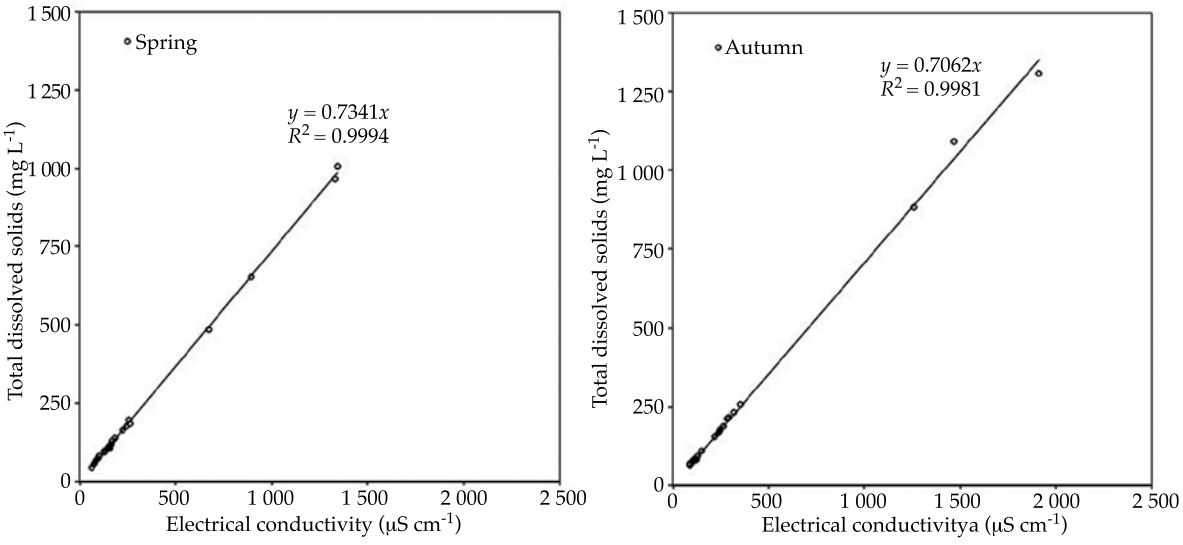

Figure 2. Concentration of salts and the relation with electrical conductivity in surface water in Sierra Norte de Puebla. Spring and autumn samples.

Table 4. Synthesis of the classification of surface water in Sierra Norte de Puebla based on sodium values. Spring and autumn sample.

Sample	SAR formulas	Classification		Sample	SAR formulas	Classification	
		S1	S2			S1	S2
Spring	SAR			Autumn	SAR		
	Samples	22			Samples	22	
	SAR_{adj}				SAR_{adj}		
	Samples	20	2		Samples	21	1
	SAR°				SAR°		
	Samples	22			Samples	22	

Table 5. Values for the sodium adsorption ratio in surface water in Sierra Norte de Puebla. Spring and autumn samples.

Sample	Station	pH	CE	SAR	SAR^{adj}	SAR°	Sample	Station	pH	CE	SAR	SAR_{adj}	SAR°
			µS cm^{-1}							µS cm^{-1}			
Spring	1	8.7	83	1.14	0.26	0.68	Autumn	1	8.0	93	0.25	0.15	0.16
	2	8.6	129	1.64	0.85	1.12		2	8.4	149	0.47	0.47	0.37
	3	7.2	263	1.69	1.85	1.40		3	7.0	321	0.37	0.58	0.35
	4	7.5	157	1.18	0.75	0.80		4	7.7	221	0.15	0.19	0.13
	5	7.6	241	1.55	1.69	1.28		5	7.8	263	0.20	0.27	0.17
	6	7.4	99	1.18	0.37	0.69		6	7.7	121	0.26	0.18	0.17
	7	7.8	78	0.88	0.17	0.51		7	7.3	89	0.33	0.18	0.20
	8	8.1	186	0.96	0.98	0.77		8	8.1	288	0.49	0.76	0.49
	9	8.0	225	1.74	1.69	1.37		9	8.0	354	0.19	0.34	0.21
	10	8.0	256	1.40	1.84	1.28		10	8.0	295	0.42	0.67	0.42
	11	7.3	897	2.26	5.17	2.59		11	6.1	1261	0.49	1.31	0.67
	12	8.0	132	1.39	0.72	0.95		12	7.2	134	0.47	0.35	0.32
	13	8.9	161	2.17	1.40	1.56		13	6.9	245	0.76	1.01	0.67
	14	7.8	1332	4.31	10.52	5.02		14	6.4	1913	1.82	5.25	2.39
	15	8.1	672	2.02	4.11	2.22		15	7.0	243	0.67	0.85	0.59
	16	7.5	1343	2.47	6.54	4.06		16	7.0	1471	1.75	4.92	2.66
	17	8.8	169	2.67	1.69	2.00		17	6.7	108	0.42	0.26	0.29
	18	9.2	149	1.57	1.12	1.16		18	6.6	238	0.48	0.62	0.41
	19	8.8	61	0.57	0.01	0.31		19	6.7	119	0.35	0.25	0.22
	20	6.7	107	0.73	0.36	0.50		20	6.4	104	0.50	0.30	0.32
	21	9.1	77	0.67	0.18	0.38		21	8.7	90	0.26	0.14	0.16
	22	8.3	156	0.96	0.86	0.76		22	7.3	116	0.53	0.32	0.34

Discussion

Ionic Concentration

Knowledge about the numerical range of the different parameters makes it possible to identify the prevalence of certain processes in the surface water and in the soil irrigated with this water. To be certain about these processes, reliable analytical data are needed. To this end, the data were evaluated as recommended by Eaton *et al.* (1995). This recommendation refers to the electroneutrality of the solutions, that is,

Table 6. Evaluation of residual sodium carbonate, boron and phosphorus in surface water in the Sierra Norte de Puebla. Spring and autumn samples.

Sample	Station	RSC	Classification	B	Clasificación			P	Classification
		$mmol_c\ L^{-1}$		$mg\ L^{-1}$	Sensitive	Semitolerantes	Tolerantes	$mg\ L^{-1}$	
Spring	1	0.29	Good	0.43	Good	Excellent	Excellent	0.02	Acceptable
	2	0.43	Good	0.28	Excellent	Excellent	Excellent	0.02	Acceptable
	3	0.01	Good	0.11	Excellent	Excellent	Excellent	0.13	Acceptable
	4	-0.13	Good	0.10	Excellent	Excellent	Excellent	0.07	Acceptable
	5	0.08	Good	0.07	Excellent	Excellent	Excellent	0.07	Acceptable
	6	0.17	Good	0.11	Excellent	Excellent	Excellent	0.08	Acceptable
	7	0.12	Good	0.14	Excellent	Excellent	Excellent	0.13	Acceptable
	8	0.23	Good	0.13	Excellent	Excellent	Excellent	0.04	Acceptable
	9	0.21	Good	0.04	Excellent	Excellent	Excellent	0.08	Acceptable
	10	0.70	Good	0.15	Excellent	Excellent	Excellent	0.10	Acceptable
	11	0.61	Good	1.54	Not recommended	Acceptable	Good	0.05	Acceptable
	12	0.13	Good	0.15	Excellent	Excellent	Excellent	0.24	Acceptable
	13	0.61	Good	0.20	Excellent	Excellent	Excellent	0.21	Acceptable
	14	2.29	Conditional	3.28	Not recommended	Not recommended	Unsafe	0.06	Acceptable
	15	0.27	Good	2.18	Not recommended	Unsafe	Acceptable	0.04	Acceptable
	16	0.84	Good	4.04	Not recommended	Not recommended	Not recommended	0.03	Acceptable
	17	0.76	Good	0.01	Excellent	Excellent	Excellent	0.28	Acceptable
	18	0.43	Good	0.06	Excellent	Excellent	Excellent	0.04	Acceptable
	19	0.05	Good	0.15	Excellent	Excellent	Excellent	0.24	Acceptable
	20	0.13	Good	0.12	Excellent	Excellent	Excellent	0.14	Acceptable
	21	0.13	Good	0.00	Excellent	Excellent	Excellent	0.14	Acceptable
	22	0.22	Good	0.42	Excellent	Excellent	Excellent	0.09	Acceptable
Autumn	1	-0.12	Good	0.23	Excellent	Excellent	Excellent	0.03	Acceptable
	2	0.02	Good	0.18	Excellent	Excellent	Excellent	0.04	Acceptable
	3	-0.85	Good	0.12	Excellent	Excellent	Excellent	0.14	Acceptable
	4	-0.89	Good	0.10	Excellent	Excellent	Excellent	0.06	Acceptable
	5	-1.20	Good	0.07	Excellent	Excellent	Excellent	0.05	Acceptable
	6	-0.41	Good	0.11	Excellent	Excellent	Excellent	0.09	Acceptable
	7	-0.11	Good	0.16	Excellent	Excellent	Excellent	0.21	Acceptable
	8	-0.38	Good	0.13	Excellent	Excellent	Excellent	0.09	Acceptable
	9	-0.86	Good	0.04	Excellent	Excellent	Excellent	0.08	Acceptable
	10	-0.41	Good	0.18	Excellent	Excellent	Excellent	0.15	Acceptable
	11	-4.42	Good	1.61	Not recommended	Aceptable	Good	0.02	Acceptable
	12	-0.26	Good	0.85	Acceptable	Good	Excellent	0.36	Acceptable
	13	-0.07	Good	0.64	Good	Excellent	Excellent	0.69	Acceptable
	14	-3.94	Good	2.95	Not recommended	Not recommended	Acceptable	0.08	Acceptable
	15	-0.38	Good	0.75	Acceptable	Good	Excellent	0.30	Acceptable
	16	-0.11	Good	4.01	Not recommended	Not recommended	Not recommended	0.02	Acceptable
	17	-0.15	Good	0.58	Good	Excellent	Excellent	0.27	Acceptable
	18	-0.56	Good	0.64	Good	Excellent	Excellent	0.39	Acceptable
	19	-0.23	Good	0.22	Excellent	Excellent	Excellent	0.25	Acceptable
	20	-0.03	Good	0.68	Acceptable	Good	Excellent	0.35	Acceptable
	21	-0.11	Good	0.01	Excellent	Excellent	Excellent	0.10	Acceptable
	22	-0.15	Good	0.85	Acceptable	Good	Good	0.30	Acceptable

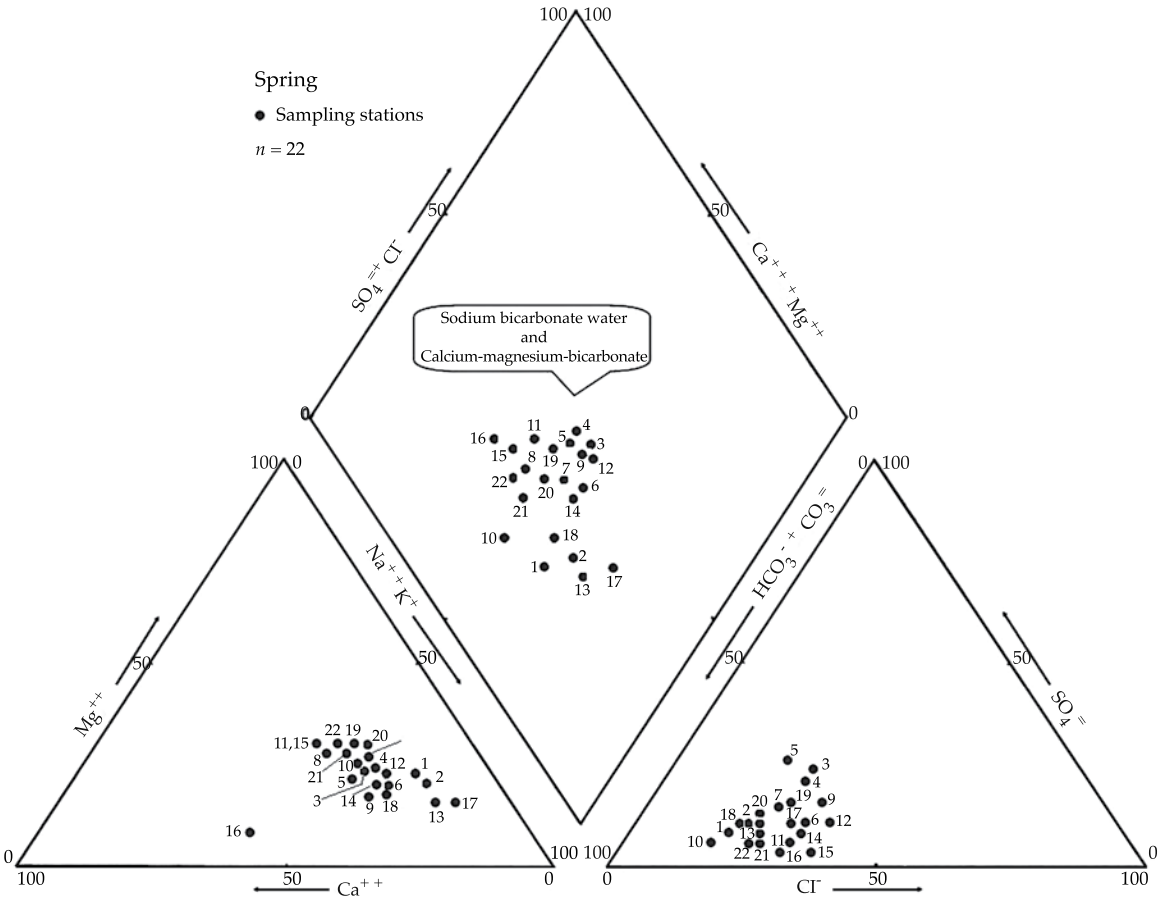

Figure 3. Hydrogeochemical classification of surface water in Sierra Norte de Puebla. Spring sample.

restrictions, except for water from sources classified as C3, which is only recommended for salinity-tolerant crops. These sources are: El Pinal thermal springs (number 11), Agua Mineral springs (number 14) and Barranca Chignahuapan thermal springs (number 16). Water from the first two, when used for irrigation, is recommended for alfalfa, oats, barley and wheat, which according to Maas (1990) tolerate those levels of salinity and are suitable for the environmental conditions in the region in which they are located (the municipalities of Chignahuapan and Zacatlan). The latter is used for therapeutic purposes (1343 μS cm^{-1}). It discharges into the Ajajalpa River, and the sample obtained downstream at the Ejido Tuliman (number 15) contained a more diluted concentration (672 μS cm^{-1}).

The sampling stations containing wastewater are number 3 in Zacapuaxtla, number 10 in Zacatlan, and 13 and 14 in Chignahuapan. The wastewater comes primarily from these towns as a result of industrial activity, specifically manufacturing, and are generally colorants that do not alter the ionic concentration.

Sodium Concentration

According to Silva (2004) and Suarez, Wood and Lesch (2008), when exchangeable sodium levels in the soil are high, the soil becomes less permeable, the porous medium is altered

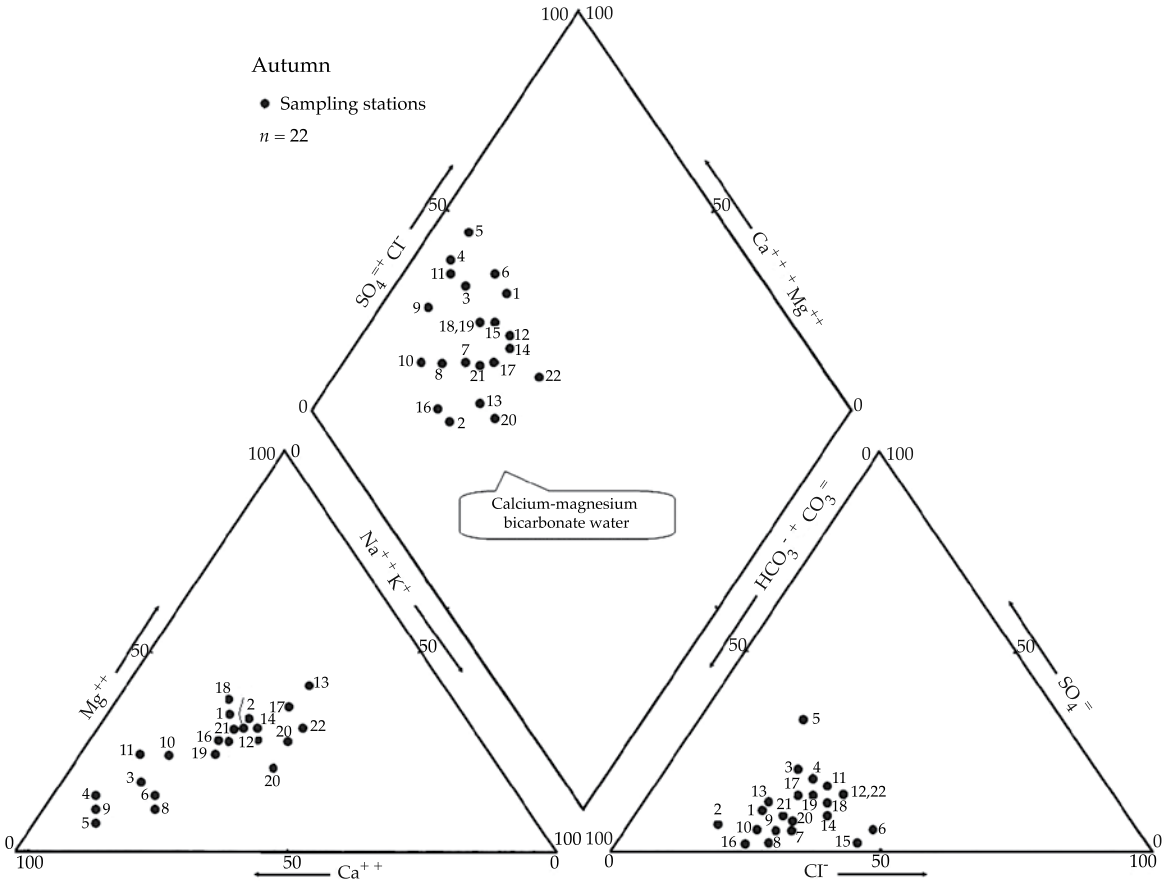

Figure 4. Hydrogeochemical classification of surface water in Sierra Norte de Puebla. Autumn sample.

the sum of anions should be similar to the sum of cations.

In spring, the mean pH was 8.1, the maximum was 9.2 and the minimum 6.7 in spring, and 7.3, 8.7 and 6.1 in autumn, respectively. Normal pH values for irrigation water, according to Ayers and Westcot (1987), range from 6.5 – 8.4. Values above 8.4, according to Ortega *et al.* (2002), will have significant implications on the availability and management of nutrients.

Works to evaluate and characterize surface water and groundwater have considered that the measurement of electrical conductivity in aqueous solutions is related to two dissolutions in water (in mg l^{-1}). Velázquez, Ortega, Martínez, Kohashi, & García (2002) showed that the value of the slope depends on the type of salt that is dominant. Jurinak and Suarez (1990), and Richards (1990), in specific investigations involving many analytical determinations of electrical conductivity and its relationship with the amount of disassociated ions by weight, established that electrical conductivity measurements are directly proportional to the disassociated molecular masses. It is important to mention that electrical conductivity measurements depend on the number of disassociated ions in the solution, but not on their masses, whereas the concentration, in mg l^{-1}, does depend on both, that is, on the number of ions and their masses.

According to the total concentration expressed as electrical conductivity, the quality of the water indicates that surface water can be used for agriculture in the Sierra Norte without

and toxic effects occur in plants sensitive to sodium ion. The relationship between SAR values and the percentage of exchangeable sodium in irrigation water is proportional, since the SAR values relate to the amount of sodium adsorbed in the soil exchange complex as a result of the application of water with a particular sodium content. As opposed to directly determining exchangeable sodium, the use of the SAR offers many advantages as an excellent diagnostic of the problems caused by sodicity in soil. The results of this investigation show three SAR expressions resulting in a range of values for each point, and based on the characteristics of the water (pH, Ca, Mg and HCO_3) it is possible to predict the effect of sodium on soil properties, and thereby on plants. Station 14 has a SAR of 4.31, a SARadj of 10.52 and a SAR° of 5.01. The Ca and Mg values indicate that the effect of the sodium is counteracted, and therefore the values of the original SAR and SAR° are low. Based on the pH value and the HCO_3 contents, it can be inferred that the Ca will form the salt $CaCO_3$. The SARadj value shows this tendency, since Ca precipitates in the presence of HCO_3. This precipitation contributes to the predominance of sodium in the soil, since its low solubility results in it remaining in the soil after calcium and magnesium have precipitated, as cited by Can-Chulim, Ramírez-Ayala, Ortega- Escobar, Trejo-López and Cruz-Díaz, in 2008.

The results of the SAR indicate that the surface water can be used in agriculture without restrictions.

Residual sodium carbonate

When carbonate and bicarbonate contents in water are greater than calcium and magnesium contents, the forming of sodium carbonate is possible since, because of its high solubility, it can remain in solution even after the calcium and magnesium carbonates have precipitated.

By evaluating the water samples using this index, only one source is classified as conditional —the Agua Mineral springs (number 14), which is not used for irrigation but directly discharges into the Ajajalpa River. Negative RSC values indicate no problems when used in agriculture and positive values show that Ca and Mg will precipitate as carbonates when coming into contact with the soil, and therefore only sodium salts will remain in the soil solution. Dhembare (2012) found negative RSC values and stated that this is because Ca and Mg do not precipitate and remain in the water. Positive RSC values are observed during the dry season because flows are reduced and the Ca and Mg concentrations precipitate in the form of carbonates. During the precipitation season, these salts and those found in the soil and rocks in general throughout the study area dissolve and are transported by streams to the main rivers. Nishanthiny *et al*. (2010) mention that the primary source of the carbonate contents is the dissolution of carbonated rocks. For this reason, the RSC values during the rainy season are negative because the rivers contain higher Ca and Mg concentration as a result of dissolution.

Boron

High boron contents are commonly associated with saline areas found in arid and semi-arid regions (Yermiyahu *et al*., 2003). But they are also found in irrigation zones, where the boron comes primarily from groundwater which acquires that content from volcanic activity or parent materials with which it comes into contact (Gméling, Németh, Eby, & Varga, 2007; Özgür, 2001). Gméling *et al*. (2007) found high boron values in groundwater in volcanic fields and associated this with geothermal activity. In an exorheic basin with agricultural use, high B values were found in groundwater, as a result of geothermal flows. In surface water, boron comes primarily from water discharged from volcanic areas, from the contact of the water with rocks rich in boron and, to a lesser degree from wastewater discharges.

In regions with a large amount of pluvial precipitation, signs of deficiency in plants are very common because of the very low concentrations of boron in soils and high leaching. On the other hand, in arid and semi-arid regions, the signs of toxicity due to boron result from large concentrations in the soil solution and from boron concentrations in irrigation water (Korzeniowska, 2008; Onthong, Yoajui, & Kaewsichan, 2011). Both deficiency as well as toxicity inhibit the growth of plants, resulting in marked reductions in crop yields and economic losses for producers (Edelstein, 2007).

The Barranca Chignahuapan thermal springs (number 16), which flows into the Ajajalpa River, is a water source not recommended for agricultural use, with a value over 4 mg l^{-1}. Nevertheless, in general, no problems exist for use in agriculture. The sources with the highest concentrations are the springs that are affected by residual volcanic activity from the Acoculco caldera. These sources are characterized by hydrothermalism and are used for therapeutic purposes.

To use water directly from the source, tolerant crops must be selected, such as oats, corn, zucchini, alfalfa and sorghum, which withstand between 2.0 and 6.0 mg B l^{-1} (Maas, 1990).

Phosphorus

Phosphorus is an essential nutrient for plants (Mendoza, Rodríguez-Martín, Fernández-Vera, Palacios-Díaz, & Hernández-Moreno, 2003) and is absorbed by the plant in the form of orthophosphates. These are the most common inorganic forms of phosphorus, and in water with little circulation they cause the development of eutrophication processes, to differing degrees of intensity. They are found in low concentrations in water, and can increase from the incorporation of water from industrial urban sources (Johnston & Dawson, 2005). The water in the Sierra Norte does not have any problems due to phosphorus contents and can be used for agricultural purposes. Eutrophication processes will be incipient in the dams.

Hydrogeochemical Classification

The stations with surface water having high concentrations are primarily the springs, which are found in a geothermal area characterized by hydrothermalism. According to Camprubí, González-Partida, Levresse, Tritlla and Carrillo-Chávez (2003), hydrothermalism is due to the contact of water with heat sources from magmatic activity, while circulating through the faults or fracture zones created by volcanic activity.

Three springs have temperatures over 30°C. One is the Barranca Chignahuapan thermal spring (number 16 with 48°C), which is used as a thermal bath for therapeutic purposes, such as those in Viterbo, Italy (Piscopo *et al*., 2006). These three springs are outside of the Acoculco caldera, but the source of the high temperature is the depth of the center of the caldera and the high permeability underneath. This source of heat raises the temperature of the water which then flows through the fissures or dissolution channels produced in the calcareous rocks and supplies these springs. The sodium and calcium bicarbonate water shows that the water that feeds these points comes from groundwater that underlies and circulates through these channels.

From the hydrogeochemical perspective, the sources of surface water are mostly bicarbonate, with variations in sodium and calcium cations. These variations are due to dilution and re-concentration. During dry periods, the less soluble ions precipitate and only those most soluble remain in solution. This is why sodium is predominant in the first sample, in which the water is classified as sodium bicarbonate. The second sampling was performed during the intense rainy season when the waters interact with the calcareous materials in the area, diluting the calcium, giving the water its calcium bicarbonate character.

Conclusions

The Sierra Norte is an area in which surface rivers are the most important source of water for agriculture. The ionic concentration of the surface water is generally low since it mostly comes from pluvial runoff. The largest variations correspond to points at which discharges from thermal springs are received, and moderate variations are observed where industrial urban discharges are received.

The quality of surface water is moderately altered at certain points along the rivers by the ionic supply of water from industrial urban sources. In general, the surface water is suitable for irrigation. The water from points corresponding to springs is not recommended. While these springs are not directly used for irrigation, they do flow into the rivers. These points of high qualitative and quantitative concentrations are localized, changing downstream from discharges —as a result of dilution or precipitation, or due to chemical processes such as oxidation and reduction.

From the hydrogeochemical perspective, the surface water is mostly bicarbonate with variations in sodium and calcium cations. These variations are due to the dilution and precipitation of calcium. Calcium is diluted during the rainy season and precipitates during the dry season. The geothermal area of the Acoculco caldera is the source of the high temperatures and ionic concentration of the surrounding springs.

References

Ayers, R. S., & Westcot, D. W. (1987). *La calidad del agua y su uso en la agricultura* (81 pp.). Estudio FAO Riego y Drenaje 29, Rev. 1. Roma: FAO.

Baccaro, K., Degorgue, M., Lucca, M., Picote, L., Zamuner, E., & Andreoli, Y. (2006). Calidad del agua para consumo humano y riego en muestras del Cinturón Hortícola de Mar del Plata. *RIA*, *35*(3), 95-110.

Bower, C. A., Ogata, G., & Tucker, J. M. (1968). Sodium Hazard of Irrigation Waters as Influenced by Leaching Fraction and by Precipitation or Solution of Calcium Carbonate. *Soil Science*, *106*(1), 29-34.

Camprubí, A., González-Partida, E., Levresse, G., Tritlla, J., & Carrillo-Chávez, A. (2003). Depósitos epitermales de alta y baja sulfuración: una tabla comparativa. *Boletín de la Sociedad Geológica Mexicana*, *56*(1), 10-18.

Can-Chulim, Á., Ramírez-Ayala, C., Ortega-Escobar, M., Trejo-López, C., & Cruz-Díaz, J. (2008). Evaluación de la relación de adsorción de sodio en las aguas del río Tulancingo, estado de Hidalgo, México. *Terra Latinoamericana*, *26*(3), 243-252.

Capra, L., Lugo-Hubp, J., & Zamorano-Orozco, J. J. (2006). La importancia de la geología en el estudio de los procesos de remoción en masa: el caso de Totomoxtla, Sierra Norte de Puebla, México. *Boletín de la Sociedad Geológica Mexicana*, *58*(2), 205-214.

Casierra, F., & Rodríguez, S. Y. (2006). Tolerancia de plantas de feijoa (*Acca sellowiana* [Berg] Burret) a la salinidad por NaCl. Agronomía Colombiana, *24*(2), 258-265.

Cuanalo, O. A., & Melgarejo, G. (2002). Inestabilidad de las laderas Sierras Norte y Nororiental del estado de Puebla. *Ciencia y Cultura*, *9*(47), 51-55.

Dhembare, A. J. (2012). Assessment of Water Quality Indices for Irrigation of Dynaneshwar Dam Water, Ahmednagar, Maharashtra, India. *Archives of Applied Science Research*, *4*(1), 348-352.

Eaton, A. D., Clesceri, L. S., & Greenberg, A. E. (1995). *Standard Methods for the Examination of Water and Wastewater* (1325 pp). 19th Edition. Washington, DC: APHA, AWWA, WEF.

Eaton, F. M. (1950). Significance of Carbonates in Irrigation Water. *Soil Science*, *69*(2), 123-133.

Edelstein, M. (2007). Grafted Melons Irrigated with Fresh or Effluent Water Tolerate Excess Boron. *J. Amer. Soc. Hort. Sci.*, *132*(4), 484-491.

Galván, A., Hernández, G., Vélez, H., Gómez, E., Becerril, A., & Luna, A. (1999). *Evaluación de impacto ambiental, informe final de actividades Sierra Norte de Puebla* (62 pp.). México, DF: Secretaría de Agricultura y Ganadería, Banco Mundial, Universidad Autónoma Metropolitana Iztapalapa.

Gméling, K., Németh, K., Eby, U., & Varga, Z. (2007). Boron Concentrations of Volcanic Fields in Different Geotectonic Settings. *Journal of Volcanology and Geothermal Research*, *159*, 70-84.

Goldberg, S., Corwin, D. L., Shouse, P. J., & Suarez, D. L. (2005). Prediction of Boron Adsorption by Field Samples of Diverse Textures. *Soil Sci. Soc. Am. J.*, *69*, 1379-1388.

Grattan, S. (2006). Irrigation Water Composition and Salinization. In B. R. Hanson, S. R.Grattan, & A. Fulton (Eds.). *Agricultural Salinity and Drainage* (pp. 5-6). Water Management Series publication 3375. Davis, California: University of California Division of Agriculture and Natural Resources.

Guevara-Romero, M. L. (2011). Tipos de vegetación de Puebla. En *La Biodiversidad en Puebla: Estudio de Estado* (pp. 75-83). México, DF: Comisión Nacional para el

Conocimiento y Uso de la Biodiversidad (Conabio), Gobierno del Estado de Puebla, Benemérita Universidad Autónoma de Puebla.

Johnston, A. E., & Dawson, C. J. (2005). *Phosphorus in Agriculture and in Relation to Water Quality* (71 pp.), Peterborough, United Kingdom: Agricultural Industries Confederation.

Jurinak, J. J., & Suarez, D. L. (1990). The Chemistry of Salt Affected-Soils and Water. In K. K. Tanji (Ed.). *Agricultural Salinity Assessment and Management* (pp. 42-63). New York: ASCE.

Korzeniowska, J. (2008). Response of Ten Winter wheat Cultivars to Boron Foliar Application in a Temperate Climate (South-West Poland). *Agronomy Research*, *6*(2), 471-476.

Langelier, W. F. (1936). The Analytical Control of Anticorrosion Water Treatment. *Journal American Waterworks Association*, *28*, 1500-1521.

López-Téllez, M. C. (2011). Usos del agua y situación de las cuencas hidrológicas. En *La Biodiversidad en Puebla: Estudio de Estado* (pp. 244-246). México, DF: Comisión Nacional para el Conocimiento y Uso de la Biodiversidad (Conabio), Gobierno del Estado de Puebla, Benemérita Universidad Autónoma de Puebla.

Maas, E. V. (1990). Crop Salt Tolerance. En: K. K. Tanji (Ed.). *Agricultural Salinity Assessment and Management* (pp. 262-304). New York: ASCE.

Martínez, M. Á., Evangelista, V., Basurto, F., Mendoza, M., & Cruz-Rivas, A. (2007). Flora útil de los cafetales en la Sierra Norte de Puebla, México. *Revista Mexicana de Biodiversidad*, *78*, 15-40.

Méndez-Ramírez, I., Namihira-Guerrero, D., Moreno-Altamirano, L., & Sosa-De-Martínez, C. (1990). *El protocolo de investigación. Lineamientos para su elaboración y análisis*. Segunda edición. México, DF: Trillas, 210 pp.

Mendoza-Grimón, V., Rodríguez-Martín, R., Fernández-Vera, J. R., Palacios-Díaz, M. P., & Hernández-Moreno, J. M. (2003). Estudio de la disponibilidad del fósforo y boro aportados por las aguas depuradas en la Isla de Gran Canaria: Metodología y resultados preliminares. En J. Álvarez-Benedí & P. Marinero (Eds.). *Actas de las VI Jornadas sobre la Investigación de la Zona no Saturada del Suelo* (pp. 355-359). Vol. 6. Valladolid, España: Instituto Tecnológico Agrario de Castilla y León (ITA).

Miyamoto, S., & Pingitore, N. E. (1992). Predicting Calcium and Magnesium Precipitation in Saline Solutions Following Evaporation. *Soil Science Society of America Journal*, 56(6), 1767-1775.

Murillo-Licea, D., López-Ramírez, E., Chávez-Hernández, P., Marañón-Pimentel, B., & Brie-Gowland, N. (2010). *Gobernanza del agua en comunidades indígenas de la región nororiental de Puebla* (256 pp.). Colección Agua y Sociedad. Jiutepec, México: Instituto Mexicano de Tecnología del Agua.

Nishanthiny, S. C., Thushyanthy, M., Barathithasan, T., & Saravanan, S. (2010). Irrigation Water Quality Based on Hydro Chemical Analysis, Jaffna, Sri Lanka. *American-Eurasian J. Agric. & Environ. Sci.*, *7*(1), 100-102.

NMX-AA-008-SCFI-2000 (2000). *Análisis de agua - determinación del Ph* (36 pp.). México, DF: Secretaría de Comercio y Fomento Industrial.

NMX-AA-034-SCFI-2001 (2001). *Análisis de agua - determinación de sólidos y sales disueltas en aguas naturales, residuales y residuales tratadas* (18 pp.). México, DF: Secretaría de Economía.

NMX-AA-073-SCFI-2001. *Análisis de agua - determinación de cloruros totales en aguas naturales, residuales y residuales tratadas* (18 pp.). México, DF: Secretaría de Economía.

NMX-AA-093-SCFI-2000 (2000). *Análisis de agua - determinación de la conductividad electrolítica* (27 pp.). México, DF: Secretaría de Comercio y Fomento Industrial.

NOM-O21-SEMARNAT-2000 (2000). *Que establece las especificaciones de fertilidad, salinidad y clasificación de suelos, estudio, muestreo y análisis* (85 pp.). México, D.F.: Secretaría de Medio Ambiente y Recursos Naturales.

Onthong, J., Yoajui, N., & Kaewsichan, L. (2011). Alleviation of Plant Boron Toxicity by Using Water to Leach Boron from Soil Contaminated by Wastewater from Rubber Wood Factories. *ScienceAsia*, *37*, 314-319.

Ortega, M. A., Castellanos, J. Z., Aguilar, R., Vázquez, A., Alaníz, E., Vargas, C., & Urrutia, F. (2002). A Conceptual Model for Increases of Sodium, SAR, Alkalinity and pH at the Independence Aquifer in Guanajuato. *Terra*, *20*, 199-207.

Özgür, N. (2001). Origin of High Boron Contents of the Thermal Waters of Kizildere and Vicinity, Western Anatolia, Turkey. *International Geology Review*, *43*(10), 910-920.

Piscopo, V., Barbiere, M., Monetti, V., Pagano, G., Pistoni, S., Ruggi, E., & Stanzioni, D. (2006). Hydrogeology of Thermal Waters in Viterbo Area, Central Italy. *Hydrogeology Journal*, *14*, 1508-1521.

Rashidi, M., & Seilsepour, M. (2011). Prediction of Soil Sodium Adsorption Ratio Based on Soil Electrical Conductivity. *Middle-East Journal of Scientific Research*, *8*(2), 379-383.

Ray, R. K., & Mukherjee, R. (2008). Reproducing the Piper Trilinear Diagram in Rectangular Coordinates. Methods Note. *Ground Water*, *46*(6), 893-896.

Richards, L. A. (1990). *Diagnóstico y rehabilitación de suelos salinos y sódicos* (172 pp.). Manual núm. 60. Sexta reimpresión. Departamento de Agricultura de los Estados Unidos, Laboratorio de Salinidad. México, DF: Limusa.

Rodier, J. (1990). *Análisis de las aguas* (pp. 186-191). Segunda reimpresión. Barcelona: Omega.

Sánchez, E., Ortega, M., Gonzáles, V., Ruelas, G., Kohashi, J., & García, N. (2002). Tolerancia de tubérculos de papa cv.

Alpha en etapa de brotación a condiciones de salinidad. *Terra*, *21*, 481-491.

Silva, H., Ortiz, M., & Acevedo, E. (2007). Relaciones hídricas y ajuste osmótico en trigo. *Agrociencia*, 41(1), 23-34.

Silva, E. I. L. (2004). Quality of Irrigation Water in Sri Lanka Status and Trends. *Asian Journal of Water*, *1*(1-2), 5-12.

Strogonov, B. P. (1964). *Physiological Basis of Salt Tolerance of Plants (As Affected by Various Types of Salinity)* (279 pp.). Jerusalem: Israel Program for Scientific Translation.

Suarez, D. L. (1981). Relation between pH and Sodium Adsorption Ratio (SAR) and an Alternative Method of Estimating SAR of Soil or Drainage Waters. *Soil Science Society America Journal*, *45*, 464-475.

Suarez, D. L., Wood, J. D., & Lesch, S. M. (2008). Infiltration into Cropped Soils: Effect of Rain and Sodium Adsorption Ratio-Impacted Irrigation Water. *J. Environ. Qual*., *37*, 169-179.

Szabolcs, I. (1989). *Salt Affected Soils* (274 pp.). Boca Raton, USA: CRS Press.

Vázquez-Martínez, I., Vargas-López, S., Zaragoza-Ramírez, J. L., Bustamante-González, Á., Calderón-Sánchez, F., Rojas-Álvarez, J., & Casiano-Ventura, M. Á. (2009). Tipología de explotaciones ovinas en la Sierra Norte del estado de Puebla. *Técnica Pecuaria en México*, *47*(4), 357-369.

Velázquez, M. A., Ortega, M., Martínez, Á., Kohashi, J., & García, N. (2002). Relación funcional PSI-RAS en las aguas residuales y suelos del Valle del Mezquital, Hidalgo, México. *Terra*, *20*, 459-464.

Velázquez, M. A., Pimentel, J. L., & Ortega, M. (2011). Estudio de la distribución de boro en fuentes de agua de la cuenca del río Duero, México, utilizando análisis estadístico multivariado. *Rev. Int. Contam. Ambie*., *27*(1), 19-30.

Wilcox, L. V. (1948). *The Quality of Water for Irrigation* (40 pp.). Tech. Bulletin 962. Washington, DC: Department of Agriculture.

Yermiyahu, U., Finegold, I., Keren, R., Cohen, Y., Yehezkel, H., & Shmuel, D. (2003). Response of Pepper to Boron and Salinity under Greenhouse Conditions. *Acta Hort*., 609, 149-154.

Institutional Address of the Authors

Dr. Álvaro Can Chulim

Unidad Académica de Agricultura
Universidad Autónoma de Nayarit
km 9 Carretera Tepic-Compostela
63780 Xalisco, Nayarit, México
Teléfono: +52 (311) 2110 128
canchulim@yahoo.com.mx

Dr. Héctor Manuel Ortega Escobar

Programa de Hidrociencias
Campus Montecillo
Colegio de Postgraduados
km 36.5 Carretera México-Texcoco
56230 Montecillo, Estado de México, México
Teléfono: +52 (959) 5201 200
manueloe@colpos.mx

Dr. Edgar Iván Sánchez Bernal

Instituto de Ecología
Universidad del Mar
Carretera a Zipolite km 1.5
San Pedro Pochutla, Oaxaca, México
Teléfono: +52 (958) 5843 149
edgarivansb@zicatela.umar.mx

Dra. Elia Cruz Crespo

Unidad Académica de Agricultura
Universidad Autónoma de Nayarit.
km 9 Carretera Tepic-Compostela
63780 Xalisco, Nayarit, México
Teléfono: +52 (311) 2110 128
ccruzc2006@yahoo.com.mx

Click here to write the autor

Current conditions in the Patcuaro wetlands, Island of Jaracuaro, Michoacan, Mexico.

Photo: Lenin Medina Orozco.

Content of Boron in Surface Water in Puebla, Tlaxcala, and Veracruz

• Oscar Raúl Mancilla-Villa* •
Universidad de Guadalajara, México
*Corresponding Author

• Ana Laura Bautista-Olivas •
Universidad de Sonora, México

• Héctor Manuel Ortega-Escobar • Carlos Ramírez-Ayala •
Colegio de Postgraduados, México

• Amada Laura Reyes-Ortigoza •
Universidad Nacional Autónoma de México

• Héctor Flores-Magdaleno •
Colegio de Postgraduados, México

• Diego Raymundo González-Eguiarte • Rubén Darío Guevara-Gutiérrez •
Universidad de Guadalajara, México

Abstract

Mancilla-Villa, O. R., Bautista-Olivas, A. L., Ortega-Escobar, H. M., Ramírez-Ayala, C., Reyes-Ortigoza, A. L., Flores-Magdaleno, H., González-Eguiarte, D. R. & Guevara-Gutiérrez, R. D. (September-October, 2014). Content of Boron in Surface Water in Puebla, Tlaxcala, and Veracruz. *Water Technology and Sciences* (in Spanish), 5(5), 93-104.

The development of agriculture depends on the quantity and quality of water available for irrigation, among other factors. Quality varies widely according to the quantity and type of salts it contains, since some elements such as boron (B) are toxic for plants. In Puebla, Tlaxcala and Veracruz over one million hectares are used for irrigation agriculture, and therefore it is imperative to know the quality of water with respect to boron contents. Therefore, this study conducted an investigation to determine the electrical conductivity (EC), pH and B content in these waters based on three samplings, performed in 2009, 2010 and 2011. A total of 91 samples were taken for each sampling. B content in water was determined in the hydro-sciences laboratory of the Postgraduates College using the Azomethine-H method. Concentrations of B in the water were low and less than 1 mg L^{-1} for 76 of the 91 samples collected for each sampling. High contents of B, above 5 mg L^{-1}, were found in 15 samples. Of the waters analyzed, 83.5% is recommended for agricultural use without restriction, while 16.5% is not recommended for agricultural, domestic or recreational uses due to the dangers and risk of toxicity from B in crops and in humans.

Keywords: Surface water, permissible limits of boron, toxicity in crops, sewage.

Resumen

Mancilla-Villa, O. R., Bautista-Olivas, A. L., Ortega-Escobar, H. M., Ramírez-Ayala, C., Reyes-Ortigoza, A. L., Flores-Magdaleno, H., González-Eguiarte, D. R. & Guevara-Gutiérrez, R. D. (septiembre-octubre, 2014). Contenido de boro en el agua superficial de Puebla, Tlaxcala y Veracruz. Tecnología y Ciencias del Agua, *5(5), 93-104.*

El desarrollo de la actividad agrícola depende, entre otros factores, de la cantidad y calidad del agua disponible para riego. La calidad varía ampliamente de acuerdo con la cantidad y tipo de sales que contenga, ya que algunos elementos, como el boro (B), son tóxicos para las plantas. En Puebla, Tlaxcala y Veracruz son destinadas a la agricultura de riego más de un millón de hectáreas y por ello resulta imperante conocer la calidad del agua en cuanto al contenido del boro. En este estudio se llevó a cabo una investigación para conocer la conductividad eléctrica (CE), el pH y el contenido de B de estas muestras de agua, con tres recorridos y muestreos de agua en 2009, 2010 y 2011; se colectaron 91 muestras de agua por cada muestreo. La determinación de B se realizó por el método de la azometina-H, en el Laboratorio de Hidrociencias del Colegio de Postgraduados. Las concentraciones de B en las muestras de agua fueron bajas, menores de 1 mg l^{-1}, en 76 de las 91 colectas de cada muestreo. En 15 muestras de agua se encontraron contenidos altos de B, mayores a 5 mg l^{-1}. De las muestras de agua analizadas, 83.5% se recomienda para uso agrícola sin ninguna restricción, mientras que 16.5% de los ríos y cuerpos de agua no es recomendable para usos agrícola, doméstico o de recreación debido a la peligrosidad y riesgos de toxicidad por B en cultivos y en humanos.

Palabras clave*: agua superficial, límites permisibles de boro, toxicidad en cultivos, agua residual.*

Received: 17/04/13
Accepted: 25/01/14

Introduction

Boron (B) is an essential element and potentially toxic to plants when it even slightly exceeds the optimal level. It is found in nearly all natural water and is one of the most toxic constituents in irrigation water. Its concentration varies from traces to several parts per million (Gupta, Jame, Cambell, Leyshon, & Nicholaichuk, 1985; Keren & Miyamoto, 1990; Singh & Singh, 1983; Verma, 1983; Elefteriou, 2001).

The toxicity of B occurs in concentrations over 1.25 mg l^{-1} for most plants (Fox, 1968; Gupta, 1983; Gupta *et al*., 1985; Munns & Tester, 2008; Ortega & Cintora, 2005; Richard, 1968; Ryan, Miyamoto, & Stroehlein, 1977; Singh & Randhawa, 1980; Verma, 1983; Brady & Weil, 2002). For plants growing in sand, they can develop normally with traces of boron (0.03-0.04 mg l^{-1}), while toxicity is present when concentrations reach 1 mg l^{-1} (Richard, 1968; Richards, 1973; Ayers & Westcot, 1989). This level is sufficient to cause sensitivity in lime and orange plants, while alfalfa reaches its maximum development if irrigation water contains 1 to 2 mg l^{-1} (Kelley, 1963; Brady & Weil, 2002).

Natural surface water rarely contains toxic levels of B, whereas water in springs and wells primarily near tectonic faults and geothermal areas can contain toxic concentrations, (Carrera *et al*., 2011; Velázquez & Pimentel, 2006). The classification of water for agricultural use based on B contents is presented in Table 1.

Boron has nutritional benefits, if not essential, for humans and animals. Boron deficiency can lead to potential health risks (Coughlin, 1998). Fruits, vegetables and nuts are a source of B in the human diet and a daily acceptable consumption is 0.3 mg kg^{-1} in weight (Murray, 1998). The maximum permissible limits for B in potable water can differ depending on the various norms which exist.

For Mexico, the official norm for water for human consumption and use (SSA, 1996) does not include reference values for B and the ecological criteria for water quality (Sedue, 1989) indicates a maximum permissible limit of 1 mg l^{-1} (1 000 µg l^{-1}) for public urban use. This value coincides with the European Directive (Weinthal, Parag, Vengosh, Muti, & Kloppmann, 2005). The World Health Organization established a limit of 500 μg^{-1} (WHO, 2008), although it is currently revising it and is provisionally establishing a limit of 2.6 mg l^{-1} (WHO, 2010). The health problems associated with excessive consumption of B range from damages to the digestive system (stomach and intestine), liver, kidneys, brain and even death (Selinus, 2004; WHO, 2008).

B is a ubiquitous element that enters surface water and groundwater through two main routes: the weathering of rocks containing boron (tourmaline type borosilicate and axinite) and wastewater, where B comes from cleaning products and industrial waste from

Table 1. Classification of irrigation waters based on boron contents.

Water class	Crop group		
	Sensitive	Semi-tolerant	Tolerant
	mg l^{-1}		
Excellent	< 0.33	< 0.67	< 1.00
Good	0.33 - 0.67	0.67 - 1.33	1.00 - 2.00
Acceptable	0.67 - 1.00	1.33 - 2.00	2.00 - 3.00
Unsafe	1.0 - 1.25	2.00 - 2.50	3.00 - 3.75
Not recommended	> 1.25	> 2.50	> 3.75

Source: Scofield, 1936; Wilcox, 1948.

paint, varnish, textile, tanning of hides and electronics, among others (Dyer & Caprara, 2009; Velázquez, Pimentel, & Ortega, 2011). Wastewater from different systems can reach surface and groundwater and cause contamination (Wolf, Held, Eiswirth, & Hötzl, 2004; Schmidt, 2007).

An additional source of B in surface water is agricultural drainage (Seiler, 2007), such as that detected in arid regions in the western United States (Lemly, Finger, & Nelson, 2009). In areas with volcanic activity, where groundwater is affected by high temperatures (roughly 200°C), B is regularly found in concentrations as high as 150 mg l^{-1} (Morell, Pulido-Bosch, Daniele, & Cruz, 2008). The relationship of B with volcanic areas is relevant in Mexico, considering that some 2 334 geothermal springs have been identified, of which approximately 27 are located in the states of Puebla and Veracruz (Iglesias, Arellano, & Torres, 2005).

In previous works about water quality in basins in the states of Tlaxcala, Puebla and Veracruz, B has been found to be added to surface water through wastewater discharged into the hydrographic network, while the groundwater can contain high concentrations of B due to geothermal conditions (Velázquez & Pimentel, 2006; Can *et al.*, 2011). These concentrations can present a potential danger of toxicity to crops in the region and health problems in the population if these water sources are used for human consumption.

In spite of its environmental importance, the distribution of B in surface water in Puebla, Tlaxcala and Veracruz is unknown. No data exist about B in surface and groundwater from natural and anthropogenic origins. Given this background, the objective of the present work is to analyze the distribution of B in surface water in the states mentioned and its potential toxic effect on crops and human health. The latter will be analyzed in terms of the maximum permissible limits established by the Mexican norm for different water uses.

Materials and Methods

Study area

The study area is located in the state of Puebla and the north-central portion of the state of Veracruz, Mexico (Figure 1). The water sampled is used for irrigation and domestic uses. The rivers, springs and reservoirs sampled in Puebla includes: Atoyac, Izúcar, Salado and Chiahutla. Those in Veracruz included: Blanco, San Miguel, Chocamam, Coscomatepec, Pescados, Consolapa, Alseseca, Tlapacoyan, Filobobos, Nautla, Tecolutla, Cazones, Tuxpan, Tempoal, Pánuco, Tampico, Nogales, Ojo de Agua, Puente de Dios, El Carmen and Pancho Pozas. The geographic coordinates of the study area are from 22° 00′ north latitude and 97°00′ west longitude to 18°00′ north latitude and 99°00′ west longitude. The altitude of the sampling sites ranges from 1 to 3 000 m.

The field sampling began at the border of Puebla and Tlaxcala, followed by southern Puebla, then north-central Veracruz and ending at the Necaxa dam in Puebla. Three samplings were collected during the dry season in the autumn of 2009, 2010 and 2011. The water samples were placed in 0.5 l polypropylene containers which were cleaned three times prior to collection —twice with distilled water and the third time with deionized water. The bottle was filled completely to eliminate introducing possible air bubbles into the water, thereby reducing possible reactions between the fluid and oxygen. The sampling stations were located with Garmin MAP 60 GPS, which was also used to determine the approximate altitude, in meters, of each site.

The chemical parameters measured at the time of sampling were pH and EC, in accordance with APHA (1995). The B contents in the water samples were determined at the Environmental Sciences of Hydro-sciences laboratory, at the Postgraduate College, Campus, Montecillo. The B was analyzed using azomethine-H, which has a detection range from 0.5 to 10 µg ml^{-1} (Bingham, 1982;

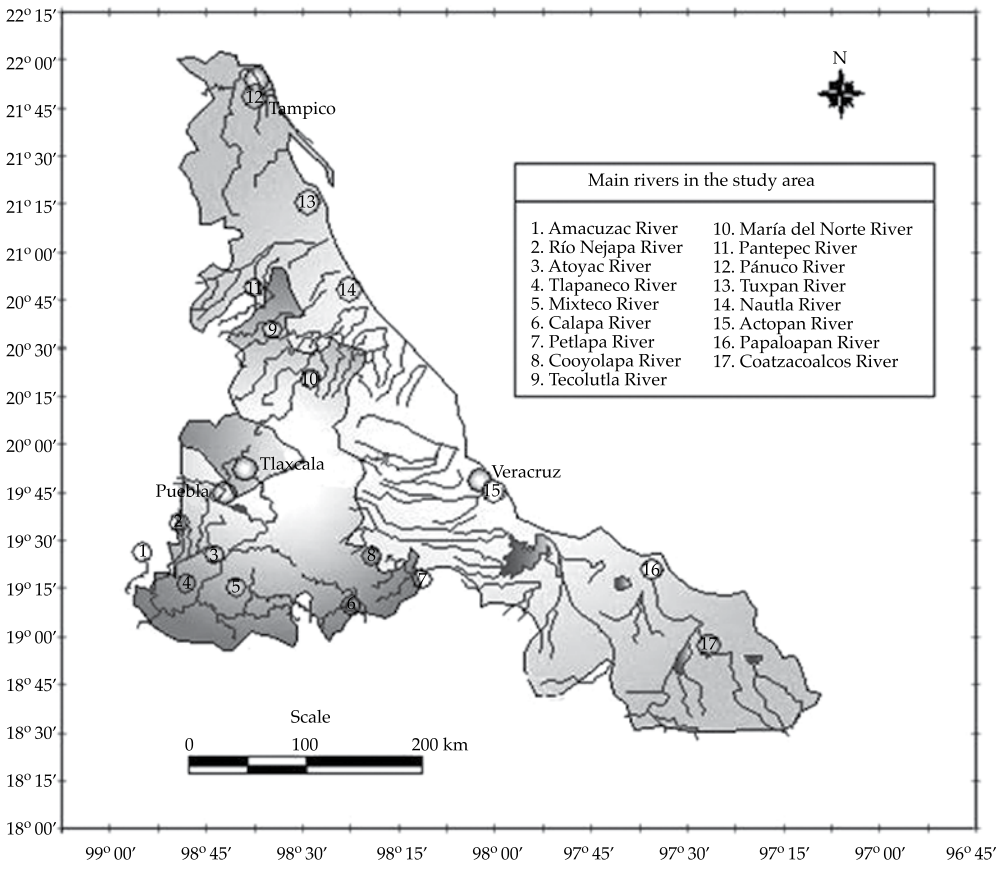

Figure 1. Location of the study area.

Rodier, 1978; Rhoades, Ingvalson, & Hatcher, 1970). The data were analyzed with the Tukey mean statistical analysis ($\alpha = 0.05$) to determine the existence of significant differences in B contents among the water samples.

Results and Discussion

Table 2 presents the geographic location, altitude and names of the sampling stations included in the present investigation. It is important to mention that the stations were located at an altitude range from sea level up to 3 000 m. The rivers and reservoirs important to irrigation in the states of Puebla and Veracruz were included. The information pertaining to the results from the 91 sampling stations was managed jointly.

Figure 2 presents the pH and EC measured in the rivers, springs and reservoirs in Puebla and Veracruz. The values of these parameters were corrected for temperature. Ninety percent of the samples had a pH between 6.9 and 9 (the maximum permissible limit is 5 to 10 units). In 85% of the samples, the electrical conductivity was less than 2 000 μS cm^{-1}. Based on these two parameters, the water analyzed was generally acceptable for agricultural use, according to Ayers and Westcot (1989). Nevertheless some restrictions were indicated for 15% of the samples with high EC levels, which came from water affected by sea water and saline groundwater.

Table 2. Geographic location and names of sampling stations.

No.	Place	Geographic position		Altitude (m)	No.	Place	Geographic position		Altitude (m)
		Lat. north	Long. west				Lat. north	Long. west	
1	Tepozontitla, Puebla Dike	19 °30.556	98 °31.98	2 933	**47**	Río Puente Pescados, Veracruz	19°21.821	96°49.574	486
2	Nanacamilpa Dam, Puebla	19°28.848	98°31.115	2 887	**48**	Afluente a río Pescados	19°23.121	96°51.058	687
3	River in Atotonilco, Puebla	19°21.665	98°27.517	2 492	**49**	Río Lomas, Veracruz	19°26.076	96°54.711	1 107
4	Atoyac River, Puebla	19°19.374	98°27.678	2 502	**50**	Río Cosolapa, Veracruz	19°27.837	96°56.850	1 270
5	Atoyac River, Puebla	19°18.918	98°27.729	2 452	**51**	Lago cráter Alchichica	19°24.579	97°23.791	2 500
6	Chiautla Lagoon, Puebla	19°19.011	98°28.250	2 478	**52**	Lago cráter La Preciosa	19°22.471	97°23.008	2 510
7	Chiautla Spring, Puebla	19°19.065	98°28.472	2 524	**53**	Lago cráter Quecholac	19°22.471	97°23.008	2 510
8	Chiautla Spring no. 2, Puebla	19°19.065	98°28.472	2 524	**54**	Nacimiento Manantiales, Puebla	19°16.307	97°21.343	2 512
9	Atoyac River, Puebla	19°04.121	98°14.515	2 268	**55**	Nacimiento Bicencio	19°17.524	97°40.148	2 530
10	Manuel Ávila Camacho Dam, Puebla	18°54.645	98°06.502	2 220	**56**	Nacimiento El Carmen	19°19.026	97°37.945	2 532
11	San José Aguacate Dike	18°51.634	98°11.152	2 099	**57**	Lago cráter Aljojuca	19°05.550	97°32.223	2 545
12	Huehuetlán River, Puebla	18°45.700	98°10.553	1 485	**58**	Lago cráter San Miguel Tecuitlapa	19°07.408	97°32.680	2 551
13	Huehuetlán Stream, Puebla	18°43.910	98°11.648	1 445	**59**	Lago cráter Atexcac	19°20.211	97°26.979	2 529
14	River in Izúcar	18°35.370	98°27.843	1 436	**60**	Arroyo en San José Capillas	19°13.544	97°22.705	2 635
15	Epatlán Stream, Puebla	18°38.559	98°22.408	1 437	**61**	Nacimiento Pancho Pozas Altotongo	19°44.375	97°15.145	2 646
16	Epatlán Lagoon, Puebla	18°37.764	98°21.098	1 442	**62**	Río Pancho Pozas Altotongo	19°44..603	97°14.915	2 165
17	El Rodeo Stream, Puebla	18°35.757	98°15.407	1 384	**63**	Río Tlapacoyan, Veracruz	19°50.034	97°13.206	1 303
18	Atoyac River in Coatzingo, Puebla	18°36.708	98°10.784	1 251	**64**	Río Alseseca, Puente Tomata, Veracruz	19°55.311	97°13.363	1 309
19	Aximilpa River, Tepejí, Puebla	18°36.570	97°55.882	1 684	**65**	Cascada El Encanto Veracruz	19°58.865	97°10.435	601
20	Puente de Dios River, Puebla	18°44.076	97°55.606	1 811	**66**	Arroyo de Piedra, Tlapacoyan, Veracruz	23°01.934	97°07.069	127
21	Tepeyahualco River, Puebla	18°48..959	97°52.758	2 076	**67**	Río Filobobos, Veracruz	20°08.025	96°57.045	7
22	La Purísima sprinkler irrigation, Puebla	18°49.967	97°46.965	2 131	**68**	Río Nahuatla, Veracruz	20°12.770	96°46.718	18
23	San Antonio Tecolco Well, Puebla	18°51.575	97°46.234	2 150	**69**	Río en Nautla, Veracruz	20°12.891	96°45.686	5

24	Francisco Villa Well, Puebla	18°50.759	97°45.365	2 144	**70**	Nautla River, Puente Remolino	20°23.949	97°14.247	24
25	Salado River, Puebla	18°23.008	97°26.497	1 687	**71**	Tecolutla River tributary streams	20°23.160	97°18.362	48
26	Tilapa waterfall, Puebla	18°16.349	97°29.236	1 696	**72**	Tecolutla River	20°26.939	97°05.005	58
27	Salado River in Zapotitlán, Puebla	18°19.098	97°30.618	1 622	**73**	Cazones River, Cazones, Veracruz	20°42.101	97°15.656	3
28	Stream in Salinas Zapotitlán, Puebla	18°20.809	97°26.930	1 642	**74**	Cazones River, in La Unión, Veracruz	20°41.619	97°20.422	14
29	Well in Salinas Zapotitlán, Puebla	18°20.809	97°26.930	1 642	**75**	Stream in Países Bajos	20°54.140	97°21.946	6
30	Basin in Salinas, Puebla	18°20.809	97°26.930	1 642	**76**	Tributary of the Tuxpan River	20°56.448	97°23.471	3
31	El Agua de Noé Alcutzingo, Puebla	18°44.927	97°14.518	1 649	**77**	Tuxpan River, Puente Tuxpan	20°56.884	97°23.664	3
32	Blanco River, Ojo Zarco, Veracruz	18°46.843	97°12.379	1 435	**78**	River in Tuxpan, Veracruz	20°58.416	97°18.473	2
33	Nogales Lagoon, Veracruz	18°49.233	97°09.876	1 450	**79**	Tributary river of Tuxpan	21°06.030	97°47.966	96
34	Blanco River in Río Blanco, Veracruz	18°49.758	97°09.031	1 358	**80**	Tributary stream of the Calabozos River, Veracruz,	21°03.900	98°08.644	103
35	Ojo de Agua, Orizaba, Veracruz	18°51.800	97°04.617	1 244	**81**	La Puertar, Calabozos River	21°03.835	98°09.230	92
36	Spring in Matzinga, Veracruz	18°48.280	97°05.651	1 254	**82**	Terrero River in Alagualtitla, Veracruz	20°56.629	98°10.681	98
37	River in Matzinga, Veracruz	18°48.280	97°05.651	1 254	**83**	Mezcatlán Spring, Veracruz	20°58.663	98°09.203	447
38	Los Manantiales Spring, Veracruz	18°47.836	97°06.351	1 265	**84**	River in Platón Sánchez, Veracruz	21°17.920	98°21.403	61
39	Río Blanco, Orizaba outlet	18°49.964	97°05.266	1 256	**85**	Tempoal River, Veracruz	21°30.037	98°24.699	36
40	San Miguel River, Veracruz	18°53.582	97°00.700	938	**86**	Pánuco River, Veracruz	22°03.629	98°10.566	2
41	Meltac River, Veracruz	18°53.582	97°00.700	938	**87**	Bridge Cortadura Lagoon Chila, Veracruz	22°10.990	98°01.125	1
42	Blanco River, Córdoba, Veracruz	18°52.192	96°52.537	724	**88**	Pánuco River, out to sea	22°13.414	97°53.717	4
43	Spring in the Atyoca River	18°55.564	96°52.713	646	**89**	Cazones River in Coronel Tito Hdez	20°27.239	97°43.968	144
44	Choacaman River, Veracruz	19°01.994	97°01.671	1 449	**90**	Necaxa Dam	20°13.196	97°59.966	1308
45	Consomatepec River, in Jamapa Veracruz	19°06.004	97°02.037	1 458	**91**	River in Texcapa Bridge II	20°13.196	97°59.966	1393
46	Huatuzco River, Veracruz	19°09.072	96°49.574	486					

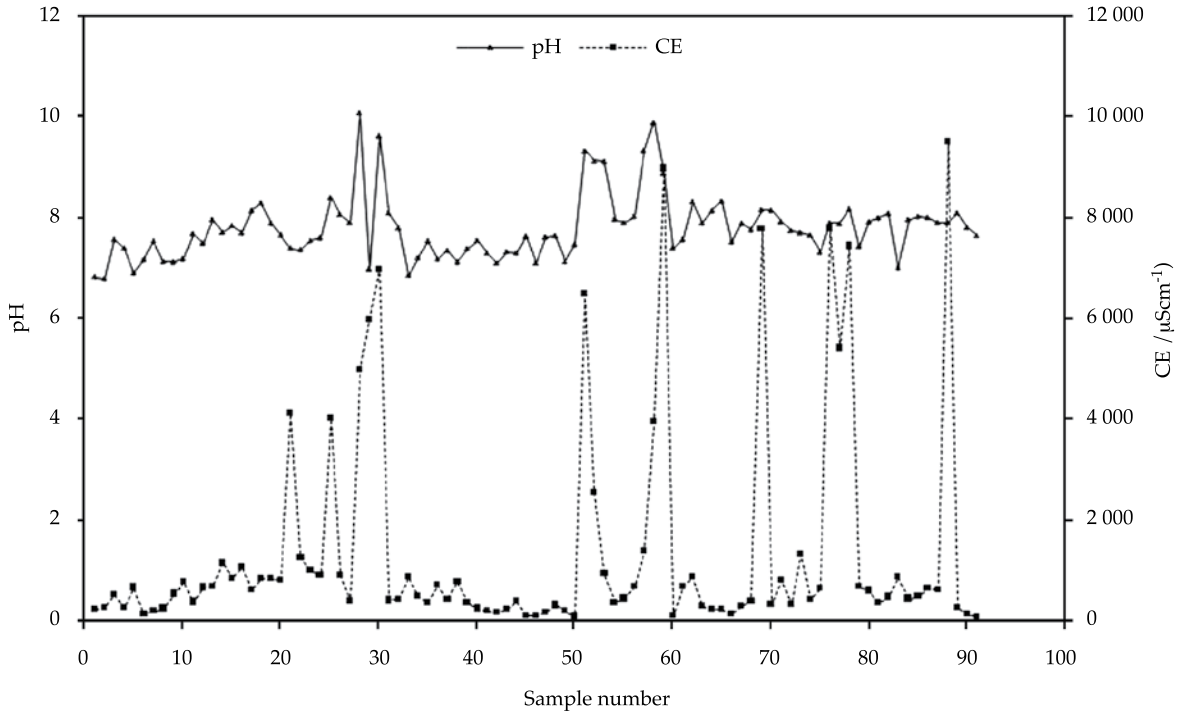

Figure 2. Electrical conductivity and pH measured in sampled water.

Boron contents

Can *et al.* (2011) performed an investigation related to boron contents in groundwater in the Oriental Watershed, Mexico, which includes the states of Tlaxcala, Puebla and Veracruz. They found that most of the surface water contained acceptable amounts of boron, while water from deep wells in some areas contained toxic amounts due to contact with igneous rocks in the region. The main volcanic rocks in the region are andesites, basalts and rhyolites. Predominant among these are sodic rhyolites, olivine phenocrysts and pyroclastic sediments, which are mostly defined as tuffs.

The surface water is affected by discharges from domestic wastewater and agricultural drainage, which are the two primary sources of salts in the rivers (Velázquez *et al.*, 2011). A third source is the geothermal flows (Iglesias *et al.*, 2005).

The B contents were low —less than 1 mg l^{-1}— in the surface water in Puebla, Tlaxcala and Veracruz for the three samples (Figure 3). Nevertheless, some water samples presented levels over the maximum permissible limit for plants (3.75 mg l^{-1}) (Scofield,1936; Wilcox, 1948).

The surface water in Tlaxcala, Puebla and Veracruz with low concentrations of B, less than 1 mg l^{-1}, is in contact with sedimentary rocks which cover over 75% of the land, including limestone, lutites, diatomite, limonite, gypsum and laterite (Tarbuck & Lutgens, 2008).

The water with low B concentration is presented in Figure 4, where it can be seen that the contents did not exceed 0.03 mg l^{-1}.

The water samples in Figure 4 are acceptable for irrigation of tolerant crops such as cotton, asparagus, sorghum, alfalfa, lettuce and corn, among others (Van Der Leeden, Troise & Todd, 1990), as well as sensitive crops such as lime, avocado, oranges and barley (Can *et al.*, 2011). That is, in terms of B contents, this water is acceptable to irrigate any of the crops.

Fifteen surface water sampling points had high concentrations of B, over 5 mg l^{-1}

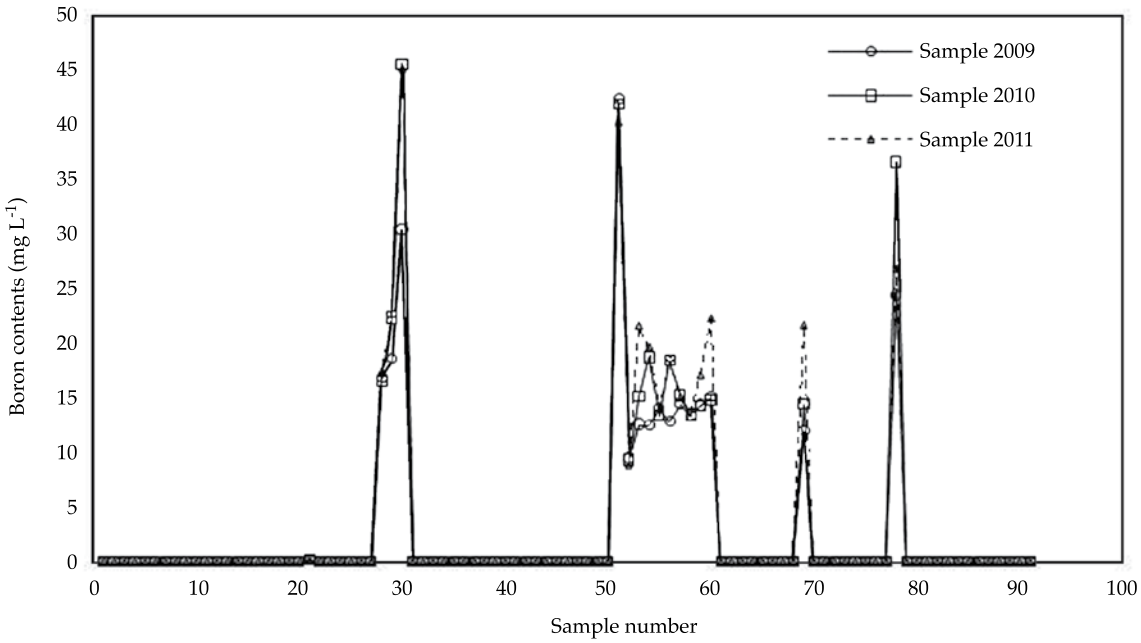

Figure 3. Boron concentration in surface water in Puebla, Tlaxcala and Veracruz.

(Velázquez *et al.*, 2011): Salado River, Atoyac River, Zapotitlan stream, and the crater lakes of Alchichica, La Preciosa, Quecholac, Aljojuca, Tecuitlapa, Atexcac, in Puebla. The samples analyzed from these sites show concentrations from 9 to 45 mg l^{-1}. In Tlaxcala, El Carmen spring had a high concentration, 12 mg l^{-1}, and in Veracruz, the Nautla and Tuxpan rivers had Boron concentrations over 12 and 24 mg l^{-1}, respectively (Figure 5).

Figure 5 shows the water samples with high B contents, over 5 mg l^{-1}. The sampling sites from which these aliquots were collected are near mountains areas in the Trans-Mexican Volcanic Belt, whose geological composition is primarily composed of igneous rocks, including colemanite, borax, olivine, sasolites and pegmatites, among others (Tarbuck & Lutgens, 2008). In addition, the water samples with high B contents in the study area can be affected by hydrothermalism, as a result of recent volcanism in the region (Alcocer, Escolero, & Marín, 2005).

The samples with higher B contents also have higher electrical conductivity, and therefore more dissolved solids, which can be affected by salts from sea intrusions (Salas, 1949; Reyes-Cortés, 1979). It is important to mention that the innumerable number of saline springs in the region of Zapotitlan are due to buried evaporites and carbonate saline sediments from the volcanic explosions that raised the Zapotitlan region during the Tertiary period (Calderón-García, 1958; Salas, 1949; Villada, 1905; Reyes, 1998). The type of salinity of the salt water in Zapotitlan is also due to pluvial water flowing through sedimentary limestone in that region (Cortés, 2009).

Therefore, the water samples pertaining to the 15 sampling points with high B concentrations are not recommended for agricultural irrigation because they would be toxic even to more tolerant crops. In addition, it is restricted for human use (WHO, 2010) as well as domestic and recreation uses (Sedue, 1989).

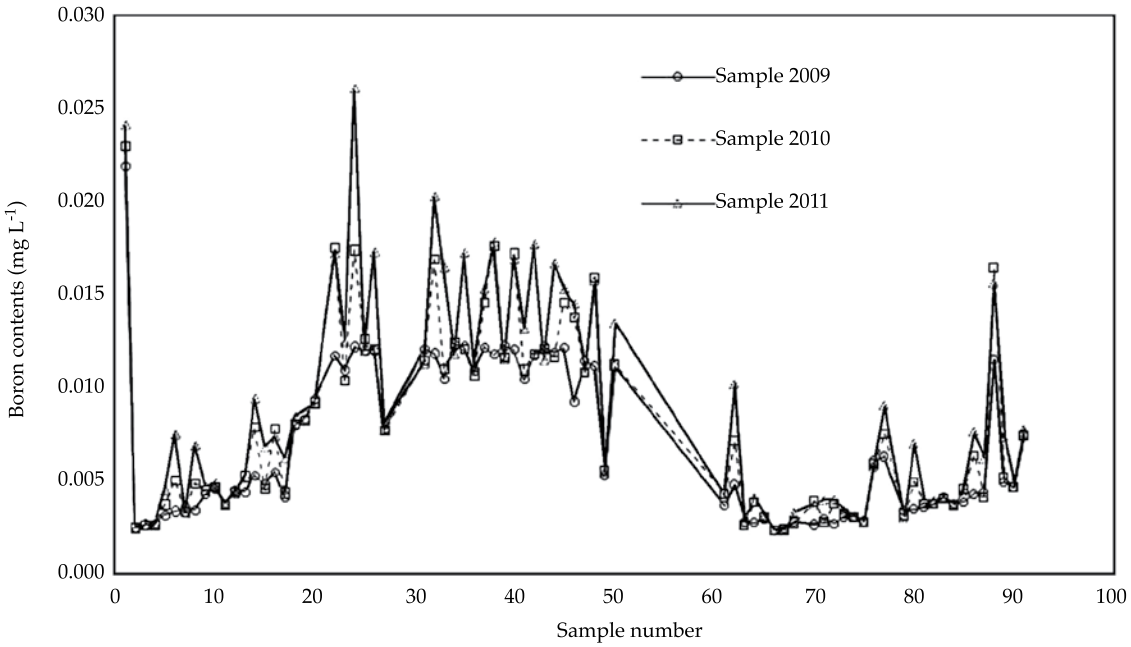

Figure 4. Low boron concentrations in surface water, Puebla, Tlaxcala and Veracruz.

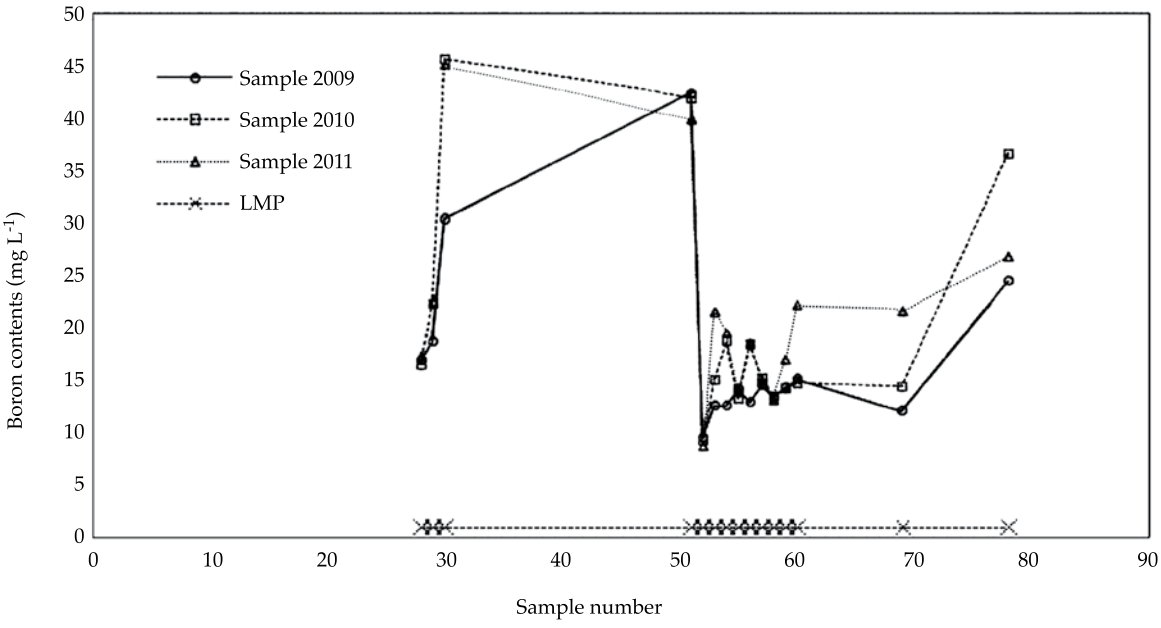

Figure 5. High boron concentrations in surface water, Puebla, Tlaxcala and Veracruz.

Other factors related to the high concentrations of B may be agricultural, urban and industrial wastewater discharges from anthropogenic activities, particularly with regard to the Nautla and Tuxpan rivers in Veracruz.

Table 3 presents the analysis of the Tukey means for B contents per site, for surface water in Puebla, Taxcala and Veracruz. According to the statistical analysis, a significant differences exist in B contents between the water with the highest EC and that with the lowest dissolved salts contents.

No significant differences exist among the water found near recent volcanic activity, such as the crater lakes in the Oriental Basin (Can, 2011), or among the water in the rivers that are significantly contaminated by wastewater, such as the Nautla and Tuxpan rivers in Veracruz. Furthermore, no significant differences were found in boron contents among water samples containing lower B contents located far from the areas affected by hydrothermalism, and which have been reported as being less affected by contamination from wastewater.

Conclusions

The values of the electrical conductivity in 90% of the surface water samples in Puebla, Tlaxcala and Veracruz were between 100 and 200 μS cm^{-1} —optimal values for water for agricultural use.

The surface water analyzed had slightly alkaline pH values, which suggests a significant presence of dissolved carbonates and bicarbonates, but it is not restricted for agricultural use.

The B contents in surface water was low in 76 of the samples analyzed, and therefore this water is acceptable for irrigation without restrictions, as well as for domestic and recreational uses.

The 15 surface water samples with high B concentrations are affected by hydrothermalism, rocks containing B and the presence of salts from sea intrusions.

The water with high concentrations of B —found in 15 of the 91 sampling sites in Puebla, Tlaxcala and Veracruz— is restricted for agricultural, domestic and recreational uses because of the risks of toxicity to crops and humans.

A significant difference in B contents exists among sampling sites, and between the water samples with high ionic concentrations and samples with low dissolved salts and less contamination from wastewater.

References

Alcocer, D. J., Escolero, F. Ó. A., & Marín, S. L. E. (2005). Problemática del agua de la Cuenca Oriental, estados de Puebla, Veracruz y Tlaxcala. En B. Jiménez & L. Marín (Eds.). *El agua en México vista desde la academia* (pp. 57-77). México, DF: Academia Mexicana de Ciencias.

APHA (1995). *Standard Methods for Examination of Water and Wastewater* (1035 pp.). Washington, DC: American Public Health Association (APHA), American Water Works Association (WWA), Water Pollution Control Federation (WPCF).

Table 3. Statistical analysis with Tukey means analysis in terms of B contents, per site, for the three samplings of surface water, Puebla, Tlaxcala and Veracruz.

Site	Range of boron means (mg l^{-1})	Tukey $\alpha = 0.05$ (¥)
30 and 51	40.42 to 41.59	A
78	29.34	B
29	21.2	C
28, 53, 54, 56, 60 y 69	16.058 to 17.424	CD
57 and 59	14.93 to 15.20	D
55 and 58	13.37 to 13.85	DE
52	9.2	E
1 to 27; 31 to 50; 61 to 68; 70 to 77; 79 to 91	0.002 to 0.138	F

¥ literal different means significant difference.

Ayers, R. S., & Westcot, D. W. (1989). *La calidad del agua y su uso en la agricultura. Estudio FAO Riego y Drenaje 29 Rev. 1* (174 pp.). Trad. al español por J. F. Alfaro (Water Quality and Use in Agriculture). Roma: FAO.

Bingham, F. T. (1982). Boron. In A. L. Page (Ed.). *Methods of Soil Analysis* (pp. 435-436). Part 2. Chemical and microbiological properties. Agronomy 9. Madison, USA: ASA, SSSA, WI.

Brady, N. C., & Weil, R. R. (2002). *The Nature and Properties of Soils* (960 pp.). (13 ed.). New Jersey: Prentice Hall.

Calderón-García, A. (1958). *Bosquejo geológico de la región de San Juan Raya, Puebla* (pp. 9-27). XX Congreso Geológico Internacional, Libreto-Guía de la Excursión A-11, México, D.F.

Can, C. A., Ortega, E. M., García, C. N., Reyes, O. A., González, H. V., & Flores, R. D. (2011). Origen y calidad del agua subterránea en la Cuenca Oriental de México. *Terra Latinoamericana*, *29*(2), 189-200.

Carrera-Villacres, D. V., Ortega-Escobar, H. M., Ramírez-García, J., Ramírez-Ayala, C., Trejo-López, C., & Becerril-Román, A. E. (2011). Boro, fosfatos e índices de salinidad del sistema hidrográfico Zahuapan-Atoyac, México. *Tecnología y Ciencia del Agua*, *2*(2), 5-21.

Cortés, M. N. (2009). *Geoconservación y cultura: un análisis de paisaje en Zapotitlán Salinas-El Encinal, Puebla* (186 pp.). Tesis de maestría en Geografía. México, DF: UNAM.

Coughlin, J. R. (1998). Inorganic Borates: Chemistry, Human Exposure, and Health and Regulatory Guidelines. *J. Trace Elem. Experim. Med*., *9*, 137-151.

Elefteriou, P. (2001). *Boron in Groundwater of the Island of Cyprus 2001* [en línea]. Citado el 26 de febrero de 2013. Recuperado de http://www.hydroweb.com/jehabs/eleftabs.

Dyer, S. D., & Caprara, R. J. (2009). A Method for Evaluating Consumer Product Ingredient Contributions to Surface and Drinking Water: Boron as a Test Case. *Environ. Tox. Chem*., *16*, 2070-2081.

Fox, R. H. (1968). The Effect of Calcium and pH on Boron Uptake from High Concentrations of Boron by Cotton and Alfalfa. *Soil Sci*., 106(6), 435-439.

Gupta, I. C. (1983). Concept of Residual Sodium Carbonate in Irrigation Waters in Telation to Sodic Hazard in Irrigated Soils. *Curr. Agric*., *7*(3,4), 97-113.

Gupta, U. C., Jame, Y. W., Cambell, C. A., Leyshon, A. J., & Nicholaichuk, W. (1985). Boron Toxicity and Deficiency: A Review Can. *J. Soil Sci*., *65*(3), 381-409.

Iglesias, E., Arellano, V., & Torres, J. R. (2005). Estimación del recurso y prospectiva tecnológica de la geotermia en México [en línea] Citado el 10 de febrero de 2013. Recuperado de http://www.sener.gob.mx/webSener/res/168/A3_Gtermia.pdf 12/06/2010.

Kelley, W. P. (1963). Use of Saline Irrigation Water. *Soil Sci*., *95*, 385-391.

Keren, R., & Miyamoto, S. (1990). Reclamation of Saline, Sodic and Boron Affected Soils. In K. K. Tanji (Ed.). *Agricultural Salinity Assessment and Management* (pp. 410-431). Chapter 19. ASCE. Manuals and Reports on Engineering Practice No. 71. New York: American Society of Civil Engineers.

Lemly, A. D., Finger, S. E., & Nelson, M. K. (2009). Sources and Impacts of Irrigation Drainwater Contaminants in Arid Wetlands. *Environ. Tox. Chem*., *12*, 2265-2279.

Morell, I., Pulido-Bosch, A., Daniele, L., & Cruz, J. V. (2008). Chemical and Isotopic Assessment in Volcanic Thermal Waters: Cases of Ischia (Italy) and Sâo Migul (Azores, Portugal) [en línea]. Citado el 5 de diciembre de 2012. Recuperado de http://www3.interscience.wiley.com/journal/118720600/.

Munns, R., & Tester, M. (2008). Mechanisms of Salinity Tolerance. *Annu. Rev. Plant Biol*., *59*, 651-681.

Murray, F. J. (1998). Issues in Boron Risk Assessment: Pivotal Study, Uncertainty Factors, and ADIs. *J. Trace Elem. Exp. Med*., *9*, 231-243.

Ortega, Y. M., & Cintora, M. J. S. G. (2005). *Boro, fósforo, e índices de salinidad en las aguas residuales para riego agrícola en el valle del Mezquital, Hidalgo* (125 pp.). Tesis de Licenciatura en Biología. México, DF: UNAM.

Reyes, G. J. C. (1998). *La sal en México II* (473 pp.). Colima, México: Universidad de Colima.

Reyes-Cortés, M. (1979). *Geología de la Cuenca de Oriental, estados de Puebla, Veracruz y Tlaxcala* (62 pp.). Colección Científica, Prehistoria 71. México, DF: SEP-INAH.

Rhoades, J. D., Ingvalson, R. D., & Hatcher, J. T. (1970). Laboratory Determination of Leachable Soil Boron. *Soil Sci. Soc. Am. Proc*., 34, 871-875.

Richard, H. F. (1968). The Effect of Calcium and pH on Boron Uptake from High Concentrations of Boron by Cotton and Alfalfa. *Soil Sci*., *106*(6), 435-439.

Richards, L. A. (Ed.). (1973). Suelos salinos y sódicos. Personal del Laboratorio de Salinidad de los Estados Unidos de América. *FAO, Manual de Agricultura*, *60*, 172.

Rodier, J. (1978). *Análisis de las aguas* (pp. 186-191). Barcelona: Ediciones Omega.

Ryan, J., Miyamoto, S., & Stroehlein, J. L. (1977). Relation of Solute and Sorbed Boron to the Boron Hazard in Irrigation Water Short Communication. *Plant and Soil*., *47*, 253-256.

Salas, G. P. (1949). Bosquejo geológico de la cuenca sedimentaria de Oaxaca. *Bol. Asoc. Mexicana Geóls. Petrols*., *1*(2), 79-156.

Schmidt, K. D. (2007). Groundwater Quality in the Cortaro Area Northwest of Tucson, Arizona. *J. Am. Water Res. Assoc*., *9*, 598-606.

Scofield, F. E. (1936). *The Salinity of Irrigation Water* (pp. 275-283). Washington, DC: Smith. Instit. Ann. Rep.

Sedue (13 de diciembre de 1989). Norma CE-CCA-001/89. Acuerdo por el que se establecen los Criterios Ecológicos de Calidad del Agua. Secretaría de Desarrollo Urbano y Ecología. *Diario Oficial de la Federación*, *430*(9), 7-15.

Seiler, R. L. (2007). Synthesis of Data from Studies by the National Irrigation Water-Quality Program. *J. Am. Water Res. Assoc*., *32*, 1233-1245.

Selinus, O. (2004). Medical Geology: An Emerging Specialty. *Terrae*, *1*(1), 8-15.

Singh, J., & Randhawa, N. S. (1980). Boron Leaching and Regeneration Capacity in Saline Sodic Soils. *J. Indian Soc. Soil Sci*., *28*(3), 307-311.

Singh, V., & Singh, S. P. (1983). Effect of Applied Boron on the Chemical Composition of Lentil Plants. *J. Indian Soc. Soil Sci*., *31*, 169-170.

SSA (18 de enero de 1996). Norma Oficial Mexicana NOM-127-SSA1-1994. Salud ambiental, agua para uso y consumo humano. Límites permisibles de calidad y tratamientos a que debe someterse el agua para su potabilización. *Diario Oficial de la Federación*, 1-7.

Tarbuck, E. J., & Lutgens, F. J. (2008). *Ciencias de la Tierra* (721 pp.) (8a edición). Madrid: Pearson Prentice Hall.

Van Der Leeden, F., Troise, F. L., & Todd D. K. (1990). *The Water Encyclopedia* (808 pp.). Washington, DC: Island Press.

Velázquez, M., & Pimentel, J. L. (del 24 al 26 de mayo, 2006). Salinidad, P, B y *E. coli* en el río Duero, Michoacán. *Memorias XV Congreso Nacional 2006 de la Federación Mexicana de Ingeniería Sanitaria y Ciencias Ambientales* (CD-ROM), Guadalajara, Jalisco, México.

Velázquez, M. A., Pimentel, J. L., & Ortega, H. M. (2011). Estudio de la distribución de boro en fuentes de agua de la cuenca del río Duero, México, utilizando análisis estadístico multivariado. *Rev. Int. Contam. Ambie*., *27*(1), 19-20.

Verma, L. P. (1983). Tolerance of Wheat to Boron in Irrigation Water. *J. Indian Soc. Soil Sci*., *31*, 167-168.

Villada, M. (1905). Una exploración a la cuenca fosilífera de San Juan Raya, Estado de Puebla. *Anales del Museo Nacional* (pp. 126-164). Tomo II. México.

Weinthal, E., Parag, Y., Vengosh, A., Muti, A., & Kloppmann, W. (2005). The EU Drinking Water Directive: The Boron Standard and Scientific Uncertainty. *Europ. Environ*., *15*, 1-12.

WHO (2008). *Guidelines for Drinking-Water Quality. Incorporating First and Second Addenda. Vol. 1. Recommendations.* (3a ed.) World Health Organization [en línea] Citado el 11 de enero de 2011. Recuperado de http://www.who.int/water_sanitation_health/dwq/gdwq3rev/en/index.html 12/04/2010.

WHO (2010). *Chemical Hazards in Drinking-Water-Boron*. World Helth Organization 2010 [en línea]. Citado el 12 de abril de 2010. Recuperado de http://www.who.int/water_sanitation_health/dwq/chemicals/boron/en/12/04/2010.

Wilcox, L. V. (1948). The Quality of Water for Irrigation Use. US Department of Agriculture. *Tech. Bulletin*, *962*, 40.

Wolf, L., Held, I., Eiswirth, M., & Hötzl, H. (2004). Impact of Leaky Sewers on Groundwater Quality. *Act. Hydroch. Hydrob*., *32*, 361-373.

Institutional Address of the Authors

Dr. Oscar Raúl Mancilla-Villa

Universidad de Guadalajara
Centro Universitario de la Costa Sur
Departamento de Producción Agrícola
Avenida Independencia Nacional 151
48900 Autlán de Navarro, Jalisco, México
Teléfono: +52 (317) 3825 010, extensión 57026
oscar.mancilla@cucsur.udg.mx

Dra. Ana Laura Bautista-Olivas

Universidad de Sonora
Departamento de Agricultura y Ganadería
Carretera Bahía de Kino km 21
83000 Hermosillo, Sonora, México
Teléfono: +52 (662) 5960 295
analaura@colpos.mx

Dr. Héctor Manuel Ortega-Escobar
Dr. Carlos Ramírez-Ayala
Dr. Héctor Flores-Magdaleno

Colegio de Postgraduados, Campus Montecillo
Hidrociencias
Carretera México-Texcoco km 36.5
56230 Montecillo, Estado de México, México
Teléfono: +52 (55) 5804 5900, extensión 1167
manueloe@colpos.mx

Dra. Amada Laura Reyes-Ortigoza

Departamento de Ecología y Recursos Naturales
Facultad de Ciencias
Universidad Nacional Autónoma de México
Área de Biología
Colonia Universidad Nacional Autónoma
de México, CU, delegación Coyoacán
04510 México, D.F., México
Teléfono: +52 (55) 5622 4827, extensión 24922
amadalaura@ciencias.unam.mx

Dr. Diego Raymundo González-Eguiarte

Profesor Investigador del Centro Universitario de Ciencias Biológicas y Agropecuarias (CUCBA)
Universidad de Guadalajara
Camino Ramón Padilla Sánchez #2100
Nextipac Zapopan, Jalisco, México
Telefono: +52 (33) 3777 1150, extensión 3040 y 3190
diegonz@cucba.udg.mx

Dr. Rubén Darío Guevara Gutiérrez

Centro Universitario de la Costa Sur
Universidad de Guadalajara
Avenida Independencia Nacional núm. 151
48900, Autlán de Navarro, Jalisco, México
Telefono: +52 (317) 3825 010, extensión 57165
rguevara@cucsur.udg.mx

Click here to write the autor

Wetland Soils from Lake Patzcuaro, Michoacan, Mexico

• Lenin E. Medina-Orozco* •
Universidad de la Ciénega del Estado de Michoacán de Ocampo, México
*Corresponding Author

• Norma E. García-Calderón • Felipe García-Oliva •
Universidad Nacional Autónoma de México

• Elena Ikkonen •
Academia Rusa de las Ciencias

Abstract

Medina-Orozco, L. E., García-Calderón, N. E., García-Oliva, F., & Ikkonen, E. (September-October, 2014). Wetland Soils from Lake Patzcuaro, Michoacan, Mexico. *Water Technology and Sciences* (in Spanish), 5(5), 105-117.

In Mexico and particularly in the state of Michoacan, the genesis, morphology and function of hydromorphic soils has not been sufficiently studied, despite having large areas of continental wetlands such as the vadose region of Lake Patzcuaro. We studied two wetlands representative of the shore of Lake Patzcuaro, Michoacan. One was permanently saturated with Gleysols development and the other was had periodic flooding and fluvisols development in a large floodplain. The results indicate the presence of haplic gleysol (colluvic, eutric) (WRB, 2006), dark brown in color, with moderate amounts of organic carbon (0.87 % average), clay> 30 %, predominant structure of subangular polyhedra and prisms with segregation of sesquioxides ferromanganese protruding from hypo-coatings of iron oxides, and the presence of traces of ostracods throughout most of the profile. Lithological discontinuity is prominent. The alluvial wetlands contain haplic fluvisol (hyperhumic, eutric) (WRB, 2006) with soil having a grayish brown matrix, a high content of organic matter throughout the profile (> 7 %), and traces of ostracods. These soils have a high base saturation (> 50 %). Three wet zones are well defined within the soil: a lower permanent endosaturation zone, an intermediate zone resulting from capillarity and an alternating wetting-drying zone in the epipedons.

Keywords: Hydric soils, hydromorphic features, lithological discontinuity, vadose region.

Resumen

Medina-Orozco, L. E., García-Calderón, N. E., García-Oliva, F., & Ikkonen, E. (septiembre-octubre, 2014). Suelos de humedal del lago de Pátzcuaro, Michoacán, México. Tecnología y Ciencias del Agua, *5(5), 105-117.*

En México, en particular en el estado de Michoacán, el estudio sobre la génesis, morfología y función de los suelos hidromórficos no ha sido explorado de forma suficiente, pese a contar con grandes extensiones de humedales continentales, como la zona vadosa del lago de Pátzcuaro. Se estudiaron dos humedales representativos de la costa del lago de Pátzcuaro, Michoacán: uno de ellos saturado permanentemente, con desarrollo de gleysoles, y un humedal con inundación periódica, fluvisoles, desarrollados en una gran planicie aluvial. Los resultados indican la presencia de un gleysol háplico (colúvico, éutrico) (WRB, 2006), de coloración pardo oscuro, con cantidades moderadas de carbono orgánico (0.87% promedio), arcilloso > 30%, de estructura predominante de poliedros subangulares y prismas con segregación de sesquióxidos ferromanganosos, sobresaliendo los hiporrevestimientos de óxidos de fierro, y presencia de restos de ostrácodos en la mayor parte del perfil. Destaca una discontinuidad litológica. Por su parte, en el humedal aluvial se presenta un fluvisol háplico (hiperhúmico, éutrico) (WRB, 2006), un suelo con matriz de color pardo grisáceo, con altos contenidos de materia orgánica en todo el perfil (> 7 %) y restos de ostrácodos. Son suelos con alta saturación de bases (> 50 %). Tres zonas de humedad son bien definidas al interior de los suelos: una zona baja de endosaturación permanente, una zona intermedia producto de la capilaridad, y una zona de secado-humedecimiento alternado en los epipedones.

Palabras clave: *zona vadosa, suelos hídricos, rasgos hidromórficos, discontinuidad litológica.*

Received: 03/12/12
Accepted: 12/02/14

Introduction

Hydromorphic soils have a high phreatic level, or prolonged saturation conditions due to flooding or pooling during periods long enough for the development of anaerobic conditions to be produced in the soil. These soils are also known as wetlands or hydric (USDA-NRCS, 2006).

Few studies have been conducted in Mexico of soils that are temporally submerged or underwater, except for very local research. And, although a direct relationship is generally accepted between the temporary flooding of soil and the appearance of redoximorphic features, this is not completely certain, as in the case of soils with interstitial water rich in dissolved oxygen, or in which dissolved oxygen is continually renewed (Van Diepen, 1984; Driessen, Deckers, Spaargaren, & Nachtergaele, 2001).

The studies conducted in our country about hydromorphic soil can be divided into three groups: 1) soils in upper mountain basins without drainage, 2) in upper mountain basins with artificial drainage (both entirely with continental influence), and 3) soils in coastal lagoons with oceanic influence.

The first group of studies has been performed with lacustrine soil in mountain basin depressions, in temperate sub-humid climates typical of central Mexico. Included are those called the "Chinampas" (terric anthrosols) in Mexico City, with a marked discontinuity in the physical and chemical properties of the profile (Ramos, Cajuste, Flores, & García, 2001; Bello, García, Ortega, & Krasilnikov, 2011; Reyes-Ortigoza & García-Calderón, 2004). With regard to mountain soil in Michoacan, Ramos (2008) reported gleysols recently formed from clayey soil in the vadose zone of the Umecuaro dam.

The second group of soils studied was formed in conditions similar to the previous group, in upper basins with a temperate climate but with artificial drainage, such as the former Texcoco Lake, most of which currently contains crops. These are soils formed by deposits in calm waters where abrupt dewatering has occurred (Segura, Gutiérrez, Ortiz, David, & Gómez, 2000), with pH between neutral and alkaline (6.9 – 10-6 saline). Micro-morphological features have been reported in these soils, pertaining to calcium carbonate formed in the different environments through which the lake evolved, with a loss of redoximorphic features (Gutiérrez, Stoops, & Ortiz, 1998; Ortiz *et al.*, 2000; Segura *et al.*, 2000).

The third group of soils developed from the affects of the ocean and mangrove vegetation, such as in the state of Tabasco. Gleysols and fluvisols have been reported (Gutiérrez & Zavala, 2001; Rivera, Ferrera, Volker, Fernández, & Rodríguez, 2002), in addition to histosols containing sulphydric material (Moreno *et al.*, 2002; Rivera *et al.*, 2002). In the state of Yucatán, Sedov *et al.* (2007) reported saturated soils in a topo-sequence of the state, classified as gleyic leptosol and calcisol, with a neutral pH (6.3 – 7.5). Solleiro-Robelledo *et al.* (2011) showed the distribution of soils in wetlands in Yucatan, reporting leptosol, calcisol, histosols and fluvisols.

Three of the largest lakes in Mexico are located in the state of Michoacan: Chapala, Cuitzeo and Pátzcuaro. Lacustrine wetland soils are found here. Nevertheless, there is little information in Patzcuaro related to soils in the vadose zone. Therefore, it is relevant to identify the morphology and classify the hydromorphic soils on the lake's coast.

The objective of the present study is to describe the morphology and hydromorphic features of soils in the field, and classify them based on IUSS Working Group WRB 2007 criteria, for two Patzcuaro Lake wetlands in the state of Michoacan.

Materials and methods

Patzcuaro Lake is located in the Trans-Mexican Volcanic Belt (TMVB), where over 1 000 volcanic cones have been reported. It is an endorheic basin of tecto-volcanic origin, dominated by basaltic and andesitic lava flows (Garduño-Monroy *et al.*, 2009). The first

wetland studied is located on the the shoreline in Ichupio, municipality of Tzintzuntzan, with coordinates 19º 38′ 22.6″ N and 101º 35′ 34.3″ W, at an altitude of 2 040 masl. Grazing is prohibited. The soil formed from the collapse of basaltic lava from the El Metate mountain (Garduño-Monroy *et al*., 2009), in a piedmont that goes into the lake with an average slope of 5%. The second site is located in the Jaracuaro wetlands, municipality of Erongaricuaro, with coordinates 19° 34′ 00″ N and 101° 41′ 17.1″ W, and an altitude of 2 040 masl (Figure 1).

The soil has formed out of a sequence of sediments and deposits of volcanic ash from the Quaternary period —Holocene and Pleistocene on top of the Patzcuaro graben— composing a large alluvia plain (Israde-Alcántara, Garduño-Monroy, Fisher, Pollar, & Rodríguez- Pascua, 2005; Garduño-Monroy *et al*., 2009) with an average slope under 2%. The site is used as a pasture for extensive livestock grazing. The main sources of food for the herds are rooted emergent hydrophytic grasses and vegetation (Figure 2).

Climatic Regime of the lacustrine region

According to the modification by Garcia (1988), the climate of the region is temperate sub-humid with summer rains from June to September, a total annual precipitation of 880 mm and a mean annual temperature of 16.8 °C. June is the hottest month, and the climate code is $(w^2)(w)b(e)g$ (Table 1).

Description and Collection of soil samples

Five profiles were taken in the vadose zone of each wetland, as representative of the local diversity of the soil (Ibáñez & Saldaña, 2011). The morphological description and redoximorphic features are based on Schoeneberger, Wysocki, Benham, & Broderson, (2002) and USDA-NRCS (2006). The first soil was described in 2008 in Ichupio (gleysols). The second was described in 2009 in Jaracuaro (fluvisols). Test pits were opened to 110 and 100 cm deep, respectively.

Samples of roughly 2 kg of soil were collected per horizon. The samples were

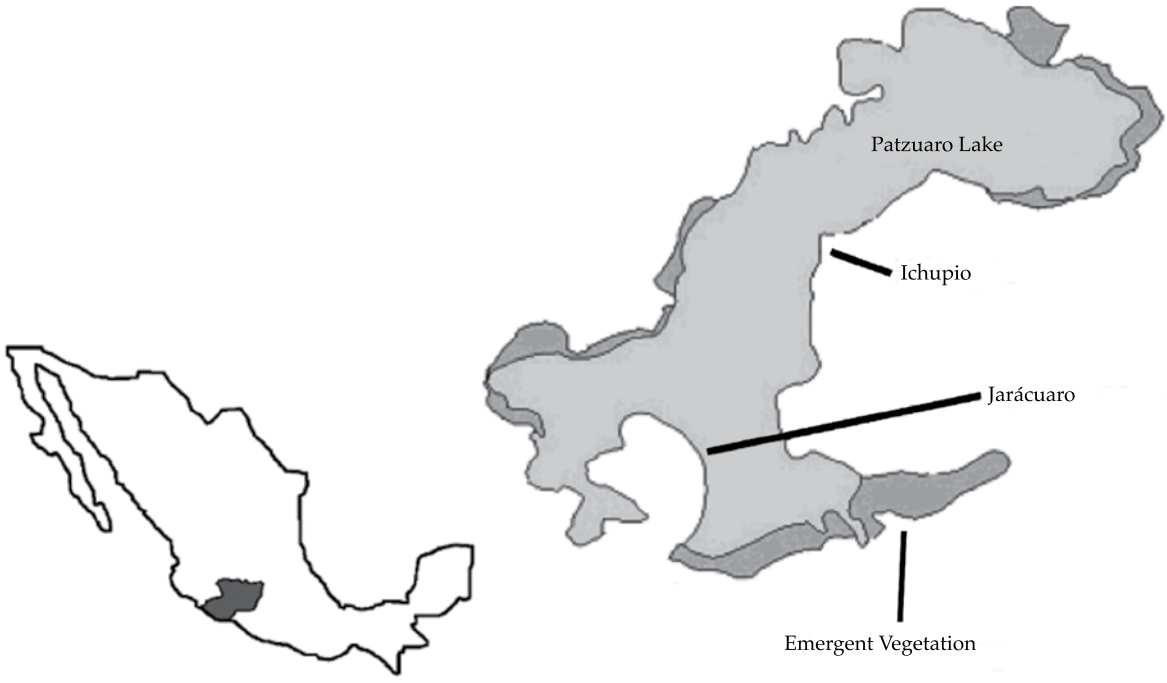

Figure 1. Location of wetlands studied, Ichupio (gleysol) and Jaracuaro (fluvisol).

Figure 2: Study site: Ichupio (left) and Jaracuaro (right).

Table 1. Hydric balance for 29 years of records from the Patzcuaro weather station.

Variable	Months												Total annual*
	Jan.	Feb.	Mar.	Apr.	May.	Jun.	Jul.	Aug.	Sep.	Oct.	Nov.	Dec.	
Precipitation (mm)	37.1	13.8	6.4	8.4	37.1	145.1	206.0	196.4	166.5	72.7	19.4	11.1	919
ETP (mm)	26.3	35.3	46.4	58.7	67.0	68.1	58.5	57.8	55.7	49.6	38.8	30.7	593
Hydric balance (mm)	-28.2	-49.7	-61.6	-90.4	-82.2	47.1	**224.4**	**285.9**	**249.3**	**133.9**	3.8	-39	
Mean air *T* (°C)	13.0	14.3	16.4	18.4	19.6	19.7	18.3	18.2	17.9	16.9	15.0	13.3	16.8
Maximum air *T* (°C)	22.6	24.4	27.1	29.2	29.6	27.2	25.0	24.9	24.4	24.5	23.9	22.7	25.5
Minimum air *T* (°C)	3.6	4.0	5.7	7.6	9.7	12.2	11.7	11.5	11.3	9.3	6.0	4.1	8.1

*29 years of records.

placed in plastic bags and transported to the laboratory for the analysis of basic physical and chemical properties (Tables 4 and 5). In addition, soil samples were collected with a cylinder of known volume to determine the apparent density of the soil (Blake & Hartge, 1986). The soil was placed in hermetically sealed plastic bags for later weighing and drying in the laboratory.

Morphological Description and Classification of the soils

The designation of the horizons was determined initially in the field based on the morphological description and perceptible diagnostic properties, according to the FAO guidelines for soil description (2009). These were later reviewed by laboratory analyses. The soils were classified according to the Reference Base for Soil Resource code (IUSS Working Group, 2007).

Chemical Response of the Soil in the Field

The following tests were performed with the soil profiles and aggregates in field conditions: electrical conductivity (EC) and pH in a 1:1 solution (water:soil) with a portable Hanna® meter, test recommended for soils with oxido-reduction conditions (Schoeneberger *et al.*, 2002); Fe^{++} reduction test, adding α solution, α' dipyridyl at 0.2% of (M/V) in an acetic acid solution at 10% (V/V), recording the test

as positive when a change in color occurred and negative when no change occurred (Schoeneberger *et al*., 2002); presence of carbonates was tested by adding HCL (10%). Effervescence was recorded and class of effervescence analyzed using a 10X magnifying lens to observe the presence or absence of secondary carbonates. H_2O_2 (30%) was used as an indicator of magnesium oxides (MnO_2), which is sometimes masked by organic matter (Schoeneberger *et al*., 2002). The odor of rotten eggs was used as an indicator of the possible presence of H_2S (hydrogen sulfur) and recorded as an indicator of sulfurous compounds (USDA-NRCS, 2006).The color of the soil matrix in moist conditions and of the redoximorphic features were registered in the field using standard Munsell® reference table (Munsell Soil Color Charts, 2000) with an aggregate or mass of recently exposed soil in order to avoid changes in color caused by the oxidation of the soil (Schoeneberger *et al*., 2002).

Laboratory Analysis

The soils were analyzed according to standardized methods and in duplicate for each of the physical and chemical properties. The basic analyses were: texture using the Bouyocous hydrometry method (Gee & Bauder, 1986); apparent density of the soil using the cylinder method (Blake & Hartge, 1986); density of particles with the pycnometry method (Blake & Hartge, 1986); total porosity of the soil (Danielson & Sutherland, 1986); organic matter and organic carbon using Walkley-Black wet combustion (Nelson & Sommers, 1996); CEC (cation exchange capacity) with ammonium acetate 1M, pH 7 (Rhoades, 1982); color of dry and wet soil by comparing Munsell® tables (Munsell Soil Color Charts, 2000). Due to the difficulty involved in measuring hydraulic conductivity in the field in saturated soil, this was estimated according to the model proposed by Saxton and Rawls (2006), for each horizon, using as input parameters the relative percentage of fine soil, organic matter, apparent density and electrical conductivity.

Results and Discussion

Morphology and classification of soil

Morphology of gleysols in Ichupio

The soil consists of eight layers with the sequence Ao-ABg1-Bg2-Bg3-2Wgr1-2Wgr2-2Wgr3. It is a well-developed mineral soil dominated by clay and silt, with a mostly angular and sub-angular block structure with medium and thick sizes from the surface to 36 cm. From 36 to 60 cm the structure is prismatic and well-defined, associated with a zone with periods of slow drying and wetting (Ciolkosz & Waltman, 1995). The block structure continues, associated with the permanent saturation zone. At 85 cm a lithological discontinuity occurs, with no evidence of being different parent material than that of the overlying material.

The increase in clay in horizon B is not associated with the migration of clay, as shown by the absence of coating, which suggests *in situ* formation possibly connected to drying and wetting cycles. The profile has a uniform brownish yellow color in the first 36 cm, in dry, and dark brown in moist soil, which corresponds to temporarily flooded layers. No specks are present in the first four layers, suggesting an oxic character. Below this depth and up to 90 cm, the soil matrix is brown in dry soil and very dark brown in wet soil. There is a contrast between the matrix and the presence of red specks as hypo-coating in peds and abandoned root channels, which suggests a zone with long periods of water saturation. The deeper layers, over 90 cm, are yellowish brown to brown in dry soil and very dark brown in wet soil, corresponding to endosaturated water table zones (Table 2).

The moisture conditions of the soil do not prevent the good development of roots in the first 85 cm, which are abundant and common, with medium and fine sizes. Nevertheless,

after 85 cm, blackish roots are present and a sulfurous odor, or rotting of the roots, is detected. This suggests it is a boundary zone for the development of roots and corresponds to the phreatic level. The saturated hydraulic conductivity inside the profile is low, possibly because of the high clay contents of the profile (over 20%), with lower conductivity values of 10 mm h^{-1} in the epipedon and under 4 mm h^{-1} in the rest of the profile (Table 3). This suggests a pedotransfer of water and slow drying and wetting in the horizons, with interpedal zones with preferential flow.

Lithological discontinuity of gleysol. This discontinuity is found between 85 and 90 cm. It consists of an accumulation of fine sediments characteristic of soils undergoing colluvial processes. In addition, there is no evidence of different materials in the lithological discontinuity and the overlying horizons, characteristic of the lithological discontinuities (Phillips, 2004; FAO, 2009). In addition, this discontinuity coincides with the zone observed to be a boundary for root growth.

Redoximorphic features. The redoximorphic features of the soil are present from 27 cm to 110 cm, in which segregation of iron and manganese sesquioxides is observed in the soil matrix. Yellowish-red specks with diffuse edges are seen in this zone (5 YR 5/8), with coatings in the peds and in interpedal zones, which contrast with the color of the soil matrix. In addition, brownish specks of manganese are observed with diffuse edges and small in size (under 5 cm) (Table 2 and Figure 3). There is a prominent contrast in luminosity and intensity between the color of the specks and the soil matrix, except for the lithological discontinuity (85 to 90 cm). The specks suggests the presence of lepidocrocite (FeOOH), with is a metastable goethite polymorph (Fanning & Fanning, 1989). Brownish specks are also present, suggesting the presence of manganese. No concretions or hard nodules were detected in the soil profile, which can be interpreted as slow diffusion of oxygen in the profile and inside the aggregates, which has not permitted the formation of concretions. The reddish specks are found primarily in the middle of the profile, while manganese is found mostly in lower zones of the profile, as a result of greater mobility (Ponnamperuma, 1972).

The reaction of the soil is positive to alpha dipyridyl during the rainy season, which suggests the presence of reduced iron (Fe^{++}), indicating reduction conditions in the soil, and the odor of sulfate reduction is present and stronger at greater depths. In contrast, during the dry season no positive reaction occurs in the Ao and A1 horizons, which correspond to the horizons with no sesquioxide specks.

The soil is slightly calcareous, but no evidence of secondary carbonates is observed. This reaction is caused by mollusk shells distributed throughout the soil profile.

Classification. Based on the field description and the results of laboratory analyses (Tables 2, 4, 5 and 6), the soil is classified as haplic gleysol (colluvic, eutric) in WRB (2006). The gleysol classification is based on the pattern of red and brown colors on the face of the aggregates and between the aggregates, and indications of reduction conditions. The presence of discontinuity and the irregular distribution of the sands gives it a colluvic character. Lastly, it is classified as eutric because of a base saturation over 50% (Table 6).

Morphology of the fluvisols in Jaracuaro

The soil has the genetic horizon sequence Ah-Ae1-Ae2-Ae3-Ar-Wr. Bioturbate epipedon was notable as polygonal crusts form 5 cm deep when the surface is dry. It contains 42% clay and 21% silt and fibrous compound material primarily consisting of dead roots (Figure 3). The soil has reversible cracks from the surface to a depth of 30 cm, where the soil is wet from the capillary movement of the water from the phreatic layer. The cracks are wide enough (over 1 cm) to enable aeration of the these strata when the soil is dry. The structure is massive when wet and angular polyhedral are observed when the soil is exposed, which is

very hard when dry in spite of the high organic matter contents (over 7%). The aggregates do not form wedges and friction faces were not seen.

When wet, the color of the soil matrix is black (10 YR 2/1), turning to very dark brown as the depth increases (10 YR 2/2). And it is gray-brown (10 YR 5/2) when dry. The organic matter content is 11% on the surface, gradually decreasing as depth increases (± 7. 0%). There is little thick gravel (under 5 cm) in the soil, which is sub-angular and white, with irregular arrangement, and is immersed in the soil matrix, suggesting fluvial origin. While the sedimentary strata are not easily observable in the field, the sediments suggest low energy processes (slope under 2%), masking the mineral deposit sequences (Bradley & Stolt, 2003).

The feel of the texture is sandy clay throughout the profile, with clay contents over 28% and an irregular distribution of the sands, which suggests fluvial origins. The average porosity of the profile is very high (55%), with abundant fine pores, decreasing to a depth of 44 cm. Below the 44 cm of depth are notable macropores not associated with roots, mostly non-dendritic vesicles, which can be interpreted as the formation of gases escaping in the form of bubbles, leaving behind this formations. In addition, the phreatic level is found at 44 cm. Because of porosity the saturated hydraulic levels are very high, with rates over 30 mm h^{-1}, which enables rapid water flow through the horizons. The presence of roots is very common in the soil and are thin in the first 20 cm, and rare below this depth, with restricted growth below 44 cm, just above the phreatic level. The apparent density is very low (0.7 to 0.8 g cm^{-3}) throughout the depth and the real density is 1.9 to 1.6 g cm^{-3}, associated with high organic matter contents (Table 5). Shell remains are observed throughout the profile, decreasing with increased depth, and reacting to HCl, while no secondary carbonates were observed.

Redoximorphic features. A browned matrix, colors 10 YR 5/2 and 10 YR 6/2-4 in dry, and 10 YR 2/1-2 in wet. It is moderately reduced, with a color intensity from 6 to 1 and brightness under 4, but is possibly masked by high organic matter contents (over 7%) throughout the profile. Ferromanganese sesquioxide segregation is not observed, nor are hard nodules in the matrix or soil aggregates. Nevertheless specks corresponding to organic matter in an intermediate state of composition were present, which disintegrate when rubbing between the fingers.

Colors characteristic of reductimorphic conditions are not discarded, which may be masked by high levels of organic matter, as reported in other soils (Ponnamperuma, 1972; Fanning & Fanning, 1989; Grimley & Vepraskas, 2000).

Reaction of the soil. The soil has an alkaline reaction, with pH values from 8.8 on the surface

Figure 3. a) Gleysol profile, Ichupio; b) prismatic gleysol aggregate showing hydromorphic features; c) fluvisol profile.

Table 2. Morphology of gleysol in Ichupio.

Horizon Depth, cm	Soil features
Horizon Ao 0 - 10	Dry color (10 YR 5/4 yellowish brown), wet color (7.5 YR 3/2 dark brown), with no specks. Sandy-loam texture to the touch; moderate granular structure and in sub-angular medium blocks; firm consistency, not adhesive, slightly plastic, not rocky; abundant fine and medium pores; slight development of oxides in biopores; abundant and thin roots; slow drainage, weak transition to next horizon, wavy.
Horizon A 10 - 15	Dry color (10 YR 5/6 yellowish brown), wet color (7.5 YR 3/2 dark brown), with no specks. Sandy-loam texture to the touch; moderate granular structure and in sub-angular medium blocks; firm consistency, not adhesive, slightly plastic, not rocky; abundant fine and medium pores (root channel pores); slight development of oxides in biopores; medium and fine roots; slow drainage; diffuse transition to next horizon by color and marked by hardness; boundary shape wavy horizontal.
Bg1 Horizon 15 - 27	Dry color (10 YR 5/6 yellowish brown), wet color (7.5 YR 3/3 dark brown), with no specks. Silty clay texture to the touch; moderate granular structure and in sub-angular medium and thick blocks; firm consistency, medium adhesiveness, slightly plastic, not rocky; medium porosity (root channel pores); slight development of oxides in biopores; abundant and thin roots; presence of shell remains; slow drainage; horizontal transition to next horizon wavy horizontal marked by hardness
Bg2 Horizon 27 - 36	Dry color (10 YR 5/6 yellowish brown), wet color (7.5 YR 3/3 dark brown), with no specks. Silty clay texture to the touch; strong structure and in sub-angular large blocks; firm consistency, more stable than the previous; moderately adhesive and moderately plastic; rocky, few under 5%, 2 to 5 cm, rounded; medium porosity (root channel pores); common fine roots; moderate development of iron oxides in macropores, mesopores and biopores color (5 YR 5/8 yellowish-red); dead bivalves and snails; slow drainage; transition to next horizon marked by color and texture; shape of boundary wavy horizontal.
Bg3 Horizon 36 - 60	Dry color (7.5 YR 5/4 brown), wet color (7.5 YR 4/4 brown); presence of specks in masses as reddish bands (5 YR 5/8 yellowish-red); abundant outside and inside the aggregates; clay texture to touch; strong and very thick (over 20 cm) prismatic structure; very firm consistency, very adhesive and very plastic; not rocky; very few pores; dendritic tubular from roots; presence of interpedal spaces between prisms when not saturated from 3 to 4 cm of depth and under 1 cm width; no coatings or stress features observed, or sliding faces between aggregates; common thin roots; presence of dead bivalves and snails in a lower quantity than the previous; drainage; transition to next horizon marked by color; horizontal irregular boundary shape.
2Wgr1 Horizon 60 - 85	Dry color (7.5 YR 5/4 brown), wet color (7.5 YR 2.5/3 very dark brown); presence of specks common in masses as red bands (5 YR 5/8 yellowish-red color) in lesser quantity than the previous, inside the aggregates and as hypo-coatings; clay texture to the touch; strong structure in angular and sub-angular blocks; medium and thick size; very firm consistency, very adhesive and very plastic; not rocky; fine tubular dendritic pores, few medium; common medium roots; no drainage, saturation zone; transition to next horizon marked by color; horizontal wavy boundary.
2Wgr2 Horizon 85 - 90	Dry color (10 YR 5/8 yellowish-brown), wet color (10 YR 3/3 dark brown), no presence of specks; sandy texture to the touch; no structure; no consistency, no adhesion or plasticity; not rocky; high interstitial porosity; absence of specks and concentrations; common medium roots, some rotting; presence of sulfurous odor, hydrogen sulfur (rotten egg odor); no drainage (phreatic layer); transition to next horizon marked by abrupt texture; horizontal wavy boundary
3Wgr3 Horizon 90 - 110	Dry color (7.5 YR 5/4 brown), wet color (7.5 YR 3/3 dark brown), presence of speck on some of the aggregates in lesser amounts than the underlying, color (5 YR 5/8 yellowish-red): clay texture to the touch; strong angular block structure, thick; firm consistency, moderately adhesive and moderately plastic; not rocky; medium porosity (root channel pores); medium roots in state of rotting, strong sulfurous odor; permanently saturated by water.

Table 3. Morphology of fluvisol in Jaracuaro.

Horizonte profundidad, cm	Soil features
Ah Horizon 0 - 5	Dry color (10YR 5/2 gray-brown), wet color (10YR 2/1 black); no presence of specks or concretions; sandy-clay texture to the touch; laminar structure forming a medium-sized reversible crust (average 5 cm), beginning at the surface, extremely strong; extremely strong consistency in dry soil, moderately adhesive and plastic; not rocky; abundant and fine pores; common and thin roots with presence of fibrous matter; slow drainage; transition to next horizon abrupt from the horizontal crust
Ae1 Horizon 5 - 12	Dry color (10YR 5/2 grayish-brown), wet color (10YR 2/2 very dark brown); no presence of specks or concretions; reversible cracks throughout the horizon; sandy-clay texture to the touch; strong structure, massive in wet and medium polyhedrons in dry; very firm consistency, moderately adhesive, slightly plastic; rocky, very few; abundant fine pores; common and thin roots; presence of fibrous matter and remains of mollusk shells; slow drainage; transition to the next horizon marked by color and structure.
Ae2 Horizon 12 - 20	Dry color (10 YR 5/2 grayish-brown), wet color (10YR 2/2 very dark brown); no presence of concretions; specked by organic matter, moderately decomposed, hemic type, mixed by bioturbation (trampling by livestock); reversible cracks beginning at the surface; sandy-clay texture to the touch; strong massive structure in wet and sub-angular medium blocks in dry; very firm consistency, moderately adhesive, slightly plastic; rocky, very few; abundant fine pores; common and fine roots; remains of mollusk shells; slow drainage, weak transition to the next horizon.
Ae3 Horizon 20 - 30	Dry color (10YR 5/2 grayish-brown), wet color (10YR 2/2 very dark brown); no presence of concretions; specked by moderately decomposed organic matter, hectic type; mixed by bioturbation (trampling by livestock): reversible cracks beginning at the surface; sandy-clay texture to the touch; strong massive structure in wet and sub-angular medium blocks in dry; very hard consistency, adhesive and plastic; rocky, very few; fine but few pores; medum roots, rare; remains of mollusk shells; slow drainage; transition to next horizon weak by color and abrupt from the absence of cracks.
Ar Horizon 30 - 44	Dry color (10YR 6/2 light yellowish-brown), wet color (10YR 3/2 very dark grayish-brown); no presence of concretions or specks; sandy-clay texture to the touch; very massive strong structure in wet and sub-angular medium blocks in dry; very hard consistency, moderately adhesive and plastic; rocky, very few; fine pores, but few; roots very rare, medium; remains of mollusk shells; strong sulfurous odor (rotting egg); slow drainage, transition to the next horizon weak in color and texture and marked from the absence of cracks.
Wr Horizon 44 - 100	Dry color (10YR 6/4 light yellowish-brown), wet color (10YR 2/2 very dark brown); no presence of concretions or specks; sandy-clay texture to the touch; strong massive vesicular structure in wet and dry; very hard consistency, moderately adhesive and plastic; not rocky; fine pores, and few; roots very rare, medium; remains of mollusk shells, strong sulfurous odor; no drainage, static level of the phreatic layer (water is free inside the profile); weak transition to next horizon.

to 8.2 in the deeper layers. The EC values are less than 1.3 dS m^{-1}, discarding soil salinity. It reacts positively to alpha-alpha dipyridyl throughout the year, which is more evident at greater depths, suggesting accumulation of reduced iron. The soil reacts slightly but continuously to H_2O_2 throughout the profile, suggesting reduced manganese free in the soil. A strong sulfurous odor is present (rotten egg odor) mostly in the horizons below 30 cm.

Classification. The soil is classified as haplic fluvisols (hyperhumic eutric) according to WRB (2006). It is classified as fluvisols because of the fluvial matter contents, as indicated by the irregular distribution of rocky fragments and sands inside the pedon. It is also classified as hyperhumic because of the high organic matter contents (over 7%). Lastly, it has a eutric classification because of a base saturation over 50% throughout the profile (Table 6).

Table 4. Chemical properties of wetland soils.

Profile	Genetic horizon	Depth cm	pH Field	MO %	CO %	EC dS m^{-1}	Wet fieldo (V/V)	Field reactions		
								α, α dipyridyl	H_2O_2*	HCl**
Ichupio (gleysol)	Ao	0 - 10	8.5	2.2	1.2	0.8	21.6	- , +	++	MO
	A	10 - 15	7.9	1.4	0.8	0.5	20.9	- , +	++	MO
	Bg1	15 - 27	7.8	1.1	0.6	0.3	22.0	+	++	MO
	Bg2	27 - 36	8.0	1.2	0.7	0.2	25.8	+	++	MO
	Bg3	36 - 60	8.4	1.1	0.6	0.2	24.7	+	++	SL
	2Wgr1	60 - 85	7.7	0.8	0.5	0.2	24.9	+	++	SL
	2Wgr2	85 - 90	7.7	0.7	0.4	0.2	19.4	+	+++	MO
	2Wgr3	90 - 110	7.7	0.8	0.4	0.2	28.0	+	+++	MO
Jarácuaro (fluvisol)	A	0 - 5	8.8	11.3	6.6	1.3	9.6	+	++	MO
	Ae1	5 - 12	8.5	9.9	5.7	0.7	57.2	+	++	MO
	Ae2	12 - 20	8.4	9.1	5.3	0.4	62.5	+	++	MO
	Ae3	20 - 30	8.4	8.5	4.9	0.4	67.5	+	++	MO
	Ar	30 - 44	8.3	8.1	4.7	0.3	62.0	+	++	MO
	Wr	44 - 100	8.2	7.2	4.2	0.2	181.1	+	++	MO

* - Negative; + =, slight reaction, ++= strong reaction; +++ very strong reaction
**Carbonate reaction in the soil matrix: N = Not calcareous, not visibly detectable or audible effervescence; ST - strongly calcareous, strongly visible effervescence, bubbles forming foam; EX = extremely calcareous, extremely strong reaction, thick foam is formed rapidly (FAO, 2009). CEC = total cation exchange capacity.

Table 5. Physical properties of wetland soils.

Profile	Genetic horizon	Depth cm	Texture (%)			Texture Class*	Apparent density	Real Density	Pores	HC**
			Sand	Silt	Clay		(g cm^{-3})	(g cm^{-3})	(%)	(mm h^{-1})
Ichupio (gleysol)	Ao	0 - 10	53	33	14	SaL	1.1	2.4	38	9.6
	A	10 - 15	41	39	20	L	1.4	2.3	42	3.7
	Bg1	15 - 27	23	57	20	SiL	1.4	2.3	45	3.0
	Bg2	27 - 36	19	57	24	SiL	1.0	2.3	44	3.5
	Bg3	36 - 60	31	39	29	SaL	1.0	2.3	37	2.0
	2Wgr1	60 - 85	11	61	27	SiC	1.2	2.4	46	2.5
	2Wgr2	85 - 90	67	27	6	SaL	1.2	2.3	45	37.9
	2Wgr3	90-110	41	39	20	L	1.2	2.3	38	3.6
Jarácuaro (fluvisol)	Ah	0 - 5	37	21	42	C	0.8	1.9	55	24.1
	Ae1	5 - 12	47	25	28	CL	0.8	1.8	54	26.1
	Ae2	12 - 20	28	34	38	CL	0.8	1.6	49	16.9
	Ae3	20 - 30	32	35	33	CL	0.8	1.9	57	20.9
	Ar	30 - 44	44	28	28	CL	0.7	1.7	58	35.7
	Wr	44-100	47	14	38	C	0.7	1.6	55	32.2

*L=Loam, SaL = sandy loam, SiL = silty loam, SiCL=Silty clay loam, CL=clay loam, CrC=Crumbly clay, CrSiC=crumbly silty clay, SiC=silty clay, CrSa= Crumbly sand, C=clay
**HC = hydraulic conductivity.

The most important modification in the classification of the soil, with respect to what has been reported by the INEGI cartography, was the change from gleysol to fluvisols.

Conclusion

The wetland soil in Ichupio has formed from colluvial processes. It has a well-defined

Table 6. Chemical properties of the wetland soils.

Profile	Genetic horizon	Depth cm	CEC $Cmol_c\ kg^{-1}$	Ca^{++} $Cmol_c\ kg^{-1}$	Mg^{++} $Cmol_c\ kg^{-1}$	Na^{+} $Cmol_c\ kg^{-1}$	K^{+} $Cmol_c\ kg^{-11}$	SB %
Ichupio (gleysol)	Ao	0 - 10	15	5.9	4.1	0.6	2.4	86.5
	A	10 - 15	20	6.2	3.4	1.5	2.1	65.5
	Bg1	15 - 27	19	6.7	3.4	1.3	1.6	68.6
	Bg2	27 - 36	18	8.2	3.6	1.6	2.2	86.7
	2Wgr1	36 - 60	20	6.4	4.0	1.4	1.7	67.4
	2Wgr2	60 - 85	19	5.7	4.5	1.7	1.8	71.8
	2Wgr3	85 - 90	16	4.2	4.4	1.2	1.6	71.0
	Ah	90 - 110	16	3.8	4.4	1.1	1.8	69.5
Jarácuaro (fluvisol)	A	0 - 5	44	9.6	7.3	4.6	4.2	58.4
	Ae1	5 - 12	40	9.4	7.1	4.2	3.9	61.2
	Ae2	12 - 20	39	9.6	5.5	3.5	2.9	55.2
	Ae3	20 - 30	37	9.8	5.6	3.5	2.5	57.9
	Ar	30 - 44	36	7.5	4.7	2.2	2.1	46.1
	Wr	44 - 100	34	8.2	5.6	3.3	2.0	56.4

structural development compared to the wetland soil in Jaracuaro, which is formed from low energy sedimentary processes. The soils studied have a shallow phreatic level and alternating periods of drying and wetting in the upper layers, which significantly affects the redoximorphic features and the structure of the horizons. In the case of the soil in the Ichupio wetlands, well-defined block and prism structures have been formed, while the structure of the Jaracuaro wetland soil is massive and hard, in spite of the high organic matter contents.

The Ichupio soils have shown redoximorphic features in most of the horizons, result of iron and manganese sesquioxide segregation, which indicates alternating drying and wetting conditions. The soil in the Jaracuaro wetlands contains an accumulation of organic matter (carbon reservoirs) and the redoximorphic features may be masked by the high organic matter contents. Vesicle pores not associated with roots and with a strong sulfur odor are prominent in the lowest zone of the fluvisol, which suggests the formation of gases such as methane, forming bubbles that escape from the soil and leave behind characteristic features.

Lastly, the Ihcupio wetlands were classified as gleysols, as reported previously by INEGI, while the classification of soil in the Jaracuaro wetlands was changed from gleysol to fluvisol.

Acknowledgements

The authors thank the project *"Focos rojos de gases con efecto de invernadero en México: estructura y funcionamiento de los suelos saturados de humedad Semarnat-Conacyt 23489"* and Project *"PAPIIT-IN224410: estructura y funcionamiento de la materia orgánica en suelos de humedales: importancia de los almacenes de carbono en ecosistemas tropicales costeros."*

References

Bello, R. R., García, N. E., Ortega, H. M., & Krasilnikov, P. (2011). Artificial *Chinampas* Soils of Mexico City: their Properties and Salinization Hazards. *Spanish Journal of Soil Science*, *1*(1). DOI: 10.3232/SJSS.2011.V1.N1.05.

Blake, G. R., & Hartge, K. H. (1986). Bulk Density. In A. Klute (Ed.). *Methods of Soil Analysis. Part 1. Physical and Mineralogical Methods* (pp. 363-375). 2nd edition. Monograph N° 9. Madison: Soil Science Society of America.

Bradley, M. P., & Stolt, M. H. (2003). Subaqueous Soil-Landscape Relationship in Rhode Island Estuary. *Soil Sci. Soc. Am. J.*, *67*, 1487-1495.

Ciolkosz, E. J., & Waltman, W. J. (1995). *Cambic Horizons in Pennsylvania Soils* (26 pp.). Agronomy Series Number 133. University Park. USA: Agronomy Department, The Pennsylvania State University.

Danielson, R. E., & Sutherland, P. L. (1986). Bulk Density. In: A. Klute (Ed). *Methods of Soil Analysis. Part 1. Physical and mineralogical methods*. 2nd Edition. Monograph N° 9. Madison: Soil Science Society of America.

Driessen, P., Deckers, J., Spaargaren, O., & Nachtergaele, F. (2001). *Lecture Notes on the Major Soils of the World* (334 pp.). Rome: FAO.

FAO (2009). *Guía para la descripción de suelos* (99 pp.). 4ª ed. Rome, Wageningen (The Netherlands): FAO, ISRIC.

Garduño-Monroy, V. H., Chávez-Hernández, J., Aguirre-González, J., Vázquez-Rosas, R., Mijares-Arellano, H., Israde-Alacántara, I., Hernández-Madrigal, V. M., Rodríguez-Pascua, M. A., & Pérez-López, R. (2009). Zonificación de periodos naturales de oscilación superficial en la ciudad de Pátzcuaro, Mich., México, con base en microtremores y estudios de paleosismología. *Revista Mexicana de Ciencias Geológicas*, *6*(3), 623-637.

Gee, G. W., & Bauder, J. W. (1986). Particle-Size Analysis. In A. Klute (Ed.). *Methods of Soil Analysis. Part 1. Physical and Mineralogical Methods* (pp. 383-411). 2nd edition. Monograph N° 9. Madison: Soil Science Society of America.

Grimley, D. A., & Vepraskas, M. J. (2000). Magnetic Susceptibility for Use in Delineating Hydric Soils. *Soil Sci. Soc. Am. J.*, *64*, 2174-2180.

Gutiérrez, C. Ma. C., Stoops, G., & Ortiz, C. A. (1998). Carbonatos de calcio en los suelos del ex lago de Texcoco. *Terra*, *16*(1), 11-19.

Gutiérrez, C. Ma. C., & Zavala, J. (2001). Rasgos hidromórficos de suelos tropicales contaminados con hidrocarburos. *Terra Latinoamericana*, *20*, 101-111.

Israde-Alcántara, I., Garduño-Monroy, V. H., Fisher, C. T., Pollar, H. P., & Rodríguez-Pascua, M. A. (2005). Lake Level Change, Climate, and the Impact of Natural Events: The Role of Seismic and Volcanic Events in the Formation of the Lake Patzcuaro Basin, Michoacan, Mexico. *Quaternary International*, *135*, 35-46.

WRB (2007). *World Reference Base for Soil Resources 2006, first update 2007* (128 pp.). Iuss Working Group, World Soil Resources Reports No. 103. Rome: FAO.

Ibáñez, J. J., & Saldaña, A. (2011). Capítulo 9. Edafodiversidad: concepto, estimación y utilidad en el análisis global de suelos (145-172 pp.). In P. Krasilnikov, F. J. Jiménez, T. Reyna, & N. E. García (Eds.). *Geografía de suelos de México*. México, DF: UNAM.

Munsell Soil Color Charts (2000). *Revised Washable Edition*. New Windsor: Gretag Macbeth.

Nelson, D. W., & Sommers, L. E. (1996). Total Carbon, Organic Carbon and Organic Matter. In D. L. Sparks (Ed.). *Methods of Soil Analysis. Part 3. Chemical Methods* (pp. 573-579). Monograph N° 5. Madison: Soil Science Society of America.

Ortiz, S. C. A., Gutiérrez, C. Ma. C., López, A. G., Rodríguez, T. S. A., & Segura, M. A. (2000). *Guía de la gira técnica en el Municipio de Texcoco, México*. Congreso Universitario Internacional de Edafología, "Nicolás Aguilera", octubre.

Phillips, J. D. (2004). Geogenesis, Pedogenesis, and Multiple Causality in the Formation of Texture-Contrast Soils. *Catena*, *58*, 275-295.

Ponnamperuma, F. N. (1972). The Chemistry of Submerged Soils. *Advances in Agronomy*, *24*, 96.

Ramos, A. R. (2008). *Relación entre el tiempo de cambio de uso y el nivel de degradación de suelos en la cuenca de Cointzio Michoacán* (108 pp.). Tesis de Maestría en Conservación y Manejo de Recursos Naturales. Morelia, México: Universidad Michoacana de san Nicolás de Hidalgo (UMSNH).

Ramos, B. R., Cajuste, L. J., Flores, D., García, N. E. (2001). Metales pesados, sales y sodio en suelos de chinampa en México. *Agrociencia*, *35*(4), 385-395.

Reyes-Ortigoza, A. L. & García-Calderón, N. E. (2004). Evolución de las fracciones húmicas de suelos en la zona chinampera de la ciudad de México. *Terra Latinoamericana*, *22*(3), 289-298.

Rhoades, J. D. (1982). Cation Exchange Capacity. In A. L. Page, R. H. Miller, & D. R. Keeney (Eds.). *Methods of Soil Analysis. Part 2. Agron. Monogr. 9*. (pp. 149-157). Madison: Am. Soc. Agron.

Rivera, C. M. del C., Ferrera, R., Volker, V., Fernández, L., & Rodríguez, R. (2002). Poblaciones microbianas en perfiles de suelos afectados por hidrocarburos del petróleo en el estado de Tabasco. *Agrociencia*, 36(2), 149-160.

Saxton, K. E., & Rawls, W. J. (2006). Soil Water Characteristic Estimates by Texture and Organic Matter for Hydrologic Solutions. *Soil Sci. Soc. Am. J.*, *70*, 1569-1578. Doi:10.2136/sssaj2005.0117.

Schoeneberger, P. J., Wysocki, D. A., Benham, E. C., & Broderson, W. D. (Eds.) (2002). Field Book for Describing and Sampling Soils, version 2.0. Natural Resources Conservation Service, National Soil Survey Center, Lincoln, NE.

USDA-NRCS (2006). *Field Indicators of Hydric Soils in the United States, version 6.0*. G. W. Hurt & L. M. Vasilas (Eds.). United States Department of Agriculture (USDA), Natural Resources Conservation Service (NRCS), in Cooperation with the National Technical Committee for Hydric Soils.

Sedov, S., Solleiro-Rebolledo., E., Fedick., S. L., Gama-Castro., J., Palacios-Mayorga, S., & Vallejo-Gómez, E. (2007). Soil Genesis in Relation to Landscape Evolution and Ancient Sustainable Land Use in the Northeastern Yucatán Peninsula, Mexico. *Atti. Soc. Tosc. Sci. Nat., Mem., Serie A*, *112*, 115-126.

Segura, C. M. A., Gutiérrez, M. del C., Ortiz, C. A., David, Y., & Gómez, J. (2000). Suelos arcillosos de la zona oriente del estado de México. *Terra Latinoamericana*, *18*(1), 35-44.

Solleiro-Rebolledo, E., Cabadas-Báez, H. V., González, A., Fedick, S. L., Chmilar, J. A., & Leonard, D. (2011). Genesis of Hydromorphic Calcisols in Wetlands of the Northeast Yucatan. *Geomorphology*, *135*, 322-331. Doi:10.1016/j.geomorph.2011.02.009.

Van Diepen, C. A. (1984). *Wetland Soils of the World, their Characterization and Distribution in the FAO-UNESCO Approach* (23 pp.). VII International Soil Classification Workshop on Characterization, Classification and Utilization of Wetland Soil. Los Banos, Philippines, March 26 to April 16.

Institutional Address of the Authors

M.C. Lenin E. Medina-Orozco

Licenciatura en Genómica Alimentaria
Universidad de la Ciénega del Estado de Michoacán de Ocampo
Avenida Universidad # 3000
59000 Sahuayo, Michoacán, México
Teléfono: +52 (353) 5320 762
leninmed@gmail.com

Dra. Norma E. García-Calderón

Unidad Multidisciplinaria de Docencia e Investigación
Facultad de Ciencias
Universidad Nacional Autónoma de México
Boulevard Juriquilla # 3001
76230 Juriquilla, Querétaro, México
Teléfono: +52 (442) 1926 201
negc@ciencias.unam.mx

Dr. Felipe García-Oliva

Centro de Investigaciones en Ecosistemas
Instituto de Biología
Universidad Nacional Autónoma de México
Antigua carretera a Pátzcuaro # 8701
Col. ExHacienda de San José de la Huerta
58190 Morelia, Michoacán, México
Teléfono: +52 (443) 3222 704
fgarcia@cieco.unam.mx

Dra. Elena Ikkonen

Academia Rusa de las Ciencias
Petrozavodsk
185610 Rusia
Teléfono: (8142) 769 810
likkonen@gmail.com

Click here to write the autor

Quetzalapan Falls, Tuliman Communal Lands, Puebla, Mexico.

Photo: Álvaro Can Chulim.

Perceptions and Realities about Pollution in the Mining Community of San José de Avino, Durango

• María de Lourdes Corral-Bermúdez • †Noelia Rivera-Quintero •
• Eduardo Sánchez-Ortiz*•
Instituto Politécnico Nacional, México
*Corresponding of Author

Abstract

Corral-Bermúdez, M. L., †Rivera-Quintero, N., & Sánchez-Ortiz, E. (September-October, 2014). Perceptions and Realities about Pollution in the Mining Community of San José de Avino, Durango. *Water Technology and Sciences* (in Spanish), 5(5), 119-134.

Water pollution in the town of San José de Avino has been attributed to mining activity. Residents were the first to detect it due to the color of a stream coming from some of the wells that traditionally supplied drinking water. They initially presumed that norms regulating mining activity (which has been conducted for 500 years) have not been observed. This created tensions between the residents and the mining company, demanding on several occasions the intervention of the authority. No explanation was being provided as to the origin of the pollution or a solution, with the focus getting lost in the debate about natural versus anthropogenic origins. This investigation analyzed the perception of residents and mine owners about the problem and demonstrated that the pollution was caused by mining activity. Nevertheless, it did not occur as a result of failure to follow regulations. The regulations were primarily aimed at processes regarding the benefit of the mineral and its waste. The preliminary activities had been set aside. For example, in this particular case, banks of inert material have formed which have released significant amount of heavy metals into the environment due to leaching. This would require systematic regulation. The environmental impact statements related to "dumps" can be approved without considering these factors.

Keywords: Minning polution, enviromental regulations, enviromental perceptions.

Resumen

Corral-Bermúdez, M. L., †Rivera-Quintero, N., & Sánchez-Ortiz, E. (septiembre-octubre, 2014). Percepciones y realidades de la contaminación en la comunidad minera San José de Avino, Durango. Tecnología y Ciencias del Agua, *5(5), 119-134.*

En la localidad de San José de Avino se presenta un fenómeno de contaminación del agua atribuido a la actividad minera. Los primeros en detectarlo fueron los pobladores debido a la coloración del arroyo por los derrames de algunas de las norias con las que tradicionalmente se abastecían de agua potable; de forma inicial, ellos han supuesto alguna inobservancia normativa de la actividad minera que tiene una antigüedad de casi 500 años. Esto provocó tensiones entre los pobladores y la minera, que ha demandado en diversas ocasiones la intervención de la autoridad sin que se haya dado una explicación al origen del fenómeno y aún menos una solución, perdiéndose en el debate entre las causas de origen natural y el origen antropogénico. En esta investigación se analizó la percepción de los pobladores y de los dueños de la mina sobre el problema y además se logró demostrar que el fenómeno sí es originado por la actividad minera; sin embargo, no obedece al incumplimiento normativo, por el contrario, dado que la reglamentación se orienta principalmente a los procesos de beneficio del mineral y sus desechos, ha dejado de lado las actividades preliminares, como la formación de terraplenes de material considerado inerte, que en este caso particular aporta importantes cantidades de metales pesados al entorno por lixiviación que requerirían una sistemática regulación, ya que las manifestaciones de impacto ambiental referidas a los "terreros" pueden ser aprobadas sin contemplar estos aspectos.

***Palabras clave**: contaminación minera, normatividad ambiental, percepciones ambientales.*

Received: 11/06/13
Accepted: 04/03/14

Introduction

San Jose de Avino is located in the central portion of the municipality of Panuco de Coronado, in the state of Durango, Mexico. Its founding is closely related to mining activities, one of the objectives of Spain's expansion. Nevertheless, the intermittence of this industrial activity has broken the town's economic dependence on it. Currently, most of the population works in farming and livestock.

Several waterwheels exist in the town, which used to be the only source of water for human consumption. Today, the town has a filtration system connected to the supply network, while some waterwheels continue to provide water to homes in the oldest part of the town.

In recent years, residents have been concerned about water from some of the waterwheels that function as artesian wells, because the streams flowing out of them have become increasingly greener. They began to relate this with the mining activity, convinced because evidence of pollution was detected when the exploitation of the mine was reactivated.

This situation generated a series of tensions between the residents and the company, which have not become very serious but continue to be latent. At different times residents have requested the intervention of authorities and certain institutions, presuming that the way in which the mineral is exploited pollutes the groundwater.

The mining company states that this phenomenon has been occurring for a long time and even began during the break in its activities, and therefore does not assume responsibility, indicating that it complies with all the related regulations.

Speaking economically, mining is the most significant activity, followed by livestock and farming, and therefore an eventual closing of the mine from social pressure would involve a significant deterioration in the region's economy. At the same time, the pollution could be affecting other economic activities in the locality.

Therefore, the overall objective of this investigation was to describe the effect of loopholes in regulations according to social and environmental indicators, as follows:

1. Determine the social perception of the problem.
2. Evaluate the type and levels of pollution in the water.
3. Identify the source of the water pollution.

All of the above was conducted under circumstances in which the company did not make itself very available, in terms of opening its doors and allowing for verifying its operations, as well as distrust by the population.

The investigation was conducted based on the hypothesis that the pollutants in the water are of anthropogenic origin and due to a loophole in regulations. To this end, information was collected from documents and in the field. The documents were obtained from official institutions such as the National Institute for Statistics and Geography (INEGI, Spanish acronym) and the Mexican Geological Service (SGM, Spanish acronym). The regulations were also reviewed. The field information consisted of taking water samples and administering a survey in the locality of San Jose de Avino. In addition, with the use of geographic information systems, several themes for analysis were overlain and a geohydrological profile was defined, which enabled more completely observing what is likely occurring.

Methodology

Preliminary Studies

A document search was conducted of demographic information registered by the INEGI, and different layers of information related to topography, geology, hydrology, etc. were obtained. Information was provided

by the Mexican Geological Service, and background related to the mining activity, the explorations and the different mineralogical contents was obtained.

The field in the locality and its surroundings was toured in order to locate the environmental problem and adjust the methodology of the investigation. Key actors and informants were also identified during this process.

Social-environmental Investigation

For the social stage, action research (Ander-Egg, 1990) was used with the following instruments:

Participant observation: During the first stage, a preliminary diagnostic was developed and recorded and the official and informal leaders, problems and community resources were identified.

Semi-structured interview. This was performed in order to present the social and water quality investigation that would be conducted in the community, with its support and authorization.

Open Interview. This was conducted in order to determine the perception of the mine owner as well as obtain information about the recent history of the mine and unpublished technical information.

Survey. The investigation included 164 occupied homes, with a confidence level of 80% and an error of 0.76; a sample size of 51 homes was obtained. The survey consisted of closed and open questions to obtain information related to the following variables:

- Demographics: age, sex, marital status, schooling and economic activities.
- Infrastructure and equipment: home and public services.
- Health: Childhood and adult morbimortality.
- Environment: water and soil.

The purpose of this phase of the investigation was to explore the relationship between the residents of San Jose de Avino with their natural environment from various points of view, generating indicators for a systematic description.

Chemical analysis

The sampling of the water and soil involved two stages. One corresponded to an exploration stage (March 7, 2011) and the other was a focused sampling (September 3, 2011). For the exploratory sampling, three points were selected in the locality of Panuco de Coronado, located north of the mining area, and three points were selected in San Jose de Avino located south of the mining area. The criteria followed were in accordance to the geographic position such that the largest area possible could be covered and extensive influence by the pollution problem could be discarded. All the samples were taken in duplicate. Field parameters were measured during the collection of samples, including potential of hydrogen (pH), temperature *T* (°C) and electrical conductivity EC (mS/cm). The location of the exploratory sampling is shown in Table 1.

The focused sampling was designed based on the results from the first sampling, combined with the results from the initial interviews. Nine sites were selected, which included six waterwheels in the locality, two points at the dam (which receives runoff downstream and is used as a watering hole) and a filtration system which supplies water to the town and is located approximately 1 km away (Table 2).

The water samples were analyzed in the laboratory to determine the concentration of arsenic (As), cadmium (Cd), chromium (Cr), lead (Pb), copper (Cu), manganese (Mn), iron (Fe), nickel (Ni) and zinc (Zn).

In addition, two samples of soil polluted by sediments were taken at coordinates N 24° 31.045′ W 104° 18.052′ and 2 140 masl, in the micro-watershed of the stream with evidence of water pollution, upstream from the dam. These were analyzed to determine concentrations of cadmium (Cd), copper (Cu), iron (Fe), manganese (Mn), nickel (Ni), lead (Pb) and zinc (Zn).

Table 1. Geographic coordinates of exploratory water sampling points.

Sample	Site	Coordinates
M1	Pánuco de Coronado Plaza	N 24° 32.3′ W 104° 19.6′
M2	Pánuco de Coronado's main well	N 24° 3.2′ W 104° 19.3′
M3	Middle school in Pánuco de Coronado	N 24° 32.2′ W 104° 19.3′
M4	Avino dam	N 24° 30.8′ W 104° 18.1′
M5	Avino well	N 24° 30.8′ W 104° 17.9′
M6	Avino house	

Table 2. Focused water sampling coordinates.

Sample	Site	Coordinates
M1	Avino shallow dam	N 24° 30′ 52.1″ W 104° 18′ 6.5″
M2	Well known as Noria	N 24° 31′ 27.7″ W 104° 17′ 47.5″
M3	Francisco Betancourt waterwheel	N 24° 31′ 27.7″ W 104°17′49.9″
M4	Mrs. Bertha waterwheel	N 24°31′26.1″ W 104° 17′ 54.2″
M5	Plaza well	N 24° 31′ 27″ W 104° 17′ 55.1″
M6	Mrs. Manuela waterwheel	N 24° 31′ 22.7″ W 104° 17′ 59.6″
M7	Well entrance	N 24° 31′ 21.3″ W 104° 17′ 57″
M8	Tajo Well	N 24° 30′ 3.6″ W 104° 18′ 12.2″
M9	Avino deep dam	N 24° 30′ 51.7″ W 104° 18′ 8.7″

Preparation of the samples

Before analyzing the water and soil samples, they underwent digestion for the oxidation of the organic matter and to dissolve analytes, in order to avoid interference from the matrix. The preparation was performed according to NMX-AA-051-SCFI-2001 (DOF, 2001). The process will briefly be described next.

Digestion of the water samples to determine total metals

1. Digestion were performed in duplicate and a target to corroborate the results was obtained.
2. Three milliliters of nitric acid were added and heated until reaching a volume of 2 to 5 ml.

3. Five milliliters of nitric acid were added to the product and heated again, covering the container with a watch glass.
4. Ten milliliters of chlorhydric acid 1:1 and 15 ml of bidistilled water were added.
5. Heated for 15 minutes, then washed, filtered and measured, to 100 ml.

Since vapors are produced throughout digestion, this was performed in an extractor hood for additional safety.

Digestion of soil samples

1. The soil was left to dry at room temperature for 24 hours.
2. It was triturated and sifted with a #10 mesh.
3. A 0.15 g sample was weighed, in duplicate, and deposited in a precipitate glass.
4. Five milliliters of reactive grade HNO_3 and 10 ml of reactive grade HCL were added. These were covered and heated on an electric burner to evaporate until obtaining approximately 2 ml of liquid.
5. The previous step was repeated.
6. Five milliliters of HCL (1:1) and 7.5 ml of bidistilled water were added; heated for 10 minutes.
7. This was filtered and measured, to 100 ml.

Characterization of samples

The concentrations of arsenic (As) and heavy metals (iron (Fe), manganese (Mn), copper (Cu), lead (Pb), zinc (Zn), cadmium (Cd), chromium (Cr) and calcium (Ca)) were determined by atomic absorption.

The samples were analyzed in the Instrumentation Center of the CIIDIR-IPN, Durango Unit. A PerkinElmer brand, AAnalyst 700 model atomic absorption spectrophotometer (AAS) was used.

AAS Analysis

A graphite furnace was used to read As, Cd, Cr and Ni in the water samples. The other elements and the metals in the soil samples were analyzed using flame analysis.

Hollow-cathode lamps were used. The equipment was calibrated according to prepared calibration standards from certified dissolution guides for each element and for class A volumetric material (Table 3).

To verify the reliability of the analysis, quality control standards were prepared, which consisted of dissolution of known concentrations prepared based on the certified dissolution guides.

The quality control standard was analyzed after calibration and upon completing the

Table 3. Calibration standards.

Element	Concentration of the calibration curve	Certified dissolution guide
As	5, 10, 20, 30, 40 µg/l	Hycel
Cd	2, 4, 8 µg/l	Cenam
Cr	5, 10, 20, 30 µg/l	Cenam
Pb	5, 10, 20, 30 mg/l	Cenam
Ni	5, 10, 20, 30 µg/l	PerkinElmer
Cu	1, 2, 4, 10 mg/l	PerkinElmer
Fe	1, 5, 10, 20 mg/l	PerkinElmer
Mn	1, 2, 4, 8 mg/l	PerkinElmer
Zn	2, 4, 6 mg/l	PerkinElmer

analysis of the samples. The NXM-052-AA-SCFI-2002 recommends that the recovery percentage of the quality control standard not exceed 15%.

Geohydrological Transect

The heights of the waterwheel wellheads were obtained, from the water mirror and from the bottom, in order to compare them with data from the mine's flood elevation. This generated an elevation profile which included the geological profile of the exploratory wells in the region. This information was used to verify or discard a relationship between the water level in the mine and the levels in the artesian wells, consider the belief by persons in the locality that a relationship exists.

Analysis of the regulations related to mining residues

The public policy regarding mining residue as established by related legislation and norms was reviewed. In particular:

1. The Mining Law and its regulation.
2. General Law on Ecological Balance and Environmental Protection (articles 28 and 35).
3. General Law for the Prevention and Comprehensive Management of Toxic Wastes (article 17).
4. Regulation pertaining to the General Law for the Prevention and Comprehensive Management of Toxic Wastes (articles 33 and 34).
5. Official Mexican Norms:
   a) NOM-052-SEMARNAT-2005.
   b) NOM-120-SEMARNAT-1997.
   c) NOM-141-SEMARNAT-2003.
   d) NOM-147-SEMARNAT/SSA1-2004.
   e) NOM-155-SEMARNAT-2007

Discussion and Results

Social-environmental Profile

Location

San Jose de Avino is located in the municipality of Panuco de Coronado, in the state of Durango, Mexico. It is located at 2 160 masl, at the coordinates 24° 31´ north latitude and 104° 18´ west latitude (INEGI, 2005). It measures 4 670.525 hectares and contains two human settlements —the residents who occupy 68.79 hectares and the mine (INEGI, 2000).

Demographic Structure

In 2010, San Jose de Avino had a total population of 760 inhabitants, of which 386 were men and 374 were women. In addition, there was a total of 209 homes, 164 of which were inhabited. Of these 164, 17 had dirt floors and 6 had only one room. A total of 108 of all the homes had sanitary facilities, 155 were connected to public services and 162 had access to electricity (INEGI, 2010).

The data from the 2010 INEGI census shows that most of the population in the locality at that time was adult, with 65% of the population 18 years of age or older. The population of children and youth did not represent the base of the population pyramid, which indicates aging over a mid-range period of time (Figure 1).

The population has been decreasing due to migration out of the locality. From 1990 to 2005 it decreased 33%, with a small recovery by 2010, according to the census for that year, ending in 21.7% (Figure 2).

Schooling

In terms of education, according to the survey (preschool-high school), 61% of the population has an elementary level, 37% a secondary level education and only 2% high school; this reflects a relatively low level of studies. Public schools

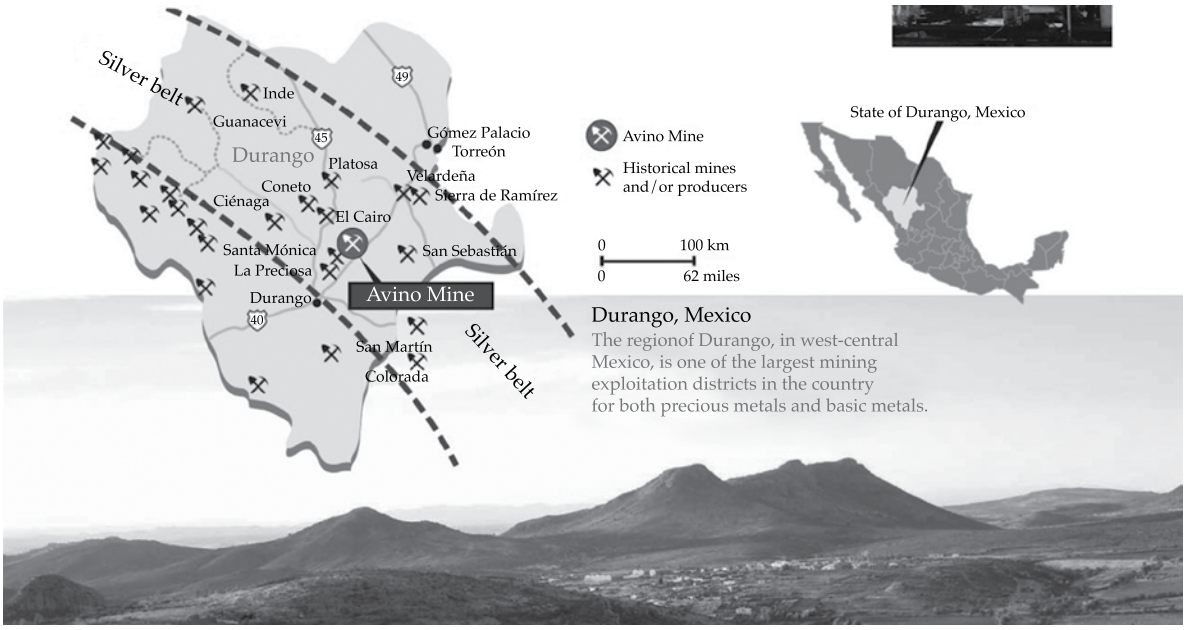

Figure 1. Location of the San Jose de Avino mine (from www.avino.com, *Avino Fact Sheet Spanish*, march 2010).

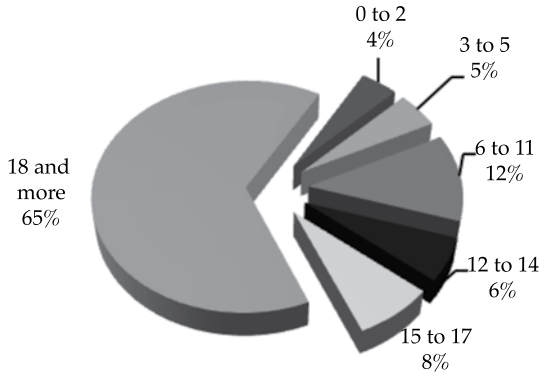

Figure 2. Distribution of the population, by ages (INEGI, 2010).

exist in the community that teach preschool, elementary, and distance-learning secondary education.

Housing

The urban development of the locality has been concentric. Other than the historic downtown, housing located in the center of the community is old, with colonial architectural styles. The housing on outer edges of the town are recent.

In terms of housing ownership, most of the population (86%) owns the house in which they live, 12% have loans and 2% rents the house in which they live (Figure 3). In addition, 67% has lived in their houses over 15 years, and 24% has lived in their houses under 5 years (Figure 4).

Most of the houses belonging to persons interviewed had adobe walls (84%), panel roofing (68%) and nearly all had concrete floors throughout.

Public Services and Infrastructure

In relation to public services, the survey results showed that most of the population possessed all the services, such as connection to the potable water network, electricity, drainage and garbage collection (Table 4).

In the community of San Jose de Avino, the waterwheels that were originally the main source of supply to the homes were conserved. San Jose de Avino has two supply sources. One is in this locality and comes from the well

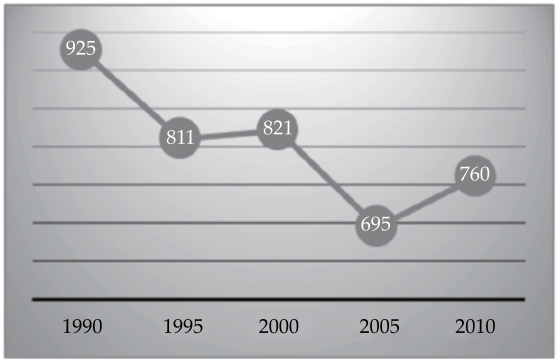

Figure 3. Population growth in San Jose de Avino (INEGI, 1990, 1995, 2005, 2010).

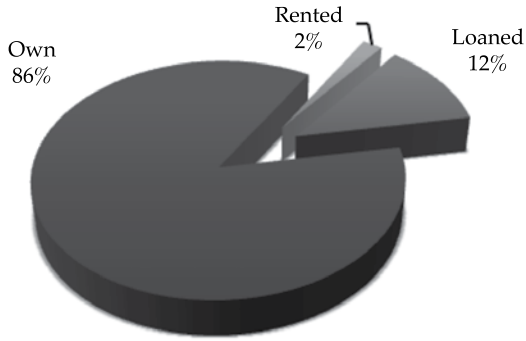

Figure 4. Ownership of homes.

called "El Tajo," located at 2.5 km, and the second source is a well located in Zaragoza, at 5.7 km. Due to this situation, the availability and accessibility of the water is not sufficient for pumping and conduction. In addition, the community's distribution network is divided into sectors, requiring management in turns.

Health

Since there are no health institutions in San Jose de Avino, this indicator was considered as a first approximation of the health situation in the study area. It is worth mentioning that although the survey does not reflect illnesses associated with the presence of heavy metals, this is a point to be more thoroughly investigated later.

When people become ill they are treated in nearby communities, primarily in Zaragoza, Madero and Panuco de Coronado, demonstrating a lack of health care facilities in the community. This may be because the community has a small population, and investment in infrastructure is made in larger communities.

Economic activities

The community was settled when the mine began to be exploited, around which the primary economic activities of the population arose —livestock, farming and mining (Figure 5).

Community Perceptions

The community surveyed perceives the soil to be eroded. This is understandable since the population is located in the foothills of a mountainous formation. The population surveyed indicated that pollution was the

Table 4. Coverage of services.

Service	INEGI 2010 census data	Survey data
Piped water	95%	98%
Drainage	74%	72.6%
Electricity	98.8%	94%
Garbage collection	NA	94%

NA = Not available.

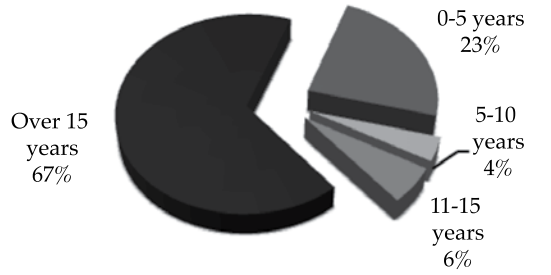

Figure 5. Length of residence.

main problem involving the water quality of the rivers and streams (Figure 6).

Even so, these rivers and streams are used for washing and as drinking water for cattle. In addition, gravel and sand are extracted from the banks of the rivers and streams for use in manufacturing material for the walls of homes. A relevant result of the social aspect of the investigation is that the residents of San Jose de Avino perceive water quality as one of their main problems, along with lack of work.

Perceptions of the Mine Owner

The San Jose de Avino mine has been exploited since colonial times. It has been managed by the Spanish, English, and Mexicans, and is currently run by a Canadian capital firm, with a smaller portion held by Mexican interests. Its production has included copper, silver and gold.

In a semi-structured interview, the former owner of the mine, Mr. Isita, stated: "In 1968, the exploration phase began. In 1974, the mine was established with an installed capacity of 1 000 tons daily, of which only 40 tons/day were produced from the open pit mine, from which gold and silver was being extracted. From 1990 to 1992, gold and silver continued to be extracted, but in lesser quantities, and larger amounts of copper began to be mined from the bottom of the pit. In 1992, the exploration of the underground mine began. By 1994 underground exploitation began, with copper, gold and silver." He considers the mine to be productive and indispensable to the life of the locality, "given that it has been exploited for

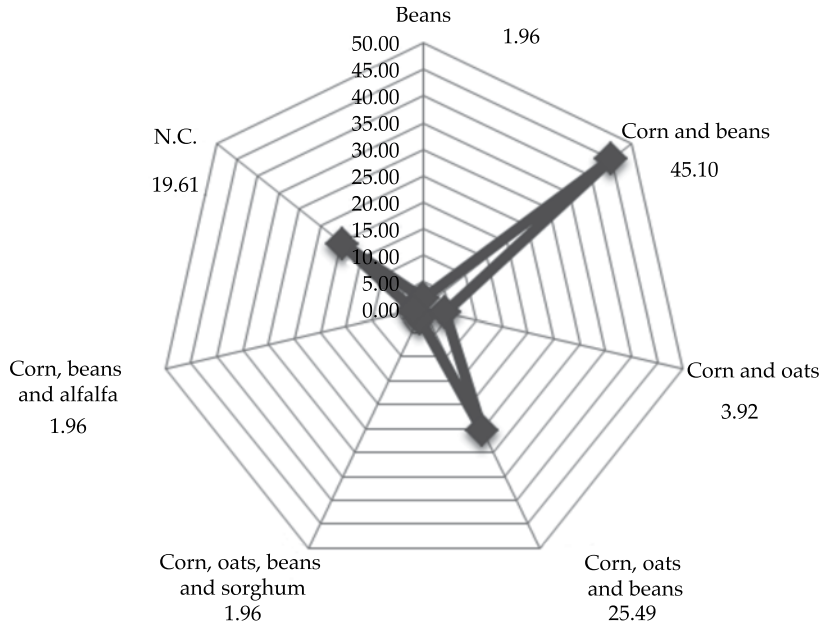

Figure 6. Diversification of crops (percentages).

over 400 years. It is abundant, but the quality is poor. It is also called "cargo" since the recovery is 60%, obtaining 250 g/t for silver and 1.5 g/t for gold (…). The presence of the mine was beneficial to the region, since because of the mining activity, and because there was no electricity or water in the zone, it sought to establish service for the mine and, therefore, for the community of San Jose de Avino, as well as the construction of the El Caracol dam and the drilling of the "El Barranqueño" well near the dam, to a depth of 400 m. In addition to providing jobs, which decreased migration because the mine offers good salaries and contributes taxes to fund public works." He also mentioned that the useful life of the mine is over 100 years. He thereby establishes a position of ongoing benefit to the locality and has repeatedly not assumed responsibility for the pollution, mentioning that a "Sign of cattle deaths" has been made repeatedly, and were never proven. On one occasion, an autopsy was performed on a cow, with no results attributable to pollution." And in 2004 he was informed of a "burst in the tailings dam because there was a spill in the area of the town, and in the presence of the authorities from Conagua and Profepa, the origin of the spill was traced back to a waterwheel," identified as the waterwheel at the house of Mrs. Manuelita, which corresponds to sampling point M6.

Surface Hydrography

The locality is in Administrative Hydrological Region III and belongs to Hydrological Region 11 of the Durango River sub-watershed, in the headwaters of the Las Casa River. Inside the community, small intermittent streams flow into a dam located on the access to the town (Figure 8).

Results from Laboratory Analyses

To measure the water quality of the aquifer that supplies the population, samples were taken at 9 sites, taking care that they were representative of the water from the waterwheels. Two samplings were performed —an exploratory sampling and a focused sampling. In addition, surface water was included from the El Tajo dam, which is used as a watering hole.

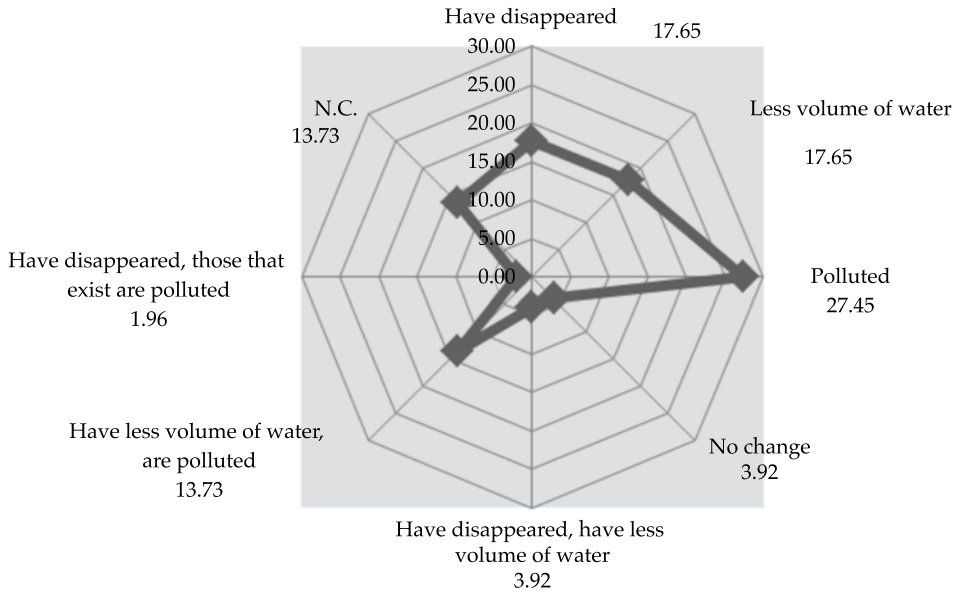

Figure 7. Perception about the water quality of the rivers and streams.

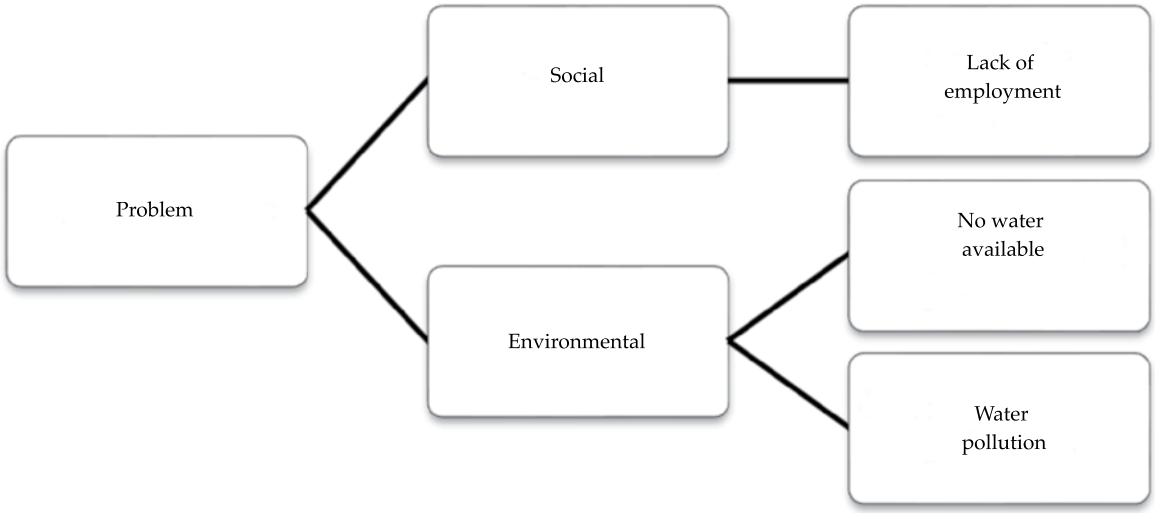

Figure 8. Perception of the problems in San Jose de Avino.

Field Parameters

The field parameters analyzed were pH, T (°C) and EC (mS/cm). Tables 5 and 6 show these results from the samples. The first sampling included 6 sites, since this was related to observing the behavior of the aquifer. Nine sites were sampled in the second sampling, of which only 2 corresponded to the first sampling stage. The sites were modified based on the analysis of the data collected from the surveys.

Table 5. Results from exploratory sampling of water.

Sample	pH	Temperature (°C)	Conductivity (mS)
M1	7.2	24	0.59
M2	7.2	24	0.59
M3	7.3	24	0.59
M4	8.4	24	1.34
M5	7.9	23	2.45
M6	8.2	24	0.68

Table 6. Results from focused sampling of water.

Sample	pH	Temperature (°C)	Conductivity (mS)
M1	6.6	21	0.64
M2	7.0	23	1.086
M3	7.0	19	2.10
M4	7.18	20	0.969
M5	7.33	21	4.5
M6	5.79	20	1.992
M7	7.61	19	1.995
M8	7.27	21	0.738
M9	7.4	22	0.61

Laboratory Parameters

Concentrations of arsenic (As), cadmium (Cd), chromium (Cr), lead (Pb), copper (Cu), manganese (Mn), iron (Fe), nickel (Ni) and Zinc (Zn) were determined in the laboratory. Tables 5 and 6 show the results from the concentrations of these elements.

Standing out among the results obtained from the focused sampling is the finding of metals Cd, Pb, Ni, Mn, Fe and Cu in amounts above allowable limits established by NOM-127-SSA1-1994, in samples M1, M6 and M9, and up to 947 times in the case of Pb (Table 7).

From the results obtained in the focused sampling, M1, M6 and M9 also stand out because of a higher presence of metals Cd, Pb, Ni, Mn, Fe and Cu, which were correlated among each other (Figure 9).

Soil samplings

Two soil samples were collected from the site at coordinates N 24° 31.045', W <c and at 2 140 masl. Table 8 shows the results obtained. Visually, the pollution from sedimentation from water transport can be seen to be coming from the mining tailings and from the waterwheel.

Another notable result is the presence of copper, which as seen in Table 6, exceeds by 300% the concentration recommended for there to be no negative impact on the soil from this type of activity (Bowie & Thornton, 1985).

Geohydrological Profile

Interpreting the results from the geohydrological profile, the flood level in the mine, identified as level 14 by the mine owner as well as employees, is several tens of meters below the soil saturation level measured at the waterwheels sampled. Therefore, there are no evident connections with underflows that would support the supposition that the flood level of the mine affects the strata which supply water to the waterwheels, thereby negating the perceived effect from within the mine.

Table 7. Results from focused sampling of water (September 2011).

Sample	As	Cd	Cr	Pb	Cu	Fe	Mn	Ni	Zn
LMP	0.025	0.005	0.050	0.01	2.00	0.30	0.15	0.050	5.00
M1	< 0.005	0.007 ± 0.000	< 0.010	1.74 ± 0.083	< 1.00	2.246 ± 0.093	3.200 ± 0.011	0.008 ± 0.002	1.571 ± 0.075
M2	< 0.005	< 0.002	< 0.010	< 0.03	< 1.00	< 0.200	< 0.06	< 0.005	0.438 ± 0.029
M3	< 0.005	0.003 ± 0.001	< 0.010	< 0.03	< 1.00	0.597 ± 0.020	0.069 ± 0.047	< 0.005	0.392 ± 0.016
M4	0.008 ± 0.001	< 0.002	< 0.010	0.127 ± 0.035	< 1.00	0.343 ± 0.177	0.069 ± 0.029	< 0.005	0.323 ± 0.005
M5	< 0.005	< 0.002	< 0.010	0.152 ± 0.000	< 1.00	< 0.200	1.245 ± 0.811	< 0.005	0.130 ± 0.000
M6	0.010 ± 0.002	1.859 ± 0.000	< 0.010	0.516 ± 0.021	13.791 ± 0.357	0.969 ± 0.044	2.294 ± 0.022	0.176 ± 0.001	3.906 ± 0.003
M7	0.006 ± 0.001	0.004 ± 0.000	< 0.010	0.065 ± 0.029	< 1.00	0.242 ± 0.039	0.212 ± 0.026	< 0.005	0.548 ± 0.036
M8	0.012 ± 0.000	< 0.002	< 0.010	< 0.03	< 1.00	0.242 ± 0.028	< 0.06	< 0.005	0.293 ± 0.017
M9	0.010 ± 0.001	0.125 ± 0.017	0.012 ± 0.005	9.47 ± 0.170	4.895 ± 0.07	21.711 ± 0.089	8.207 ± 0.664	0.023 ± 0.000	3.361 ± 0.018

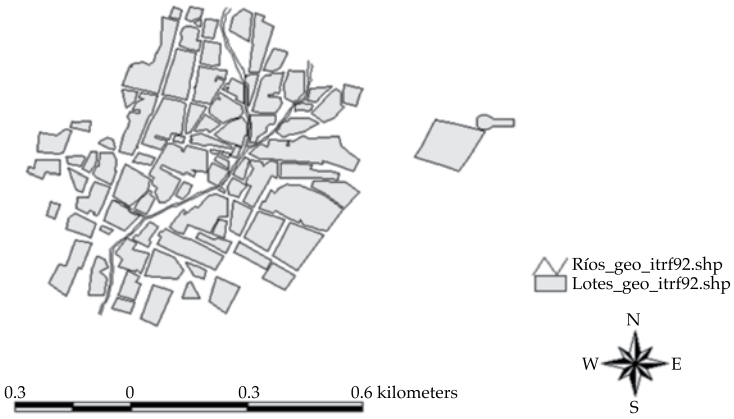

Figure 9. Intermittent streams that run through the town.

Table 8. Results from the analysis of the soil samples.

Concentration, in mg/g							
Sample	**Cd**	**Cu**	**Fe**	**Mn**	**Ni**	**Pb**	**Zn**
B & T	< 0.001 - 0.002	< 2	--	--	0.002 - 0.1	0.01 - 0.15	0.025 - 0.2
A	0.082 ± 0.001	270 ± 8.48	43 ± 2.35	1.43 ± 0.27	0.029 ± 0.002	3.14 ± 0.46	21.51 ± 0.32
B	< 0.001	8.1 ± 0.61	73.33 ± 0.004	3.03 ± 0.44	0.01 ± 0.002	7.36 ± 0.23	2.15 ± 0.15

Conclusions

Mining production generates a significant amount of "inert" material for use by the mining industry. This is generated from the movement of large volumes of material for exploratory excavation, in order to build different systems to permit both horizontal and vertical access, until reaching the mining exploitation zone itself.

In the case of San Jose de Avino, at least three groups of spoil banks (Figure 10) are located upstream from the town, very near the channel. They are composed of material that is not useful to mining, consisting of fractured rock with particles under 60 cm in diameter and a large range of sizes. It has a green color because of the naturally high copper oxide contents. At the foot of each of these spoil banks are zones with copper oxide concentrations from the leaching of rainwater and later surface evaporation. Right in the spot where the stream begins, at the foot of one of the spoil banks, is a gully with evident signs of leachate deposits from the level of the underflow to a depth of 30 to 35 cm (Figures 10, 11, 12 and 13, 14 and 15).

All this is located upstream from the town, at a distance of 500 meters from the first house and at the head of the stream, as well as on its right banks.

Norms NOM-052-SEMARNAT-2005, NOM-120-SEMARNAT-1997, NOM-141-SEMARNAT-2003, NOM-147-SEMARNAT/SSA1-2004 and NOM-155-SEMARNAT-2007 do not in any case consider restrictions for any of the spoil banks, nor do they require the mining industry to classify them or evaluate their possible activation when exposed to the elements.

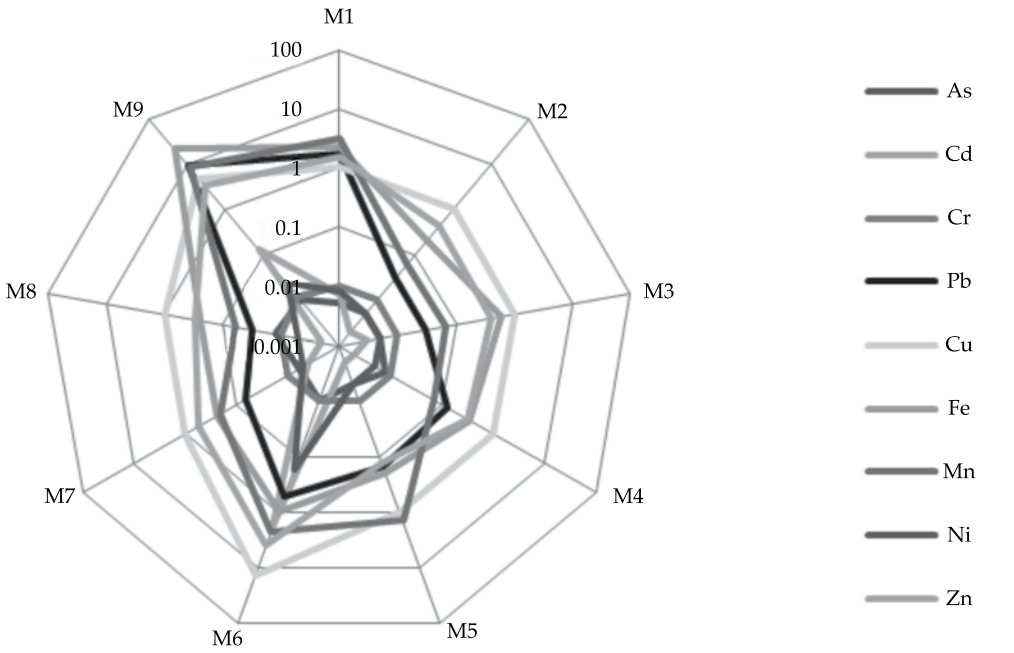

Figure 10. Diagram of concentration of heavy metals in field samples.

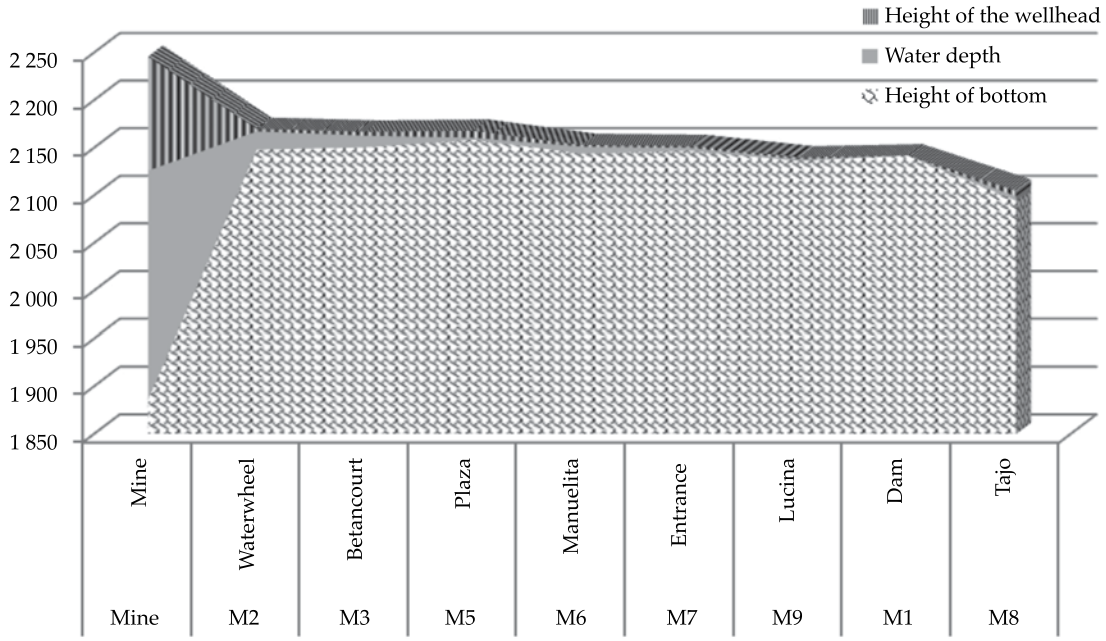

Figure 11. Geohydrological profile.

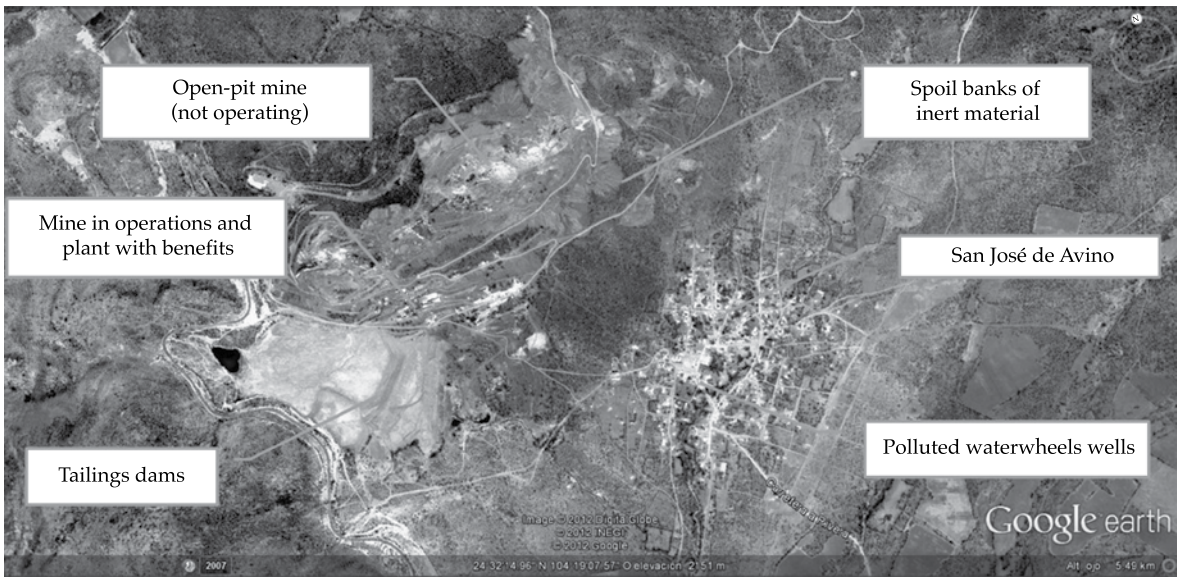

Figure 12. Overall map of the San Jose de Avino area.

Figure 13. Appearance of the stream downstream from the waterwheels producing water, with high copper oxide contents.

Figure 14. Spoil banks and evidence of leachates at the bottom.

The environmental impact statement for these mining projects does not consider this type of extraction of inert matter as a risk and does not establish measures to evaluate or recover the leachates. Only dumping sites are considered which, nevertheless, require the approval of the Ministry of Natural Resources and the Environment.

Although the pollution in San Jose de Avino is caused by mining activity, it is not related to a lack of compliance with existing regulations, but rather a loophole in them.

Therefore, the Mexican Official Norms or the review criteria for environmental impact statements need to require the characterization and evaluation of heavy metal contents and certain other pollutants from material in the spoil banks, and the consequent construction of leachate recovery systems. They must also prohibit their placement upstream from sources

Figure 15. Appearance of leachates in a gully downstream from San Jose de Avino.

supplying water for human consumption, among other pertinent actions.

Recommendations and Suggestions

There are three aspects to the recommendations resulting from the present study. The first is social, for which it is helpful to foster relationships between the community and the company, clearly articulate the problem and determine joint solutions, such as the construction of leachate traps and the creation of some type of process for the treatment and final disposal of sediments.

The second aspect is the search for effects on livestock that drink at the El Tajo dam, which receives runoff with high heavy metal loads.

Lastly, similar sites need to be studied to identify leaching of heavy metals and other compounds from mining spoil banks, where they may not be as evident as this case but are present. The purpose of this is to initiate the consultations needed for issuing regulations that require the characterization of risks from the leaching of heavy metals in mining spoil banks.

References

Ander-Egg, E. (1990). *Repensando la Investigación Acción Participativa*. Buenos Aires: Grupo Editorial Lumen Humanitas.

Bowie, S. H. U., & Thornton, L. (1985). *Enviromental Geochemistry and Health*. Hingham, USA: Kluwer Academic Publ.

Diario Oficial de la Federación. Normas Oficiales Mexicanas (NOM-052-SEMARNAT-2005 NOM-120-SEMARNAT-1997, NOM-141-SEMARNAT-2003, NOM-147-SEMARNAT/SSA1-2004, NOM-155-SEMARNAT-2007).

INEGI (2010). *Censos de Población y Vivienda*. Consultado en diciembre de 2011. Recuperado de http://www.censo2010.org.mx.

Ley Minera y su reglamento, http://www.diputados.gob.mx/LeyesBiblio/ref/lmin.htm.

Ley General del Equilibrio Ecológico y Protección al Ambiente, http://www.diputados.gob.mx/LeyesBiblio/ref/lgeepa.htm.

Ley General para la Prevención y Gestión integral de los Residuos Peligrosos, http://www.diputados.gob.mx/LeyesBiblio/index/htmre.

Reglamento de la Ley General para la Prevención y Gestión integral de los Residuos Peligrosos, http://www.diputados.gob.mx/LeyesBiblio/index.

Institutional Address of the Authors

M.C. María de Lourdes Corral Bermúdez

Egresada de la Maestría en Gestión Ambiental
Instituto Politécnico Nacional, CIIDIR Unidad Durango
Sigma 119, Fraccionamiento 20 de Noviembre II
Durango, Durango, México
Teléfono: +52 (618) 814 2091
freelucobel@hotmail.com

Dr. Eduardo Sánchez Ortiz

Investigador del Instituto Politécnico Nacional, CIIDIR Unidad Durango
Calle Sigma 119, Fraccionamiento 20 de Noviembre II
34220, Durango, Durango, México
Teléfono: +52 (618) 8142 091, extensión 82622
esanchezo@ipn.mx

A Geostatistical Approach to the Optimal Design of the "Saltillo-Ramos Arizpe" Aquifer Monitoring Network for Proper Water Resources Management

• Martín A. Díaz-Viera •
Instituto Mexicano del Petróleo

• Félix Canul-Pech* •
Instituto Nacional de Estadística y Geografía, México
*Corresponding Author

Abstract

Díaz-Viera, M. A., & Canul-Pech, F. (September-October, 2014). A Geostatistical Approach to the Optimal Design of the "Saltillo-Ramos Arizpe" Aquifer Monitoring Network for Proper Water Resources Management. *Water Technology and Sciences* (in Spanish), 5(5), 135-153.

The purpose of this study is to determine the optimal design of the piezometric level monitoring network in the "Saltillo-Ramos Arizpe" aquifer using a geostatistical approach. To identify the best wells for monitoring, two options were considered —one fixed the level of variance in the estimation error and the other fixed the number of wells regardless of the resulting estimation error. Both options applied the optimal successive inclusions technique in combination with the ordinary kriging method as a spatial estimator. The data used were taken from 750 hydraulic installations (wells and treadmills) in a geohydrological study conducted in the aquifer in 2007. Groundwater levels showed spatial trends —i.e., lack of stationarity— which was estimated by a first degree polynomial fit and then subtracted from the original data, thereby obtaining residuals. With these residuals, semivariograms were calculated and an isotropic spherical model was fitted. The resulting optimal network consists of 144 wells, with a standard deviation of error of 21 meters determined by ordinary block kriging. This represented 19.2% of the 750 existing hydraulic installations in the study aquifer, and implies a 80.8 % savings in the cost of monitoring the wells. The best 50, 100, 200, 300, 400 and 500 monitoring wells were also determined, and represent options which can be considered depending on the material, financial and human resources available for this activity.

Keywords: Estimation, kriging, optimization, successive inclusions, geostatistics, aquifer, monitoring network, optimal network design.

Resumen

Díaz-Viera, M. A., & Canul-Pech, F. (septiembre-octubre, 2014). Diseño óptimo de la red de monitoreo del acuífero "Saltillo-Ramos Arizpe" para el adecuado manejo del recurso hídrico, aplicando un enfoque geoestadístico. Tecnología y Ciencias del Agua, *5(5), 135-153.*

El presente estudio tiene la finalidad de realizar el diseño óptimo de la red de monitoreo de los niveles piezométricos en el acuífero "Saltillo-Ramos Arizpe", aplicando un enfoque geoestadístico. Para determinar los mejores pozos para el monitoreo se consideran dos alternativas: en la primera se fija un nivel de varianza del error de estimación, mientras que en la segunda se fija la cantidad de pozos, independientemente del error de estimación que resulte. En ambas opciones se aplica la técnica de optimización de las inclusiones sucesivas óptimas, en combinación con el método de kriging ordinario como estimador espacial. Los datos utilizados fueron tomados de 750 aprovechamientos hidráulicos (pozos y norias) de un estudio geohidrológico realizado en el acuífero en 2007. Los niveles piezométricos presentaron el fenómeno de tendencia espacial, es decir, falta de estacionaridad, la cual fue estimada por medio de un ajuste polinomial de primer grado y posteriormente restada a los datos originales, obteniéndose valores residuales. A dichos residuales se les calcularon semivariogramas y se les ajustó un modelo esférico e isotrópico. La red óptima consta de 144 pozos, determinada para una desviación estándar del error de estimación por kriging ordinario en bloques de 21 metros. Lo anterior representa un 19.2% de los 750 aprovechamientos hidráulicos existentes en el acuífero de estudio, lo cual implica un ahorro en un 80.8% de costo de monitoreo en pozos. Asimismo, se determinaron los mejores 50, 100, 200, 300, 400 y 500 pozos para el monitoreo, opciones que se pueden tomar en cuenta dependiendo de los recursos materiales, financieros y humanos disponibles para realizar dicha actividad.

***Palabras clave**: estimación, kriging, optimización, inclusiones sucesivas, geoestadística, acuífero, red de monitoreo, diseño óptimo de redes.*

Received: 05/12/12
Accepted 15/03/14

Introduction

The study of fresh water resources is justifiable given the water demanded for consumption by living beings. It is therefore important to monitor the behavior of groundwater and, especially, of aquifers subject to high demand.

The Saltillo metropolitan region is an interesting area to apply the methodology pertaining to the work herein. According to the results from the population census published by the National Institute for Statistics and Geography (INEGI, 2010), this region has undergone very significant growth over recent years, where the water demand is primarily met by the Saltillo-Ramos Arizpe aquifer since no other significant fresh water sources exist.

The methodology used takes advantage of the fact that the kriging estimation-error variance does not depend on the value of the variable, according to Samper and Carrera (1990). Therefore, this variance can be calculated before taking measurements and obtaining the location of measuring points, in this case wells, in such a way as to minimize the uncertainty of the estimation. This uncertainty can also be minimized with a preset number of wells.

Some of the reference works include: Prakash and Singh (2000), who designed an optimal network for the upper Kongal basin, district of Nalgonda, A.P. (India) by applying kriging; Banjevic and Switzer (2002) compared recooked simultaneous simulation optimization strategies and algorithms for sequential selection points; Dixon, Smith and Chiswell (1999) applied geographic information systems and recooked simulation algorithms; Lloyd and Atkinson (1999) designed optimal sampling configurations using ordinary kriging and indicator kriging; Cousens, Brown, Mcbratney, & Moerkerk (2002) applied different sampling strategies to generate maps of underbrush; Wang and Qi (1998) studied the effect of sample distribution on the analysis of the spatial structure of polluted soil, among others.

The purpose of this study is to establish and apply a methodology to determine the optimal network of wells for monitoring piezometric levels in the aquifer in question, in order to manage it. To this end, a geostatistical approach was applied consisting of: performing a preliminary and exploratory analysis of the data; obtaining a variogram model of the spatial correlation; performing estimations with ordinary and optimal kriging; and applying the successive inclusion technique.

Objectives

General

To establish and apply a methodology that makes it possible to systematically obtain the optimal design of monitoring networks in order to manage piezometric levels based on the geostatistical analysis of data.

Specifics

- Obtain a model of the spatial variability of the data pertaining to existing piezometric levels using geostatistical analysis.
- Evaluate the spatial behavior of the estimation-error variance by applying ordinary kriging to estimate piezometric levels.
- Determine the optimal network of wells for the monitoring of piezometric levels in the Saltillo-Ramos Arizpe aquifer, based on different scenarios.

Methodologies for the optimal design of monitoring networks

To determine the optimal design of groundwater monitoring networks, methodologies using geostatistical approaches and "Kalman filtering" have been proposed in various parts of the world. The former enables evaluating the level of uncertainty by determining the estimation-error variance at points in a network based on the spatial correlation of a variable. The other

enables evaluating the degree of uncertainty by coupling a filtering algorithm with a hydrodynamic flow model, and helps to improve the accuracy of the results and the calibration of the model. The two approaches are considered to be equivalent.

To apply the geostatistical approach, a function is needed that describes the spatial correlation of the study property (Z(x)). A semivariogram can usually be used (Chiles & Delfiner, 1999; Olea, 1999; Isaaks & Srivastava, 1989; Moral-García, 2003).

The most common estimator of the semivariogram or semivariance, according to Omre (1984) can be expressed as:

$$\gamma^*(h) = \frac{1}{2N}\sum_{i=1}^{N}\left[Z(x+h) - Z(x)\right]^2 \qquad (1)$$

Where N is the number of pairs of $[Z(x + h) – Z(x)]$ separated by a distance h. When the random function is stationary, the following relation is met:

$$\gamma(h) = Var(Z) - C(h) \qquad (2)$$

Thereby, in this case the semivariogram and the covariance are defined.

Normally, the semivariogram is an increasing monotonic function, since when distance h increases the difference $|Z(x + h) – Z(x)|$ increases. If Z is a stationary random function, γ reaches a limit value, called "sill," which is equivalent to the variance of Z. The sill is reached for a value of h known as the range. The range determines the zone of influence, outside of which the spatial correlation is zero. By definition, $\gamma(0) = 0$, but $\gamma(0)$ often has a positive value, called the nugget effect.

Nevertheless, not all the semivariograms reach a sill. Some may not asymptotically tend to the variance but rather to infinity when h tends to infinity. In addition, the range does not have to be equal in all directions, in which case it reflects the existence of anisotropy. It is also possible to have more than one range for a determined direction, which would indicate the presence of different correlation structures acting at difference scales.

Ordinary point kriging (Isaaks & Srivastava, 1989) can be described as:

$$\hat{Z}_0 = \sum_{i=1}^{n} W_i Z(x_i) \qquad (3)$$

$$\sum_{j=1}^{n} W_j \hat{C}_{ij} + \mu = \hat{C}_{i0} \quad \forall i = 1,\ldots,n$$

$$\sum_{i=1}^{n} W_i = 1$$

Where $\hat{Z}_0$ is the estimator, W_i the weights for ordinary point kriging, μ is a Lagrange multiplier; $\hat{C}_{ij}$ and $\hat{C}_{i0}$ are the covariances which can be substituted by the semivariances in the case of the intrinsic hypothesis, that is, second order stationarity of the variable to be estimated.

The variance of the minimized error can be expressed as:

$$\hat{\sigma}_R^2 = \hat{\sigma}^2 - \left(\sum_{i=1}^{n} w_i \hat{C}_{i0} + \mu\right) \qquad (4)$$

This minimizes the estimation-error variance, typically known as ordinary kriging variance.

The block kriging estimation (Moral-García, 2003) will have the form:

$$Z_{KB}^*(x) = \sum_{i=1}^{n} w_i Z(x_i) \qquad (5)$$

Where w_i is the weights assigned to the data $(Z(x_i))$ in ordinary block kriging. As in the case of ordinary point kriging, the estimation of the block must be unbiased in order to minimize the error variance:

$$\sum_{j=1}^{n} w_j C(x_i - x_j) + \mu = \bar{C}(x_i - V(x)) \qquad (6)$$

$$i = 1,\ldots n$$

$$\sum_{i=1}^{n} w_i = 1$$

The system is identical to point kriging, except that the right term $\bar{C}(x_i - V(x))$ represents the covariance between point x_i and block $V(x)$, that is, the mean covariance between the random variable $Z(x_i)$ and the random variable $Z(x)$, the latter corresponding to all points in block V.

In practice, the covariance $\bar{C}(x_i - V(x))$ is calculated with the arithmetic mean of the covariance between sampling points x_i and the m points obtained by discretizing block V:

$$\bar{C}\left(x_i - V\left(x\right)\right) = \frac{1}{m}\sum_{j=1}^{m} C\left(x_i - x_j'\right) \qquad (7)$$

The block variance is:

$$\sigma_{KU}^2 = \bar{C}\left(V\left(x\right), V\left(x\right)\right) - \sum_{i=1}^{n} w_i \bar{C}\left(x_i, V\left(x\right)\right) - \mu \qquad (8)$$

Where the block covariance $\bar{C}(V(x),V(x))$ is calculated with the arithmetic mean of the covariances between the points that discretize the block:

$$\bar{C}\left(V\left(x\right), V\left(x\right)\right) = \frac{1}{m^2}\sum_{j=1}^{m}\sum_{k=1}^{m} \bar{C}\left(x_j' - x_k'\right) \qquad (9)$$

The following methods are applied to determine the optimal design of monitoring networks using the geostatistical approach (Samper & Carrera, 1990).

Fictitious point method

Where n number of measurements exist corresponding to n spatially distributed points $\{xi,\ i = 1,...,n\}$, to determine the value of the measurement of an additional point x_{n+1}:

1. A fictitious additional point $n + 1$ is first considered.
2. The value in x_{n+1} is estimated using kriging.
3. The variance of the kriging estimation is obtained.

Lastly, points 1, 2 and 3 are repeated, changing the position of the point until obtaining the optimal position, which minimizes the variance.

The methods can be classified as *global* and *local*, depending on whether the mean value of the property is calculated globally or whether a local improvement of the estimation is desired.

Global estimation

This is intended to minimize the variance of the estimation of the mean value of the overall property —that is, the design of the network for the overall region. The index $R(x)$ is defined by the relative reduction of the uncertainty:

$$R\left(x\right) = \frac{\sigma_0^2 - \sigma^2\left(x\right)}{\sigma_0^2} \qquad (10)$$

Where:

σ^2_0 = variance of the estimation with n existing points.

$\sigma^2(x)$ = variance of the estimation with an additional point $n + 1$ at position x.

Algorithm 1

If predefined positions exist for x_{n+1}, then $\sigma^2(x)$ is calculated for all positions and the one with the largest $R(x)$ is selected.

Algorithm 2

If position x_{n+1} has no restrictions, then it is possible to calculate $\sigma^2(x)$ on a grid and to draw the level curves for $R(x)$.

Local estimation

The variance in a certain zone of the network is to be minimized locally.

This approach requires calculating both variances as well as points, and therefore only the largest uncertainties can be eliminated.

1. A point is added in the zones with the largest uncertainty.
2. The level curves are calculated for the typical deviations for cases with and without the point, and the results are compared.

This continues until finding the point that most reduces the uncertainty.

In both approaches, the algorithm can be repeated by adding other points. Efficient strategies exist to include more than one point, such as:

- The successive inclusion method
- Optimal successive exchanges method
- Complete enumeration method
- Branch and boundary method, etc.

Optimization strategies using more than one point

For the case of irregular networks, this represents a discreet problem intended to select the best subset of points from a given set.

a) Successive inclusion method

The points that minimized the variance are successively added in each step until completing a number of preset points or arriving at a given variance level.

b) Optimal successive exchanges method

A set X_0 of points is selected such that when exchanging one of its elements for a remaining one, the variance does not decrease, which is a necessary condition but not sufficient for obtaining the optimal set.

Algorithm

1. Let $X_0 = \{t_1, t_2, ..., t_{n-k}\}$ and $\{X_1 = t_{n-k+1}, ..., t_N\}$ and j_1.
2. The j-th element in X_0 is systematically exchanged with all those from X_1 and the corresponding variances are calculated.
3. When the variance decreases, then the permanent exchange is made.
4. The value of j is modified as follows:

$$j = \begin{cases} j+1, \text{ si } j < N \\ 1, \quad \text{si } j = 1 \end{cases}$$

and the process returns to step 2. It stops when none of the elements in X_0 can be exchanged in such a way that the variance of the estimation decreases.

c) Complete enumeration method

All the subsets of set $T = \{t_1, t_2, ..., t_N\}$ with $n - k$ elements are examined. The one with the smallest variance is the optimal subset.

The total number of subsets to be evaluated would be:

$$\binom{N}{n-k} = \frac{N!}{(N-n+k)!(n-k)!} \qquad (11)$$

A systematic approach would be to use a tree search. This begins with a null or empty set. The difficulty with this approach is the need to perform a large number of operations.

d) Branch and boundary method

This is similar to the above, with the following differences:

- The tree is constructed based on the total set of points.
- One point is eliminated when advancing forward through the tree, and one is added when going backward.
- An additional condition is compared —that the variance of the estimate be less than or equal to the smallest calculated variance up to this moment with $n - k$ points. Otherwise, the process does not continue advancing, since by doing so it would increase. This has the same advantage as the previous, of reducing estimation time.

The optimization technique used in this study is successive inclusion, (Carrera, Usunoff, & Szidarovszky, 1984; Carrera & Szidarovszky, 1985; Díaz- Viera, 1997, 1998). The algorithm consists of set m with existing points designated by $X = \{x_1, x_2, ..., x_m\}$, and the optimal subset, with n points, which minimizes the variance of the estimation is designated by $X = \{x_{o1}, x_{o2}, ..., x_{on}\}$.

Algorithm

1. For $j = 0$, $X = \{x_1, x_2, ..., x_m\}$ and $X_o = \{\varnothing\}$, donde $\varnothing$ = empty.
2. The estimation-error variance for i is calculated with kriging $\sigma^2(x_i)$, from 1 to m, and the one with the largest value is selected, such that point x_i is extracted from set X and included in set X_0, resulting in:

$$X = \{x_1, x_2, ..., x_{m-j}\} \text{ and } X_o = \{x_{o1}\}$$

3. $j = j + 1$ is increased.
4. Expression (10) is evaluated for all values of i, from 1 to $(m - j)$, that is, $R(x_i) = \dfrac{\sigma_j^2 - \sigma_{j+1}^2(x_i)}{\sigma_j^2}$, which is the relative reduction index.

where:

σ_j^2 = estimation-error variance with the j points that belong to X_0.

σ_{j+1}^2 = estimation-error variance with an additional point $j + 1$ at position x_i.

5. The point x_i that most reduces the estimation-error variance —that is, that has the largest value of $R(x_i)$— is selected by extracting it from set X and adding it to set X_0, resulting in:

$$X = \{x_1, x_2, ..., x_m\} \text{ and } X_o = \{x_{o1}, x_{o2}, ..., x_{oj}\}$$

6. As long as $j < n$ o $\sigma_j^2 <$ tolerance, the procedure returns to step 3, otherwise it terminates.

The equations to calculate the inverse of the kriging matrix and the variance of the estimation with $j + 1$ and $j - 1$ points, based on the values obtained with j points, according to Samper and Carrera (1990), are solved as follows: Let G.l = g and λ_0 = the solution of this system. If a new point x_{j+1} is added the new equations can be written as:

$$\begin{pmatrix} G & \vdots & g \\ \cdots & \cdots & \cdots \\ g^t & \vdots & 0 \end{pmatrix} \begin{pmatrix} \lambda \\ \vdots \\ \lambda_{j+1} \end{pmatrix} = \begin{pmatrix} \gamma \\ \vdots \\ \gamma_{vj+1} \end{pmatrix} \tag{12}$$

Where $g^t = (\gamma_{j+1,1}, \ldots, \gamma_{j+1,j+1})$. The inverse of the new coefficients matrix is given as:

$$\begin{pmatrix} X & \vdots & y \\ \cdots & \cdots & \cdots \\ y^t & \vdots & s \end{pmatrix} \tag{13}$$

where:

$$s = \frac{1}{g^t G^{-1} g} \tag{14}$$

$$y = -G^{-1} g s$$

$$X = G^{-1} + s^{-1} y y^t$$

And the solution of the system can be expressed as:

$$\lambda_{j+1} = s\left(\gamma_{vj+1} - g^t \lambda_o\right) \tag{15}$$

$$\lambda = \lambda_0 - G^{-1} g \lambda_{j+1} \tag{16}$$

The new variance, after adding point $x_{j\,i+1}$ is:

$$\sigma_{j+1}^2 = \sigma_j^2 - \left(\gamma_{vj+1} - g^t G^{-1} g\right)^2 / \left(g^t G^{-1} g\right) \tag{17}$$

These expressions are very useful to calculate the variances of the estimations by adding a point.

The geostatistical methodology used consists of the following stages: preliminary analysis of the data, exploratory analysis, variogram analysis and spatial estimation.

In the *preliminary analysis* stage, the piezometric levels are calculated by subtracting from it the heights of the wellheads and the depths of the static level. A vector file of points is generated in shape format with the attributes of the associated wells (code, depth of static level, wellhead height and piezometric level), and is transformed from NAD27 to ITRF92, from a universal transverse Mercator projection (UTM) to a Lambert conformal conic (LCC) projection using the equations cited in Leick (1990).

The layer of the topographic curves is superimposed at a scale of 1:250 000. The local urban borders (data from the National Institute for Statistics and Geography) and the polygon of the aquifer in question are superimposed to verify the position of the wells and their attributes.

During the *exploratory analysis*, basic statistical parameters are calculated, including mean, variance, standard deviation, quartiles, maximum value, minimum value, kurtosis coefficient and asymmetry. In addition, a frequencies histogram is generated, as well as the *Q*-*Q* Plot and box plots. Atypical values are sought and separated from the other data, and the basic statistical parameters are calculated again. The idea is to perform a graphic-numerical analysis of the nature of the data, evaluate some of the suppositions (such as normality, linearity and homoscedasticity) (Armstrong & Delfiner, 1980), and evaluate the presence of atypical values, which are the values that exceed the limits established by the following expressions (Díaz-Viera & Barandela, 1994; Díaz-Viera, Hernández-Maldonado, & Méndez- Venegas, 2010):

$$\text{Upper limit} = q(0.75) + 1.5\, iq$$
$$\text{Lower limit} = q(0.25) - 1.5\, iq$$

Where $q(p)$ are the quantiles and iq is the interquartile range (difference between the third and first quartiles); the atypical values can significantly affect the later stages of the geostatistical analysis (Cressie & Hawkins, 1980; Díaz-Viera, 2002) as well as the absence of data.

During the *variographic analysis* stage, first the dimensionless semivariances are calculated, followed by the semivariances for directions 45, 90 and 270° at different distances, analyzing them to determine the possible presence of anisotropy. In case of its presence, its direction and the minimum and maximum values are calculated. In addition, the semivariogram model that best fits the data according to the Akaike information criterion (AIC)(Akaike, 1974,1977) is obtained. This relates the complexity of the model (number of parameters) and the goodness of fit (mean square error). Cross validation is applied, specifically the "leave one out" method mentioned by Journel and Huijbregts (1978), which consists of leaving a known point out of the estimation and proceeding to calculate the ordinary kriging value using the parameters from the semivariogram model obtained. The same procedure is applied to the rest of the points, obtaining the differences between the real and calculated values. The statistics related to these differences are analyzed and the expectations are that the mean value will be near zero, the variance will be small and the normalized variance near one, according to Omre (1984).

If a spatial trend $M(x,y)$ is detected, this is calculated by first and second degree polynomials. Then, the difference between the known value $Z(x,y)$ is determined, leaving a residual $R(x,y)$, that is $R(x, y) = Z(x, y) - M(x, y)$. Then the entire geostatistical procedure is applied to the residuals $R(x, y)$.

The main purpose of this stage is to calculate and model a function that reflects the spatial correlation of the piezometric levels based on a reasoned adoption of the most suitable hypothesis regarding its variability.

A grid of points in the study area is generated according to the *spatial estimation*, taking into

account the end coordinates of the polygon representing the aquifer. The resolution of this grid is 500 by 500 meters, given the spatial resolution of the known data. Then, based on the parameters of the semivariogram model obtained through the variographic analysis, the variable studied (piezometric level or its residual) and the estimation-error variance are calculated for each node in the grid. To this end, the 16 wells closest to each node are determined. Moral-Garcia (2003) recommends a little over 10 for this operation. Ordinary point kriging is used for these estimations.

Characteristics of the area and study data

The study area (Figure 1) is the "Saltillo-Ramos Arizpe" aquifer. It is located in southeastern Coahuila de Zaragoza, Mexico, and covers portions of the municipalities of Saltillo, Ramos Arizpe and Arteaga. Its location is between coordinates 101° 06′ and 100° 47′ west longitude and 25° 35′ and 25° 20′ north longitude (ITRF92 datum). Its borders are the Zapaliname mountain to the south and southeast, the Areaga mountain, San Lucas and San Jose de los Nuncios mountains to the east, and the El Asta and Palma Gorda mountains to the west. The city of Saltillo, capital of the state of Coahuila de Zaragoza, and the towns of Ramos Arizpe and Arteaga are located within the area of the aquifer.

The coordinates of the vertices that compose the polygon of this aquifer and the location of the wells were transformed to ITRF92 datum and the following parameters were used in the Lambert conformal conic (LCC):

- False easting: 2 500 000 m.
- False northing: 0 m.
- First parallel: 17.5°
- Second parallel: 29.5°.
- Parallel of origin: 12° north.
- Meridian of origin: 102° west.

The zone is located in the physiographic province of mountains and watersheds, on the border of the Sierra Madre Oriental (Conagua, 2010). There are two types of physiographic characteristics: a) a relatively smooth topographical area corresponding to the Valley of Saltillo-Ramos Arizpe, with an elevation that decreases towards the north, with values from 1 800 to 1 200 masl, and b) a western mountainous area, with an east-west orientation, characterized by an abrupt topography with a maximum elevation of 2 400 masl.

In the valley, the aquifer is composed of alluvial deposits, Reynosa conglomerates and fractured lutites from the Parras Formation. In the mountainous areas located in the west and northwest portions of the valley, the aquifer is composed of fractured arsenic rocks.

This is a semi-confined aquifer with a hydrogeological base —defined as the depth at which the fractures in the Parras Formation disappear or close up— between 250 and 450 m.

The boundaries of the impermeable aquifer are the contact between the fractured Parras Formation and the low permeable Indidura Formation, in the west and southeast of the valley.

The aquifer contains 750 wells. The registries for these were provided by the National Water Commission (Conagua), from a geohydrological study performed in 2007.

Results

Preliminary Analysis

Of 750 the wells (Figure 1), 413 have records to the depth of the static level. The heights of the 413 wellheads were reviewed with respect to the level curves from the INEGI series III topographic card, with a scale of 1:250 000. One height was detected to be inconsistent (well SRA-071), with a value of 5 261 m, located between topographic level curves 1 500 and 1 600 m. Another four (SRA-292, SRA-423, SRA-424, SRA-425) did not contain this value, resulting in 408 wells with consistent data. The

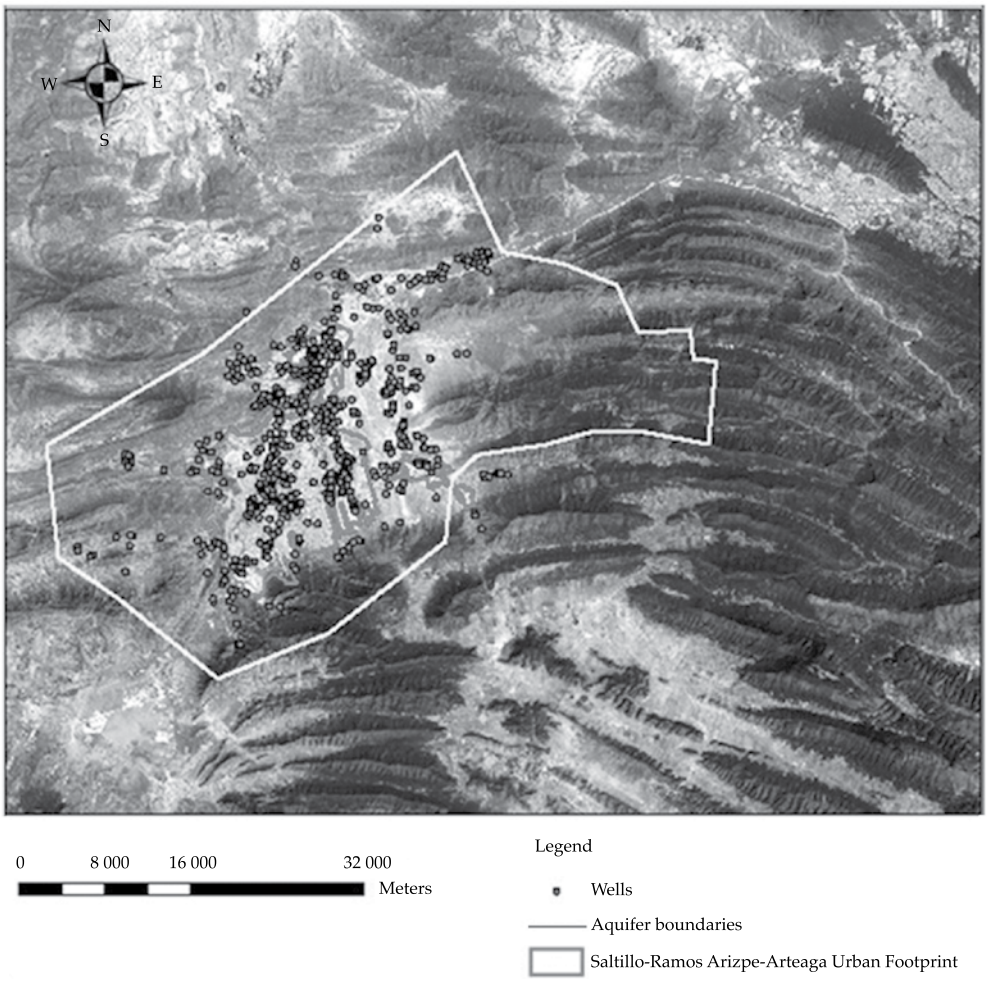

Figure 1. Location of the "Saltillo-Ramos Arizpe" aquifer and the 750 wells.

piezometric levels were calculated for the next analysis.

Exploratory analysis

The 408 piezometric levels present a spatial trend, given that the semivariances calculated are not bounded by the variance line (Figure 2). To eliminate the spatial trend, a first-degree polynomial fit of the data is performed. The following coefficients are obtained:

a = 29 674.64084 m
b = –0.002119162 m
c = –0.0151855557 m

This variable is expressed as:

$$Z(x,y) = M(x,y) + R(x,y) \tag{18}$$

Where $M(x,y) = a + b * X + c * Y$ is the trend and $R(x) = Z(x) - M(x,y)$ are the residuals of the piezometric levels.

The exploratory analysis of the residuals $R(x)$ is conducted. Twenty-six atypical values are detected and eliminated.

Table 1 shows a positive asymmetry with a value of 0.2883 m; the mean (-2.9250) is larger than the median (-5.2860), and the resulting interquartile range is 71.24 m.

The frequency histogram (Figure 2) presents a positive asymmetry. The box plot shows that the mean is larger than the median, and some atypical values are observed.

Variographic analysis

The semivariances were estimated, which are now bounded by the variance line (Figure 3), resulting in a dimensionless semivariogram with the following parameters:

- Model: Spheric
- Nugget: 130.4765 m.
- Sill-nugget: 739.8475 m.
- Range: 6 708.8846 m.
- AIC: 4527.1123.

In addition, the cross validation of the semivariogram model is graphically shown, in which a regression coefficient of 0.984 is observed. The statistics obtained from the validation are:

Mean of the differences between the real and estimated value	-0.21699 m
Variance of the differences between the real and estimated value	59 365.26
Mean of the normalized differences	-0.111604
Variance of the normalized differences	9.755

The normalized difference is the difference between the real and estimated values of the variables, inversely proportional to the standard deviation of the estimation-error variance.

Anisotropy analysis

Figure 4 shows that the values of the semivariances are similar in all directions. An isotropic behavior is observed, determining that there is no anisotropy, or not enough elements exist to determine its presence.

Spatial estimate

With the parameters of the semivariogram model obtained from the variographic analysis, the spatial estimation is performed by applying ordinary point kriging, using a 500 by 500 meter grid which covers the space of the polygon representing the aquifer in question.

Figure 5 shows the 3D map of the estimated residuals of the piezometric levels. The values represented range from -60.8 to 73.9 meters.

Figure 6 shows the standard deviations of the largest estimation-error (29.5), located at the periphery of the mapped zone. The smallest deviations (14.2) are distributed throughout the map from southwest to northeast, near the wells used to determine the semivariogram model.

After estimating the residuals $\hat{R}(x,y)$, the trend $M(x,y)$ is added using equation (18) to obtain the estimated piezometric levels $\hat{Z}(x,y)$.

Figure 7 shows the 2D map of the piezometric levels estimated, in the southwest-northeast direction, with values from 1 786.96 to 1 181.94 m.

Optimization using successive inclusion

The results from the optimization are shown next. Two variants are presented, as follows.

Optimization considering a tolerance for the standard deviation of the estimation-error.

Figure 8 shows the behavior of the standard deviation of the estimation-error with ordinary block kriging as wells are added by successive inclusion.

Beginning at 144 wells, the value of the standard deviation of the estimation-error presents a variance in centimeters, resulting in a value of 21 m, as can be observed in Table 2.

Figure 9 shows the spatial distribution of the 144 wells. They can be seen to cover most of the aquifer, except for the northeast zone where there are no wells.

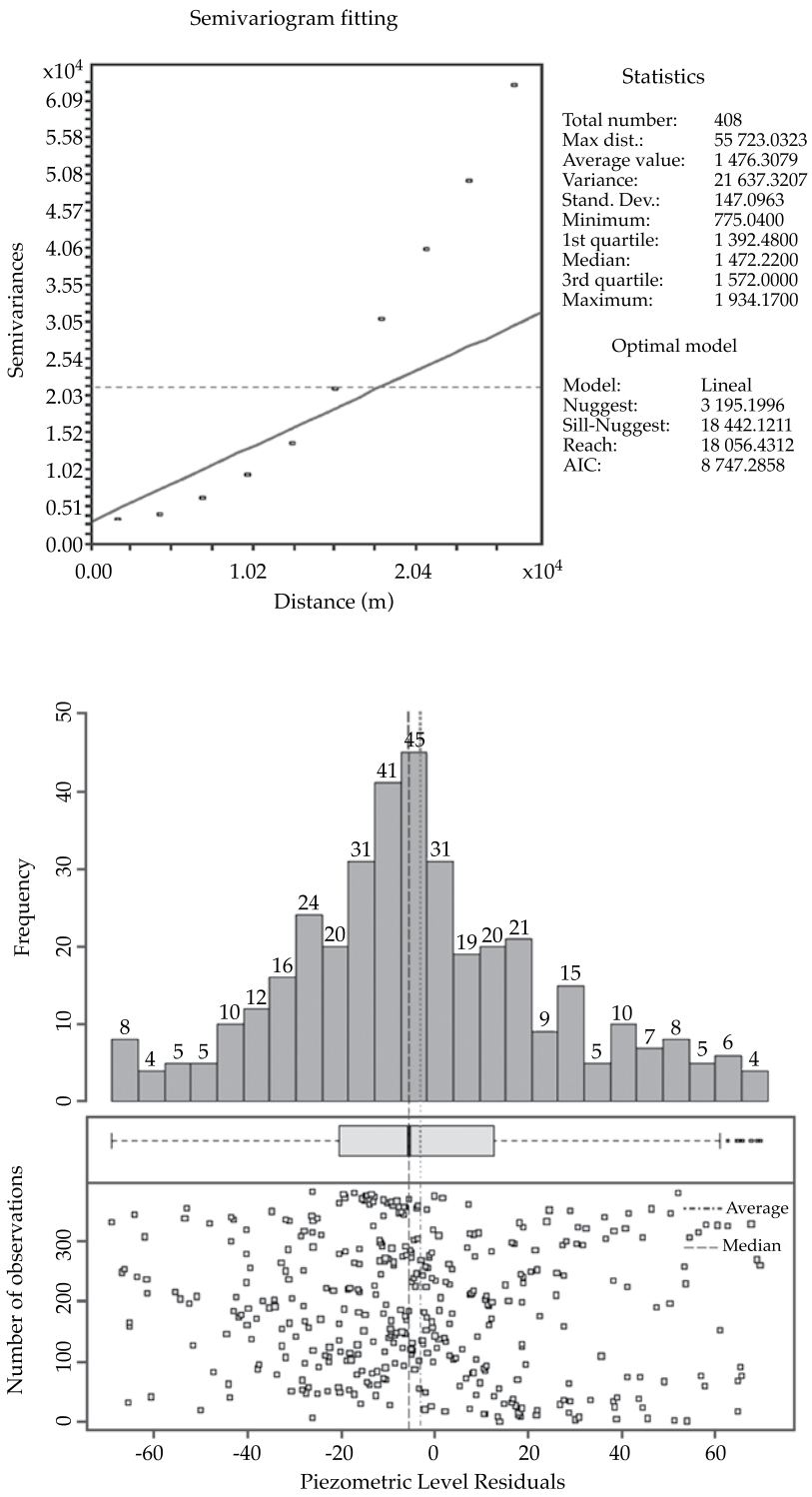

Figure 2. Presence of spatial trend, histogram of frequencies and box plot of the piezometric level residuals without the 26 outliers (382 data).

Table 1. Basic statistical parameters of the residuals without the 26 atypical values.

Parameters	Value
Total data	382
Maximum distance	50 078.43
Mean	-2.9250
Variance	826.2219
Standard deviation	28.7441
Variation coefficient	9.8285
Median	-5.2860
First quartile (Q1)	-20.32
Third quartile (Q3)	13.24
Interquartile range	71.24
Asymetry	0.2883
Kurtosis	3.0251
Maximum value	71.2412
Minimum value	-68.9487

Table 2. Variation in the standard deviation of the estimation with respect to the number of wells.

No. of wellss	Standard deviation of the estimation-error (m)
1	862.96
50	24.73
60	23.54
70	22.78
80	22.22
90	21.84
100	21.58
110	21.38
120	21.22
130	21.11
140	21.03
144	**21.00**
150	20.96
160	20.9
200	20.76
300	20.65
400	20.63
450	20.62

Optimization by presetting the number of wells

Table 3 compares the basic statistical parameters pertaining to the standard deviation of the ordinary point kriging estimation-error for the best wells for monitoring, obtained through optimization by presetting the number of wells.

The mean and median are observed to decrease as the number of wells increases. The opposite occurs with the variance and, therefore, with the standard deviation.

Figure 10 shows the location of the best 50 wells. They are distributed throughout the aquifer, except in the eastern portion where no wells exist.

Discussion

This study was performed based on the piezometric levels of the wells in the area of the aquifer in question. The data presented spatial trends, which were estimated using a first-degree polynomial fit and subtracted from the original data to obtain residuals.

The subsequent geostatistical analysis and the optimization were performed using the residuals obtained so as not to be affected by the lack of stationarity.

The semivariogram model obtained is spherical. Anisotropy is not detected, that is, it resulted in being isotropic.

In the spatial estimation of the piezometric levels, the calculated spatial trend was added to the calculated residuals. The ordinary point kriging estimation was performed in a large portion of the aquifer, leaving only some areas not covered because of a lack of neighboring wells. Drawdown cones are seen in the aquifer.

In the optimization, considering a tolerance for the standard deviation of the estimation-error, a convergence of the error is observed near the 50 wells added using successive inclusions. Nevertheless, a variation of centimeters in the levels was observed as of 144 wells, which was the criterion chosen to stop the inclusion of more wells.

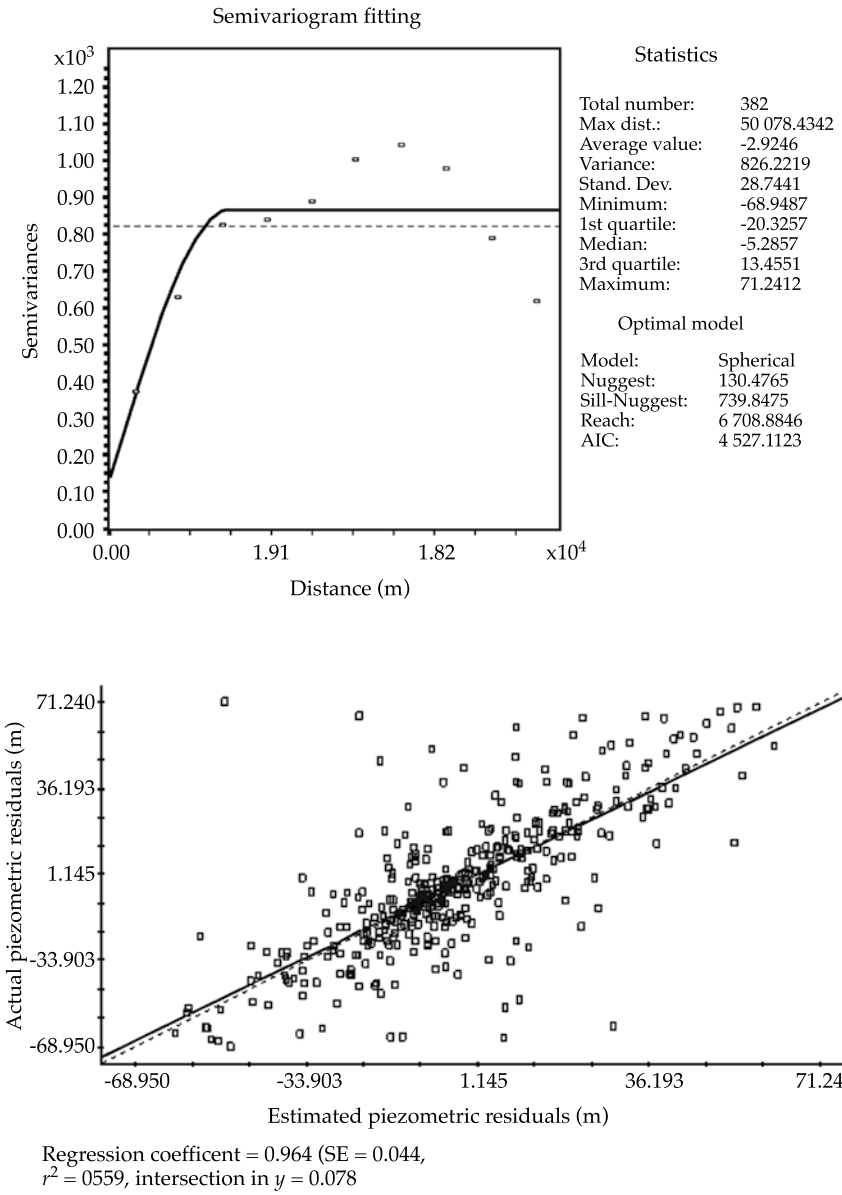

Figura 3. Ajuste y validación cruzada del modelo de semivariograma.

It is important to mention that the values of the relative reduction index are highest for the wells obtained through optimization by presetting the number of wells. That is, they are the best 50, 100, 200, 300, 400 and 500 wells for the monitoring of the aquifer.

Conclusions

The present work met the stated objectives, applying the method to obtain the optimal design of a monitoring network for the management of the Saltillo-Ramos Arizpe aquifer. This was achieved through a geostatistical analysis of piezometric level data, using ordinary kriging for the estimation and the successive inclusion technique for the optimization.

The optimal design of the network took into account the boundaries of the aquifer as defined by Conagua, without considering other geohydrological parameters in the study area.

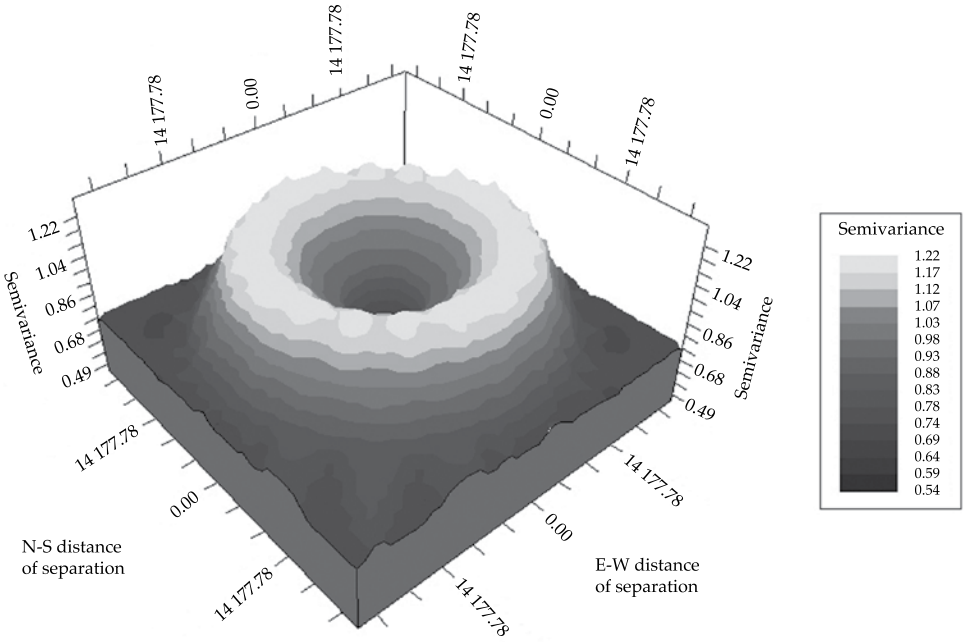

Figure 4. Semivariances for directions 0, 45, 90 and 135, and at different distances.

Calculation of the piezometric level residuals. Ordinary point kriging

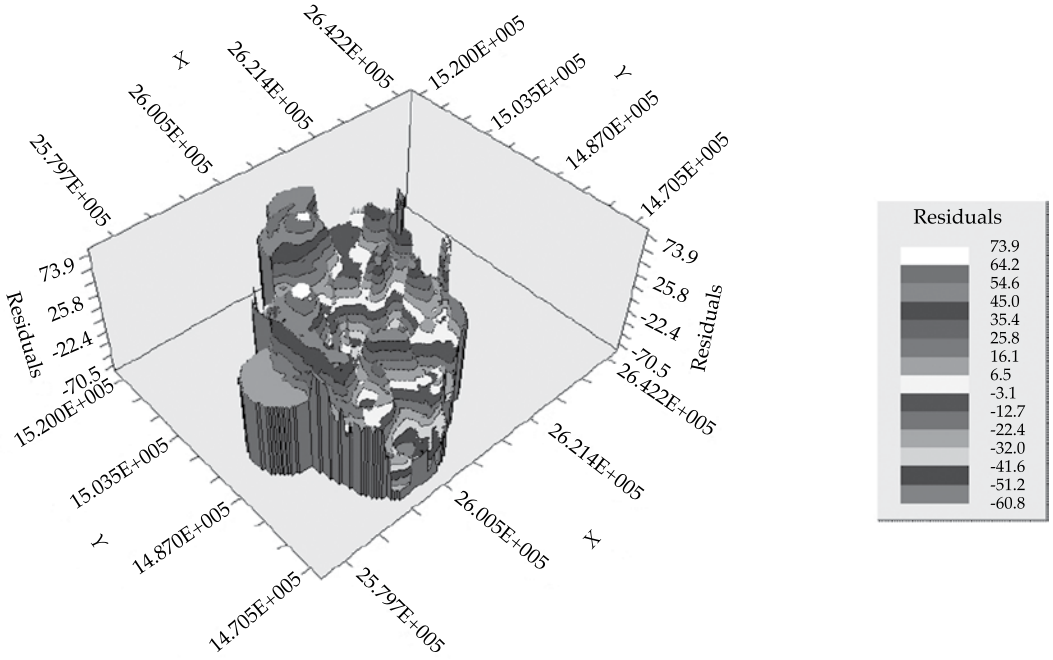

Figure 5. 3D map of the estimated piezometric level residuals.

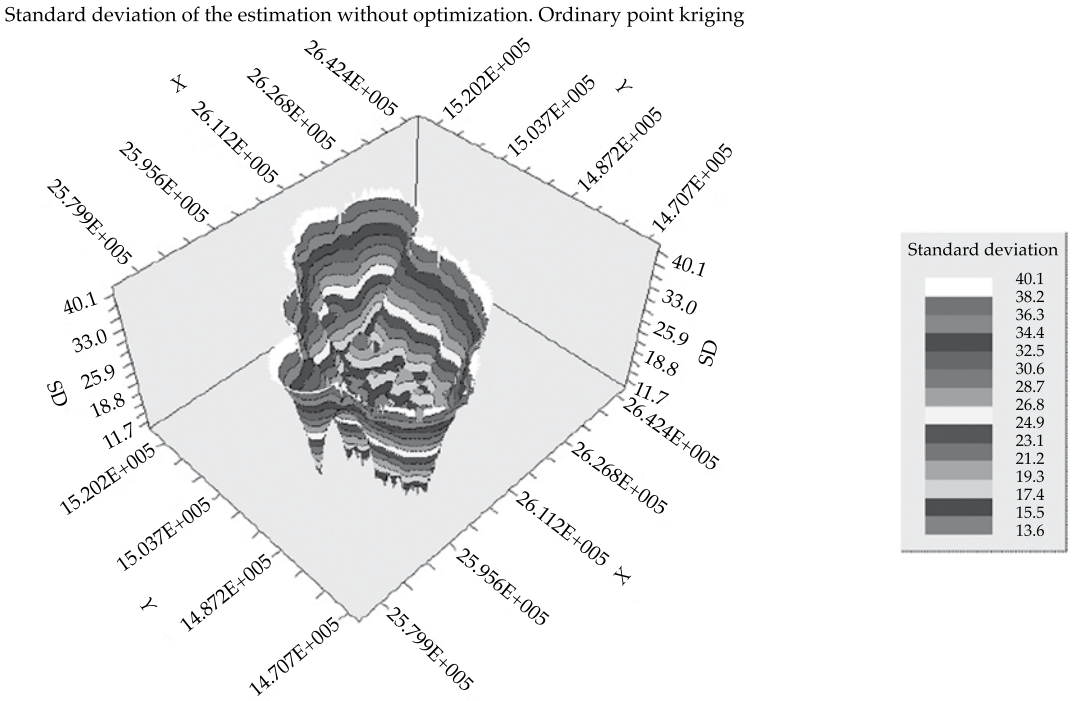

Figure 6. 3D view of the standard deviations of the estimation-error of the residuals.

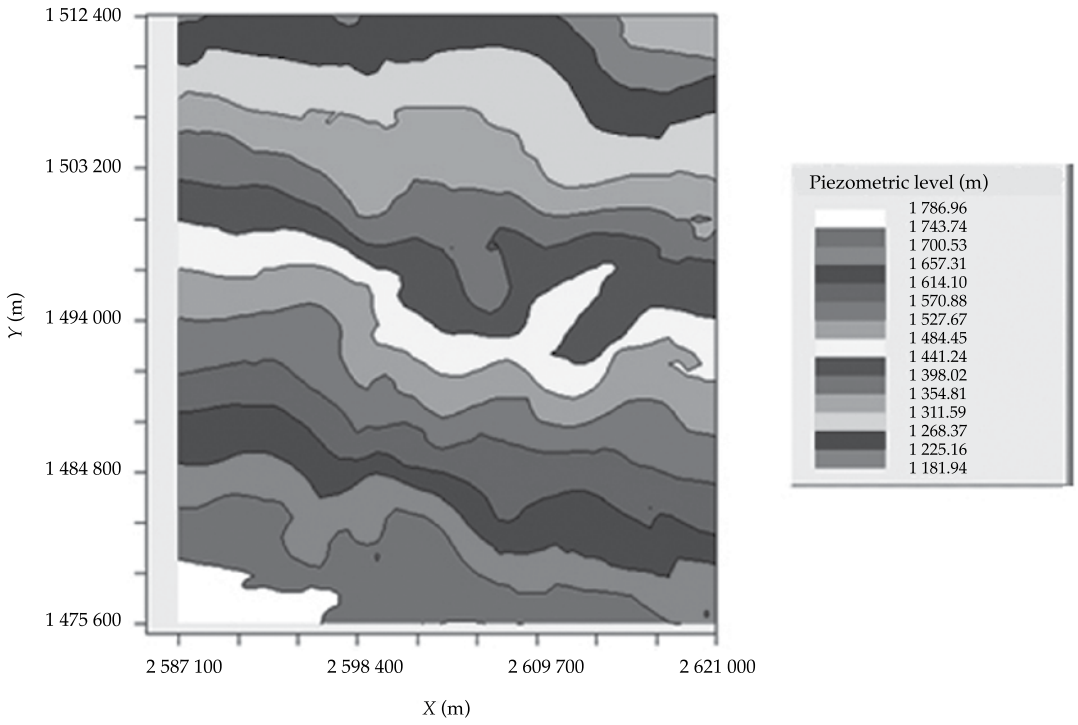

Figure 7. 2D map of the estimated piezometric levels using ordinary point kriging.

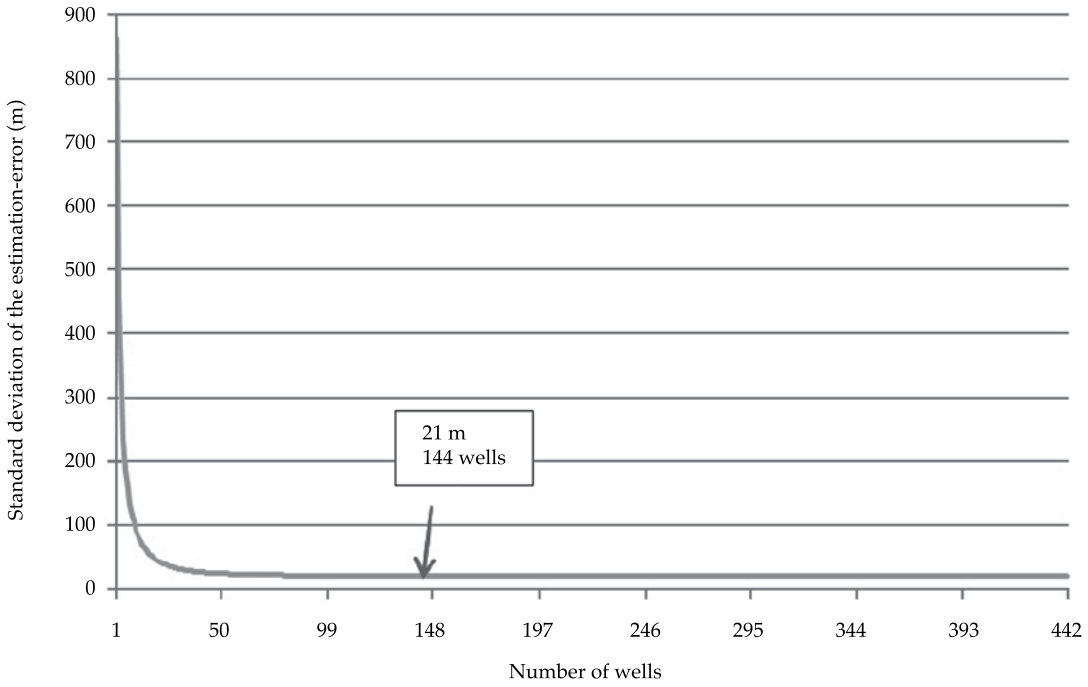

Figure 8. Behavior of the standard deviation of the estimation-error wtih ordinary block kriging.

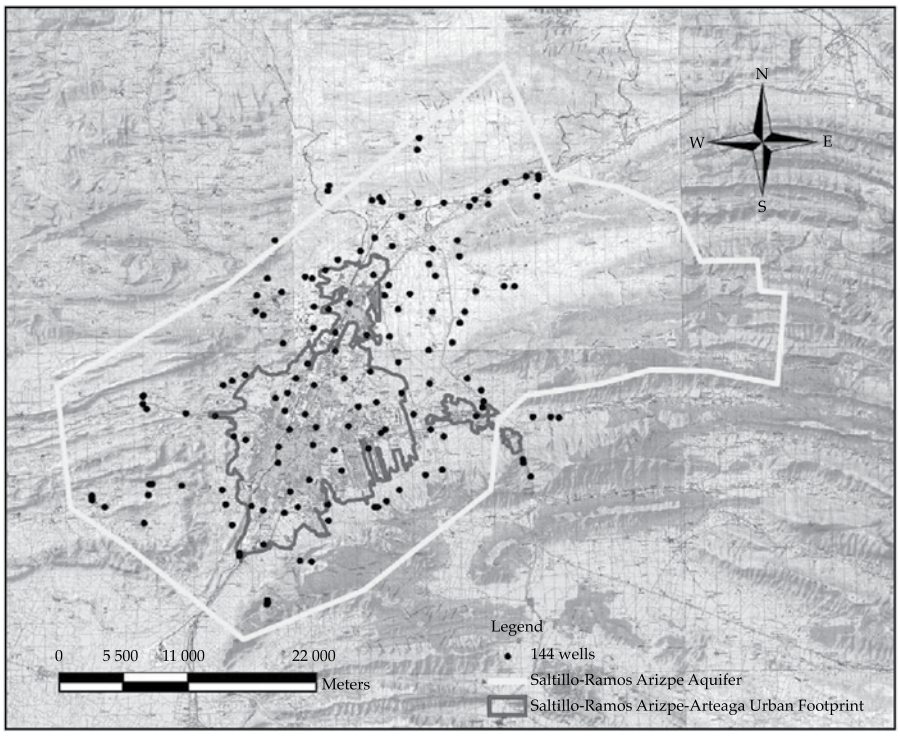

Figure 9. Spatial distribution of the 144 wells that make up the optimal network determined.

Table 3. Comparison of the basic statistical parameters of the standard deviation of the estimation-error for the best wells..

Statistical parameter	Entire network	Optimal Network (21 m)	Wells that offer the estimation with the highest certainty					
Number of wells	750	3 144	50	100	200	300	400	500
Mean	26.9734	27.6769	29.8205	28.1804	27.3404	27.1512	27.0601	26.9889
Variance	87.9695	73.9683	54.0006	68.5659	78.8585	82.3256	84.8264	86.5767
Standard deviation	9.3792	8.6004	7.3485	8.2805	8.8802	9.0733	9.2101	9.3047
Variation coefficient	0.3477	0.3107	0.2464	0.2938	0.3248	0.3342	0.3404	0.3448
Minimum value	11.6435	11.7095	11.7134	11.7095	11.7089	11.7089	11.6436	11.6436
First quartile (0.25)	18.4486	20.0717	24.4888	21.1941	19.2468	18.8975	18.6577	18.4234
Median	26.1632	29.1670	27.8962	26.4394	26.0529	26.0700	26.0860	26.1025
Third quartile (0.75)	35.1362	35.0940	35.6206	35.2252	35.0515	35.0223	35.0644	35.0713
Maximum value	43.2565	43.2565	43.2565	43.2565	43.2565	43.2565	43.2565	43.2565
Asymetry	0.1899	0.3257	0.3394	0.3487	0.2971	0.2594	0.2314	0.2144
Kurtosis	1.7406	1.8237	2.1486	1.8832	1.7776	1.7635	1.7464	1.7401

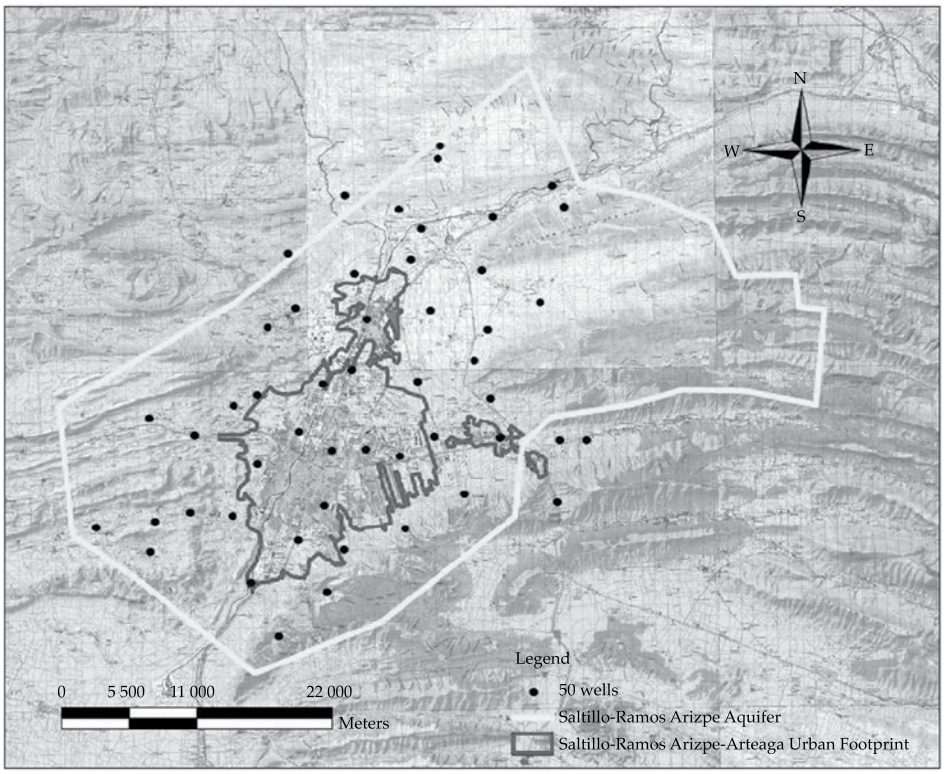

Figure 10. Location of the 50 wells that offer the estimation with the highest certainty.

It is worth mentioning that the methodology used is applicable to any area and type of regionalized study variable.

A total of 382 piezometric level data were used to generate a semivariogram model of 750 existing wells, representing 50.9% of the total.

It is therefore concluded that this is a sufficient amount to model the spatial correlation of said variable.

The optimal network was determined to contain 144 wells, with a standard deviation of the estimation-error of 21 meters with ordinary block kriging, representing 19.2% of the 750 wells existing in the aquifer and a savings of 80.8% in the cost of monitoring the wells.

Optimization with a fixed number of wells enables determining the best wells for monitoring. The number of wells are selected depending on the resources available.

For future works of this type in this aquifer, it is recommended to subdivide the aquifer based on its hydrogeological nature and incorporate existing groundwater flow models.

Acknowledgements

The Geophysical Institute of the National Autonomous University of Mexico, the National Institute for Statistics and Geography, Northeast Regional Division, and the National Water Commission, Saltillo District, Coahuila de Zaragoza, for the support provided to perform this study.

References

Akaike, H. (1974). A New Look at Statistical Model Identification. *IEEE Transactions on Automatic Control*, *AC-19*, 716-722.

Akaike, H. (1977). An Entropy Maximization Principle. In P. R. Krishnaiah (Ed.). *Aplications of Statistic.* Amsterdam: North Holland.

Armstrong, M., & Delfiner, P. (1980). Towards a More Robust Variogram: Case Study on Coal. Note n_671. Fontainebleau, France: CGMM.

Banjevic, M., & Switzer, P. (2002). *Optimal Network Designs in Spatial Statistics*. Stanford: Stanford University.

Carrera, J., Usunoff, E., & Szidarovszky, F. (1984). A Method for Optimal Network Design for Groundwater Management. *Journal of Hydrology*, *73*, 147-163.

Carrera, J., & Szidarovszky, F. (1985). Numerical Comparison of Network Design Algorithms for Regionalized Variables. *Appl. Math. Comput.*, *16*, 189-202.

Chiles, J. P., & Delfiner, P. (1999). *Geostatistics Modeling Spatial Uncertainty* (157-158 pp.). New York: John Wiley & Sons.

Cressie, N., & Hawkins, D. M. (1980). Robust Estimation of the Variogram. *Math. Geol.*, *12*, 115-126.

Conagua (junio de 2010). *Sección Aguas Nacionales. Sistema Nacional de Información del Agua (Sina)*. Comisión Nacional del Agua. Recuperado de http://www.cna.gob.mx/.

Cousens, R. D., Brown, R. W., Mcbratney, A. B., & Moerkerk, M. (2002). Sampling Strategy is Important for Producing Weed Population Maps: A Case Study Using Kriging. *Weed Science*, *50*, 542–546.

Díaz-Viera, M. (2002). *Notas del Curso: Geoestadística Aplicada* (135 pp.). México, DF: Instituto de Geofísica, UNAM, Instituto de Geofísica y Astronomía, Ministerio de Ciencia, Tecnología y Medio Ambiente de Cuba.

Díaz-Viera, M., Hernández-Maldonado, V., & Méndez-Venegas, J. (2010). *RGEOESTAD: un programa de código abierto para aplicaciones geoestadísticas basado en R-Project*, México. Recuperado de http://mmc2.geofisica.unam.mx/gmee/paquetes.html.

Díaz-Viera, M., & Barandela, R. (agosto de 1994). *GEOESTAD: un sistema de computación para el desarrollo de aplicaciones geoestadísticas*. Memorias del II Taller Internacional Informática y Geociencias, GEOINFO'94, Ciudad de la Habana, Cuba.

Díaz-Viera, M. (11-15 noviembre de 1997). *DISRED: una herramienta para el diseño de redes de monitoreo usando un enfoque geoestadístico*. Primer Congreso Nacional de Aguas Subterráneas, Mérida, México.

Díaz-Viera, M. (24-27 de marzo de 1998). El diseño de redes óptimas de monitoreo en aguas subterráneas usando un enfoque geoestadístico. *Memorias del IV Taller Internacional Informática y Geociencias* (pp. 66-69). GEOINFO'98, Ciudad de la Habana, Cuba.

Dixon, W., Smyth, G. K., & Chiswell, B. (March, 1999). Optimized Selection of River Sampling Dites. *Water Research*, *33*(4), 971-978.

Journel, A. G., & Huijbregts, Ch. J. (1978). *Mining Geostatistics* (590 pp.). London: Academic Press.

INEGI (junio de 2010). *Apartado Geografía*. Instituto Nacional de Estadística y Geografía. Recuperado de http://www.inegi.org.mx/.

Isaaks, E. H., & Srivastava, R. M. (1989). *An Introduction to Applied Geoestatistics* (278-279 pp.). New York/ Oxford: Oxford University Press.

Leick, A. (1990). *GPS Satellite Surveying* (pp. 284-301). Orono, USA: University of Maine.

Lloyd, C. D., & Atkinson, P. M. *Designing optimal sampling configurations with ordinary and indicator kriging*. In Proceedings of the 4th International Conference on GeoComputation. 1999.

Moral-García, F. A. (2003). *La representación gráfica de las variables regionalizadas. geoestadística lineal* (pp. 71-74). Cáceres, España: Universidad de Extremadura.

Olea, R. A. (1999). *Geostatistics for Engineers and Earth Scientists* (pp. 7-16) Lawrence, USA: Kansas Geological Survey, The University of Kansas.

Omre, H. (1984). *The Variogram and its Estimation. Geostatistics for Natural Resources Characterization* (107-125 pp.). Vol. 1. Verly *et al*. (Eds.). Hingham: NATO ASI Series. Reidel.

Prakash, M. R., & Singh, V. S. (April, 2000). Network Design for Groundwater Monitoring – A Case Study. *Environmental Geology*, *39*(6), 628-632.

Samper, C. F. J., & Carrera, R. J. (1990). *Geoestadística. Aplicaciones a la Hidrogeología Subterránea* (pp. 409-427). Barcelona: Centro Internacional de Métodos Numéricos en Ingeniería.

Wang, X. J., & Qi, F. (December 11, 1998). The Effects of Sampling Design on Spatial Structure Analysis of Contaminated Soil. *The Science of the Total Environment*, *224*(1-3), 29-41.

Institutional Address of the Authors

Dr. Martín A. Díaz-Viera

Investigador
Instituto Mexicano del Petróleo
Programa de Recuperación de Hidrocarburos
Eje Central Norte Lázaro Cárdenas 152
Col. San Bartolo Atepehuacan
Delegación Gustavo A. Madero
Apdo. Postal 14-805
07730 México, D.F., México
Teléfonos: +52 (55) 9175 6473 y 9175 6993
Fax: +52 (55) 9175 6993
mdiazv@imp.mx
mdiazv64@yahoo.com.mx

M. en C. Félix Canul-Pech

Instituto Nacional de Estadística y Geografía
Dirección Regional Noreste
Pino Suárez No. 602 Sur, Col. Centro
64000 Monterrey, Nuevo León, México
Teléfonos: +52 (81) 8152 8250 y 8152 8249
felix.canul@inegi.org.mx
fcanul2003@yahoo.com.mx

Click here to write the autor

Upper Pixquiac River Watershed, Veracruz, Mexico.

Photo: Marta Magadalena Chávez Cortés.

Charging Scheme for Hydrological Services Provided by the Upper Pixquiac River Watershed

• Marta Magdalena Chávez-Cortés* • Karla Erika Mancilla-Hernández •
Universidad Autónoma Metropolitana, Xochimilco, México
*Corresponding Author

Abstract

Chávez-Cortés, M. M., & Mancilla-Hernández, K. E. (September-October, 2014). Charging Scheme for Hydrological Services Provided by the Upper Pixquiac River Watershed. *Water Technology and Sciences* (in Spanish), 5(5), 155-170.

From a hydrological point of view, forests provide multiple benefits to society; among them, water collection and purification. Yet they are still subjected to alarming rates of deforestation, which is why the payment of environmental services is seen as a promising conservation strategy. The goal of this work was to determine a water tariff that can be applied to water users in the Pixquiac River watershed, using the opportunity cost method. Our results show cattle to be the main economic activity competing for land use. The study determined that the amount consumers should pay for water services provided by the forest is $0.473/m^3 during the first year and $0.232/m^3 from year two to year ten. It concludes that that the market price for the activity competing with forest conservation is a determinant of the feasibility of applying a water tariff. The applicability of the tariff will also depend on the consumers' willingness to pay and their income level. Hence the need to complement this research with a contingent valuation study to determine the amount consumers would be willing to pay to have water in enough quantity and quality to satisfy their current needs.

Keywords: Economic-ecological evaluation, payment for environmental services, water collection, hydrological monetary rate.

Resumen

Chávez-Cortés, M. M., & Mancilla-Hernández, K. E. (septiembre-octubre, 2014). Esquema de cobro del servicio hidrológico que provee la cuenca alta del Pixquiac. Tecnología y Ciencias del Agua, *5(5), 151-170.*

Desde el punto de vista hidrológico, los bosques otorgan múltiples beneficios a la sociedad, entre ellos la captación y limpieza del agua. Sin embargo, siguen siendo sujetos a dimensiones alarmantes de deforestación, por lo que el pago por servicios ambientales puede verse como una estrategia prometedora para su conservación. En tal contexto, este trabajo se orientó a construir una propuesta de tarifa hídrica que pudiera ser aplicada a los usuarios del agua en la cuenca del río Pixquiac, para lo cual se utilizó el método de costo de oportunidad para asignarle valor al bosque. Los resultados indican que la principal actividad económica que compite con el uso de suelo forestal es la ganadería, y que el monto de la compensación que deben pagar los usuarios por los servicios hídricos que presta el bosque asciende a $0.473/m^3 durante el primer año y $0.232/m^3 del año dos al diez. Se concluye que el precio del mercado de la actividad que compite con la conservación del bosque es un factor determinante en la factibilidad de la aplicación de una tarifa hídrica. También que la aplicabilidad de la tarifa dependerá de la voluntad de pago de los usuarios del agua y de su nivel de ingresos. De aquí la necesidad de complementar esta investigación con un estudio de valoración contingente en donde se determine el monto que los usuarios estarían dispuestos a pagar por seguir contando con agua suficiente en calidad y cantidad para satisfacer sus necesidades reales.

Palabras clave: *pago por servicios ambientales, captación de agua, tarifa hídrica.*

Received: 29/10/13
Accepted: 19/03/14

Introduction

Water is one of the strategic resources of this century, locally as well as globally. Its profuseness on the planet (38 million km^3) contrasts with its unequal distribution, and its being an essential element for life currently makes it the center of many conflicts. Water availability —along with soil degradation and losses in biodiversity— are considered to be the principal factors threatening natural resources and the preservation and good functioning of the systems that support life (Chávez, 2007).

In Mexico, water availability has been reported to be one of the most serious problems the country will face over the next two decades, with roughly 11% of the population affected by water scarcity. In addition, the development of

our country has been inverse to the availability of water, with 76% of the population living where only 20% of the available fresh water is located. As a result, overexploitation of aquifers, expensive transfers from one watershed to another to satisfy growing demands and conflicts among competing users have increased over the past 20 years (Chávez, 2007).

Among the factors contributing to the water problem are: a) lack of understanding of the relationship between water and the ecosystem; 2) lack of knowledge about the benefits provided by ecosystems; 3) limited understanding of how ecosystems sustain a wide range of production and consumptions processes; and 4) low valuation of ecosystems in terms of decision-making because of the lack of markets for the goods and services they provide (Emerton & Bos, 2004; Ramírez-Chasco, Cabrejas-Palacios, Seco-Meneses, & Torres-Escribano, 2004; MEA, 2007).

These four factors apply to the case of forest ecosystems, which continue to be subjected to alarming rates of deforestation in spite of the hydrological benefits they provide to society: water catchment and storage; minimization of flooding and drought cycles, and control of erosion and sediment in water bodies; water quality; and local and regional regulation of the climate (Emerton & Boss, 2004; Manson, 2004). It is important to mention that the principal report that evaluates the world's forest resources indicates that the loss in forest area in Mexico from 2000-2010 increased to 195 000 hectares, and the main factor affecting the deforestation of forests and jungles is land use changes from forest to urban and farming activities (FAO, 2011). In the case of Veracruz, data indicate that this state lost the largest percentage (19%) of natural vegetation from 1993-2000 (Semarnat, 2006b). In addition, at the Third Mexican Ecology Congress held in April 2011 in Veracruz, the state was reported to have lost over 80% of its original vegetation cover, and the red light corresponded to the deforestation occurring in the upper watersheds, particularly in Cofre de Perote and Pico de Orizaba. As a result of this loss of natural capital, added to drought conditions, the city of Xalapa —which receives a good part (40%) of its water from the Pixquiac River watershed— has faced serious water supply problems, leading authorities to resort to rationing (Contreras & Solano, 2010).

In contrast, many specialists consider environmental services and ecosystems to be among the most important reasons for conserving forests and managing them more carefully. In fact, the degree to which environmental forest services are maintained is one of the main criteria used to distinguish between sustainable and unsustainable management schemes (Higman, Bass, Judd, Mayers, & Nussbaum, 1999). This recognition has led to developing strategies that are complementary to soil regulation and post-disaster restoration, in order to more successfully respond to the challenge of conserving forests (Landell-Mills & Porras, 2002). The economic valuation and generation of markets for the environmental services offered by ecosystems represent examples of this new approach (Silva-Flores, Pérez-Verdín, & Navar-Cháidez, 2010).

The concept of environmental services, or ecosystems markets, is based on the principle that the providers of these services should be economically compensated by the society that uses them, as a way to conserve the ecosystems in which these services are generated. Generally, the owners of ecosystems are not compensated for the environmental services provided by their land, and so the benefits from these services are not considered when deciding how to use the land. This reduces the likelihood of adopting economic practices that favor ecosystems. Sustainable use is more likely if owners are compensated for the environmental services provided by their lands. (Landell-Mills & Porras, 2002). In theory, this promotes a more effective and sustainable use of natural resources, contributing to reversing the tendency to treat the environment as "free goods" (Cordero, 2003).

According to the literature, this alternative is considered to be promising for forests, since the market for the environmental services they provide is growing rapidly thanks to national and regional policies and the influence of international treaties and agreements, such as the Framework Convention on Climate Change and the Kyoto Protocol, the Convention on Biodiversity and the North American Free Trade Agreement in the case of Mexico (FAO, 2004). In fact, some authors, such as Rosa *et al.* (2004) (cited in Silva-Flores, 2010) believe that favorable conditions exist in the country for the development of these initiatives. They see good opportunities for carbon capture, genetic diversity, natural attractions and environmental water services. In addition, the Report on the Proposal for Payment for Environmental Services (PES) in Mexico describes three conditions which favor a national conservation strategy: 1) Mexico's comparable advantages in terms of international markets for biodiversity, forest cover (current and desired) and ecotourism; 2) climate vulnerability and access to water and other resources are significantly at risk nationally, as reported by civil and academic organizations and recognized by the government; and 3) Mexican socioeconomic policies are favorable to the use of market solutions as a complement for addressing the environmental problem. In addition, the creation of policies for markets for ecosystem services is supported by a set of legal instruments, including the General Law for Ecological Balance and Environmental Protection, the Wildlife Law, the Biosafety Law, the Forestry Law, the Agrarian Law the Soil Conservation Law and the Water Law.

In Mexico, the environmental services market was formally adopted in 2003 as a national strategy, when the Payment Program for Environmental Hydrological Services (PEHS) was initiated in order to address areas with strategic hydrological importance (Corbera & González, 2007). This program was created to provide usufructuaries or legitimate owners of forest resources with economic incentives to reduce deforestation in areas with severe water supply problems caused by land use changes (Semarnat, 2006a). Nevertheless, before these programs, Mexico had already created some initiatives involving payment for environmental services. These included one of the first carbon capture projects in the world and a strategy at the watershed level in the municipality of Coatepec, Veracruz, which was one of the first in Latin America to establish a trust through which water consumers compensated forest managers for the maintenance of the forest cover in the upper part of the local watershed (Corbera, González, & Brown, 2009).

In general, the effectiveness of this type of strategy to conserve forests and promote sustainability is believed to be positive, though modest. The National Evaluation Council on Social Development Policies (Coneval, Spanish acronym), for example, in its 2008-2009 specific performance evaluation reported a direct relationship between the reduction of deforestation and the provision of supports. It also indicated that land owners affirmed that without the payment program for environmental services they would dedicate their land to other uses. In addition, some authors recognize that this strategy has been successful in various cases, including the community of Puerto Bello Metzabok in Chiapas, the Oaxaca Communitarian System for Biodiversity, the Sinaloa Water Factory Project (Faces, Spanish acronym), the Monarch Biosphere Reserve, the Scolel Tea Project in Chiapas and the Local Mechanism for Environmental Service Compensation in Quintana Roo, among others. These projects are engaged in a variety of activities to conserve ecosystems and generate monetary benefits for communities (Chávez & Mancilla, 2013).

Furthermore, there is agreement that projects such as these have generated other types of benefits, such as strengthening the social capital of groups (training, organization) to improve forest management; autonomy in the management of territories; recognizing

usage and property rights; contributing to implementation rules that improve the monitoring of illegal felling; and creating long-term financing strategies to conserve globally important biodiversity, such as Concurrent Funds and the Biodiversity Heritage Fund (Corbera *et al*., 2009). Nevertheless, authors such as Muñoz-Piña, Guevara, Torres and Braña (2008), and García-Amado, Ruiz, Reyes, Barrasa and Contreras (2011) believe that while this mechanism is encouraging, its operation still needs to be refined in order to fully meet the objectives. Therefore, it is important to continue to work in this direction, generating information based on case studies in order to better understand the issue of providing water in connection with the quantitative valuation of environmental services, especially in the national context (Silva-Flores *et al*., 2010).

Any estimation of the economic value of environmental services involves the selection of a method. The primary methods among which to choose are grouped into different categories: valuation at market prices, including opportunity cost; estimation of consumption benefits and subsistence production; market substitution methods, including the travel cost model, hedonic modeling and substitute goods models; methods related to production functions, including biophysical relationships between environmental functions and market activities; expressed preference methods, primarily contingent valuation and its variants; and methods based on costs, including replacement costs and defensive expenses (Dixon, Scura, Carpenter, & Sherman, 1994; Van den Bergh, 1996). The present work uses the *opportunity cost* method to calculate the economic-ecological value of forests as water catchment areas, given its validity and theoretical acceptance, information requirements and its ease in use (Munasinghe & Lutz, 1993; Van den Bergh, 1996). According to this method, cost implies something more than just making a payment or sacrifice to obtain a good or service through purchase, exchange or production. With this approach, if a consumer pays an amount of money to receive a good, implicitly they would not use that money to purchase other goods that could provide more or less satisfaction. If a company uses its resources to produce something, it obviously looses the opportunity to spend those same resources to create other products. This leads to a central concept in modern economic science —*opportunity cost*, which is understood as the benefit that is sacrificed by not taking an alternative course of action (Munasinghe & Lutz, 1993).

In the case of intangible goods or services, such as pure air or water catchment and storage, the opportunity cost is based on the idea that the cost of using a resource for purposes that have no market price, or are not sold, can be estimated using a proxy of the income lost by not using the resources for other purposes. For example, consider the case of preserving a wooded area instead of using it for livestock farming. The income not earned from livestock farming represents the opportunity cost of the forest. Thus, instead of directly determining the value of the benefits from the forest, the income not earned as a result of preserving the area is estimated, and based on this a value can be assigned to the alternative use. The opportunity cost is then considered the cost of preservation (Barrantes & Castro, 2002).

The work by Cordero-Camacho (2001) is an example of research in Latin America that uses this approach to value water services provided by forests. They developed a charging and payment scheme for environmental water services in the province of Heredia, Costa Rica. Other examples include: Hernández, Cobos and Ortiz (2002), who developed an environmental valuation for water regulations in the Sierra Biosphere Reserve in Guatemala; Barzev (2004), who developed an economic valuation of water supply and demand for the source of the Chiquito River, in Honduras; and Bastidas (2009), who generated an economic valuation for water regulations for a forest in a watershed of the Gaucha River, in Colombia. In the case of Mexico, although very little

has been published on the topic, Semarnat in Queretaro conducted a prospective study in the municipalities of Landa de Matamoros and Amealco in 2002 (Fregoso, 2006); Coila (2005) performed an economic valuation of the environmental water services in the forests in the sub-watershed of the Santa Catarina River; and Silva-Flores *et al*. (2010) developed one for El Salto, Pueblo Nuevo, Durango.

Given this context, the objective of the work herein is to construct a water fee that can be applied to water users in order to recover the equivalent amount that would be earned by the main economic activity competing with the conservation of the forest, and use this as compensation to discontinue that activity. This contributes to advances in the possible use of a financing instrument for comprehensive water management in the Pixquiac River, as proposed in the "soft approach" to water management by Brandes, Ferguson, M'gonigle and Sandborn (2005).

Study Area

The Pixquiac River watershed is in the state of Veracruz, Mexico. It is located in the western portion of the city of Xalapa and northwestern Coatepec, between the coordinates UTM 2148010.5 and 2164990.5 north latitude and 694007.18 and 72049.18 west longitude. The altitude ranges from 1 040 to 3 800 masl (see Figure 1). In terms of hydrology, this watershed belongs to hydrological region number 28 of the Papaloapan River and is part of the Lerma La Antigua River watershed (Manson, 2007). The area of the Pixquiac River watershed is approximately 10 303.53 hectares and it is 30.72 km long. It covers part of the municipalities of Acajete (11.64%), Coatepec (1.25%), Las Vigas de Ramírez (48.75%), Tlanehuayocan (6.52%), Perote (28.02%) and Xico (3.79%).

The area of interest for the present study is located in the upper watershed, with an area of 7 371.99 hectares. The upper watershed is in the mountainous areas, or in the upper portions of the mountains. The upper boundary is the water divide. It is also called a headwater zone, where the hydrological flows originate, and its main function is water catchment (Paldeyra, 2003, cited in García, Martínez, & Vidriales, 2008). The study herein is limited to this area.

Because of its location, this watershed represents one of the most important water supplies for the Xalapa region and its surrounding area. In addition, with adequate management and care this hydrological system has the potential of being inexhaustible. This is why conservation in the upper watershed is particularly important and warrants studies such as the one herein. It is also worth mentioning that the site contains a large variety of flora and fauna, constituting one of the most important ecological environments in the region, which strengthens interest in this area (García-Calva, 2010).

Methodology

In terms of the design and implementation of systems for payment for water services, this case study focused on the first two aspects proposed by Pagiola (2002): the identification and quantification of water services generated by the forest in the upper Pixquiac River basin and the calculation of fees that users should be charged after including the environmental dimension.

In terms of methodology, the first aspect was addressed using the model by Barrantes and Castro (2002) as a reference to determine the value of the water resources provided by the forests. This is based on the opportunity cost of the use of the land. This model takes two factors into account in the valuation (*VB*) —the value or cost of the water captured by the forests (*VC*) and the value or cost of the recovery of soil used for livestock farming, or exposed soil (*VR*). That is:

$$VB = VC + VR \qquad (1)$$

The cost of catchment, *VC*, in $\$/m^3$, is calculated as follows:

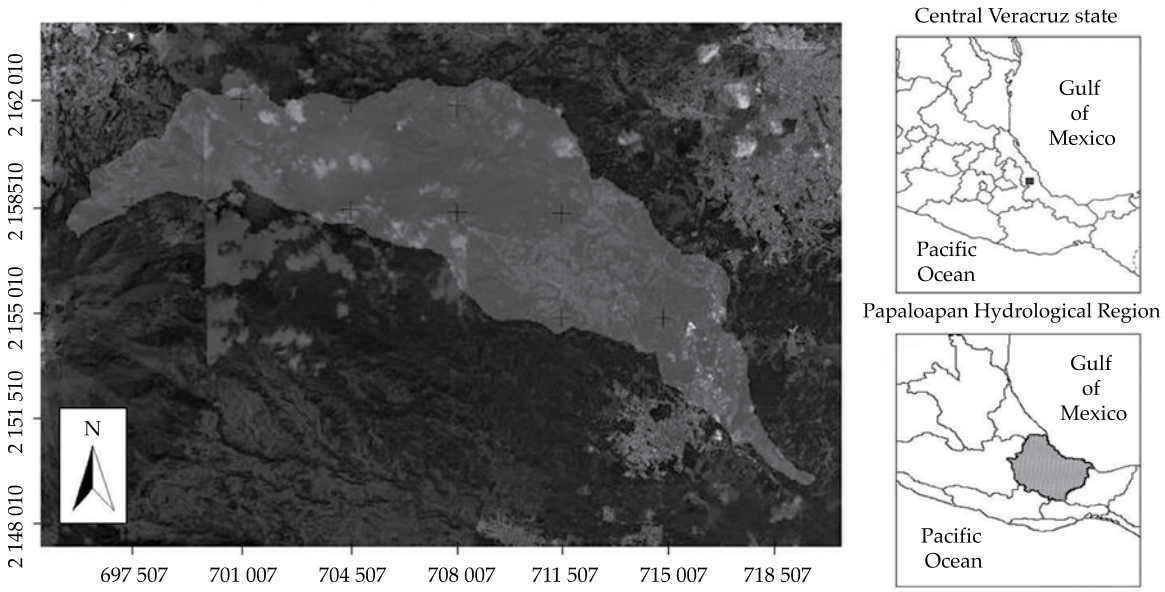

Figure 1. Geographic location of the Pixquiac River Watershed.

$$VC = \frac{\alpha BAb}{Oc}(1+\beta) \qquad (2)$$

Where α is the relative importance of the forest in terms of the water resource it provides (dimensionless value between 0 = no importance and 1=maximum importance); *B* is the opportunity cost of the forest *versus* livestock farming [$/(ha x year)]; *Ab* is the area of the study region covered by the forest (ha); *Oc* is the volume of water captured by the wooded area in the study region (m^3/year); and β is the value of the water quality of the runoff captured by said forest (dimensionless value between 0= very poor and 1 = very good).

The recovery cost, *VR*, in $/$m^3$, is equal to:

$$VR = \frac{\alpha CAr}{Oc} \qquad (3)$$

Where α is the relative importance of the forest in function of the water resource it provides (dimensionless value between 0 = no importance and 1 = maximum importance); *C* is the cost of the activity involving the recovery of the forest in the study area [($/(ha x year)]; *Ar* is the area in the study region to be recovered (ha); *Oc* is the volume of water captured by the wooded area in the study region (m^3/year).

The methodology by Barrantes and Castro (2002) considers a period of five years for the establishment and initial management of the forests. The present study is based on 10 years to estimate the total recovery value, including its establishment, as recommended by Silva-Flores *et al*. (2010).

The area pertaining to forest land and the area to be recovered were calculated by developing a vegetation and land use map using remote sensing technologies and geographic information systems.

The importance assigned to the forest in terms of water resources was determined by administering a survey to a total of 60 users with domestic intakes supplied by the water in the study area. These users expressed their opinions about the importance of the forest in terms of water catchment and the quality of the water they receive. The survey was administered according to a stratified sampling and using closed questions. The sample size

was determined based on saturation criteria (Serbia, 2007). The responses to the surveys regarding these two aspects were measured on a scale of 1 to 10 and were integrated by calculating the mean. Lastly, the average values (α and β) were normalized to obtain values between 0 and 1.

Livestock farming was identified as the activity responsible for the change in land use from forest to pasture (INEGI, 2012). Following the suggestion by INE (2002), the opportunity cost of livestock farming was calculated as the income generated by meat production, rather than cattle production. This is because the income from meat that is sold can be assumed to include the production costs of an animal unit. It is important to clarify that the two largest types of meat production in the state of Veracruz are bovine and ovine (INEGI, 2012), and therefore both production values were included.

The method consisted of obtaining, from INEGI documents, the value of the production of bovine (*VPB*) and ovine (*VPO*) meat, for each of the municipalities in the study area and for the area in each municipality dedicated to livestock farming (*LF*). The areas dedicated to farming by each municipality in the study area (*FA*) were calculated based on information from remote sensors. Then, the meat production values for both types of cattle were added, for each municipality, to obtained the accumulated value of this variable (*VAP*). These accumulated values were divided by the area of the municipality dedicated to farming in order to obtain the value of the income from production per municipality (*RP*). Since the information from INEGI is aggregated by municipality and a value is needed to represent the opportunity cost for the entire study area, the mean income from production was calculated per municipality and weighted according to the portion of the municipal area used for livestock farming.

Following the recommendations by Silva-Flores *et al*. (2010), the volume of water captured by the forests in the study area was estimated by multiplying the net catchment in the watershed by an adjustment factor obtained from dividing the wooded portion of the study area by the area of the watershed. The annual net catchment value was taken from García *et al.* (2008) who performed a comprehensive study of this watershed.

Finally, to calculate the new fees, the value of the water resource provided by the forests (*VB*) was added to the current charges for potable water services in the study area.

Results

Ground cover

The land use and vegetation maps produced include five categories: 1) crop area, 2) pasture, 3) exposed soil, 4) coniferous forests; 5) pine-oak forest. Since the middle-upper wooded portion of the watershed was the area of interest in terms of hydrology, the cover and land use map that originally included the entire watershed was cropped from 2 100 masl and above. The area corresponding to each of these covers is shown in Table 1. As can be seen, the most abundant cover is coniferous forest, with 2 846.7 ha, equivalent to 71.8% of the study area. The least abundant is pine-oak forest, covering 1.15% of the study area, equal to 45.72 hectares.

The resulting calculated areas of the coniferous forest and the pine-oak forest (2 982.42 ha) was taken as a reference to calculate the value of the forest's water catchment. In

Table 1. Cover for each land use category (ha).

Land Use	Cover (ha)
Crop areas	199.17
Pasture	271.26
Exposed soil	601.38
Coniferous forest	2 846.70
Pine-Oak forest	45.72
Total	**3 964.23**

Source: developed by authors.

the case of the recovery value, the area to be recovered was the result of the sum of the areas pertaining to pasture and exposed soil (872.64 ha).

Water catchment volume

According to García *et al.* (2008) and Ballesteros (2010), the net catchment of the watershed is as much as 145 430 260 (m^3/year). The wooded part of the study area represents 0.29 = 2 982.42/10 303.53 of the total area of the watershed. Therefore, the amount of water captured by the forest in question is 42 174 775.4 (m^3/year) = 145 430 260.0 * 0.29.

Estimation of the Index of Importance of the Forest to Users, in Relation to Water Catchment and Quality

The results indicate that 79.17% of those surveyed rates the importance of the forest in terms of water resources as 10, and 20.80% rates it as 9. According to the recommendations by Cochran (1977), the mean of these scores was calculated as a representative measurement of the data, and by normalizing it the value of this service to users was determined to be 0.97. This percentage represents the portion of the opportunity cost for which water users should compensate the land owners who are involved in protecting and recovering the forest. The other portion (0.021) can be attributed to other forest services, such as recreation or carbon capture. In terms of the quality of the runoff water, 12.5% of those surveyed assigned a value of 6 to the water quality, 16.6% a value of 8, 25% a value of 9 and 48.5% rated it as 10. To summarize, the average rating by users of the water quality of runoff is 0.89.

Estimation of the opportunity cost of forests versus livestock farming activity

The results obtained for the estimation of the opportunity cost and the data used to calculate it are shown in Table 2. As can be seen in this table, the opportunity cost for using forest land is 2 059.76 $/(ha x year).

Estimation of the costs for recovery and reforestation for the rehabilitation of the watershed

As shown in Table 3, the total cost of this activity is $17 300.56/ha for a temperate, cold ecosystem, according to data established by the National Forest Commission (DOF, 2011), with an adjustment for inflation of 4.05%. During the first year, the cost is 84.69% of the total, equal to $14 652.1/ha. Over the following nine years, the costs to maintain the forest area decrease to a fixed amount of $2 648.44/ha.

Calculation of catchment and recovery in the watershed

Substituting in equation (2), the catchment value is $0.266/$m^3$, as seen below:

$$VC = \left(\frac{(0.97)(2\,059.76)(2\,982.42)}{42\,174\,775.4}\right) * (1 + 0.89) = 0.266$$

Substituting in equation (3), the recovery value for the first year is $0.294/ m^3 and $0.053/ m^3 for years 2 to 10, as seen below:

$$VR[1] = \left(\frac{(0.97)(14\,652.1)(872.64)}{42\,174\,775.4}\right) = 0.294$$

$$VR[2-10] = \left(\frac{(0.97)(2\,648.44)(872.64)}{42\,174\,775.4}\right) = 0.053$$

Using equation (1) and substituting, the value of the forest for the first year is $0.560/ m^3 and $0.319/$m^3$ for the next nine years, as shown in the following equations:

$$VB[1] = VC + VR[1] = 0.266 + 0.294 = 0.560 \ \$/m^3$$

$$VB[2-10] = VC + VR[2-10] = 0.266 + 0.053$$
$$= 0.319 \ \$/m^3$$

Environmentally Adjusted Water Fee

The new proposed fee model is shown in Tables 4 and 5, which compare current fees to suggested fees by applying the value of the forest for the first year and the following nine years, respectively. The new fee is adjusted according to the range of consumption, based on the criteria applied by the water operations entity for charging for the use of the resource.

This environmentally adjusted water fee is the mechanism employed to charge users in order to compensate land owners to take responsibility for protecting and recovering the forest, to fulfill its hydric functions. In this way, the forest is considered a producer of environmental services, with profits that can be equal to or more attractive than traditional land uses, such as livestock farming as in the case of this study.

Discussion

For an indication of the economic impact of the environmentally adjusted fee on family income, the current payment and suggested payments were compared. To put this comparison in context, the current minimum salary in the study area was obtained, as well as the salary distribution by social strata.

According to data for 2013 from the National Minimum Salary Commission, the study area pertains to geographic region "B," where the minimum daily salary is $61.38 ($1 841.40 monthly)(STPS-Conasami, 2013). In terms of the upper social stratum, the National Jobs and Employment Survey (STPS-INEGI, 2013) reports earnings of over five times the minimum salary for this group (over $9 207.00 per month), while the middle class earns between two and five minimum salaries ($3 682.00 to $9 207.00 per month) and the low social stratum from zero to two minimum salaries ($0.00 to $3 682.00).

Using this information as a reference and the data from Ochoa, Rodríguez and Delgado (1993) regarding the amount of water provided, we can say that for the low social stratum, with an estimated water consumption between 70 and 172 m^3 per year, the suggested payment is always under 3.8% of the annual salary, equivalent to $833.76/year. For the middle class, with an estimated consumption between 182 and 355 m^3 per year, the maximum annual fee is under 7.5% of the annual income (($3 269.52); and for the lower-middle (cuadro4) stratum, which consumes between 273 and 456 m^3, the fee does not exceed 4.8% of the annual income, equivalent to $5 280.48/year. This implies a maximum payment of $2.28 for a daily consumption of 471.23 liters per intake for the lower stratum, a maximum of $8.95 per daily consumption of 972.6 liters per intake for the middle class, and a maximum of $14.46 per daily consumption of 1 249.31 liters per intake for the middle-upper stratum (residential). This analysis suggests that the fee would initially be affordable for all those who earn at least a minimum salary, considering, for example, what can be spent daily on bottled drinks (a 600 ml bottle of soda costs $9.00 (Anguiano & Mendoza, 2013) and a bottle of water costs roughly $10.00). These results suggest that the new environmental component has a relatively low impact on the consumer of the resources. This is contrary to the common assumption that the fees would significantly increase, thereby reducing the competitiveness of the economic instruments intended to encourage the conservation of ecosystem services ((Bastidas, 2009)).

Nevertheless, in the case concerning the present study, it is important to mention that even though the largest increase in the percentage of monthly income does not apply to the lower stratum, the income for this group could fall be below the minimum salary, and therefore the available payment could be negative. Given this context and in terms of sustainability, the establishment of a fee should be a priority, where the government guarantees

Table 2. Estimation of the opportunity cost of forest land use.

Municipality	Value of bovine (VPB) meat production $/year	Value of ovine (VPO) meat production $/year	Accumulated value of meat production VPB + VPO $/year	Area dedicated to livestock farming (LF) ha	Earnings from meat production RP = (VPB + BPO)/LF $/year x ha	Municipal area pertaining to the study area and dedicated to livestock farming (FA) ha	(*RP* x *SMAEG*) $/year	Weighted average of income from opportunity cost of production (total of RP x FA/total FA) $/year x ha
Acajete	13 502 000	1 224 000	14 726 000	2 990	4 925.08	1 019.59	5 021 562.31	10 425 617.55 / 5 061.55
Coatepec	7 863 000	1 709 000	9 572 000	3 647	2 624.62	1 714.09	4 498 834.89	
Las Vigas de Ramírez	9 811 000	899 000	10 710 000	1 168	9 169.52	1.168	10 709.99	
Perote	2 974 000	4 084 000	7 058 000	20 862	338.31	2 211.37	748 128.58	
Tlalnehuayocan	0	892 000	892 000	511	1 745.59	35.25	61 532.04	
Xico	4 327 000	4 158 000	8 485 000	8 009	1 059.43	80.09	84 849.74	
					Totales	5 061.55	10 425 617.55	**2 059.76**

Source: developed by authors based on INEGI data (2012).

Table 3. Reference cost for reforestation or restoration and maintenance.

Type of activity	Measurement unit	Cost ($)
Cost of restoration of soil	Hectare	9 669.15
Cost of reforestation	Hectare	4 982.95
Cost of maintenance	Hectare	2 648.44
Total Cost	Hectare	**17 300.56**

Source: developed by authors based on DOF data (2011).

Table 4. Fees for potable water service (2013) compared to fees that include the value of the forest (VB), corresponding to the first year.

Consumption range m^3/month	Low Stratum w/o VB	Low-middle Stratum with VB	Low-middle w/o VB	Social Interest with VB	Middle domestic w/o VB	Middle domestic with VB	Middle-upper w/o VB	Middle-upper with VB
(0-10)	**46.71**	**46.71**	**66.80**	**66.8**	**84.69**	**84.69**	**100.12**	**100.12**
(11-20)	4.70	5.26	6.72	7.28	9.03	9.59	10.90	11.46
(21-30)	5.25	5.81	7.02	7.58	9.24	9.8	11.22	11.78
(31-40)	5.39	5.95	7.41	7.97	9.53	10.09	11.58	12.14
(41-60)	5.76	6.32	7.71	8.27	10.03	10.59	12.24	12.8
(61-80)	6.11	6.67	8.97	9.53	10.70	11.26	12.99	13.55
(81-100)	6.47	7.03	9.61	10.17	11.98	12.54	14.63	15.19
(101-120)	7.35	7.91	9.85	10.41	12.34	12.9	15.08	15.64
(121-150)	7.90	8.46	10.73	11.29	13.33	13.89	16.27	16.83
(151-200)	8.93	9.49	11.98	12.54	14.98	15.54	18.23	18.79

Source: developed by the authors based on data from the Xalapa Municipal Potable water and Treatment Commission (2013). The dark gray boxes represent the base fee for each type of user, considering a maximum consumption of 10 m^3. The rest of the boxes refer to the cost of extra consumption expressed in $/$m^3$), whose value is adjsuted according to the range of consumption and type of user.

Table 5. Fees for potable water service (2013) and their comparison with fees that include the value of the forest (VB), corresponding to years 2 through 10.

Consumption range m^3/month	Low Stratum w/o VB	Low-middle Stratum with VB	Low-middle w/o VB	Social Interest with VB	Middle domestic w/o VB	Middle domestic with VB	Middle-upper w/o VB	Middle-upper with VB
(0-10)	**46.71**	**46.71**	**66.80**	**66.8**	**84.69**	**84.69**	**100.12**	**100.12**
(11-20)	4.70	5.019	6.72	7.03	9.03	9.34	10.90	11.21
(21-30)	5.25	5.569	7.02	7.33	9.24	9.55	11.22	11.53
(31-40)	5.39	5.709	7.41	7.72	9.53	9.84	11.58	11.89
(41-60)	5.76	6.079	7.71	8.029	10.03	10.34	12.24	12.55
(61-80)	6.11	6.429	8.97	9.28	10.70	11.01	12.99	13.30
(81-100)	6.47	6.789	9.61	9.92	11.98	12.29	14.63	14.94
(101-120)	7.35	7.669	9.85	10.16	12.34	12.65	15.08	15.39
(121-150)	7.90	8.219	10.73	11.04	13.33	13.64	16.27	16.58
(151-200)	8.93	9.249	11.98	12.29	14.98	15.29	18.23	18.54

Source: developed by the authors based on data from the Xalapa Municipal Potable water and Treatment Commission (2013). The dark gray boxes represent the base fee for each type of user, considering a maximum consumption of 10 m^3. The rest of the boxes refer to the cost of extra consumption expressed in $/$m^3$), whose value is adjsuted according to the range of consumption and type of user.

users the supply needed to satisfy minimum survival needs, established as 50 l/inhab/day (Glieck, 2001). This is highly important given that, as Tello (2006) states, "access to potable water reflects aspects that are fundamental to life and factors that are indispensable to social development, since it involves notable improvements in the living conditions of persons, which are observed in the economic, social and cultural realms."

On the other hand, while incorporating the value of the forest into fees can reflect an advance in the valuation of ecosystem services and their maintenance, the fee system used by the water operator entity needs to be adjusted. This can be seen in the following example. Supposing 355 m^3/year is consumed by middle domestic as well as residential users, the cost of consuming this amount would be higher for the former than for the latter, in relation to salary (3 and 2.95%, respectively). And this takes into account the possibility that the residential user may earn only one minimum salary more than the highest salary category for the middle domestic user. When considering two or more minimum salaries, the percentage for the residential users decreases to 2.5%. This shows the limitations of the fee scheme used by the operating entity as a basis for charging for the hydrological services provided by the forest. It also reflects the importance of addressing aspects related to equity when establishing and charging fees (Brandes *et al*., 2005).

Therefore, it is necessary to emphasize that the applicability of a fee will depend on the income levels of water users and their willingness to pay. This points to the need to complement this investigation with a contingent valuation study, to determine the amount that users would be willing to pay to continue to receive enough water with sufficient quality to satisfy real needs (Barrantes & Castro, 2002). These amounts were found to differ considerably between two national studies related to the willingness to pay for the hydrological services provided by forests. In one case, the users were willing to pay $29.76 /year (López-Paniagua, 2007), and in the other, $216.16 /year (Silva-Flores, 2010). With regard to water users in the Pixquiac watershed, the former is an amount that, if accepted as feasible, would be very close to the annual payment required of the low stratum (for minimal consumption) to maintain the watershed as a water catchment and storage area. Nevertheless, this is insufficient because the level of consumption by the lower stratum does not reflect the actual consumption of water in the watershed. In contrast, the second amount would be more than sufficient to compensate the land owners in order to prevent land use changes in the forest. Nevertheless, this would require charging all domestic users, across the board, for a much higher consumption than what they actually use, worsening the situation for the lower stratum. Therefore, it is clear that much care must be taken when extrapolating the results from studies to other places or regions, since they are based on biophysical, social and economic characteristics that are specific to a study area. Nevertheless, it is important to continue these types of investigations in the country in order to encourage the use of a PES strategy as a disincentive to deforestation, and thereby improve our watersheds' hydrological regulation capacities (Silva-Flores *et al*., 2010).

The contrast between the fees derived from the study herein and the amount users are willing to pay could lead to a compromise between the two amounts, with the idea of gradually introducing these mechanisms over time in order to create a culture of payment for services provided by the forest. Given this perspective, care should also be taken so that there is transparency and effectiveness in the fee payment mechanisms and the final destination of the income generated; otherwise the policy would be useless (Merino, 2005). It is also important to keep in mind that the willingness to pay is related to the opportunity —in time and form— and the quality of the resource received by the users. Therefore, infrastructure solutions that provide timely and appropriate distribution of the resource must continue, as

a mechanism that complements the financial aspect of water management (Brandes *et al*., 2005; Marañón-Herrera, Chávez-Cortés, Martínez-Espinosa, & Ruelas- Monjardin, 2008).

Furthermore, it is evident that the market price of the activity that competes with forest conservation is a determining factor in the feasibility of applying a water fee, since the earnings from forest activities are not the same as those from farming, for example. In circumstances such as this one, the income of those in possession of forest land would need a compensation in addition to fee payments, perhaps through synergetic activities or environmental tourism, in which the forest supports the habitats of species and provides ecosystem services related to recreation, education and culture. Other alternatives include complementing the income of owners of forests through community forest management (CFM) (Merino, 2005) and environmental services programs by the government, such as carbon capture, water production and conservation of biodiversity (Silva-Flores, 2010).

From the methodological perspective, the instrument used is clearly highly dependent on market dynamics and collective opinion, since it is based on opportunity cost and the values identified. Therefore, the calculations herein are not reproducible for different contexts, such as place, time, conditions and type and number of users. Therefore it should be approached carefully. Nevertheless, it is still valuable since it enables obtaining some approximate values of the economic worth of the upper watershed's forest, as a means towards long-term sustainability (Aguilera, 2006). In addition, the forest values obtained constitute a first approach and can be used as a reference for future analyses of this type in the Pixquiac watershed.

Finally, based on this investigation, the need for water and its importance to users in the Pixquiac River watershed are evident. Therefore, the development and implementation of environmental management policies are relevant, particularly water management policies. To this end, a genuine compromise is needed as well as relationships between state level environmental authorities and the different social actors (Brandes *et al*., 2005). As a complement, substantial efforts are needed by both parties in order to emphasize the importance of education and raising awareness of the population about water management and the natural resources in the area in which they live (López- Paniagua, 2007).

Conclusions

The overall objective of this investigation was met, which consisted of constructing a water fee that could be applied to domestic water users for the purpose of recuperating an amount equivalent to that which would otherwise be earned by engaging in the primary economic activity that competes with forest conservation, and use that compensation as an incentive for discontinuing that activity.

The market price of the activity that competes with the conservation of the forest is a determining factor in the feasibility of applying a water fee. Therefore, other activities to complement the income of forest owners should be considered in the management proposal.

Studies of this type should be complemented by contingent valuation studies to address the viability of applying a water fee. It is also important to mention that this type of study needs to continue in order to analyze other services provided by forests and include them in the construction of fees.

It is known that a sudden application and standardization of regulations to motivate changes in behavior of persons is not met with acceptance. Therefore, in this case it is important to consider the usefulness of gradually applying and adjusting a water fee. In addition, transparency in collecting and allocating funds will be crucial to the success of any policy related to payment for environmental services.

The experiences gained from the investigations performed in Costa Rica and other regions have demonstrated that PES has played an important role in the conservation of ecosystems and stopped degradation. This shows how the adaptability of the system to different contexts and environmental services makes PES programs applicable to a large number of situations throughout the country. In this sense, the results of this investigation should provide a basis for discussing forest conservation and the maintenance of the environmental services they provide.

Acknowledgements

We thank the reviewers for their valuable comments and suggestions to improve this document.

References

Aguilera, U. D. (2006). El valor económico del medio ambiente. *Ecosistemas*, *15*(2), 66-71.

Anguiano, D., & Mendoza, A. (2013). *Suben el precio de los refrescos de Coca-Cola* [en línea]. Ciudad de México. Milenio-Negocios. Consultado el 26/05/2013. Recuperado de http://monterrey.milenio.com/cdb/doc/noticias2011/607e5689c02bb47f9d4ecb72088b911f.

Ballesteros, P. E. (2010). *Balance hídrico preliminar de la microcuenca del río Pixquiac* (46 pp.). Tesis para obtener la Especialidad en Diagnóstico y Gestión Ambiental. Veracruz, México: Universidad Veracruzana.

Barrantes, G., & Castro, E. (2002). Experiencias replicables de valoración económica de bienes y servicios ambientales y establecimiento de sistemas de pago por servicios ambientales. Implementación de un esquema de cobro y pago por servicio ambiental hídrico: el caso de la empresa de servicios públicos de Heredia S.A. En R. Barsev (Ed.). *Guía metodológica para la valoración de bienes, servicios e impactos ambientales. Un aporte para la gestión de ecosistemas y recursos naturales en el CBM. Serie Técnica 04* (pp. 108-112) Managua, Nicaragua: Corredor Biológico Mesoamericano-CCAD-PNUM/GED.

Barzev, R. (2004). *Estudio de la valoración económica de la oferta y demanda hídrica del bosque en que nace la fuente del río Chiquito (Finca El Cacao-Achuapa), Nicaragua-Implementación de mecanismos de pagos por servicios hídricos* [en línea]. Managua, Nicaragua. Pasolac. consultado el 10/10/2013. Recuperado de http://201.116.60.96:8080/wb/ceeaa/ficha_de_estudio_economico?id=298.

Bastidas, P. D. (2009). *Valoración económica del servicio ambiental de regulación hídrica del bosque de roble en la cuenca del río Guacha, Encino-Santander, Colombia* (85 pp.). Tesis para obtener el grado de maestro. Asunción, Paraguay: Universidad Nacional de Asunción.

Brandes, O. M., Ferguson, K., M'gonigle, M., & Sandborn, C. (2005). *At a Watershed: Ecological Governance and Sustainable Water Management in Canada* [en línea]. Victoria, Canada. The POLIS Project on Ecological Governance, University of Victoria. Consultada el 30/08/2013. Recuperado de https://www.google.com/#q=at+a+watershed.

Cochran, W. (1977). *Sampling Techniques.* Third Edition (150 pp.) New York, USA: John Wiley and Sons.

Coila, Y. (2005). *Valoración económica del servicio ambiental hídrico de los bosques de la subcuenca del río Santa Catarina, México* [en línea]. Boletín de la Fundación Equitas, Santiago, Chile. MERCOSUR/GMCRES N° 80/962005. Consultado el 30/09/2013. Recuperado de www.boletin.fundacionequitas.org/11/11.13.htm.

Contreras, T. C., & Solano, C. F. A. (2010). *Caracterización del agua pluvial en el periodo de verano para su uso doméstico en Xalapa, Veracruz* (71 pp.). Tesis para obtener el grado de especialista en Diagnóstico y Gestión Ambiental. Xalapa, México: Universidad Veracruzana.

Comisión Municipal de Agua Potable y Saneamiento de Xalapa (2013). *Tarifas para el cobro de agua potable del mes de septiembre* [en línea]. Xalapa, México. CMAS. Consultado el 25/09/2013. Recuperado de www.aguaxalapa.gob.mx.

Corbera, E., & González, C. (2007). *Pago por servicios ambientales en México: situación actual y objetivos de futuro* (95 pp.). Memoria del taller. México, DF: Instituto Nacional de Ecología.

Corbera, S., González, S. C., & Brown, K. (2009). Institutional Dimensions of Payment for Ecosystem Services: An Analysis of México´s Carbon Forestry Program. *Ecological Economics*, 68, 743-761.

Cordero, D. (2003). *Lineamientos para la formulación de una estrategia para la sostenibilidad financiera del programa PROCUENCAS de la ESPH S.A. bajo un modelo de inversión ambiental compartida* (76 pp.). Heredia, Costa Rica: Escuela de Ciencias Forestales, Universidad Nacional.

Cordero-Camacho, D. (2001). *PROCUENCAS, un esquema de cobro y pago por servicio ambiental hídrico en la Provincia de Heredia, Costa Rica* [en línea]. Heredia, Costa Rica. Empresa de Servicios Públicos de Heredia. Consultado el 2/09/2013. Recuperado de http://www.undp.org.cu/eventos/aprotegidas/Pago_Serv_Amb_Agua_D_Cordero_Heredia.pdf.

Chávez, C. M. M. (2007). Usos y abusos del agua. *Ciencias*, *85*, 30-36.

Chávez, C. M. M., & Mancilla, H. K. E. (2013). El pago por servicios ambientales y la conservación de los bosques. *ContactoS*, *88*, 27-35.

DOF (febrero de 2011). *Acuerdo por el cual se emiten los costos de referencia para reforestación o restauración y su mantenimiento para compensación ambiental por cambio de uso de suelo en terrenos forestales y la metodología de su estimación*. México, DF: Diario Oficial de la Federación.

Dixon, J., Scura, L. F., Carpenter, R. A., & Sherman, P. B. (1994). *Análisis económico de impactos ambientales* (249 pp.). Traducción de Tomás Saravi A. Segunda edición. Turrialba, Costa Rica: CATIE, Unidad de Producción de Medios.

Emerton, L. & Bos, E. (2004). *Valor. Considerar a los ecosistemas como un componente económico de la infraestructura hídrica* (94 pp.). Traducción de José M. Blanch. San José, Costa Rica: UICN-ORMA.

FAO (2004). *Payment Schemes for Environmental Services in Watersheds* [en línea]. Arequipa, Perú. Organización de las Naciones Unidas para la Agricultura y la Alimentación, Land and Water Discussion Paper 3, Regional Forum. Consultado el 1/10/2013. Recuperado de *ftp://ftp.fao.org/agl/aglw/docs/lwdp3_es.pdf*.

FAO (2011). *Situación de los bosques del mundo 2011* (190 pp.). Roma: Organización de las Naciones Unidas para la Agricultura y la Alimentación.

Fregoso, A. (2006). La oferta y el pago de los servicios ambientales hídricos: una comparación de diversos estudios. *Gaceta Ecológica*, *78*, 29-46.

García, C. I., Martínez, O. A., & Vidriales, C. G. (2008). *Balance hídrico de la cuenca del río Pixquiac*. (31 pp.). Documento Técnico del Proyecto NCMA 3-08-03. Delimitación de zonas prioritarias y evaluación de los mecanismos existentes para el pago de servicios ambientales hidrológicos en la cuenca del río Pixquiac, Veracruz, México. Xalapa, México: Senderos y Encuentros para un Desarrollo Autónomo Sustentable, A.C.

García-Amado, L. R., Ruiz, P. M., Reyes, E. F., Barrasa, G. S., & Contreras, M. E. (2011). Efficiency of Payments for Environmental Services: Equity and Additionality in a Case Study form Biosphere Reserve in Chiapas, México. *Ecological Economics*, *70*, 2361-2368.

García-Calva, L. (2010). *Ordenamiento territorial de la subcuenca del río Pixquiac, Ver., a partir de la identificación de áreas ecológicamente sensibles* (110 pp.). Tesis para obtener el grado de Biólogo. México, DF: Universidad Autónoma Metropolitana Xochimilco.

Glieck, P. H. (February, 2001). Safeguarding our Water. Making Every Drop Count. *Scientific American*, *284*(2), 40-45.

Hernández, O., Cobos, C., & Ortiz, A. (2002). *Valoración económica del servicio ambiental de regulación hídrica. Lado sur de la reserva de la Sierra de las Minas Guatemala* [en línea]. Guatemala, Guatemala: FIPA/AID-USAID. Consultado el 7/10/2013]. Recuperado de ftp://*pdf.usaid.gov/pdf_docs/pnacx128.pdf*.

Higman, S., Bass, S., Judd, N., Mayers, J., & Nussbaum, R. (1999). *The Sustainable Forestry Handbook* (231 pp.). London: Earthscan.

INE (2002). *Estimación del costo de oportunidad del uso de suelo forestal en ejidos a nivel nacional* (13 pp.). México, DF: Instituto Nacional de Ecología-Secretaría de Ecología, Medio Ambiente y Recursos Naturales.

INEGI (2012). *Anuario Estadístico Veracruz* (500 pp.). México: Instituto Nacional de Estadística Geografía e Informática.

Landell-Mills, N., & Porras, I. (2002). *Silver Bullets or Fools' Gold? A Global Review of Markets for Forest Environmental Services and their Impacts on the Poor. Instruments for Sustainable Private Sector Forestry Series* (75 pp.). London: International Institute for Environment and Development.

López-Paniagua, C. (2007). *Estudio de mercado del servicio ambiental hidrológico en la cuenca de Tatalpa Jalisco* [en línea]. Tesis para obtener el grado de maestro. Texcoco, México. Colegio de Postgraduados (COLPOS). Consultada el 2/10/2013. Recuperado de http://www.biblio.colpos.mx:8080/xmlui/handle/10521/1606.

Manson, R. H. (2004). Los servicios hidrológicos y la conservación de los bosques en México. *Madera y Bosques*, *10*(1), 3-20.

Manson, H. R. (2007). *Efectos del uso de suelo sobre la provisión de servicios ambientales hidrológicos: monitoreo del impacto del pago por servicios ambientales hidrológicos (PSAH)* (14 pp.). México, DF: Instituto Nacional de Ecología-Secretaría de Medio Ambiente y Recursos Naturales.

Marañón-Herrera, S., Chávez-Cortés, J. M., Martínez-Espinosa, D., & Ruelas-Monjardin, L. C. (2008). Los modelos de manejo del agua y su influencia en las políticas de los procesos acuícolas. Estudio de caso. La piscicultura de ornato en el estado de Morelos, México. *Ingeniería hidráulica en México*, *23*(4), 145-159.

MEA (2007). *Millenium Ecosystem Assessment: A Toolkit for Understanding and Action. Protecting Nature's Services. Protecting Ourselves* (28 pp.). Washington. DC: Island Press.

Merino, P. L. (enero-marzo, 2005). El desarrollo institucional de esquema de pago por servicios ambientales. *Gaceta Ecológica*, *74*, 29-42.

Munasinghe, M., & Lutz, E. (1993). Environmental Economics and Valuation in Development Decision Making. En M. Munasinghe (Ed.). *Environmental Economics and Natural Resource Management in Developing Countries* (560 pp.). Washington, DC: The World Bank.

Muñoz-Piña, C., Guevara, A., Torres, J. M., & Braña, J. (2008). Paying for the Hydrological Services of Mexico's Forest: Analysis, Negotiations and Results. *Ecological Economics*, *65*(4), 725-736.

Ochoa, A. L., Rodríguez, V. M., & Delgado, B. A. (1993). *Análisis de la información del estudio de actualización de dotaciones del país* (20 pp.) Jiutepec, México: IMTA, 1983.

Pagiola, S. (2002). Paying for Water Services in Central America: Learning from Costa Rica. En S. Pagiola, J., Bishop, & N. Landell-Mills (Eds.). *Selling Forest Environmental Services: Market-based Mechanisms for Conservation and Development* (pp. 40-63). London: Earthscan.

Serbia, J. M. (2007). Diseño, muestreo y análisis en la investigación cualitativa. *Hologramática* (año 4), *3*(7), 123-146.

Ramírez-Chasco, F., Cabrejas-Palacios, J., Seco-Meneses, A., & Torres-Escribano, J. L. (2004). El valor ecológico de los medios fluviales urbanos. *Ingeniería hidráulica en México, 19*(4), 21-32.

Semarnat (2006a). *Introducción a los servicios ambientales* (73 pp.). México, DF: Secretaría de Medio Ambiente y Recursos Naturales.

Semarnat (2006b). *El medio ambiente en México 2005: en resumen* (91 pp.). México, DF: Secretaría de Medio Ambiente y Recursos Naturales-United Nations Development Programme.

Silva-Flores, R., Pérez-Verdín, G., & Navar-Cháidez, J. J. (2010). Valoración económica de los servicios ambientales hidrológicos en El Salto, Pueblo Nuevo, Durango. *Madera y Bosques*, *16*(1), 31-49.

STPS-Conasami (2013). *Nuevos salarios mínimos 2013, por área geográfica generales y profesionales* [en línea]. México, DF: Secretaría del Trabajo y Previsión Social-Comisión Nacional de Salarios Mínimos. Consultado el 23/10/2013. Recuperado de http://www.conasami.gob.mx/nvos_sal_2013.html.

STPS-INEGI (2013). *Encuesta nacional de Ocupación y Empleo* (10 pp.). México, DF: Secretaría del Trabajo y Previsión Social-Instituto Nacional de Estadística, Geografía e Informática.

Tello, M. L. F. (2006). *El acceso al agua potable, ¿un derecho humano?* [en línea]. México, DF. *Revista Derechos Humanos México. Revista del Centro Nacional de Derechos Humanos*, 2. Consultado el 23/10/2013. Recuperado de http://www.juridicas.unam.mx/publica/rev/indice.htm?r=derhumex&n=2.

Van Den Bergh, J. (1996). *Ecological Economics and Sustainable Development. Theory, Methods and Applications* (354 pp.). Cheltenham, UK: Edward Elgar.

Institutional Address of the Authors

Dra. Marta Magdalena Chávez Cortés
Biól. Karla Erika Mancilla Hernández

Laboratorio de Planeación Ambiental
Departamento El Hombre y su Ambiente
Universidad Autónoma Metropolitana, Xochimilco
Calzada del Hueso 100, Col. Villa Quietud, delegación Coyoacán
04960 México, D.F., México
Teléfono: +52 (55) 54837 225
ccmm1320@correo.xoc.uam.mx
kalita280183@hotmail.com

Click here to write the autor

Technical Note

Mathematical Modeling of Recessive Flows in the Andean Mediterranean Region of Maule; Case Study of Estero Upeo, Chile

• Francisco Balocchi •
University of Arizona, USA

• Roberto Pizarro* • Carolina Morales •
Universidad de Talca, Chile
*Corresponding Author

• Claudio Olivares •
Ministerio de Obras Públicas, Chile

Abstract

Balocchi, F., Pizarro, R., Morales, C., & Olivares, C. (September-October, 2014). Mathematical Modeling of Recessive Flows in the Andean Mediterranean Region of Maule; Case Study of Estero Upeo, Chile. *Water Technology and Sciences* (in Spanish), 5(5), 171-180.

This study analyzed four mathematical models for recessive flow estimation in order to determine which one would provide the best results for an Andean basin in Maule, central Chile. This was accomplished through the analysis of 25 summer floods occurring between 1971 and 2003, which identified groundwater as the exclusive supply as of the third inflection point of the falling limb of the storm's hydrograph. The results indicate that the exponential model 3 provides the best estimates. According to the Bland and Altman agreement test, the best model adjustment period was 240 hours.

Keywords: Hydrograph, recessives flows, falling limb, mathematics models.

Resumen

Balocchi, F., Pizarro, R., Morales, C., & Olivares, C. (septiembre-octubre, 2014). Modelamiento matemático de caudales recesivos en la región mediterránea andina del Maule; el caso del estero Upeo, Chile. Tecnología y Ciencias del Agua, *5(5), 171-180.*

En el presente estudio se analizaron cuatro modelos matemáticos de estimación de caudales recesivos, con el fin de determinar cuál de ellos obtiene los mejores resultados en una cuenca andina del Maule, zona mediterránea de Chile central. Esto se realizó a través del análisis de 25 crecidas en la época estival 1971-2003, en donde se consideró el aporte exclusivo de las aguas subterráneas a partir del tercer punto de quiebre de la curva de bajada del hidrograma. Los resultados obtenidos demuestran que el modelo exponencial 3 es el que presenta las mejores estimaciones. En el caso del mejor lapso para el ajuste de los modelos, el tiempo de 240 horas es el que obtiene los mejores resultados, según el test de Bland y Altman.

Palabras clave: *hidrograma, caudales recesivos, curva de bajada, modelos matemáticos.*

Received: 25/03/13
Accepted: 19/03/14

Introduction

The prediction of flow recession is a widely used method for hydrological planning and investigations (Smakhtin, 2001). It has thus become an important hydrological tool, especially during summer when the population's water supply depends on the reserves in a watershed (Wittenberg, 1999). Therefore, knowledge about these water reserves is vitally important to a country's human and economic development.

Thus the need to calculate the availability of this resource for use during summer months. To this end, mathematical modeling serves as

an important analytical tool and contributes to understanding the behavior of water during these periods, given that these models can study the behavior of complex systems in situations that are difficult to observe in the real world (Sujono, Shikasho, & Hiramatsu, 2004). Estrela (1992) indicates that mathematical models for calculating flows are a valid way to solve theoretical water problems and, in addition, better reflect physical and hydrological conditions.

In addition, Linsley, Kohler and Paulhus (1949) and Pizarro (1993) report that the flow of rivers during droughts or low water periods can be calculated if the shape of the recession curve of the hydrograph is known. The hydrograph shows the behavior of flows over time, and is composed of a concentration curve, a descending limb and a recession curve (Maidment, 1992; Pizarro, 1993; Aparicio, 2003; Bedient & Huber, 2002; Brodie, Hostetler, & Slatter, 2007). The recession curve is that for which the flow is exclusively supplied by groundwater and enables calculating the availability of water during floods, which is particularly important during summer months. Figure 1 shows the beginning of the recession curve, or depletion, from point C and onward (Linsley *et al.*, 1949). According to the third breakpoint method, the beginning of recession flows are indicated for the case of the second breakpoint and point C′ (Pizarro *et al.*, 2013). The present study uses the third breakpoint method since flow data is more stable when taking that point as the beginning of the recession curve, thereby reducing the variability in the data and improving levels of fit.

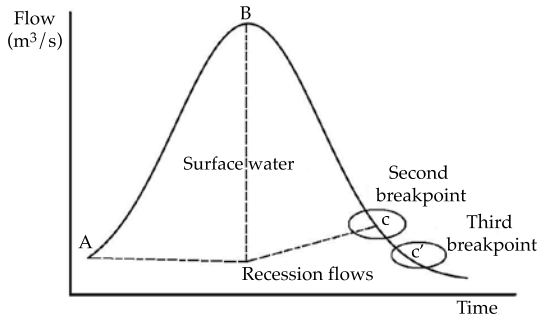

Figure 1. Flood hydrograph.

The separation of the hydrograph proposed by Linsley *et al.* (1949) and corroborated by Pizarro (1993) is what is most used in Chile. This separation consists of drawing the descending curve of the hydrograph on a semi-logarithmic graph, in which the second breakpoint corresponds to the beginning point of the hydrograph, in which the supply comes only from recession flows (Vilaró, 1976; Bedient & Huber, 2002). Other types of methodologies for the separation of hydrographs exists, such as Bedient and Huber (2002), and Viessman and Lewis (2003), which offer good approximations that generally do not present significant variations in determining the beginning point of the recession flows (Ponce,1989). In the academic field, the theory for the separation of hydrographs by Hewlet and Hibbert (1967) is the most highly accepted. This methodology shows that new water from rain pushes the old water out from the soil and the latter joins with the surface and/or groundwater flow. Nevertheless, Brooks, Barnard, Coulombe and Mcdonnell (2009) demonstrate that this behavior does not necessarily occur. Lastly, the Linsley separation methodology was held constant to determine the behavior of the different mathematical recession models.

Considering the above, and with knowledge acquired from recession curves, the behavior of groundwater flows was modeled for the Upeo Estuary in the Lontue River, Chile. The purpose of this was to identify the model with the best fit for the study area, given the decrease in water availability in the Mediterranean region in Chile, especially during summer. This, in addition to determining the correct model for the watershed studied, would ensure adequately calculating recession flows and reserves in the watershed.

The station used for the present study was the Upeo Estuary, in Upeo, located at coordinates UTM 309 573 E –6 105 697 N (WGS84/h19). Precipitaiton in the study area (Figure 2) is 1 800 mm/year. The area corresponds to the Lontue River sub-basin, located between 309 340 E – 6 095 942 N and 342 916 E – 6 114 754 N (WGS84/h19), which, along with the Teno River, covers an area of 2 784 km^2. Both have a snow regime. They begin in the Andes mountains and are the source of the Mataquito River. The Lontue River receives water in the north from two estuary tributaries —Upeo and Chenquelmo.

The temperature recorded at this station ranged from 20 to 4°C. The maximum flow recorded at the station was 490 m^3/s during the year 2000.

The Andes mountain range is the main geomorphology in the region. In terms of the geology, Paleozoic Mesozoic is predominant, with Cenozoic in some sectors. The sector also contains moraines glacial sediments (CNR,1978).

Methodology

The factors considered for selecting the watershed were having a natural flow regime, monitoring by a flow meter station and containing a water stage recorder. The station selected contains data from 1964 to the present. The Upeo Estuary station was thereby chosen, located in Upeo, in the Mataquito watershed, region of Maule (Figure 2).

The information required included discharge curves and water stage recorder data from 1964 to 2003, corresponding to the Upeo Estuary Station. This information was provided by the General Water Department, an official institution responsible for the management and measuring of water resources in Chile.

The period with clearly identifiable floods during summer months (October-April) was selected from the information collected. Accordingly, 25 floods were selected during hydrological years 1971-2003, based on which flood hydrographs for each storm was constructed. It is worth keeping in mind that

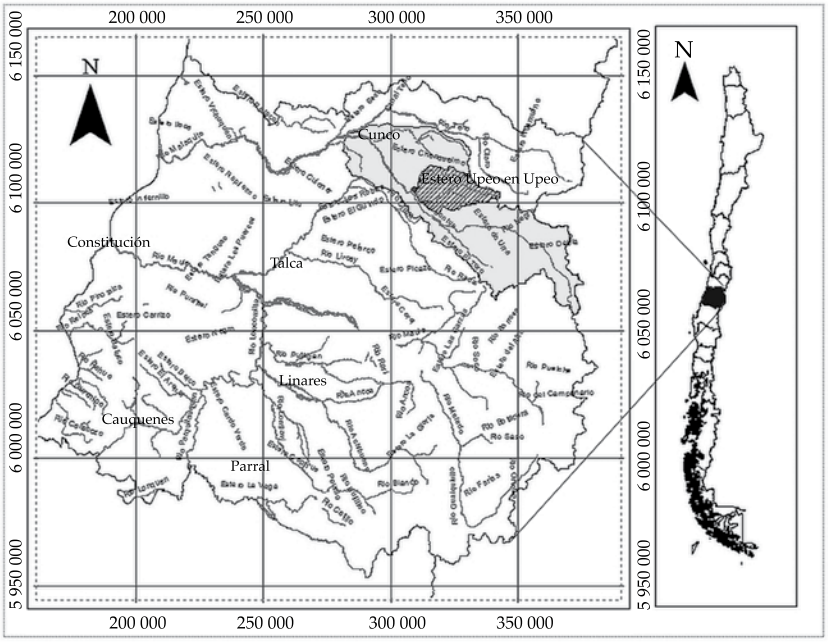

Figure 2. Location of study area.

the last floods of each year were selected, those near the end of the hydrological cycle, in order to ensure the presence of recession flows during significant periods.

The periods mentioned correspond to the amount of time between the beginning of a recession flow (Q_0) and the beginning of a new flood. These periods are essential to the calculation of the parameters in the models used. The shortest flood period identified was 11 days and the maximum was 239 days.

The present study included five periods, which correspond to 48 hours, 72 hours, 168 hours, 240 hours and the total hours of each flood selected, given the hypothesis that the longer the time from the initial coordinate (Q_0, t_0) the better the fit of each model. Thus, (Q_0, t_0), (Q_{48}, t_{48}) represent the coordinates for period t = 48 hours; (Q_0, t_0), (Q_{72}, t_{72}) for t = 72 hours, etcetera, for each period chosen. Nevertheless, for the purpose of representativeness for this study, only periods of 240 and the total hours of each flood were included.

Four types of mathematical models were used —one power and three exponential. The parameters used were initial flow (Q_0), depletion coefficient (α), a particular parameter (n) in exponential model 2, the Neper constant (e) and times t and t_0, where t_0 corresponds to the initial time in the models.

The fit of these models is based on the value of the initial flow of the recession (Q_0) produced at time $t_0 = 0$. This involves taking into account one or more points at instant $t_0 + dt$, which defines another coordinate, Q_t, with which the parameters of the equation can be obtained. Therefore, it is important to study whether the time differential affects the prediction of recession flows. The models used were:

Power model: $Q(t) = Q_0(1 + \alpha \cdot t)^{-2}$
(Cirugeda, 1985) (1)

Exponential model 1: $Q(t) = Q_0 \cdot e^{-\alpha(t-t_0)}$
(Remenieras, 1971) (2)

Exponential model 2: $Q(t) = Q_0 \cdot e^{-\alpha(t-t_0)^n}$
(Cirugeda,1985) (3)

Exponential model 3: $Q(t) = Q_0 \cdot e^{(-2\alpha\sqrt{t})}$
(prepared) (4)

A series of constructed and simulated models were generated for exponential model 3, which is proposed as a new model for the study area. It was mathematically determined as follows:

It is known that $\frac{dQ}{dt} < 0$ where Q = flow and t = time

If the change in flow over time is assumed to be proportional to the flow itself and inversely proportional to the root of time, then:

$$\frac{dQ}{dt} = -\alpha\left(\frac{Q}{\sqrt{t}}\right) \text{ operating } \frac{dQ}{Q} = -\alpha\left(\frac{dt}{\sqrt{t}}\right)$$

It is also known that when $Q = Q_0$, then $t = 0 = t_0$. Integrating between the limits t and t_0, we have:

$\ln Q \int_{Q0}^{Q} = -\alpha\sqrt{t}\int_{t0}^{t}$, which gives us:

$\ln Q - \ln Q_0 = -2\alpha\left(\sqrt{t} - \sqrt{t0}\right)$. Therefore:

$$Q(t) = Q_0 \cdot e^{\left(-2\alpha\sqrt{t}\right)}$$

To determine the parameters of the models and thus be able to fit these to the recession curves, the procedure involved determining a beginning coordinate for the beginning of the recession flows (t_0, Q_0). A second coordinate was then included to calculate the depletion coefficients of the models. In addition, exponential model 2 requires a third coordinate to satisfy the system of equations.

The models were validated using different tests and non-parametric statistical indicators. The statistical validation stage was based on the results from the 25 floods selected for the four models proposed. The following indicators and statistical tests were used.

a) Coefficient of Determination (R^2)

This coefficient, also known as the Nash-Sutcliffe, determines the proportion of the total variation of the observed flows (independent variables) that is explained by the modeled flows (dependent variable). It is determined as follows:

$$R^2 = 1 - \frac{\sum(yi - \hat{y}i)^2}{\sum(yi - \bar{y}i)^2}$$

yi: observed flows
$\bar{y}i$: average of the observed flows
$\hat{y}i$: modeled flows (5)

b) Standard Error of the Estimation (SEE)

Determines the average difference between observed and calculated flows, where values near 0 indicate that the model provides a good description of the flows, according to the indicator formula:

$$SEE = \sqrt{\frac{\sum(y - \hat{y})^2}{n-2}}$$

y: observed flows
$\hat{y}$: modeled flows
n: number of flow data (6)

c) Mann-Whitney U Test

This test determines whether two independent samples come from the same population (Montgomery & Runger, 1996; Mendenhall & Sincich, 1997). In addition, because it is a non-parametric test, normality and equality of variances are not required (Mason & Lind, 1995).

The null hypothesis and the alternative are established:

H_0: the distributions of variables R_1 and R_2 are identical.
H_a: the distributions of variables R_1 and R_2 are not identical.

Where R_1 corresponds to the real data and R_2 to the modeled data:

$$Ua = (n_1 \cdot n_2) + \left(\frac{n_1 - n_2 + 1}{2}\right) - \sum R_1$$ for small samples (n_1 and $n_2 < 25$) (7)

$$Z = \frac{\sum R_1 - \sum R_2 - \left[(n_1 - n_2)\cdot\left(\frac{n_1 + n_2 + 1}{2}\right)\right]}{\sqrt{n_1 \cdot n_2\left(\frac{n_1 + n_2 + 1}{3}\right)}}$$ for large samples (n_1 and $n_2 > 25$) (8)

Where:

n_1: size of sample R_1; n_2: size of sample R_2; $\sum R_1$: sum of the ranges for sample R_1; $\sum R_2$: sum of the ranges for sample R_2.

Decision rule: H_0 is rejected at a level of significance of α if:

$$Z \geq |Z\alpha|$$ (9)

Where Zα: critical value obtained from the standard normal table at a level of significance α of 0.05 and 0.01.

d) Bland and Altman agreement test

This test determines whether the estimation models have enough agreement to be interchangeable (Carrasco & Jover,2004; Cox, 2006). In statistical terms, the average differences (*dp*) between the real and estimated values are calculated, which represents the systematic error, while the variance of the differences (*DS*) measures inaccuracy. The 95% confidence levels are thereby established (Carrasco & Jover, 2004; Paradis, Lefebvre, Morin, & Gloaguen, 2010). This is defined by the expression:

$$LC = dp \pm 2 \cdot DS$$ (10)

Therefore, the relationship of real versus estimated values with the *dp* nearest zero in

absolute values will be the best fit. If an equality or a small difference in the *dp* value exists, the best fit will correspond to the one with the lowest *DS* value and its confidence levels will be narrower (Bland & Altman, 1999).

Results and Discussion

As a visual example, Figure 3 presents two different floods with their respective models (adjusted for all the data) and real flows, in order to show the large differences between models.

Table 1 shows the average depletion coefficients (α) for the four models proposed for the five periods and 25 floods.

In Table 1, the value of the depletion coefficient is observed to decrease as the estimation time increases, since by increasing the fit time (differential) the slope between the first and last points decreases.

For exponential model 2, the depletion coefficient increased as estimation times increased. This is because its value increases when raising time *t* to the "n" in the calculation formula. The coefficients resulting from this model were higher than the other three models.

The values of the coefficients in exponential model 3 were stable. This model also has the lowest variation coefficient, and therefore it could be a well-fitted model.

On the other hand, with parameter "n" in exponential model 2, there is an increase as the estimation time increases —0.4834 for 240 hours and 0.4940 for the total number of hours of the flood (average values). The results obtained agree with the behavior of parameter α. This may be because when parameter "n" increases, the depletion coefficient (α) also increases (according to the calculation formula).

Table 2 summarizes the results for the average coefficient of determination (R^2), the

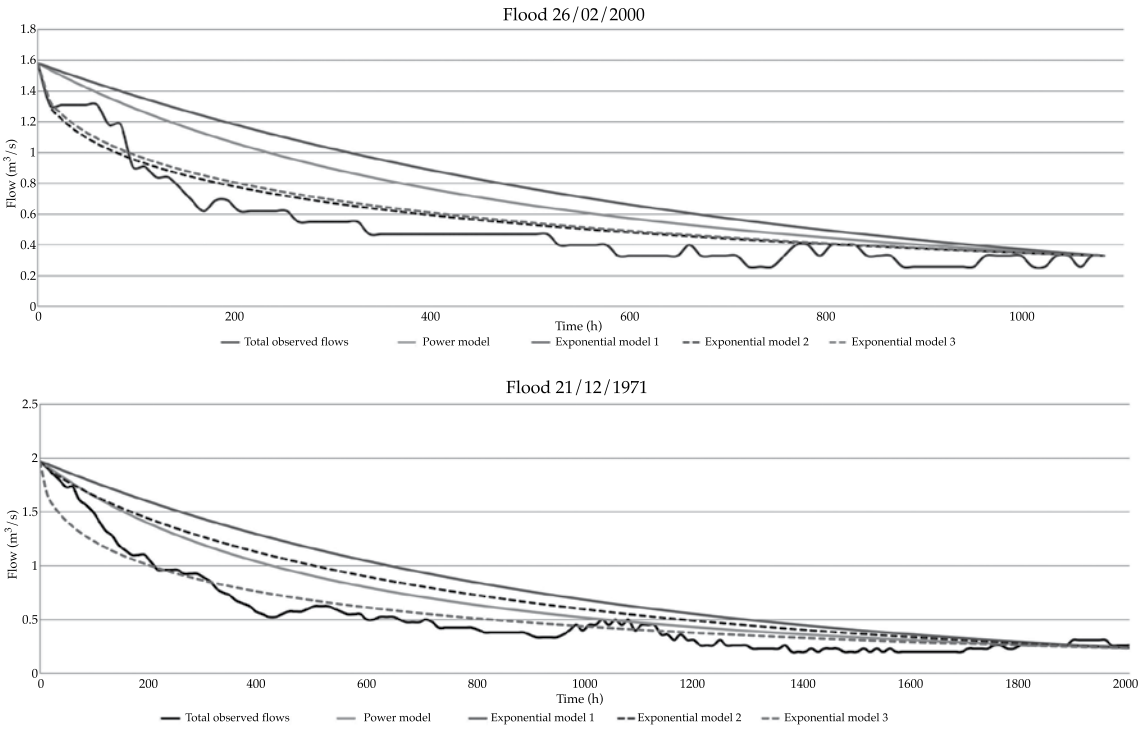

Figure 3. Example of floods with the four models used.

Table 1. Depletion coefficient (α).

		α (240 h)	α total (*)
Power model	Average	0.0021	0.0012
	Variation Coef.	0.7437	0.8070
Exponential model 1	Average	0.0031	0.0015
	Variation Coef.	0.6281	0.9102
Exponential model 2	Average	0.0244	0.0224
	Variation Coef.	0.6281	0.4604
Exponential model 3	Average	0.0244	0.0224
	Variation Coef.	0.6269	0.4601

(*) Includes the total available data; α, depletion coefficient.

Table 2. Results from statistical tests: R2, SEE and Mann-Whitney.

Test	R^2		SEE		U Mann-Whitney	
Model	α (240 h)	α total (*)	α (240 h)	α total (*)	α (240 h)	α total (*)
Power	0.22	0.49	1.27	1.45	4%	20%
Exponential 1	0.08	0.3	1.47	1.83	4%	20%
Exponential 2	0.16	0.53	1.51	1.24	0%	32%
Exponential 3	0.28	0.59	1.2	1.1	0%	44%

(*) Includes the total available data; α, depletion coefficient.

standard error of the estimation (SEE), the Mann-Whitney U test and the Bland-Altman for the four models proposed, for the two periods considered and 25 floods included in the study.

Table 2 shows that the highest average R^2 values are mostly found for the total data. This may be due to the sensitivity of the R^2 calculation formula to changes in the denominator. Nevertheless, the values for the coefficient of determination were very low and do not appear to adequately represent the behavior of the mathematical models used. In addition, exponential model 3 resulted in the highest coefficient for all the data available, although the values were low overall. In terms of R^2, the power model obtained the best results, followed by exponential model 3.

Exponential models 1 and 2 have the lowest average and their values are irregular, with no clear trend. Exponential model 1 had the lowest coefficient of determination values, indicating its use does not appear adequate.

For the case of the SEE (Table 2), the lowest average values (80% of them) are found in exponential model 3. Exponential model 1 had the highest SEE values, indicating that this model would not accurately represent the behavior of recession flows in the study basin.

The SEE values decrease as estimation time increases, which could confirm the hypothesis that the longer the duration time the better the fit of the model.

The results obtained with the Mann-Whitney U test, calculated with a significance level of 5% (Table 2), show that the total data contains the largest percentage of approved tests, with the best results provided by exponential model 3, closely followed by the power model. Exponential model 1 was discarded as a predictor of recession flows, having obtained the least satisfactory results with this test.

Lastly, the low results obtained with the Mann-Whitney U test can be explained by the level of significance used, which contains a

small range of acceptance and, therefore, is a very strict test.

In the case of the Bland and Altman test, it is worth mentioning that this was chosen considering the fact that its creators as well as other investigators disagree about the reliability of the R^2 coefficient of determination, since when two different instruments systematically measure different amounts, the correlation can be perfect even when the agreement is null (Pita & Pértegas, 1998).

Table 3 shows the results obtained for the average differences (*dp*) and the variance of the differences (*DS*) for the four models used.

According to Table 3, with respect to the average differences, the best model is exponential model 2, followed by exponential model 3. Nevertheless, the standard deviation of the differences clearly shows that exponential model 3 is better.

Exponential model 1 is again discarded as a predictor model due to the poor results obtained from the average differences, the standard deviation of the differences and the overall statistical validation.

For an even more in-depth analysis of the models, real averages of the floods were compared. To this end, the quotient between the standard error estimation and the real average flows for the 25 floods estimated was considered. That is, values near 0 represent a small proportion, and indicate the best fit. This is presented in Table 4.

As seen in Table 4, exponential model 3 had the best results —that is, the lowest quotient between the SEE and the average observed flows.

For the case of the remaining models, the results from exponential models 1 and 2 were not satisfactory, and model 1 had the lowest quality, again corroborating that it is not an adequate model for the watershed studied.

With regard to the time period, in general, the one corresponding to the total data available provided the best results. In addition, no notable evidence exists regarding

Table 3. Average differences (*dp*) and variance of the differences (*DS*) for the four models analyzed..

Model	*i*	**α (240 h)**	**α total (*)**
Power	*dp*	0.637	-0.557
	DS	0.765	1.052
Exponential 1	*dp*	0.903	-1.05
	DS	0.813	1.242
Exponential 2	*dp*	0.149	-0.104
	DS	0.819	0.975
Exponential 3	*dp*	0.187	0.035
	DS	0.758	0.912

(*) Includes the total available data; α, depletion coefficient; *i*, statistical indicator.

Cuadro 4. Cociente entre el EEE y el promedio de caudales observados de las crecidas seleccionadas.

Model	**α (240 h)**	**α total (*)**
Power	0.44	0.51
Exponential 1	0.51	0.65
Exponential 2	0.52	0.44
Exponential 3	0.41	0.39

(*) Includes the total available data;; α, depletion coefficient.

whether any particular period provides poor results, according to the statistics mentioned previously. Nevertheless, the Bland and Altman tests show the period corresponding to 240 hours (10 days) provides the best results.

Conclusions

Given the importance of correctly modeling this type of flow, especially in arid and semi-arid Mediterranean regions, this type of study is vitally important to planning for extreme events. In the case of water scarcity, it enables calculating the volume available after a flood and regulating the functioning of the reservoir, among other actions.

According to the results, exponential model 3 provides the best results when estimating recession flows in the Upeo Estuary watershed, in Upeo, Chile.

The best time period for the calculation of parameter α was determined to be the total data for each flood, as expected, having substantially obtained the best results. Nevertheless, with the Bland and Altman test, the best period was 240 hours. Given the recognized potential of this test, it is concluded that the best estimation period corresponds to 240 hours.

Lastly, the proposed model must respond to the behavior of similar flows and watersheds, and in the case of Chile, many have similar geomorphological characteristics.

References

Aparicio, F. (2003). *Fundamentos de hidrología de superficie* (303 pp.). México, DF: Editorial Limusa.

Bedient, P., & Huber, W. (2002). *Hidrology and Floodplain Analysis* (692 pp.). 3th. ed. New York: Adisson-Wesley Pub. Co.

Bland, J. M. & Altman, D. G. (1999). Measuring Agreement in Method Comparison Studies. *Statistical Methods in Medical Research*, *8*, 135-160.

Brodie, R., Hostetler, S., & Slatter, E. (2007). *Q-Lag: A New Hydrographic Approach to Understanding Stream-Aquifer Connectivity. Canberra, Australy*. Consultado el 12 de noviembre de 2007. Recuperado de http://www.affashop.gov.au/PdfFiles/q-lag.pdf.

Brooks, J. R., Barnard, H. R., Coulombe, R., & Mcdonnell, J. J. (2009). Ecohydrologic Separation of Water between Trees and Streams in a Mediterranean Climate. *Nature Geoscience*, *3*, 100-104.

CNR (1978). *Estudio integral de riego de la cuenca del río Mataquito: prefactibilidad*. Santiago, Chile: Comisión Nacional de Riego.

Carrasco, J., & Jover, L. (2004). Métodos estadísticos para evaluar la concordancia. *Med. Clin. (Barc.)*, *122*(1), 28-34.

Cirugeda, J. (1985). *Curso Internacional de Hidrología General y Aplicada* (pp. 66-77). Madrid: Centro de Estudios y Experimentación de Obras Públicas, Gabinete de Formación y Documentación.

Cox, N. (2006). Assessing Agreement of Measurement and Predictions in Geomorphology. *Geomorphology*, *76*(3-4), 332-346.

Estrela, T. (1992). *Modelación matemática para la evaluación de los recursos hídricos* (55 pp.). Madrid: Centro de Estudios Hidrográficos, Ministerio de Obras Públicas.

Hewlet, J. D., & Hibbert, A. R. (1967). Factors Affecting the Response of Small Watersheds to Precipitation in Humid Areas. *Progress in Physical Geography*, *33*(2), 288-293.

Linsley, R., Kohler, M., & Paulhus, J. (1949). *Applied Hydrology* (pp. 398-404). New York: McGraw Hill Civil Engineering Series.

Maidment, D. (1992). *Handbook of Hydrology* (147 pp.). New York: McGraw-Hill, Inc.

Mason, R. D., & Lind, D. A. (1995). *Estadística para administración y economía*. México, DF: Alfaomega.

Mendenhall, W., & Sincich, T. (1997). *Probabilidad y estadística para ingeniería y ciencias* (1176 pp.) 4a. ed. México, DF: Prentice-Hall Hipanoamericana.

Montgomery, D., & Runger, G. (1996). *Probabilidad y estadística aplicadas a la Ingeniería* (895 pp.) México, DF: Editorial McGraw-Hill.

Paradis, D., Lefebvre, R., Morin, R., & Gloaguen, E. (2010). Permeability Profiles in Granular Aquifers Using Flowmeters in Direct-Push Wells. *Ground Water*, *49*(4), 534-547.

Pita, S., & Pértegas, S. (1998). *La fiabilidad de las mediciones clínicas, el análisis de concordancia para variables numéricas*. La Coruña, España: Unidad de Epidemiología Clínica y Bioestadística, Complexo Hospitalario-Universitario Juan Canalejo.

Pizarro, R., Balocchi, F., Garcia, P., Macaya, K., Bro, P., León, L., Helwig, B., & Valdés, R. (2013). On Redefining the Onset of Base Flow Recessions on Storm Hydrographs. *Open Journal of Modern Hydrology*, *3*, 269-277.

Pizarro, R. (1993). *Elementos técnicos de hidrología III. Proyecto Regional mayor sobre el uso y conservación de recursos hídricos en áreas rurales de América Latina y el Caribe* (133 pp.). Talca, Chile: UNESCO-ORCYT, Uruguay, Ediciones Universidad de Talca.

Ponce, V. (1989). *Engineering Hydrology, Principles and Practices* (640 pp.). New Jersey: Editorial Prentice-Hall.

Remenieras, G. (1971). *Tratado de Hidrología Aplicada* (515 pp.). Madrid: Editores Asociados.

Smakhtin, V. U. (2001). Estimating Continuous Monthly Base Flow Time Series and their Possible Applications in the Context of the Ecological Reserve. *Water SA*, *27*(2), 213-217.

Sujono, J., Shikasho, S., & Hiramatsu, K. (2004). A Comparison of Techniques for Hydrograph Recession Analysis. *Hydrological Processes*, *18*, 403-413.

Viessman, W., & Lewis, G. (2003). *Introduction to Hydrology* (612 pp). 5th edition. Englewood Cliffs, USA: Prentice Hall.

Vilaró, F. (1976). *Elemento de hidrología de superficie. Hidrología subterránea* (385-398 pp.). Tomo I. Barcelona: Ediciones Omega S. A.

Wittenberg, H. (1999). Base Flow Recession and Recharge as Nonlinear Storage Processes. *Hydrological Processes*, *13*, 715-726.

Institutional Address of the Authors

Ing. Francisco Balocchi

University of Arizona
Department of Hydrology and Water Resources
1133 E James E. Rogers Way
Tucson, Arizona, USA
Teléfono: +1 (520) 6213 131
fbalocchi@email.arizona.edu

Ing. Francisco Balocchi
Dr. Roberto Pizarro
M.C. Carolina Morales

Centro Tecnológico de Hidrología Ambiental
Universidad de Talca
Casilla 747
Talca, Chile
Teléfono +56 (71) 2200 375
fbalocchi@utalca.cl
rpizarro@utalca.cl
camorales@utalca.cl

Ing. Claudio Olivares

Dirección General de Aguas
Ministerio de Obras Públicas
Riquelme 465
Block B, piso 3, Coyhaique
Teléfono +56 (67) 2572 266
claudio.olivares@mop.gov.cl

Click here to write the autor

Technical Note

Evaluation of Probabilistic Model Selection Criteria: Validation with Series of Simulated Maxima

• Roberto S. Flowers-Cano* • Robert Jeffrey Flowers • Fabián Rivera-Trejo •
Universidad Juárez Autónoma de Tabasco, México
*Corresponding Author

Abstract

Flowers-Cano, R. S., Flowers, R. J., & Rivera-Trejo, F. (September-October, 2014). Evaluation of Probabilistic Model Selection Criteria: Validation with Series of Simulated Maxima. *Water Technology and Sciences* (in Spanish), 5(5), 181-189.

In this paper, a Monte Carlo study is performed to determine the validity of using the root mean square error as a selection criterion for the frequency analysis. This statistic is compared to those from the Kolmogorov- Smirnov, the Cramer-Von Mises and the Anderson-Darling tests. The distributions chosen to compare these statistics are gamma, Weibull, Gumbel, log-normal and log-logistic. The results obtained by this study indicate that at least 50 random observations are needed to obtain good results using either the Anderson-Darling or root mean square error statistics. The Kolmogorov-Smirnov and Cramer-Von Mises tests are not recommended since they require sample sizes larger than those usually found in hydrology.

Keywords: Root mean square error, Kolmogorov- Smirnov, Cramer-Von Mises, Anderson-Darling.

Resumen

Flowers-Cano, R. S., Flowers, R. J., & Rivera-Trejo, F. (septiembre-octubre, 2014). Evaluación de criterios de selección de modelos probabilísticos: validación con series de valores máximos simulados. Tecnología y Ciencias del Agua, *5(5), 181-189.*

Se realizó un estudio de Monte Carlo para determinar la validez del empleo de la prueba del error estándar de ajuste como criterio de selección en el análisis de frecuencias. Dicho estadístico se comparó con los estadísticos de prueba de Kolmogorov-Smirnov, Cramer-Von Mises y Anderson-Darling. Las distribuciones elegidas para el propósito de comparar estos estadísticos fueron la gamma, Weibull, Gumbel, log-normal y log-logística. Los resultados obtenidos recomiendan el uso de muestras con tamaño de por lo menos n = 50 para tener un buen desempeño de las pruebas de Anderson-Darling y error estándar de ajuste. El empleo de las pruebas de Kolmogorov-Smirnov y Cramer-Von Mises no es del todo recomendable en hidrología, ya que para obtener un desempeño aceptable se necesitan muestras más grandes de las que normalmente se tienen en esta disciplina.

***Palabras clave**: error estándar de ajuste, Kolmogorov-Smirnov, Cramer-Von Mises, Anderson-Darling.*

Received: 14/10/12
Accepted: 12/02/14

Introduction

The design of control and exploitation works requires an analysis of the frequency of extreme hydrological events to calculate the probability that these events will occur. When designing hydrological works, the return period of an event often exceeds the period of observation and information must therefore be extrapolated based on recorded values. The use of graphs is one way to extrapolate historical data, which requires an experienced analyst and has the disadvantage of being subjective. A more objective technique is to determine the theoretical probability distribution that best fits the measured data and use this function for the extrapolation. Some of the probability distributions used in hydrology are normal, log-normal, gamma, Gumbel, Weibull, Pearson type III and log-Pearson type III (Aksoy, 2000;Aparicio-Mijares, 2005). A significant problem in the analysis of frequencies is the

selection of a probability distribution that is suitable for the observed data. This problem is not unique to hydrology but is also observed in other areas, such as reliability and actuary sciences. Quesenberry and Kent(1982) developed a distribution selection criterion based on statistics that do not vary with changes in scale. They demonstrated the effectiveness of their criterion by conducting a Monte Carlo study to distinguish among exponential, gamma, Weibull and log-normal distributions. Generally, models are selected using goodness-of-fit tests, which include graphic and statistical methods, the latter being preferred due to their objectivity (Shin, Jung, Jeong, & Heo, 2011). Chi-squared (x^2) and adjusted standard error (ASE) are two statistical methods most commonly used in hydrology (Ganancias-Martínez, 2009). The empirical distribution function is another method which is often used. This includes the Kolmogorov-Smirnov (KS), Cramer-Von Mises (CVM) and Anderson-Darling (AD) (for example, Laio, 2004; Suhaila & Jemain, 2007; Dan´azumi, Shamsudin, & Aris, 2010; Shin *et al*., 2011; Atroosh & Moustafa, 2012). Nevertheless, statistical tests for goodness-of-fit are not very capable of rejecting wrong distributions (Mitosek, Strupczewski, & Singh, 2002) and, therefore, in many cases a particular test may accept more than one distribution (Laio, Baldasarre, & Montanari, 2009). In this case, the concept of model selection criteria represents an alternative to goodness-of-fit tests. Various selection criteria can be defined according to the goodness-of-fit statistics just mentioned. Other selection criteria area based on likelihood functions, such as the Akaike information criterion (AIC) and the Bayesian information criterion (BIC) (Laio *et al*., 2009). Balasooriya, Low and Wong (2005) evaluated the effectiveness of the Akaike and the Quesenberry and Kent criteria. They found that while both performed well, the latter performed slightly better. Nevertheless, because of the computational difficulty of this criterion the use of the AIC preferable. Selection criteria for probabilistic models have received little attention in the hydrology literature. Mitosek *et al.*(2002) considered the Weibull, gamma, Gumbel and log-normal distributions as options for the distribution of annual peak flows, and evaluated these distributions using three indices: mean absolute deviation, mean squared and normalized likelihood function. After the Monte Carlos study was performed, they concluded that the normalized likelihood function represented the best selection criteria. Adlouni, Bobée and Ouarda (2008) used graphic techniques to select the type of distributions that provided the best fit to a set of data. They used the Werner and Upper (2002) classification criterion, dividing the distributions according to: a)stable; b)with a Pareto tail; c) changing regularly; d) sub-exponential; and e) non-existent exponential moments. The authors proposed the use of graphic methods to determine the class of the distribution and then used criteria such as the AIC, BIC and the AD to select the distribution with the best fit. Meanwhile, Laio *et al*. (2009) analyzed the performance of the AIC, BIC and AD model selection criteria to identify the probabilistic model with the best fit for extreme hydrological data. The performance of these criteria was compared to synthetic data. There was no clear winner among the three, but they were observed to be more effective when the distribution used to generate the synthetic data had two parameters instead of three. Di Baldasarre, Laio and Montanari (2009) extended the Laio *et al*. (2009) analysis and demonstrated that the use of model selection criteria performed better than a fixed probabilistic model to calculate design floods for a hydraulic work. A procedure similar to that by Laio *et al.* (2009) was used in this work. Synthetic data for a known distribution were used to compare the performance of different selection criteria (AD, KS, CVM and ASE). Nevertheless, only distributions with two parameters were used for maximum effectiveness (Laio *et al*., 2009; Haddad & Rahman, 2011; Markiewicz, Strupczewski, &

Kochanek, 2010). The result was a comparison of the performance of the ASE, recommended by Aparicio-Mijares (2005) versus the other criteria commonly used in applied statistics. The results show that the performance of the ASE was comparable to that of AD and better than the KS and CVM tests. In addition, the two latter tests were found not to be entirely recommendable for hydrology since samples larger than those normally found in this field are required for their acceptable performance.

Materials and Methods

Comparison of Selection Criteria

A numerical analysis was conducted to compare the performance of the different selection criteria for probabilistic models. The criteria considered were the adjusted standard error (ASE), Cramer-Von Mises (CVM), Kolmogorov-Smirnov (KS) and Anderson-Darling (AD). The analysis was performed with a series of Monte Carlo experiments which consisted of the following steps: a) choosing the following mother probability distributions: Gumbell, Weibull, gamma, log-normal (consult Haan (1994) for these four) and log-logistic (consult Dey and Kundu (2009)) and probability density functions (PDF); b) generating 80 000 random samples from the mother distributions, using samples sizes of n = 30, 50, 80 and 100; c) fitting the distributions of interest to the data generated and estimating the parameters based on the maximum likelihood method; d) calculating the AD, CVM, KS and ASE statistics for each of the distributions; e) for each criterion, selecting the distribution resulting in the smallest value, and if the distribution selected was equal to the mother distribution, the criterion was considered successful.

Parameters of the Distributions

The parameters of the mother distributions are shown in Table 1. These are based on the estimators by De Dios-Lara(1998).

Table 1. Parameters of the distributions used to generate synthetic data. α: form; β: scale; θ: location.

Distribution	Parameters	
Gamma	α	β
	6.17	12.75
	14.39	11.51
	12.42	13.56
	10.19	9.29
Weibull	α	β
	2.77	106.1
	4.03	152.8
	2.09	121.6
	2.25	115.5
Gumbel	θ	β
	142.33	22.73
	157.20	43.48
	94.48	37.04
	79.86	28.57
Log-normal	θ	β
	5.09	0.449
	4.80	0.356
	4.66	0.370
	4.50	0.311
Log-logística	θ	β
	4.79	0.237
	4.91	0.280
	4.68	0.180
	4.66	0.303

Model Selection Methods

The model selection criteria used in this work were based on the calculation of the ASE, KS, CVM and AD statistics. The mathematical form of the ASE can be found in Raynal-Villaseñor (2013). For the other statistics, consult Suhaila and Jemain (2007).

Sensitivity Study

A sensitivity study was performed to determine the effect of the use of a selection criterion on the estimation of the quantile x_T; that is, the value associated with return period T. For this study, Monte Carlo tests were performed as follows: a) one of the five distributions mentioned previously was selected as the mother

distribution; b) the value x_T of the mother distribution corresponding to return period T was calculated. The values of T considered were 10 and 100 years, the former representing interpolation and the second extrapolation; c) 400 000 samples of the mother distribution were generated with samples sizes $n = 30$ and $n = 50$, and the parameters shown in Table 1 were used; d) the five distributions of interest were fitted to the data from each sample using the maximum likelihood method; e) the values of the AD, CVM, KS and ASE criteria were calculated for each of the five distributions; f) for each criterion, the distribution which resulted in the smallest value was selected; g) the distribution selected for each criterion was used to calculate the INSERTAR SIMBOLO estimator of x_T; h) for the set of ADx_T values, the relative root mean squared error (δRMSE) and the relative bias (δS) were calculated using the following expressions (Markiewicz *et al.*, 2010):

$$\delta RECM = \sqrt{\frac{E\left(\hat{x}_T - x_T\right)^2}{x_T}} \quad (1)$$

$$\delta S = \frac{E\left(\hat{x}_T - x_T\right)}{x_T} \quad (2)$$

where x_T is the "real" quantile value obtained from the mother distribution; $\hat{x}_T$ is an estimator of x_T and E indicates the expected value.

Results

Comparison of the Selection Criteria

The results are shown in Table 2. The percentage of correct selections (PCS) are observed for each of the simulation scenarios generated. The PCS is the number of times that the selection criterion correctly identified the mother distribution, divided by the total number of selections. The five distributions were analyzed, for which the randomly assigned PCS would be 20%. Therefore, a good selection criterion would be above 20%. Table 2 shows the PCS increasing with n for a mother distribution and a specific set of parameters. The AD criterion is also seen to be somewhat better when the mother distribution is log-normal, gamma or Weibull, while the ASE is better when the mother distribution is Gumbel, and the CVM is better when the mother distribution is log-logistic (see Figure 1). In general, the AD seems to be the winning criterion, followed by the ASE, while KS seems to have the lowest power of selection. This figure also shows that the PCS varies not only according to the selection criterion and n but also in function of the mother distribution. All the criteria considered perform better with a Weibull or log-logistic mother distribution than with gamma, Gumbel or log-normal (see Figure 2).

This is due to the difficulty they have discriminating among similar distributions. The resulting PCS depends on the distributions to be compared. If the Weibull distribution is substituted with log-gamma, the PCS for the other distributions would be lower. Table 2 and the graphs show that if the size of the sample is small, then the selection criteria are similar. If two models make very similar predictions, it does not matter which one is chosen; rather, it is important to be able to distinguish among distributions that differ considerably, since they could make very different predictions.

Sensitivity Study

The results of the sensitivity study are summarized in Table 3.

The δRMSE and δS of the estimators obtained with the models selected based on the different criteria are shown. For each mother distribution, the values of all the sets of parameters used were averaged and classified according to the sample size and the return period used in the simulation. The following is observed:

a) The magnitude of δRMSE increases with the return period and decreases as the

Table 2. Percentage of correct selection (PCS) for different mother distributions.

Parameters	ASE				KS				CVM				AD			
	n 30	*n* 50	*n* 80	*n* 100	*n* 30	*n* 50	*n* 80	*n* 100	*n* 30	*n* 50	*n* 80	*n* 100	*n* 30	*n* 50	*n* 80	*n* 100
Gamma distribution																
$\alpha = 6.17$ $\beta = 12.75$	15.00	24.40	31.20	41.10	16.80	21.36	28.57	32.80	18.60	24.73	35.96	37.06	21.90	23.67	43.00	46.00
$\alpha = 14.39$ $\beta = 11.51$	14.50	27.20	39.40	45.00	14.89	22.80	29.40	34.70	17.08	27.07	32.97	38.86	20.60	32.80	42.70	48.00
$\alpha = 12.42$ $\beta = 13.56$	16.70	28.10	40.80	44.90	16.98	22.60	29.60	32.70	16.97	25.80	32.60	38.76	23.20	32.90	42.16	48.30
$\alpha = 10.19$ $\beta = 9.29$	17.00	28.50	40.50	45.10	20.40	22.26	29.24	34.13	20.48	25.87	33.40	40.80	25.87	32.30	43.30	50.40
Weibull distribution																
$\alpha = 2.77$ $\beta = 106.1$	62.00	70.10	80.90	82.90	56.10	64.17	72.43	77.10	64.10	69.80	76.82	81.00	69.30	75.40	82.40	85.50
$\alpha = 4.03$ $\beta = 152.8$	78.10	80.70	89.90	90.20	60.64	66.50	74.80	78.90	69.30	73.20	80.92	82.30	77.30	78.30	88.00	87.20
$\alpha = 2.09$ $\beta = 121.6$	47.20	53.10	61.90	68.10	46.75	56.39	64.00	70.40	57.54	62.21	68.10	72.30	55.30	62.40	67.70	73.90
$\alpha = 2.25$ $\beta = 115.5$	49.40	60.70	67.60	76.00	50.55	61.30	65.80	70.80	58.34	65.10	72.16	73.83	56.80	68.20	73.80	77.60
Gumbel distribution																
$\theta = 142.33$ $\beta = 22.73$	73.20	82.30	83.90	85.80	35.20	46.70	61.86	62.48	47.15	56.60	63.74	69.20	59.40	66.10	71.66	74.70
$\theta = 157.20$ $\beta = 43.48$	33.87	38.50	31.70	30.60	19.58	26.70	31.34	33.63	19.94	28.24	36.26	36.43	24.88	34.00	42.20	43.20
$\theta = 94.48$ $\beta = 37.04$	12.30	12.20	14.30	16.60	8.90	10.08	13.39	14.07	7.69	7.68	10.58	11.80	9.30	10.10	11.40	15.90
$\theta = 79.86$ $\beta = 28.57$	16.30	11.70	12.00	13.30	11.80	12.57	14.20	14.79	10.26	9.49	12.59	11.49	10.20	9.30	14.30	14.90
Log-normal distribution																
$\theta = 5.09$ $\beta = 0.449$	36.90	31.00	32.10	34.70	20.00	27.17	31.94	34.07	23.28	32.83	37.60	40.30	28.67	39.40	43.10	44.30
$\theta = 4.80$ $\beta = 0.356$	31.50	24.80	24.90	30.20	15.18	19.86	23.80	29.81	19.10	21.44	25.57	34.06	23.50	27.10	31.07	39.56
$\theta = 4.66$ $\beta = 0.370$	33.00	28.40	27.80	30.70	14.96	19.40	28.50	30.07	20.58	24.05	33.67	33.57	24.88	28.60	37.10	40.36
$\theta = 4.50$ $\beta = 0.311$	24.80	19.70	22.38	23.90	14.29	17.63	18.48	22.58	14.29	18.40	20.46	24.15	18.70	21.10	22.90	27.60
Log-logistic distribution																
$\theta = 4.79$ $\beta = 0.237$	31.80	56.50	68.50	73.50	57.19	59.54	65.53	66.97	60.56	62.00	67.10	69.23	57.50	58.30	66.40	68.70
$\theta = 4.91$ $\beta = 0.280$	34.90	53.30	70.20	74.30	53.25	64.07	65.73	61.70	57.49	65.10	68.33	65.20	61.11	63.14	66.50	65.50
$\theta = 4.68$ $\beta = 0.180$	22.60	40.70	58.20	66.90	54.25	57.94	64.10	67.90	56.54	61.20	64.30	69.70	52.40	57.60	61.50	66.50
$\theta = 4.66$ $\beta = 0.303$	38.90	52.40	68.80	70.40	57.50	58.84	65.00	69.80	57.34	62.24	65.90	70.60	54.80	61.30	64.90	69.90

sample size increases. This was expected since the variance of the estimators of x_T increases when T increases and decreases when n increases (Silva *et al.*, 2011).

b) When the mother distribution is log-logistic and for $T = 10$, the magnitudes of δRMSE and δS associated with the ASE criterion are significantly larger than for the other criteria.

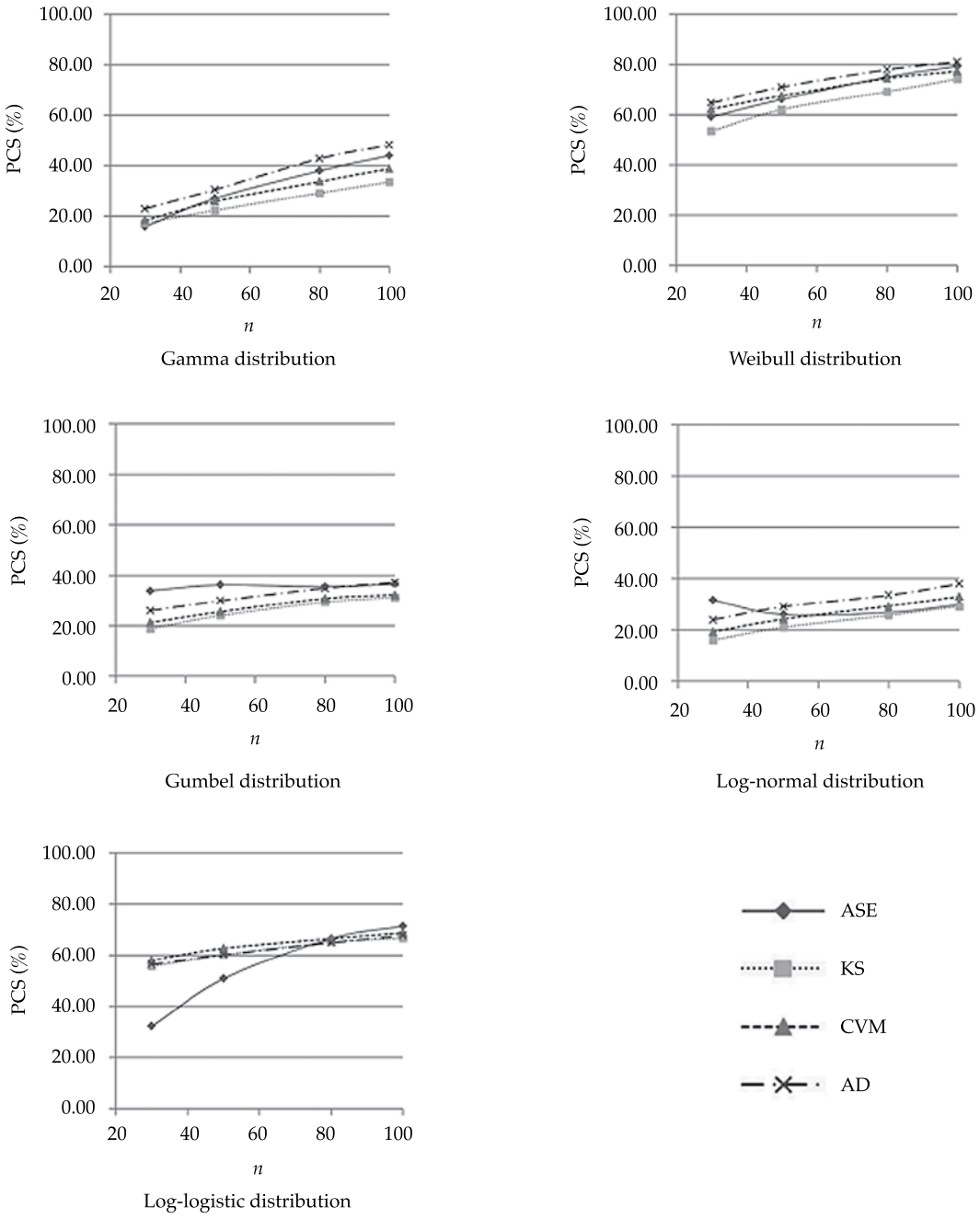

Figure 1. Graphs of the percentage of correct selections (PCS) for the different model selection criteria versus the size, n, of the sample.

c) The smallest δRMSE values indicate that the $\hat{x}_T$ estimators are closer to the real value of x_T.

d) In general, no large differences among the criteria were observed for $T = 10$.

e) For $T = 100$, the AD criterion tends to produce the most accurate estimations, which tend to be smaller than the other criteria analyzed.

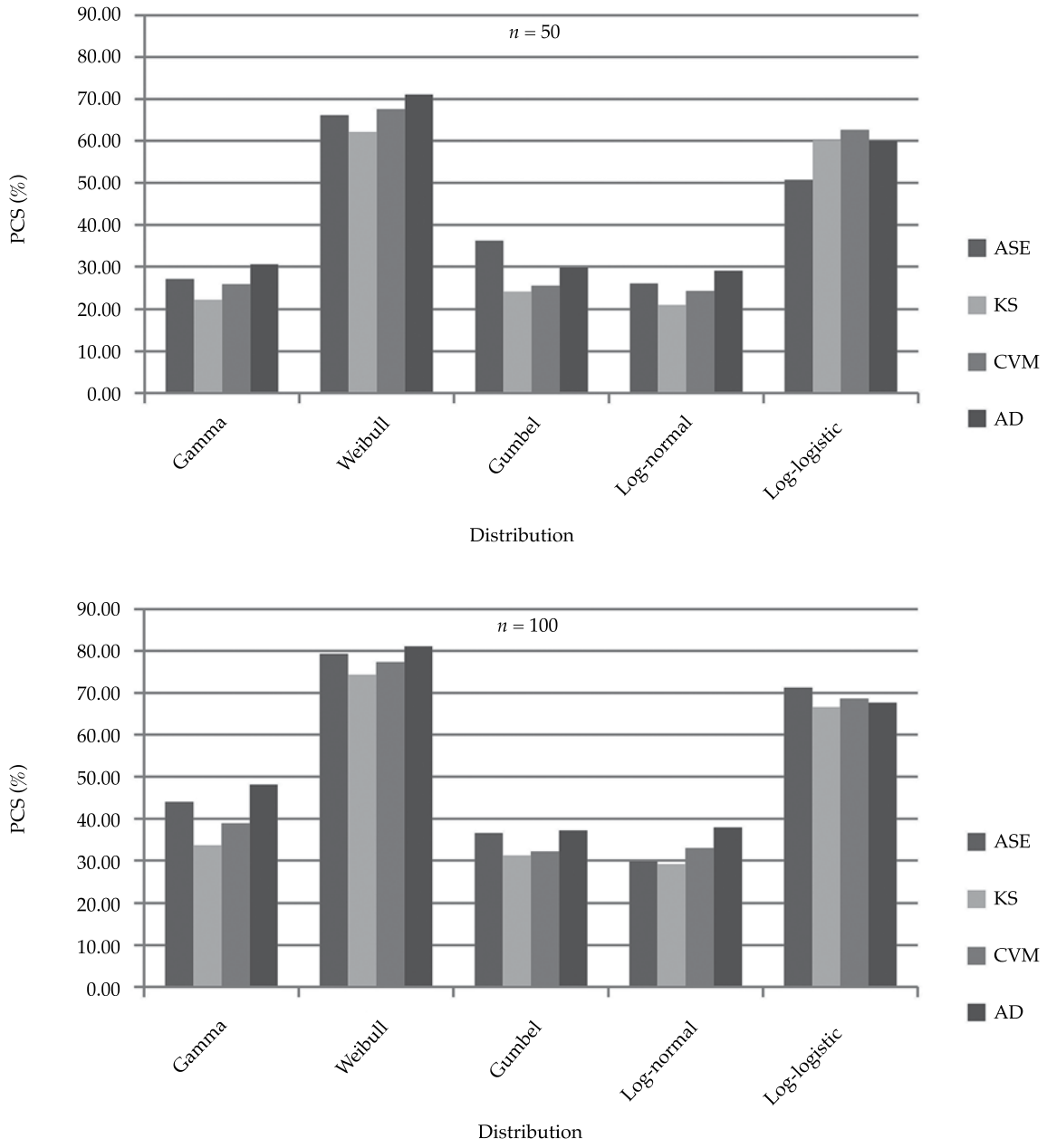

Figure 2. PCS obtained with the different selection criteria for different mother distributions.

Conclusions

The simulations show that selection criteria help to choose the best distribution for a frequency analysis. Of the criteria analyzed, the best was AD, followed by ASE. It was also observed that it was difficult to discriminate between two similar distributions. The percentage of correct selections (PCS) depends on the size, n, of the sample and the distribution of the data generated. In general, the AD criterion results in better estimations for $T = 100$, even when it does not choose the correct distribution. In addition, it tends to produce smaller estimations than the

Table 3: δRMSE and δS obtained for different mother distributions.

Sample size	Return period	ASE		KS		CVM		AD	
		δRMSE	δS	δRMSE	δS	δRMSE	δS	δRMSE	δS
Gamma distribution									
30	10	0.071	-0.007	0.071	-0.009	0.071	-0.011	0.070	-0.012
30	100	0.153	0.038	0.153	0.037	0.150	-0.033	0.115	-0.010
50	10	0.055	-0.004	0.055	-0.004	0.055	-0.006	0.054	-0.006
50	100	0.128	0.040	0.132	0.040	0.130	0.038	0.096	-0.001
Weibull distribution									
30	10	0.076	-0.004	0.086	0.007	0.078	-0.003	0.075	-0.008
30	100	0.183	0.069	0.297	0.131	0.213	0.081	0.131	0.030
50	10	0.058	-0.003	0.065	0.006	0.060	0.000	0.057	-0.004
50	100	0.123	0.040	0.229	0.096	0.175	0.062	0.104	0.024
Gumbel distribution									
30	10	0.078	-0.013	0.079	-0.019	0.079	-0.023	0.078	-0.018
30	100	0.147	-0.005	0.147	-0.015	0.147	-0.014	0.130	-0.051
50	10	0.060	-0.011	0.061	-0.015	0.061	-0.016	0.060	-0.011
50	100	0.120	0.009	0.120	-0.004	0.119	-0.003	0.102	-0.036
Log-normal distribution									
30	10	0.092	-0.029	0.092	-0.024	0.092	-0.026	0.093	-0.027
30	100	0.171	0.003	0.167	-0.010	0.164	-0.012	0.161	-0.066
50	10	0.071	-0.014	0.071	-0.017	0.071	-0.017	0.072	-0.018
50	100	0.142	0.024	0.140	0.003	0.135	0.008	0.131	-0.006
Log-logistic distribution									
30	10	0.170	0.030	0.117	-0.010	0.117	-0.012	0.117	-0.014
30	100	0.226	-0.081	0.225	-0.096	0.227	-0.096	0.229	-0.104
50	10	0.136	0.024	0.091	0.004	0.091	-0.006	0.091	-0.007
50	100	0.185	-0.055	0.184	-0.076	0.186	-0.076	0.188	-0.080

other criteria analyzed, and it underestimates the x_T value in the majority of cases. The differences among the criteria for $T = 10$ are not large. Based on the results, samples of at least $n = 50$ are recommended for the AD and ASE tests to perform well. The KS and CVM tests are not recommended unless large samples are obtained.

References

Aksoy, H. (November 2000). Use of Gamma Distribution in Hydrological Analysis. *Turkish Journal of Engineering and Environmental Sciences*, *24*(6), 419-428.

Aparicio-Mijares, F. J. (2005). *Fundamentos de Hidrología de Superficie* (304 pp.). México, DF: Limusa Noriega Editores.

Atroosh, K. B., & Moustafa, A. T. (June 2012). An Estimation of the Probability Distribution of Wadi Bana Flow in the abyan Delta of Yemen. *Journal of Agricultural Science*, *4*(6), 80-89.

Balasooriya, U., Low, C. K., & Wong, A. Y. W. (2005). Modeling Insurance Loss Data: The log-EIC Distribution. *Journal of Actuarial Practice*, *12*, 101-125.

Dan´Azumi, S., Shamsudin, S., & Aris, A. (June 2010). Modeling the Distribution of Rainfall Intensity using Hourly Data. *American Journal of Environmental Sciences*, *6*(3), 238-243.

De Dios-Lara, E. (1998). *Análisis hidrológico de tormentas de diseño para el estado de Tabasco* (215 pp.). Tesis de Maestría en Ingeniería Hidráulica. Cárdenas, México: Universidad Juárez Autónoma de Tabasco, División Académica de Ingeniería y Arquitectura.

Dey, A. K., & Kundu, D. (2009). Discriminating between the Log-Normal and Log-Logistic Distributions.

Communications in Statistics - Theory and Methods, *39*(2), 280-292.

Di Baldasarre, G., Laio, F., & Montanari, A. (2009). Design Flood Estimation using Model Selection Criteria. *Physics and Chemistry of the Earth*, *34*(10-12), 606-611.

El Adlouni, S., Bobée, B., & Ouarda, T. B. M. J. (2008). On the Tails of Extreme Event Distributions in Hydrology. *Journal of Hydrology*, *154*, 16-33.

Ganancias-Martínez, F. (2009). *Cátedra de Hidrología y Procesos Hidráulicos* (32 pp.). Clase de Estadística Hidrológica. Córdoba, Argentina: Universidad Nacional de Córdoba, Facultad de Ciencias Exactas, Físicas y Naturales.

Haan, C. T. (1994). *Statistical Methods in Hydrology* (378 pp.). Sixth printing. Ames, Iowa, USA: Iowa State University Press.

Haddad, K., & Rahman, A. (2011). Selection of the Best Fit Flood Frequency Distribution and Parameter Estimation Procedure: A Case Study for Tasmania in Australia. *Stoch. Environ. Res. Risk Assess*, *25*, 415-428.

Laio, F. (2004). Cramer-von Mises, and Anderson-Darling Goodness of Fit Tests for Extreme Value Distributions with Unknown Parameters. *Water Resources Research*, *490*, W09308, doi:10.1029/2004WR003204, 10.

Laio, F., Di Baldasarre, G., & Montanari, A. (2009). Model sSelection Techniques for the Frequency Analysis of Hydrological Extremes. *Water Resources Research*, *495*, W07416, doi:10.1029/2007WR006666, 11.

Markiewicz, I., Strupczewski, W. G., & Kochanek, K. (2010). On Accuracy of Upper Quantiles Estimation. *Hydrology and Earth System Sciences*, *14*, 2167-2175.

Mitosek, H. T., Strupczewski, W. G., & Singh, V. P. (2002). Toward an Objective Choice of an Anual Flood Peak Distribution (16 pp.). *5th ICHE, Warsaw Poland, CD Proceedings*, Track C, PDF 158.

Quesenberry, C. P., & Kent, J. (1982). Selecting Among Probability Distributions used in Reliability. *Technometrics*, *24*(1), 59-65.

Raynal-Villaseñor, J. A. (2013). Probability Weighted Moments Estimators for the GEV Distribution for the Minima. *IJRRAS*, *15*(1), 33-40.

Shin, H., Jung, Y., Jeong, C., & Heo, J. H. (April 2011). Assessment of Modified Anderson-Darling Test Statistics for the Generalized Extreme Value and Generalized Logistic Distributions. *Stochastic Environmental Research and Risk Assessment*, *26*, 105-114.

Silva, A. T., Naghettini, M., & Portela, M. M. (2011). Sobre a Estimacao de Intervalos de Confianca para os Quantis de Variáveis Aleatórias Hidrológicas. *Recursos Hídricos*, *32*(2), 63-76.

Suhaila, J., & Jemain, A. A. (2007). Fitting Daily Rainfall amount in Malasya Using the Normal Transform Distribution. *Journal of Applied Sciences*, *7*(14), 1880-1886.

Werner, T., & Upper, C. (2002). *Time Variation in the Tail Behavior of Bund Futures Returns*. Working Paper No. 199, Frankfurt: European Central Bank.

Institutional Address of the Authors

M.I.H. Roberto S. Flowers-Cano
M.C. Robert Jeffrey Flowers
Dr. Fabián Rivera-Trejo

Universidad Juárez Autónoma de Tabasco
División Académica de Ingeniería y Arquitectura
Carretera Cunduacán-Jalpa de Méndez
Km 1, Col. La Esmeralda
86690 Cunduacán, Tabasco, México
Teléfono: +52 (993) 358 1500, extensiones 6758 y 6707
flowerscano@hotmail.com
robert.flowers@basicas.ujat.mx
jose.rivera@daia.ujat.mx

Click here to write the autor

Lyttelton Bay, New Zealand.

Photo: Víctor Manuel Pineda Blancarte.

Technical Note

Extreme 24-Hour Rainfall Predictions in the State of Zacatecas, Mexico

• Daniel Francisco Campos-Aranda* •
Profesor jubilado de la Universidad Autónoma de San Luis Potosí, México
*Corresponding Author

Abstract

Campos-Aranda, D.F. (September-October, 2014). Extreme 24-Hour Rainfall Predictions in the State of Zacatecas, Mexico. *Water Technology and Sciences* (in Spanish), 5(5), 191-216.

When determining the hydrological dimensions of both large and small hydraulic works that are dangerous because of their proximity to populations or important economic areas, the use of design floods associated with high return periods is common, such as 1 000 or 10 000 years. At times, the risk to be exceeded is even eliminated by using the maximum probable flood. Generally, probabilistic methods cannot be used to obtain these design floods since annual maximum flow data do not exist. Therefore, it is estimated using hydrological methods that convert design storms into response hydrographs. Unfortunately, pluviograph data are also scarce and, therefore, annual maximum daily rainfall (MDR) records are processed, which are much more common and widespread. This study processed 98 MDR records with over 25 data available for the state of Zacatecas. Seventeen were not homogeneous and were therefore eliminated. For the remaining 81, annual maximum series predictions were obtained for high return periods varying from 100 to 10 000 years. Predictions obtained with recurrence intervals of 100, 1 000 and 10 000 years were compared with those available from maximum isocurves published in 1976 by the former Secretary of Hydraulic Resources and found that such maps are still valid for the state of Zacatecas. The David M. Hershfield statistical method was also applied for estimating probable maximum precipitation (PMP) punctually with duration of 24 hours. This PMP ranged from 196.5 to 507.0 millimeters. Regarding the ratios between the PMP and the maximum observed value of DMP, and between PMP and the prediction of 10 000 years, their practical average magnitudes are 4.20 and 2.20, respectively. The regional frequency analyses performed in two geographic regions in the state of Zacatecas made it possible to demonstrate their usefulness and accuracy in estimating predictions for sites or localities in that region that do not contain data.

Keywords: Annual daily maximum precipitation, probable maximum precipitation, Log-Pearson Type III distribution, GEV distribution, standard error of fit, regional flood frequency analysis.

Resumen

Campos-Aranda, D.F. (septiembre-octubre, 2014). Predicciones extremas de lluvia en 24 horas en el estado de Zacatecas, México. Tecnología y Ciencias del Agua, *5(5), 191-216.*

Cuando se dimensionan hidrológicamente obras hidráulicas grandes o pequeñas pero peligrosas por su ubicación cercana a centros de población o de importantes áreas económicas, es común utilizar crecientes de diseño asociadas a altos periodos de retorno como 1 000 o 10 000 años; incluso en algunas ocasiones se decide eliminar el riesgo de ser excedidas utilizando la creciente máxima probable. Por lo general, la obtención de estas crecientes de diseño no puede ser abordada con el método probabilístico, pues no existen datos de gasto máximo anual, entonces su estimación se realiza con métodos hidrológicos que transforman tormentas de diseño en hidrogramas de respuesta. Desafortunadamente, los registros pluviográficos son también bastante escasos y por ello, se procesan los registros de precipitación máxima diaria anual (PMD), que son mucho más comunes y amplios. En este estudio se procesaron los 98 registros de PMD con más de 25 datos, disponibles en el estado de Zacatecas. Se encontró que 17 son no homogéneos y por ello se eliminaron. Para el resto, 81 series anuales de máximos, se obtuvieron sus predicciones de periodos de retorno elevados variando de 100 a 10000 años. Se contrastaron las predicciones obtenidas con intervalos de recurrencia de 100, 1 000 y 10 000 años, con las disponibles como curvas isomáximas publicadas en 1976, por la extinta Secretaría de Recursos Hidráulicos y se encontró que tales mapas todavía son vigentes para el estado de Zacatecas. También se aplicó el método estadístico de David M. Hershfield para estimar la precipitación máxima probable (PMP) puntual en 24 horas. Esta PMP varió de 196.5 a 507.0 milímetros. Respecto a los cocientes entre la PMP y el valor máximo observado de PMD y entre la PMP y la predicción de 10 000 años, sus magnitudes medias de orden práctico son 4.20 y 2.20, respectivamente. Los análisis regionales de frecuencia realizados en dos zonas geográficas del estado de Zacatecas, permitieron demostrar su utilidad y precisión para estimar predicciones en sitios o localidades sin datos, pero ubicados dentro de tal región.

Palabras clave: *precipitación máxima diaria anual, precipitación máxima probable, distribución Log-Pearson tipo III, distribución GVE, error estándar de ajuste, análisis regional de frecuencia.*

Received: 16/10/13
Accepted: 16/06/14

Introduction

The use of *flood frequency analyses* enables estimating peak design flows, which are extreme events associated with a certain exceedance probability. Its opposite is known as the return period, or *average* interval, in years, for which an equal or greater event occurs. The procedure consists of fitting a probability distribution function or probabilistic model to the available sample of annual maximum instantaneous flows, based on which *predictions* are obtained.

High return periods of 1 000 to 10 000 years are used when generating these predictions, or *design floods*, in order to hydrologically determine the dimensions of large exploitation or control reservoirs and protection dikes for nuclear plants, as well as to define maximum flood levels in order to position infrastructure above them —such as important roadways, treatment plants and drinking water storage— and thereby reduce risks. To this end, the *probable maximum flood* is used, which is estimated based on the *probable maximum precipitation* (Smith, 1993; Gupta, 2008; Shaw *et al*., 2011).

Given the scarcity of gauging stations in the sites of interest, design floods were estimated using the *hydrological method*, which converts a design storm into a watershed response hydrograph. The basic procedure involved in this method is the unit hydrograph (UH), which may be identified or synthetic. The synthetic hydrograph includes dimensionless and triangular UH, which are simplifications.

Due to the lack of pluviographs in both small and large rural watersheds, *design storms* must be developed based on the largest amount and most widespread rain gauge records available. Annual maximum daily precipitation (MDP) records are processed as random variables, and a probabilistic model is fitted to obtain predictions, that is, to develop a frequency analysis.

The *objective* of this work was to analyze and process 134 MDP records pertaining to the state of Zacatecas, Mexico, in order to estimate predictions for return periods of 100, 500, 1 000, 5 000 and 10 000 years, based on two probabilistic models. A point estimation of 24-hr probable maximum precipitation (PMP) was also obtained using the David M. Hershfield statistical method. Existing maps of maximum isocontours for the country for 100, 1 000 and 10 000-year return periods (published by the former Secretary of Hydraulic Resources in 1976) were compared to the predictions obtained. It was determined that these maps are still valid. Values of 4.20 and 2.20 were identified for the relation between *PMP* versus the largest observed MDP value, and versus the MDP prediction for a return period of 10 000 years, respectively. The results of two regional frequency analyses are also presented —one for the geographic region of Juchipila and the other for Hydrological Region No. 37 (El Salado), in the state of Zacatecas, Mexico.

Data, Methods and Results

Processed Rain Gauge Records

The state of Zacatecas currently has 134 rain gauge stations with annual maximum daily precipitation (MDP) records, according to information provided by the local National Water Commission (Conagua). Only those series containing more than 25 data were used since the records were going to be probabilistically processed to obtain predictions for high return periods. Table 2 presents the general characteristics of the 98 records containing more than 25 years, as well as their unbiased statistical properties as defined by the arithmetic mean, range, asymmetry, kurtosis and first-order serial correlation coefficients. The longest period of records is 68 years and corresponds to the San Pedro Piedra Gorda station, though there are 20 series containing 50 or more years. Prior to the probabilistic and statistical processing of the MDP records, each one was reviewed to detect all values over 100 millimeters and the

Zacatecas Conagua department was asked to verify whether the data were correct, for their inclusion or rejection.

Statistical Quality Tests

In order to obtain reliable predictions based on the results of the probabilistic processing of the MDP series, a random stationary process is necessary, that is, one in which there are no changes over time. This means that the MDP series must be composed of independent values and be free of deterministic components that make them non-homogeneous. The use of only annual maximum daily precipitation values ensures that they are independent, although persistence, trends, changes in the mean or excessive or little variability can be present.

To determine the statistical quality of each record, the following seven tests were applied: (1) Von Neumann, test of non-randomness versus unspecified deterministic components (WMO, 1971; Buishand, 1982); (2) Anderson, to detect persistence based on the first-order serial correlation coefficient (Linsley *et al*., 1988); (3) Sneyers, also to test for persistence and more highly recommended for records with anomalies (WMO, 1971); (4) Kendall test to detect trends, particularly linearity (Kottegoda, 1980); (5) Spearman, for a more general test of trends (WMO, 1971); (6) Cramer test to compare means by sub-periods (WMO,1971); and lastly, (7) the Bartlett test to determine inconsistent dispersion (WMO, 1971; Ruiz-Maya, 1977).

Results of the Statistical Tests

Table 2 lists the 17 rain gauge stations that were identified as non-homogeneous according to the detection of the deterministic components indicated. The persistence, or trend, was designated as *slight* when it was detected by only one of the two specific tests applied. When the Von Neumann test resulted in a loss in randomness, the records were identified as non-random.

Twelve records showed only slight persistence, according to the Sneyers test, and were processed. These were: Ameca La Vieja, Boca del Tesorero, Camacho, Cedros, García de la Cadena, Genaro Codina, Guadalupe, Juan Aldama, Nochistlán, Palmillas, San Pedro Piedra Gorda and Villa de Cos. Thus, 81 records were processed (see Figure 1). Three non-homogeneous records which had no missing years are shown in Figures 2, 3 and 4. The linear trend shown in these figures was calculated and proven based on the Ostle and Mensing criterion (1975).

Predictions with High Return Periods

The classic definition of *probability* is the ratio of the number of cases favorable to the event over the number of possible cases. This ranges from 0 to 1, where 0 represents an improbable event and 1 a certain event. Therefore, an extreme annual event that is equaled or exceeded once every 100 years, on average, has an exceedance probability of 0.01, and its complement —0.99 or 99%— would be the probability that it is not exceeded. This means that for an extreme event whose mean recurrence interval is 10 000 years, it exceedance probability is 0.0001, which is very low, only 0.01%.

Having explained the concept of return periods for annual events, the respective predictions will be presented. These were obtained based on two probabilistic models whose application in frequency analyses has been established in the United States and England. These are Log-Pearson Type III (LP3) and the Generalized Extreme Values (GEV), respectively, and have three fit parameters.

Both probabilistic models were fitted using the two most common and consistent methods —the LP3 was fitted using the method of moments in the logarithmic (WRC,1977) and true (Bobée, 1975) domains; and the GEV was based on sextiles (Clarke, 1973) and *L* moments (Stedinger *et al*., 1993; Hosking & Wallis, 1997).

Table 3 shows the minimum standard error of fit (Kite, 1977) obtained and the predictions

Table 1. General characteristics, statistical parameters and results from tests of homogeneity of annual maximum daily precipitation records for the 98 rain gauge stations with over 25 years of recrods in the state of Zacatecas, Mexico.

Code no.[1]	Name of weather station	Records		*MDP*[3]		Statistical parameters[4]					Statistical tests[5]						
		Period	*ND*[2]	Minimum	Maximum	*Me*	*Cv*	*Cs*	*Ck*	r_1	VN	PA	PS	TK	TS	PC	PB
1-1	Achimec	1947-2012	50	20.0	82.5	44.7	0.324	0.664	3.001	0.173	H	H	H	H	H	H	H
2-2	Adjuntas del Refugio	1980-2012	31	21.0	86.0	44.7	0.369	0.893	3.561	-0.125	H	H	H	NH	NH	H	NH
3-3	Agua Nueva	1963-2012	43	17.1	76.0	36.3	0.335	0.987	4.841	0.100	H	H	H	H	H	H	H
4-4	Ameca La Vieja	1977-2011	30	25.5	73.0	44.5	0.290	0.519	2.615	0.083	H	H	NH	H	H	H	H
5-5	Boca del Tesorero	1966-2012	44	20.2	82.0	43.6	0.302	0.899	3.941	-0.022	H	H	NH	H	H	H	H
6-6	Calera de Víctor Rosales	1961-2012	51	18.5	72.0	41.0	0.295	0.770	3.503	0.069	H	H	H	H	H	H	H
7-7	Camacho	1974-2012	31	18.0	59.0	28.8	0.301	1.416	6.523	0.156	H	H	NH	H	H	H	H
8-9	Cañitas de Felipe Pescador	1974-2012	37	16.0	75.0	37.5	0.410	0.920	3.372	-0.009	H	H	H	H	H	H	H
9-10	Coapas	1971-2012	41	23.0	67.8	41.6	0.280	0.588	3.026	-0.254	H	H	H	H	H	H	H
10-11	Chalchihuites	1962-2011	47	20.0	104.5	43.7	0.386	1.102	5.336	0.027	H	H	H	H	H	H	H
11-12	Chichimequillas	1981-2011	31	20.0	70.8	42.7	0.360	0.441	2.205	0.356	NH	NH	NH	NH	NH	NH	H
12-13	Cedros	1971-2011	38	18.0	60.5	32.8	0.299	1.044	3.965	0.155	H	H	NH	H	H	H	H
13-14	Col. González Ortega	1970-2011	37	26.8	106.0	47.8	0.417	1.536	5.230	-0.171	H	H	H	H	H	H	H
14-15	Concepción del Oro	1960-2011	47	13.8	83.1	37.3	0.419	0.765	3.412	-0.093	H	H	H	H	H	H	H
15-16	Corrales	1978-2012	33	20.5	92.1	44.0	0.387	1.281	4.873	-0.221	H	H	H	H	H	H	H
16-17	Cueva Grande	1977-2012	33	9.0	85.6	43.2	0.429	0.262	2.841	0.213	H	H	NH	NH	NH	NH	H
17-18	El Arenal	1974-2012	39	20.0	100.0	49.0	0.396	0.797	3.505	-0.252	H	H	H	H	NH	H	H
18-19	El Cazadero	1958-2012	55	17.0	95.5	42.9	0.398	1.249	4.584	-0.034	H	H	H	H	H	H	H
19-20	El Nigromante	1984-2012	29	17.5	79.0	42.8	0.365	0.630	3.126	0.056	H	H	H	H	H	H	H
20-21	El Platanito	1957-2012	53	24.0	108.5	51.6	0.303	0.972	5.185	0.289	NH	NH	NH	H	H	H	NH
21-22	El Romerillo	1980-2011	30	27.3	78.2	46.4	0.296	0.588	2.803	-0.169	H	H	H	H	H	H	H
22-23	El Rusio	1967-2011	45	20.0	71.5	41.8	0.382	0.349	1.928	0.075	H	H	H	NH	NH	H	H
23-24	El Salvador	1984-2011	25	20.0	88.5	46.8	0.361	0.983	3.860	0.173	H	H	H	H	H	H	H
24-25	El Sauz	1947-2012	66	21.2	67.2	38.5	0.287	0.660	2.808	0.040	H	H	H	H	H	H	H
25-26	Espíritu Santo	1984-2012	28	24.0	85.0	46.9	0.365	0.907	3.409	-0.193	H	H	H	H	H	H	H
26-27	Excamé	1946-2012	66	30.5	82.0	52.8	0.267	0.470	2.344	0.119	H	H	H	H	H	H	H
27-28	Felipe Ángeles (S)	1979-2011	26	18.0	76.5	44.0	0.345	0.216	2.958	0.076	H	H	H	H	H	H	H

Table 1 (continued). General characteristics, statistical parameters and results from tests of homogeneity of annual maximum daily precipitation records for the 98 rain gauge stations with over 25 years of recrods in the state of Zacatecas, Mexico.

28-29	Felipe Ángeles (V)	1980-2012	33	26.0	78.0	44.3	0.326	0.794	3.044	0.240	H	H	NH	NH	NH	H	H
29-30	Fresnillo	1950-2012	54	15.5	86.2	43.9	0.354	0.795	3.919	-0.178	H	H	H	H	H	H	H
30-31	García de la Cadena	1984-2012	27	33.2	82.3	57.7	0.237	0.091	2.990	-0.016	H	H	NH	H	H	H	H
31-32	Genaro Codina	1980-2012	28	27.7	66.8	43.5	0.251	0.413	2.491	-0.051	H	H	NH	H	H	H	H
32-33	Gral. Guadalupe Victoria	1966-2011	45	9.0	95.5	43.5	0.364	1.074	5.138	-0.322	H	NH	H	H	H	H	H
33-34	Gruñidora	1964-2010	44	12.4	91.0	40.3	0.436	0.874	3.983	0.116	H	H	NH	NH	NH	H	NH
34-35	Guadalupe	1979-2012	31	16.5	86.0	43.1	0.367	0.688	4.237	0.045	H	H	NH	H	H	H	H
35-36	Huanusco	1967-2010	36	26.7	71.0	48.1	0.257	0.194	2.086	-0.108	H	H	H	H	H	H	H
36-37	Huitzila	1982-2012	25	36.3	98.5	61.7	0.271	0.520	2.776	0.125	H	H	H	H	H	H	H
37-38	Jalpa	1979-2012	34	24.0	75.7	50.3	0.210	0.505	4.198	-0.058	H	H	H	H	H	H	H
38-39	Jerez	1963-2012	42	23.0	69.3	40.8	0.286	0.820	3.265	0.067	H	H	H	H	H	H	H
39-40	Jiménez del Teúl	1963-2011	40	18.0	77.0	36.9	0.361	1.097	4.638	-0.065	H	H	H	H	H	H	H
40-41	Juan Aldama	1975-2010	34	20.0	80.0	46.8	0.345	0.558	2.953	0.165	H	H	NH	H	H	H	H
41-42	Juchipila	1947-2010	59	26.5	90.2	46.5	0.284	1.066	4.264	0.117	H	H	H	H	H	H	H
42-43	La Florida	1956-2011	53	25.5	76.0	44.2	0.270	0.765	3.364	0.075	H	H	H	H	H	H	H
43-44	La Villita	1958-2011	53	35.2	82.1	53.9	0.206	0.576	3.107	0.028	H	H	H	H	H	H	H
44-45	Las Ánimas	1980-2011	28	19.9	76.8	42.6	0.280	0.519	4.684	0.158	H	H	NH	H	H	H	NH
45-46	Loreto	1964-2011	46	20.0	106.0	51.2	0.349	1.005	4.334	0.028	H	H	H	H	H	H	H
46-47	Los Campos	1980-2011	30	18.0	98.5	48.9	0.356	1.058	4.537	0.117	H	H	NH	H	H	H	H
47-49	Luis Moya	1980-2010	27	25.5	89.7	51.7	0.336	0.572	3.164	0.177	H	H	NH	H	H	H	NH
48-50	Malpaso	1975-2011	35	17.0	71.0	39.3	0.390	0.591	2.925	0.180	H	H	NH	NH	NH	H	H
49-51	Mesillas	1980-2011	30	20.0	84.9	42.7	0.351	0.653	3.913	-0.204	H	H	H	H	H	H	H
50-52	Mezquital del Oro	1982-2011	26	37.0	102.3	59.2	0.262	1.255	4.698	0.093	H	H	H	H	H	H	H
51-53	Milpillas de Allende	1979-2011	32	19.3	80.0	48.8	0.299	0.181	2.687	0.233	H	H	NH	NH	NH	NH	H
52-55	Momax	1980-2011	25	26.5	80.0	46.4	0.320	1.195	4.049	-0.308	H	H	H	H	H	H	H
53-56	Monte Escobedo	1965-2011	44	31.5	79.3	49.5	0.228	0.546	2.989	0.038	H	H	H	H	H	H	H
54-57	Moyahua de Estrada	1980-2011	31	33.0	80.0	50.9	0.240	0.659	2.990	0.009	H	H	H	H	H	H	H
55-58	Nochistlán	1950-2011	58	19.0	101.0	48.0	0.359	0.681	3.418	0.172	H	H	NH	H	H	H	H
56-59	Nuevo Mercurio	1959-2011	38	16.2	76.0	35.3	0.422	1.151	3.934	-0.005	H	H	H	H	H	H	H
57-60	Ojo Caliente	1969-2011	50	13.4	87.0	41.6	0.380	0.770	3.951	-0.057	H	H	H	H	H	H	H
58-61	Pajaritos de la Sierra	1974-2009	29	28.0	71.2	49.5	0.237	0.088	2.171	0.415	NH	NH	NH	NH	NH	NH	H
59-62	Palmillas	1980-2011	27	22.0	82.0	44.5	0.319	1.014	4.640	0.241	H	H	NH	H	H	H	H

Table 1 (continued). General characteristics, statistical parameters and results from tests of homogeneity of annual maximum daily precipitation records for the 98 rain gauge stations with over 25 years of recrods in the state of Zacatecas, Mexico.

60-64	Pastorías	1978-2011	29	23.0	83.0	47.2	0.333	0.325	2.638	0.322	NH	NH	NH	H	NH	H	H
61-65	Pinos	1947-2011	55	25.0	93.8	48.9	0.326	0.762	3.353	-0.134	H	H	H	H	H	H	H
62-66	Pino Suárez	1980-2011	28	20.0	96.0	48.1	0.374	1.025	4.102	-0.221	H	H	H	H	H	H	H
63-68	Presa El Chique	1950-2011	59	22.4	75.2	44.4	0.255	0.534	3.358	0.044	H	H	H	H	H	H	H
64-63	Presa Palomas	1967-2011	44	30.1	78.9	48.0	0.260	0.715	2.911	0.090	H	H	H	H	H	H	H
65-69	Presa Santa Rosa	1947-2011	62	22.8	79.0	41.2	0.335	0.975	3.571	0.039	H	H	H	H	H	H	H
66-70	Puerto de San Francisco	1970-2011	40	27.3	85.0	43.5	0.262	1.270	6.304	0.193	H	H	H	H	H	H	H
67-71	Purísima de Sifuentes	1978-2011	28	18.0	96.3	40.3	0.426	1.393	6.163	0.075	H	H	H	H	H	H	NH
68-73	Río Grande	1975-2011	37	18.0	90.0	41.8	0.413	1.093	4.186	-0.192	H	H	H	H	H	H	H
69-108	Sain Alto	1987-2011	25	22.5	91.0	44.8	0.352	1.426	5.581	-0.218	H	H	H	H	H	H	H
70-74	San Andrés	1973-2011	36	19.0	93.0	47.3	0.410	0.707	3.076	-0.268	H	H	H	H	H	H	H
71-75	San Antonio del Ciprés	1970-2011	37	16.0	82.3	44.9	0.314	0.442	3.105	0.070	H	H	H	H	H	H	H
72-76	San Benito	1970-2011	28	20.0	86.0	46.2	0.434	0.683	2.623	-0.120	H	H	H	H	H	H	H
73-77	San Gil	1970-2011	36	13.0	76.0	35.5	0.417	0.770	3.645	-0.034	H	H	H	H	H	NH	H
74-78	San Isidro de los González	1976-2011	33	21.0	72.0	39.3	0.297	0.874	3.793	-0.253	H	H	H	H	H	H	H
75-79	San Jerónimo	1980-2011	30	20.5	69.0	40.0	0.307	0.543	2.991	-0.384	H	H	H	H	H	H	H
76-80	San José de Llanetes	1976-2011	30	22.0	71.2	38.3	0.328	1.322	4.634	-0.014	H	H	H	H	H	H	NH
77-81	San Juan Capistrano	1972-2011	32	23.0	76.0	46.1	0.305	0.531	2.785	0.249	H	H	NH	NH	NH	H	H
78-82	San Pedro de la Sierra	1978-2010	25	20.0	72.0	44.5	0.310	0.496	2.938	-0.252	H	H	H	H	H	H	H
79-83	San Pedro Piedra Gorda	1943-2011	68	16.0	80.0	41.5	0.266	0.409	4.058	-0.029	H	H	NH	H	H	H	H
80-85	San Tiburcio	1973-2011	37	16.0	80.0	40.1	0.384	0.839	3.441	-0.092	H	H	H	H	H	H	H
81-86	Sierra Hermosa	1978-2011	32	22.0	98.0	46.7	0.461	0.925	3.239	-0.284	H	H	H	H	H	H	H
82-113	Sombrerete	1984-2011	28	20.6	76.8	38.7	0.352	0.959	4.283	-0.020	H	H	H	H	H	H	NH
83-88	Tayahua	1965-2010	44	20.0	81.1	43.9	0.280	0.571	3.738	0.158	H	H	NH	H	H	H	H
84-89	Tecomate	1948-1999	50	27.5	76.5	46.0	0.247	0.526	3.057	-0.175	H	H	H	H	H	H	H
85-90	Tepetongo	1980-2011	28	29.0	80.0	44.5	0.297	0.892	3.599	0.426	NH	NH	NH	NH	NH	NH	H
86-91	Teúl de González Ortega	1963-2011	44	20.5	93.0	51.6	0.302	0.697	3.492	-0.184	H	H	H	H	H	H	H
87-92	Tierra y Libertad	1982-2011	28	20.0	80.0	43.4	0.354	0.626	3.202	0.048	H	H	H	NH	NH	H	H
88-93	Tlachichila	1977-2011	25	30.4	97.8	54.7	0.266	1.152	5.146	-0.136	H	H	H	H	H	H	NH
89-94	Tlaltenango	1950-2011	56	32.5	92.2	53.1	0.256	0.634	3.017	-0.061	H	H	H	H	H	H	H
90-95	Trancoso	1952-2010	54	19.6	69.5	44.0	0.277	-0.144	2.559	0.081	H	H	H	H	H	H	H
91-96	Valparaíso	1975-2011	32	26.0	66.0	41.7	0.242	0.594	3.302	0.170	H	H	H	NH	NH	H	H
92-97	Vicente Guerrero	1981-2011	25	22.6	71.0	47.4	0.266	0.171	2.936	0.182	H	H	H	H	H	H	H

Table 1 (continued). General characteristics, statistical parameters and results from tests of homogeneity of annual maximum daily precipitation records for the 98 rain gauge stations with over 25 years of recrods in the state of Zacatecas, Mexico.

93-98	Villa de Cos	1963-2011	45	21.0	100.2	49.3	0.359	0.753	3.478	0.191	H	H	NH	H	H	H	H
94-99	Villa García	1960-2011	52	20.4	81.5	47.5	0.334	0.527	2.814	0.045	H	H	H	H	H	H	H
95-100	Villa González Ortega	1978-2010	31	22.3	69.3	40.7	0.325	0.519	2.528	0.047	H	H	H	H	H	H	H
96-101	Villa Hidalgo	1966-2011	43	15.8	97.5	46.5	0.372	0.775	3.752	0.042	H	H	H	H	H	H	H
97-102	Villanueva	1963-2011	47	16.0	66.5	39.0	0.308	0.244	2.698	0.233	NH	NH	NH	H	H	H	H
98-103	Zacatecas	1953-2010	58	16.4	82.5	46.8	0.308	0.428	2.937	0.002	H	H	H	NH	NH	NH	H

Legend:

[1] number according to the local Zacatecas Conagua department.

[2] number of years (data) processed.

[3] annual maximum daily precipitation from records.

[4] *Me* arithmetic mean, in millimeters.
Cv coefficient of variation, dimensionless.
Cs coefficient of asymmetry, dimensionless.
Ck Kurtosis coefficient, dimensionless.
r_1 first-order serial correlation coefficient.

[5] VN VonNeumann test (H=homogeneous and NH = non-homogeneous).
PA Anderson Test.
PS Sneyers Test.
TK Kendall test.
TS Spearman test.
PC Cramer test.
PB Bartlett test.

Table 2. Rain gauge stations eliminated due to presenting deterministic components.

Station (code)	Deterministic components detected
1. Adjuntas del Refugio (2)	Trend and variability.
2. Chichimequillas (12)	Not random, persistence, trend and change in mean.
3. Cueva Grande (17)	Slight persistence, trend and change in mean.
4. El Platanito (21)	Non-random, persistence and variability.
5. El Rusio (23)	Trend.
6. Felipe Ángeles (29)	Slight persistence and trend.
7. Gruñidora (34)	Slight persistence, trend and variability.
8. Malpaso (50)	Slight persistence and trend.
9. Milpillas de Allende (53)	Slight persistence, trend and change in mean.
10. Pajaritos de la Sierra (61)	Non-random, persistence, trend and change in mean.
11. Pastorías (64)	Non-random, persistence and slight trend.
12. San Juan Capistrano (81)	Slight persistence and trend.
13. Tepetongo (90)	Non-random, persistence, trend and change in mean.
14. Tierra y Libertad (92)	Trend.
15. Valparaíso (96)	Trend.
16. Villanueva (102)	Non-random and persistence.
17. Zacatecas (103)	Trend and change in mean.

for return periods of 100, 500, 1 000, 5 000 and 10 000 years, for both models. The standard error of fit (SEF) is shown in bold for the method of moments in the true domain corresponding to the LP3 model and for the sextiles method corresponding to the GEV model, since these methods less frequently result in the minimum SEF. Given the large similarity in SEF between the two probabilistic models, with the 81 MDP records processed, another distribution did not need to be tested and fitted; for example, the Generalized Logistic recently established in England (Mansell, 2003; Shaw *et al*., 2011). The last column of Table 3 shows which probabilistic model resulted in the minimum SEF and, thus, which predictions corresponded to each one of the 81 records processed.

The Log-Pearson Type 3 distribution resulted in a minimum SEF only in 19 of the 81 records processed, as seen in the last column of Table 3. In relation to the fits for the GEV distribution, most resulted in Type I or Gumbel, with a shape parameter (k) near zero. Type II or Frechet was observed in only 5 stations: Corrales, El Cazadero, Mezquital del Oro, Sain Alto and Sierra Hermosa. Type III, or Weibull, was observed in 10 stations: García de la Cadena, Huanusco, Mesillas, Presa El Chique San Antonio del Ciprés, San Pedro Piedra Gorda, Tayahua, Tecomate, Trancoso and Vicente Guerrero.

Comparison of Current Predictions and those from the 1976 Study

Weiss (1964) established the factors with which to multiply precipitation measured at certain fixed intervals in order to transform them into real observed rainfall values of a particular duration. In order for daily precipitation to correspond to a duration of 24 hours, it must be multiplied by 1.13. Having made this correction, the rain gauge stations were identified that were common to both the Zacatecas study and the one conducted in the mid 1970s (SRH, 1976) which included all of Mexico. Forty-six were found, which are shown in Table 4 according to hydrological region. Region 12 was sub-divided into western, central (Juchipila) and eastern zones.

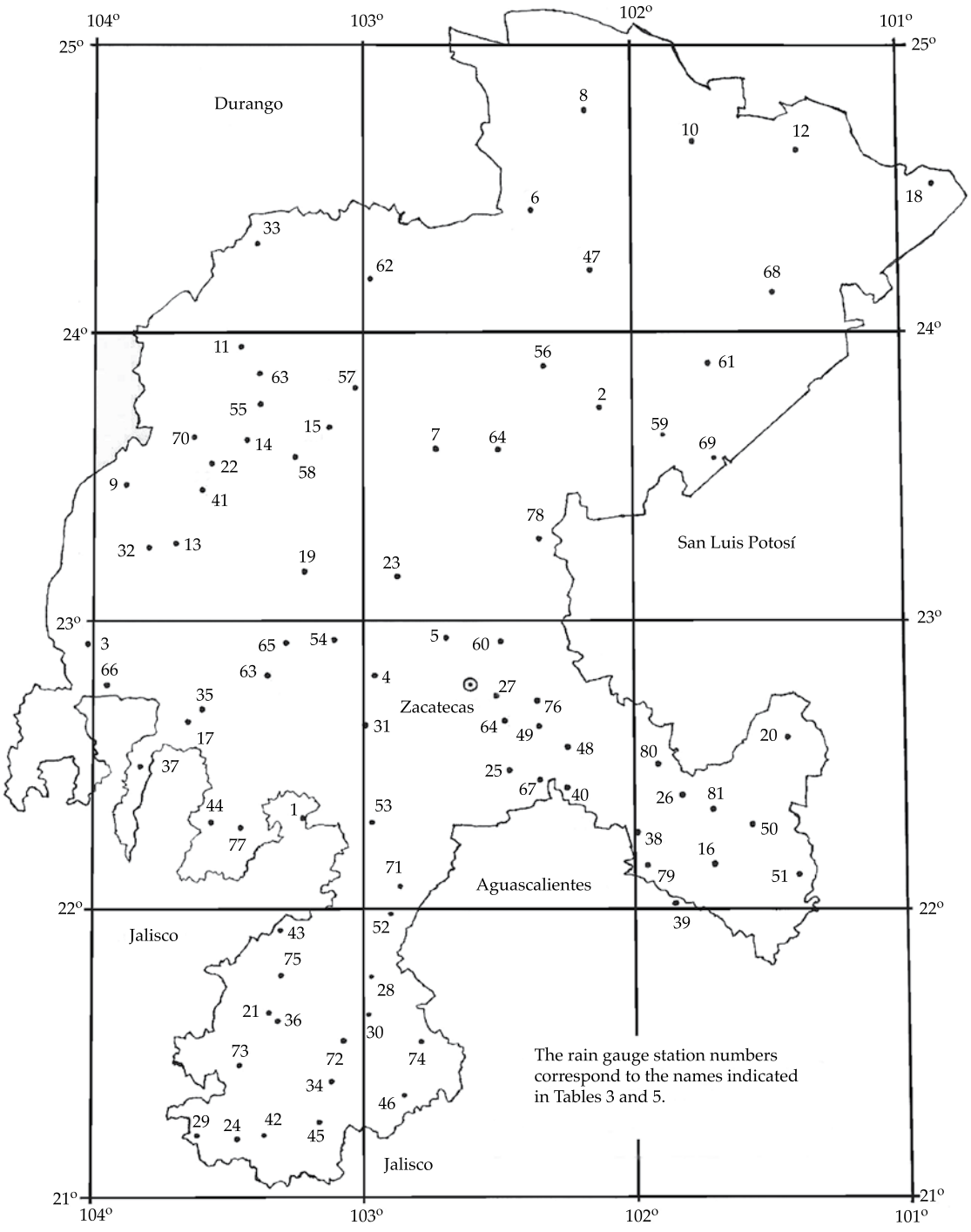

Figure 1. Geographic location of the 81 rain gauge stations processed in the state of Zacatecas, Mexico.

Table 4 shows the predictions derived from the isocontour maps (SRH, 1976) available only for return periods of 100, 1 000 and 10 000 years. It also presents the predictions adopted from the LP3 and GEV models, previously corrected by the Weiss factor. Lastly, the ratios of the

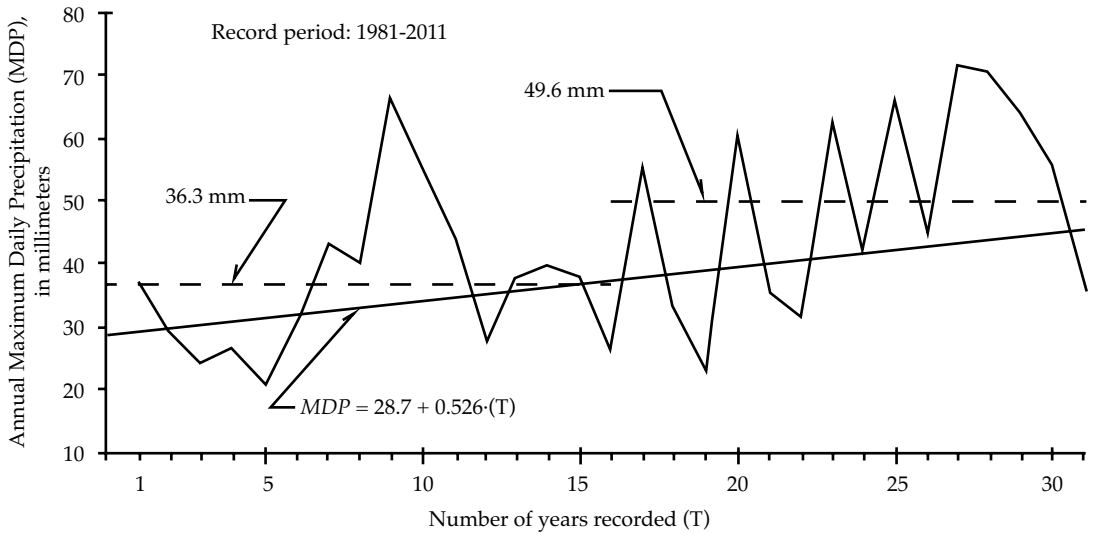

Figure 2. Chronological series of annual maximum daily precipitation for rain gauge station Chichimequillas, state of Zacatecas, Mexico.

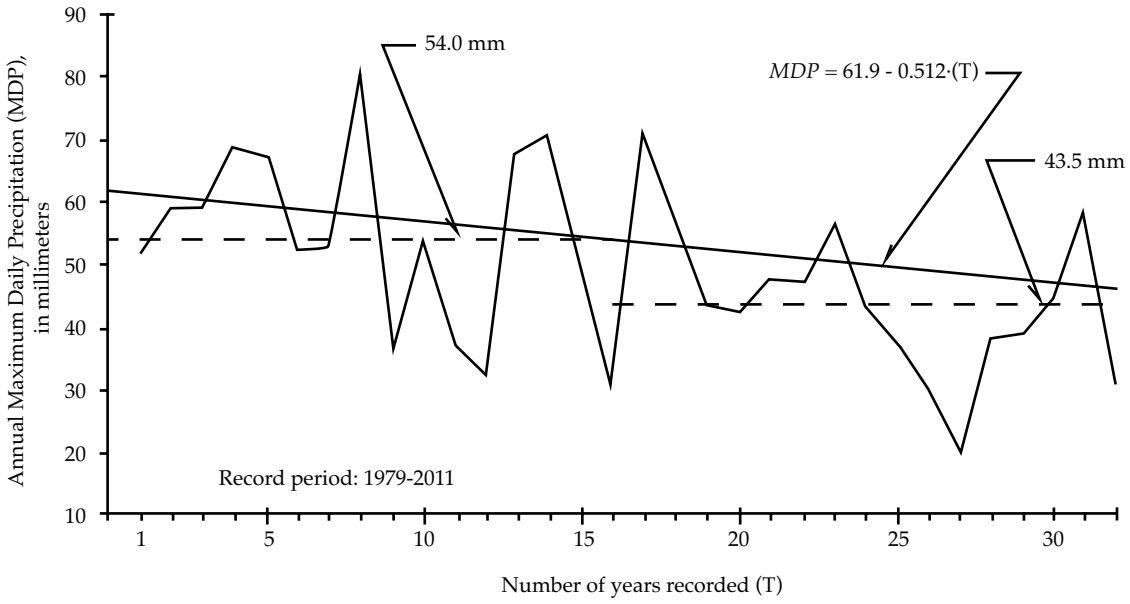

Figure 3. Chronological series of annual maximum daily precipitation for rain gauge station Milpillas de Allende, state of Zacatecas, Mexico.

values cited are presented, that is, between the recent value and the previous value, or from the maps.

Logically, a wider spread is seen in the ratios for return periods of 10 000 years than those associated with 100 years. The smallest ratios correspond to Camacho and Trancoso and the largest to El Cazadero and Villa de Cos. In general terms, the ratios are near 1 in arid or semi-arid hydrological regions (numbers

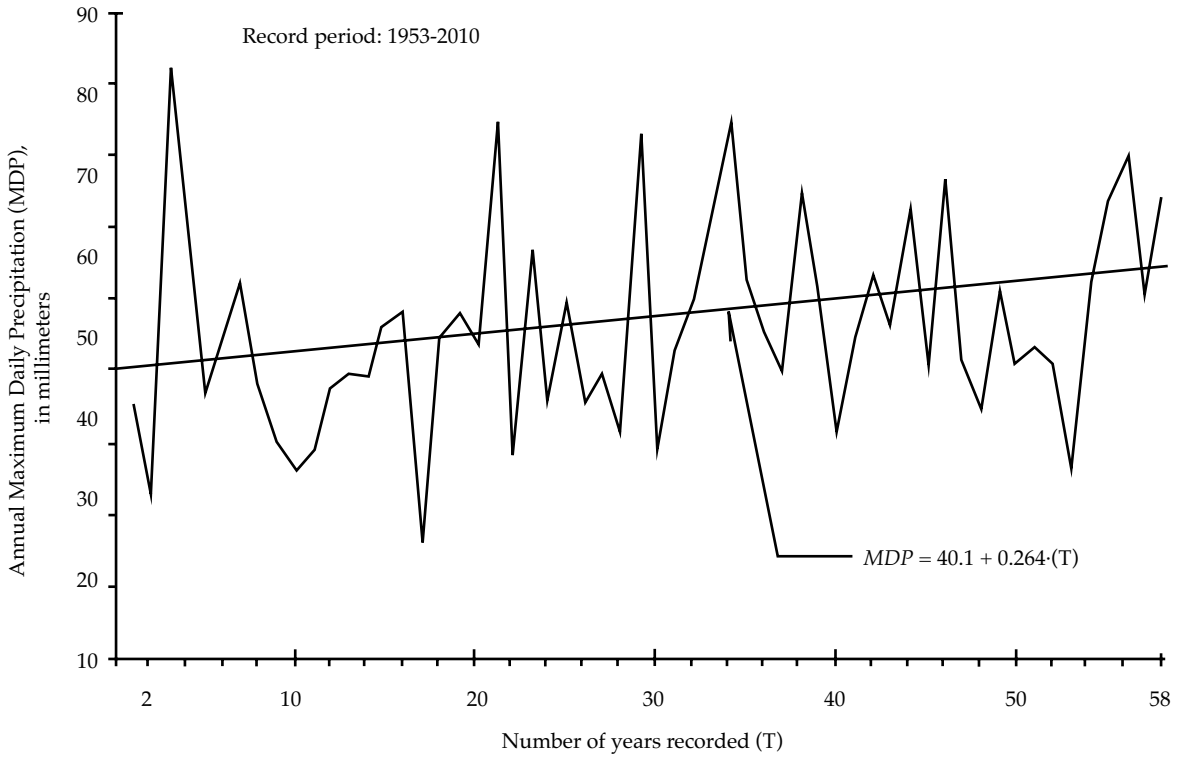

Figure 4. Chronological series of annual maximum daily precipitation for rain gauge station Zacatecas, state of Zacatecas, Mexico.

36 and 37). The smallest values correspond to hydrological region 12, the central region. The values of the middle 46 ratios are very similar, roughly 0.88. Therefore, it is concluded that the maximum isocontour maps (SRH, 1976) are still valid for design purposes. These are shown in Figures 5, 6 and 7.

Statistical Estimation of Point PMP

The David M. Hershfield statistical method to estimate the probable maximum precipitation (*PMP*) can be found in Hershfield (1961, 1965), WMO (1973) and Campos (1998). Table 5 shows the results from applying this method to the 81 MDP records. A large range in the PMP is observed, from 196.5 mm in Camacho to 507.0 mm in Sierra Hermosa. Both stations belong to Hydrological Region number 37. Nevertheless, their altitudes are quite different —658 masl in Camacho and 2 100 masl in Sierra Hermosa.

Point PMP Ratios

The last two columns of Table 5 presents the ratio of PMP versus the observed annual maximum daily precipitation (P_0) and versus the MDP prediction for 10 000 years (P_{Tr}). The arithmetic mean, the mode and the population median are 4.177, 4.117 and 4.157, for the first ratio, respectively, and 2.158, 2.044 and 2.120 for the second, respectively. The mode and the median were obtained based on the Mixed Gamma distribution. Thus, a value that is 4.20 times the P_0 and another that is 2.20 times P_{Tr} will provide a quick and approximate estimation of 24-hr point PMP. For more precise estimations, isocontour lines can be constructed for *PMP*, or a weighted transport to the site of interest can be performed according to the closest data in Table 5 that belong to the same geographic region.

Technology and Sciences. Vol. V, No. 5, September-October, 2014

Table 3. Predictions of annual maximum daily precipitation (mm) for the return periods indicated (years), using two probabilistic models with 81 rain gauge stations in the state of Zacatecas, Mexico.

No.	Rain gauge station	Log-Perason type III (LP3) Distribution						General Extreme Values (GEV)Distribution						Model Adopted
		SEF	100	500	1 000	5 000	10 000	*SEF*	100	500	1 000	5 000	10 000	
1	Achimec	1.767	89.9	107.4	115.0	133.0	140.9	1.745	90.3	107.5	114.7	130.9	137.7	GEV
2	Agua Nueva	2.274	73.5	87.7	93.9	108.3	114.6	**2.264**	75.1	91.4	98.5	115.2	122.5	GEV
3	Ameca La Vieja	2.782	84.6	100.0	106.6	122.4	129.3	2.701	83.2	96.0	101.1	112.1	116.5	GEV
4	Boca del Tesorero	1.963	84.6	100.9	108.1	125.2	132.8	1.803	87.0	104.9	112.7	131.1	139.1	GEV
5	Calera de Víctor Rosales	1.697	77.1	90.4	96.0	109.2	114.9	**1.629**	77.8	90.8	96.2	108.1	113.0	GEV
6	Camacho	2.183	59.7	75.9	83.7	104.1	114.1	2.220	58.0	71.6	77.7	92.8	99.7	LP3
7	Cañitas de Felipe Pescador	2.611	91.4	117.3	129.4	159.7	173.8	2.585	92.3	119.2	131.7	163.2	177.8	GEV
8	Coapas	1.568	76.3	88.6	93.8	105.9	111.1	1.487	76.6	88.1	92.7	102.7	106.7	GEV
9	Chalchihuites	3.208	98.9	122.7	133.3	159.2	170.9	3.376	95.2	114.5	122.6	140.8	148.5	LP3
10	Cedros	1.394	66.6	83.0	90.7	110.2	119.5	1.299	68.6	87.2	96.1	119.0	129.9	GEV
11	Col. González Ortega	4.196	131.4	192.0	224.9	322.2	375.2	4.349	133.5	201.2	239.5	357.1	423.5	LP3
12	Concepción del Oro	1.829	87.8	107.9	116.5	136.9	145.8	1.914	86.7	105.7	113.6	131.9	139.5	LP3
13	Corrales	3.432	106.4	140.5	157.1	200.9	222.4	3.403	108.9	147.2	166.4	218.4	244.4	GEV
14	El Arenal	2.301	112.1	137.9	149.3	176.3	188.3	2.410	110.3	134.0	144.0	166.8	176.5	LP3
15	El Cazadero	2.345	102.7	133.1	147.5	184.7	202.4	2.226	106.3	142.6	160.4	208.2	231.9	GEV
16	El Nigromante	2.036	89.7	106.1	113.0	128.6	135.2	1.899	92.0	109.9	117.3	134.0	140.9	GEV
17	El Romerillo	2.318	90.9	109.2	117.4	137.1	146.0	2.163	89.0	103.9	110.0	123.3	128.8	GEV
18	El Salvador	3.653	102.4	126.5	137.4	164.1	176.2	3.534	107.0	136.7	150.6	185.5	201.8	GEV
19	El Sauz	1.302	73.9	88.4	94.9	110.6	117.6	1.276	73.6	87.1	92.8	105.7	111.1	GEV
20	Espíritu Santo	3.427	108.7	140.0	154.9	193.1	211.4	3.317	108.7	139.0	153.1	188.6	205.1	GEV
21	Excamé	**2.233**	91.9	104.4	109.5	120.9	125.6	2.193	94.6	107.9	113.1	124.3	128.6	GEV
22	Felipe Ángeles (S)	2.240	80.9	88.8	91.5	96.8	98.7	2.081	81.5	89.0	91.5	96.1	97.7	GEV
23	Fresnillo	**2.756**	90.2	106.9	114.0	130.3	137.4	**2.759**	92.9	112.7	121.3	141.2	149.8	LP3
24	García de la Cadena	3.055	89.4	96.0	98.4	103.2	104.9	3.014	88.8	94.0	95.7	98.5	99.4	GEV
25	Genaro Codina	1.811	76.2	87.9	92.9	104.5	109.6	1.625	75.2	84.6	88.2	95.6	98.4	GVE
26	Gral. Guadalupe Victoria	**3.229**	92.4	111.7	120.2	140.0	148.8	2.983	96.9	122.0	133.5	162.0	175.0	GEV

Table 3 (continued). Predictions of annual maximum daily precipitation (mm) for the return periods indicated (years), using two probabilistic models with 81 rain gauge stations in the state of Zacatecas, Mexico.

27	Guadalupe	**3.790**	89.1	104.8	111.3	125.9	132.0	3.884	83.2	92.7	96.0	102.4	104.7	LP3
28	Huanusco	**2.434**	80.2	89.1	92.6	100.1	103.1	2.268	80.4	87.9	90.5	95.4	97.1	GEV
29	Huitzila	3.077	113.4	133.1	141.7	161.8	170.7	2.877	112.2	128.6	135.2	149.2	154.8	GEV
30	Jalpa	**2.711**	79.2	88.2	91.9	100.1	103.6	2.714	82.7	95.5	100.8	113.2	118.5	LP3
31	Jerez	1.700	79.0	95.7	103.3	121.8	130.3	1.598	80.3	97.4	105.0	123.1	131.2	GEV
32	Jiménez del Teúl	2.155	81.6	102.0	111.4	134.6	145.4	2.110	81.5	101.0	109.7	130.7	140.0	GEV
33	Juan Aldama	3.576	92.1	106.0	111.5	123.6	128.5	3.565	94.1	109.4	115.4	128.3	133.4	GEV
34	Juchipila	1.912	90.3	110.4	119.6	142.7	153.4	**1.815**	93.5	117.2	128.4	156.4	170.3	GEV
35	La Florida	1.591	81.2	95.8	102.2	117.5	124.4	**1.578**	80.4	93.2	98.4	110.0	114.8	GEV
36	La Villita	**1.526**	85.8	96.2	100.5	110.2	114.3	1.539	85.6	95.2	98.9	106.6	109.6	LP3
37	Las Ánimas	**2.711**	75.6	86.1	90.3	99.8	103.7	2.773	71.8	78.1	80.3	84.3	85.7	LP3
38	Loreto	**3.011**	105.8	126.8	135.9	157.3	166.7	2.732	110.3	136.1	147.6	175.2	187.4	GEV
39	Los Campos	**3.598**	102.4	123.3	132.3	153.6	162.9	3.196	110.9	142.4	157.3	195.2	213.1	GEV
40	Luis Moya	3.139	102.3	118.9	125.7	141.0	147.4	3.054	103.4	120.1	126.7	140.9	146.5	GEV
41	Mesillas	2.753	85.1	98.3	103.6	115.2	120.0	2.714	84.7	96.7	101.3	110.7	114.2	GEV
42	Mezquital del Oro	3.259	114.9	145.7	160.9	201.2	221.1	3.212	118.3	155.1	174.0	226.2	253.0	GEV
43	Momax	3.832	103.6	137.3	154.3	200.7	224.2	3.879	105.7	143.7	163.4	218.6	247.1	LP3
44	Monte Escobedo	1.172	82.8	94.8	99.9	111.8	117.0	1.030	82.2	92.2	96.0	104.1	107.2	GEV
45	Moyahua de Estrada	1.774	89.3	104.7	111.6	128.0	135.4	**1.808**	85.8	96.6	100.8	109.7	113.2	LP3
46	Nochistlán	2.013	99.6	117.8	125.4	142.6	150.0	1.972	100.0	117.8	125.0	140.8	147.2	GEV
47	Nuevo Mercurio	2.631	92.5	126.0	142.7	187.9	210.6	2.663	93.0	128.1	145.8	194.3	218.9	LP3
48	Ojo Caliente	**2.554**	88.8	105.8	113.0	129.4	136.3	2.575	86.3	100.0	105.3	116.4	120.7	LP3
49	Palmillas	3.064	88.4	105.8	113.4	131.4	139.4	**3.207**	87.2	103.2	109.9	125.1	131.4	LP3
50	Pinos	1.531	99.9	120.9	130.2	152.6	162.7	1.515	98.9	117.8	125.7	143.6	151.1	GEV
51	Pino Suárez	3.026	108.1	135.0	147.3	177.6	191.4	2.800	113.1	146.2	161.9	201.8	220.7	GEV
52	Presa El Chique	**1.115**	76.0	86.2	90.4	99.9	103.9	1.040	75.9	84.8	88.2	95.2	97.8	GEV
53	Presa Palomas	1.735	88.4	105.7	113.5	132.5	141.2	1.640	90.0	106.9	114.2	131.4	138.9	GEV
54	Presa Santa Rosa	1.885	89.5	113.4	124.7	153.6	167.3	1.834	90.4	114.6	125.9	154.4	167.7	GEV

Table 3 (continued). Predictions of annual maximum daily precipitation (mm) for the return periods indicated (years), using two probabilistic models with 81 rain gauge stations in the state of Zacatecas, Mexico.

55	Puerto de San Francisco	2.472	80.5	97.1	104.7	123.5	132.2	2.631	77.6	90.1	95.3	107.1	111.9	LP3
56	Purísima de Sifuentes	3.790	99.5	128.2	141.6	175.4	191.2	3.827	98.9	127.0	139.9	172.1	186.9	LP3
57	Río Grande	2.485	103.6	134.9	149.8	187.9	206.0	2.421	104.6	137.3	152.9	192.9	211.9	GEV
58	Sain Alto	3.671	102.3	133.8	149.3	190.4	210.6	3.653	105.3	142.6	161.7	214.3	241.2	GEV
59	San Andrés	2.471	110.3	135.4	146.3	172.0	183.3	**2.633**	112.3	140.4	152.8	182.5	195.7	LP3
60	San Antonio del Ciprés	**2.732**	83.9	96.0	100.8	111.6	116.0	2.612	84.6	95.9	100.2	109.0	112.3	GEV
61	San Benito	**4.202**	104.1	123.2	131.0	148.1	155.2	4.065	115.4	145.5	158.9	191.0	205.2	GEV
62	San Gil	1.731	81.7	98.8	106.0	122.5	129.6	1.718	81.2	97.6	104.4	119.4	125.6	GEV
63	San Isidro de los González	1.519	77.5	94.1	101.5	119.8	128.2	1.325	78.7	95.3	102.6	119.9	127.6	GEV
64	San Jerónimo	1.638	77.0	90.3	96.0	109.0	114.6	1.500	76.3	87.6	92.0	101.4	105.1	GEV
65	San José de Llanetes	2.774	86.7	115.8	130.6	171.1	191.8	2.803	88.3	120.7	137.6	185.4	210.3	LP3
66	San Pedro de la Sierra	2.410	82.8	94.4	99.1	109.4	113.6	2.267	86.1	99.6	105.0	116.5	121.1	GEV
67	San Pedro Piedra Gorda	2.096	67.4	73.0	75.0	78.9	80.4	2.084	67.6	72.7	74.3	77.3	78.3	GEV
68	San Tiburcio	2.439	90.7	112.0	121.5	144.4	154.7	2.345	92.2	114.5	124.4	148.0	158.4	GEV
69	Sierra Hermosa	4.015	131.4	180.2	204.3	268.9	300.9	3.962	128.6	174.0	196.2	254.7	283.3	GEV
70	Sombrerete	2.198	83.8	103.5	112.5	134.4	144.4	2.092	83.8	102.3	110.3	129.2	137.4	GEV
71	Tayahua	**2.232**	78.7	90.1	94.8	105.4	109.8	2.188	77.7	87.0	90.4	97.5	100.1	GEV
72	Tecomate	1.179	78.8	90.1	94.8	105.6	110.3	1.105	78.0	87.3	90.8	98.1	100.8	GEV
73	Teúl de González Ortega	**2.179**	96.7	112.3	118.8	133.6	140.0	2.020	100.0	118.1	125.6	142.6	149.7	GEV
74	Tlachichila	3.142	102.7	124.4	134.3	159.1	170.6	2.982	106.3	132.1	144.3	175.0	189.4	GEV
75	Tlaltenango	1.671	95.4	112.1	119.3	136.7	144.5	1.577	94.6	108.8	114.6	127.3	132.4	GEV
76	Trancoso	1.100	70.7	75.0	76.4	78.9	79.8	1.012	69.3	72.5	73.4	74.8	75.2	GEV
77	Vicente Guerrero	2.417	76.1	81.7	83.7	87.6	89.0	2.229	80.0	87.5	90.1	95.0	96.7	GEV
78	Villa de Cos	1.836	104.6	125.9	135.1	156.8	166.3	1.807	104.7	125.4	134.0	153.6	161.7	GEV
79	Villa García	2.086	94.5	110.4	117.1	132.1	138.4	1.991	93.7	108.0	113.5	125.1	129.6	GEV
80	Villa González Ortega	2.142	83.2	100.3	107.8	125.7	133.7	1.981	81.8	96.0	101.8	114.6	119.8	GEV
81	Villa Hidalgo	**2.449**	97.8	116.2	124.0	141.7	149.3	2.267	100.1	120.1	128.4	147.2	155.1	GEV

Legend: SEF - standard error of fit, in millimeters.

Table 4. Comparison of 24-hour rainfall prediction for return periods of 100, 1 000 and 10 000 years for 46 rain gauge stations common to both the 1976 and current study.

No.	Rain gauge station	Storm report			Probabilistic estimation			Ratio: RV/PV*		
		100	1 000	10 000	100	1 000	10 000	100	1 000	10 000
Hydrological Region No. 36										
1	Cedros	125	170	225	77.5	108.6	146.8	0.620	0.639	0.652
2	Juan Aldama	100	125	175	106.3	130.4	150.7	1.063	1.043	0.861
3	San Gil	115	155	190	91.8	118.0	141.9	0.798	0.761	0.747
4	Río Grande	105	150	180	118.2	172.8	239.4	1.126	1.152	1.330
5	El Cazadero	100	125	175	120.1	181.3	262.0	1.201	1.450	1.497
6	El Arenal	125	170	200	126.7	168.7	212.8	1.014	0.992	1.064
7	Sain Alto	115	155	200	119.0	182.7	272.6	1.035	1.179	1.363
8	El Sauz	100	125	150	83.2	104.9	125.5	0.832	0.839	0.837
9	Presa Santa Rosa	100	125	150	102.2	142.3	189.5	1.022	1.138	1.263
Hydrological Region No. 37										
10	Concepción del Oro	100	150	180	99.2	131.6	164.8	0.992	0.877	0.916
11	Camacho	125	175	225	67.5	94.6	128.9	0.540	0.541	0.573
12	Nuevo Mercurio	100	150	190	104.5	161.3	238.0	1.045	1.075	1.253
13	San Tiburcio	100	125	180	104.2	140.6	179.0	1.042	1.125	0.994
14	San Benito	130	200	250	130.4	179.6	231.9	1.003	0.898	0.928
15	Agua Nueva	100	125	150	84.9	111.3	138.4	0.849	0.890	0.923
16	Guadalupe	100	140	175	100.7	125.8	149.2	1.007	0.899	0.853
17	Cañitas de Felipe P.	100	150	200	104.3	148.8	200.9	1.043	0.992	1.005
18	Villa de Cos	100	125	150	118.3	151.4	182.7	1.183	1.211	1.218
19	Fresnillo	100	125	150	101.9	128.8	155.3	1.019	1.030	1.035
20	Calera de Víctor R.	100	125	150	87.9	108.7	127.7	0.879	0.870	0.851
21	San Antonio del Ciprés	100	125	150	95.6	113.2	126.9	0.956	0.906	0.846
22	Villa Hidalgo	125	200	250	113.1	145.1	175.3	0.905	0.726	0.701
23	Pinos	105	150	190	111.8	142.0	170.7	1.065	0.947	0.898
Hydrological Region No. 11										
24	Sombrerete	130	175	220	94.7	124.6	155.3	0.728	0.712	0.706
25	Chalchihuites	150	200	275	111.8	150.6	193.1	0.745	0.753	0.702
Hydrological Region No. 12 (west)										
26	Jiménez del Teúl	125	150	200	92.1	124.0	158.2	0.737	0.827	0.791
27	San José de Llanetes	120	150	200	98.0	147.6	216.7	0.817	0.984	1.084
28	Achimec	125	150	200	102.0	129.6	155.6	0.816	0.864	0.778
29	Monte Escobedo	125	150	200	92.2	108.5	121.1	0.738	0.723	0.606
Hydrological Region No. 12 (central)										
30	Boca del Tesorero	100	150	160	98.3	127.4	157.2	0.983	0.849	0.983
31	Presa Palomas	100	150	160	101.7	129.0	157.0	1.017	0.860	0.981
32	Tayahua	100	150	160	87.8	102.2	113.1	0.878	0.681	0.707
33	Presa El Chique	100	150	160	85.8	99.7	110.5	0.858	0.665	0.691
34	Tlaltenango	125	150	200	106.9	129.5	149.6	0.855	0.863	0.748
35	Excamé	125	150	200	106.9	127.8	145.3	0.855	0.852	0.727
36	La Villita	125	150	200	97.0	113.6	129.2	0.776	0.757	0.646
37	Tecomate	125	150	200	88.1	102.6	113.9	0.705	0.684	0.570

Table 4 (continued). Comparison of 24-hour rainfall prediction for return periods of 100, 1 000 and 10 000 years for 46 rain gauge stations common to both the 1976 and current study..

38	Teúl de González O.	125	150	200	113.0	141.9	169.2	0.904	0.946	0.846
39	Juchipila	125	150	200	105.7	145.1	192.4	0.846	0.967	0.962
40	Nochistlán	125	150	200	113.0	141.3	166.3	0.904	0.942	0.831
Hydrological Region No. 12 (east)										
41	Trancoso	120	150	170	78.3	82.9	85.0	0.653	0.553	0.500
42	Ojo Caliente	125	170	200	100.3	127.7	154.0	0.802	0.751	0.770
43	San Pedro Piedra G.	100	125	160	76.4	84.0	88.5	0.764	0.672	0.553
44	Mesillas	100	130	150	95.7	114.5	129.0	0.957	0.881	0.860
45	Loreto	100	150	200	124.6	166.8	211.8	1.246	1.112	1.059
46	Villa García	120	150	200	105.9	128.3	146.4	0.883	0.855	0.732
Minimum value		100	125	150	67.5	82.9	85.0	0.540	0.541	0.500
Maximum value		150	200	275	130.4	182.7	272.6	1.246	1.450	1.497
Arithmetic mean		-	-	-	-	-	-	0.907	0.890	0.879
Sample median		-	-	-	-	-	-	0.893	0.873	0.848
Population median		-	-	-	-	-	-	0.898	0.878	0.861

Recent value (RV), previous value (PV).

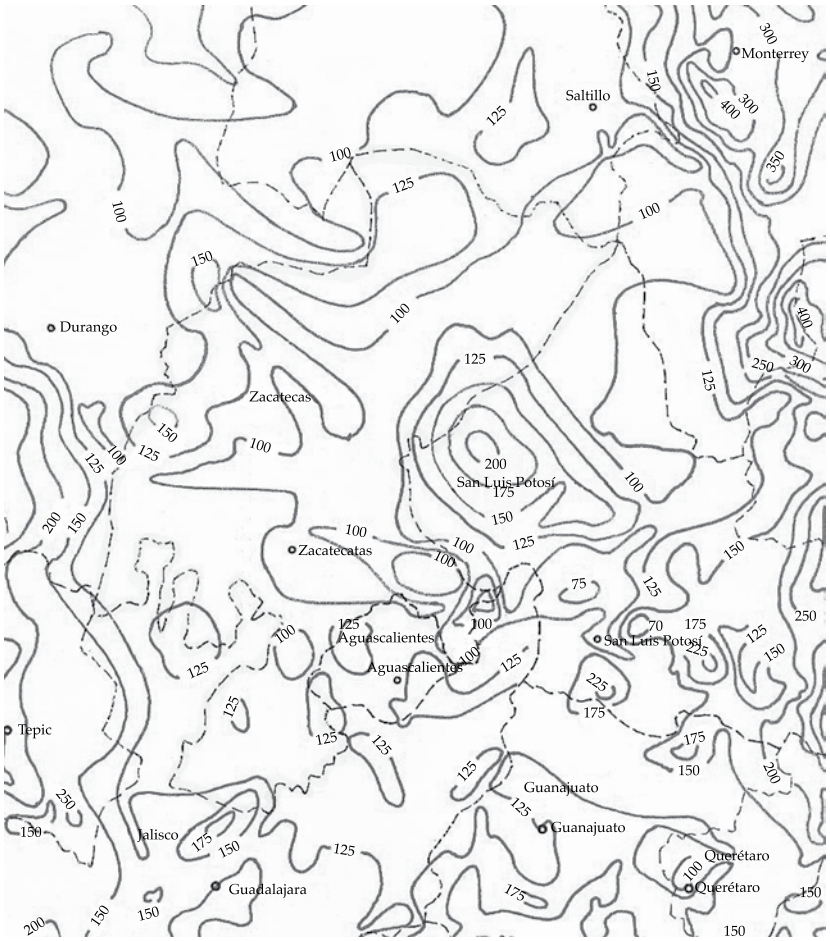

Figure 5. Maximum isocontour lines for a return period of 100 years, state of Zacatecas (SRH, 1976).

Figure 6. Maximum isocontour lines for a return period of 1000 years, state of Zacatecas (SRH, 1976).

Estimation of PMP for an Area, with Different Durations

Point PMP values obtained with the Hershfield method based on MDP rain gauge records are representative of a 25 km^2 area, as has been established. Therefore, to estimate the PMP corresponding to a certain area or watershed (A) over 25 km^2, an area reduction factor (RFA) must by applied, since all storms are reduced as they increase in area. The WMO (1973) presented some average reduction curves by area, obtained from a general P-A-D analysis of large storms. The curve corresponding to a 24-hour duration was represented by the following fourth degree polynomial:

$$RFA = 1.012021 - 5.985305 \cdot 10^{-4} \cdot A + 1.39148 \cdot 10^{-6} \cdot A^2 - 1.548155 \cdot 10^{-9} \cdot A^3 + 6.121556 \cdot 10^{-13} \cdot A^4 \quad (1)$$

in which the area A is in km^2. The above expression was obtained based on 11 points, where the coefficient of determination is 0.99874 and the standard error of the estimation is 0.00257 (Campos, 1998).

In large watersheds, which commonly contain several rain gauge stations, the

Figure 7. Maximum isocontour lines for a return period of 10 000 years, state of Zacatecas (SRH, 1976).

weighted point PMP value must first be obtained, for example, using the contour line method, Thiessen polygons or another more suitable technique.

To distribute a 24-hour point or area *PMP* into other durations, the criterion proposed by Schulz (1976) can be used, which consists of drawing, on logarithmic paper, a straight line parallel to the curve enveloping the maximum global values, for a duration of 24 hours and the value of the PMP. The enveloping curve is a straight line on the logarithmic paper whose equation is (WMO, 1973; Linsley *et al*., 1988):

$$P_{MM} = 421.64 \cdot D^{0.475} \qquad (2)$$

where P_{MM} is the maximum global precipitation, in millimeters, for duration D in hours. For example, to obtain the *PMP* for 6 hours when its value is 513.0 mm for 24 hours, the procedure is:

$$\alpha = \frac{513.0}{(24)^{0.475}} = \frac{513.0}{4.52481} \cong 113.375$$

$$PMP_6 = 113.375 \cdot (6)^{0.475} \cong 265.5 \text{ mm}$$

Regional Frequency Analysis in the Geographic Region of Juchipila

The key objective of using the *regional* procedure with the available *MDP* information was to generate predictions for sites without information or where the information was discarded because the records were not

Table 5. Results from applying the DM Hershfield test to estimate 24-hour point *PMP* (mm) for the 81 rain gauge stations indicated in the state of Zacatecas.

No.	Rain gauge station	Mean (mm)		S. D.[1] (mm)		F. F.[2]		*PMP*[3] (mm)	Ratios[4]	
		$\overline{X}_n$	$\overline{X}_{n-m}$	S_n	S_{n-m}	Km_o	Km		*PMP/Po*	PMP/P_{Tr}
1	Achimec	44.668	43.896	14.494	13.566	2.846	17.565	344.7	4.178	2.215
2	Agua Nueva	36.316	35.371	12.174	10.606	3.831	17.968	278.9	3.670	2.015
3	Ameca La Vieja	44.467	43.483	12.909	11.938	2.473	17.534	330.0	4.521	2.507
4	Boca del Tesorero	43.595	42.702	13.170	11.902	3.302	17.610	309.9	3.779	1.972
5	Calera de Víctor Rosales	40.998	40.378	12.095	11.369	2.781	17.736	295.0	4.097	2.310
6	Camacho	28.848	27.843	8.674	6.740	4.622	18.327	196.5	3.331	1.524
7	Cañitas de Felipe Pescador	37.476	36.433	15.357	14.185	2.719	17.903	370.4	4.939	1.844
8	Coapas	41.634	40.980	11.667	11.028	2.432	17.688	293.8	4.333	2.437
9	Chalchihuites	43.653	42.330	16.837	14.343	4.335	17.634	360.6	3.451	1.867
10	Cedros	32.834	32.086	9.814	8.784	3.235	18.124	241.7	3.995	1.647
11	Col. González Ortega	47.770	46.153	19.925	17.573	3.406	17.428	449.1	4.237	1.059
12	Concepción del Oro	37.300	36.304	15.627	14.213	3.292	17.929	356.2	4.286	2.162
13	Corrales	44.027	42.525	17.048	14.937	3.319	17.592	395.7	4.296	1.433
14	El Arenal	48.962	47.618	19.395	17.723	2.956	17.364	448.3	4.483	2.107
15	El Cazadero	42.905	41.931	17.056	15.596	3.435	17.666	386.1	4.043	1.473
16	El Nigromante	42.786	41.493	15.628	14.247	2.633	17.627	384.6	4.868	2.416
17	El Romerillo	46.427	45.331	13.734	12.572	2.614	17.444	345.4	4.417	2.373
18	El Salvador	46.812	45.075	16.919	14.832	2.928	17.431	404.3	4.568	1.773
19	El Sauz	38.473	38.031	11.060	10.542	2.767	17.868	271.6	4.042	2.163
20	Espíritu Santo	46.957	45.548	17.153	15.742	2.506	17.424	421.7	4.961	1.820
21	Excamé	52.759	52.309	14.089	13.713	2.165	17.195	345.4	4.212	2.377
22	Felipe Ángeles (S)	43.973	42.672	15.185	13.940	2.427	17.555	381.3	4.984	3.454
23	Fresnillo	43.900	43.102	15.519	14.506	2.971	17.609	363.2	4.213	2.339
24	García de la Cadena	57.700	56.754	13.680	13.019	1.962	16.888	363.2	4.413	3.234
25	Genaro Codina	43.532	42.670	10.905	10.095	2.390	17.565	288.2	4.314	2.592
26	Gral. Guadalupe Victoria	43.460	42.277	15.828	13.854	3.842	17.633	351.3	3.679	1.776
27	Guadalupe	43.129	41.700	15.846	13.938	3.178	17.625	374.9	4.359	2.513
28	Huanusco	48.131	47.477	12.348	11.880	1.980	17.363	323.2	4.552	2.946
29	Huitzila	61.652	60.117	16.736	15.192	2.527	16.719	416.1	4.224	2.379
30	Jalpa	50.335	49.567	10.547	9.696	2.695	17.257	277.2	3.662	2.368
31	Jerez	40.793	40.098	11.682	10.912	2.676	17.733	289.4	4.176	1.952
32	Jiménez del Teúl	36.937	35.910	13.321	11.781	3.488	17.936	309.9	4.025	1.959
33	Juan Aldama	46.824	45.818	16.170	15.303	2.234	17.436	403.4	5.043	2.676
34	Juchipila	46.547	45.795	13.206	11.977	3.707	17.488	308.1	3.416	1.601
35	La Florida	44.211	43.600	11.930	11.177	2.899	17.584	291.7	3.838	2.249
36	La Villita	53.868	53.325	11.119	10.495	2.742	17.129	282.2	3.437	2.185
37	Las Ánimas	42.607	41.341	11.918	10.044	3.530	17.631	286.2	3.727	2.442
38	Loreto	51.150	49.931	17.846	15.995	3.505	17.271	398.8	3.762	1.883
39	Los Campos	48.907	47.197	17.404	14.928	3.437	17.354	400.4	4.065	1.663
40	Luis Moya	51.744	50.285	17.397	15.966	2.469	17.191	429.0	4.783	2.591
41	Mesillas	42.687	41.231	14.972	12.897	3.386	17.644	351.5	4.140	2.724
42	Mezquital del Oro	59.011	57.346	15.218	12.767	3.521	16.860	357.4	3.494	1.250
43	Momax	46.424	45.025	14.865	13.398	2.610	17.433	370.5	4.631	1.462

Table 5 (continued). Results from applying the DM Hershfield test to estimate 24-hour point *PMP* (mm) for the 81 rain gauge stations indicated in the state of Zacatecas.

44	Monte Escobedo	49.477	48.784	11.275	10.415	2.930	17.321	280.6	3.538	2.316
45	Moyahua de Estrada	50.884	49.913	12.193	11.117	2.706	17.229	312.7	3.909	2.044
46	Nochistlán	47.986	47.056	17.230	15.846	3.404	17.427	391.4	3.875	2.353
47	Nuevo Mercurio	35.263	34.162	14.864	13.406	3.121	18.019	349.9	4.604	1.470
48	Ojo Caliente	41.632	40.706	15.817	14.548	3.182	17.719	365.1	4.197	2.370
49	Palmillas	44.489	43.046	14.208	12.308	3.165	17.542	341.5	4.165	2.168
50	Pinos	48.876	48.044	15.921	14.814	3.089	17.377	370.9	3.954	2.172
51	Pino Suárez	48.050	46.274	17.969	15.608	3.186	17.389	418.6	4.360	1.678
52	Presa El Chique	44.381	43.850	11.316	10.647	2.945	17.580	278.7	3.706	2.522
53	Presa Palomas	47.966	47.247	12.458	11.644	2.718	17.393	306.4	3.883	1.952
54	Presa Santa Rosa	41.210	40.590	13.816	13.033	2.947	17.740	327.8	4.149	1.730
55	Puerto de San Francisco	43.468	42.403	11.369	9.279	4.591	17.616	256.5	3.018	1.717
56	Purísima de Sifuentes	40.257	38.181	17.169	13.447	4.322	17.787	365.6	3.796	1.692
57	Río Grande	41.811	40.472	17.270	15.447	3.206	17.703	400.2	4.447	1.671
58	Sain Alto	44.760	42.833	15.770	12.754	3.777	17.541	354.3	3.893	1.300
59	San Andrés	47.319	46.014	19.406	18.015	2.608	17.432	461.4	4.961	2.228
60	San Antonio del Ciprés	44.905	43.867	14.117	12.803	3.002	17.538	341.0	4.143	2.687
61	San Benito	46.175	44.700	20.032	18.800	2.197	17.466	493.3	5.736	2.127
62	San Gil	35.464	34.306	14.806	13.265	3.143	18.008	350.0	4.605	2.466
63	San Isidro de los González	39.327	38.306	11.685	10.267	3.282	17.800	285.4	3.964	1.979
64	San Jerónimo	40.007	39.007	12.276	11.182	2.682	17.755	310.3	4.497	2.613
65	San José de Llanetes	38.340	37.207	12.583	11.139	3.052	17.845	308.5	4.333	1.423
66	San Pedro de la Sierra	44.540	43.396	13.802	12.831	2.229	17.514	356.6	4.953	2.606
67	San Pedro Piedra Gorda	41.535	40.961	11.066	10.078	3.874	17.728	262.7	3.284	2.969
68	San Tiburcio	40.135	39.028	15.419	14.067	2.913	17.775	368.3	4.604	2.058
69	Sierra Hermosa	46.672	45.016	21.496	19.667	2.694	17.467	507.0	5.173	1.584
70	Sombrerete	38.650	37.237	13.602	11.579	3.417	17.835	320.9	4.178	2.067
71	Tayahua	43.939	43.074	12.314	11.027	3.448	17.592	290.9	3.587	2.572
72	Tecomate	45.962	45.339	11.333	10.550	2.954	17.497	280.0	3.660	2.458
73	Teúl de González Ortega	51.566	50.602	15.584	14.381	2.948	17.236	366.7	3.943	2.168
74	Tlachichila	54.680	52.883	14.556	11.700	3.839	17.055	333.4	3.409	1.558
75	Tlaltenango	53.143	52.433	13.599	12.633	3.148	17.175	325.9	3.535	2.178
76	Trancoso	44.004	43.523	12.208	11.797	2.202	17.589	304.8	4.386	3.587
77	Vicente Guerrero	47.408	46.425	12.597	11.849	2.074	17.366	334.4	4.710	3.060
78	Villa de Cos	49.276	48.118	17.678	16.065	3.242	17.354	400.9	4.001	2.194
79	Villa García	47.523	46.857	15.871	15.277	2.268	17.428	381.8	4.685	2.607
80	Villa González Ortega	40.713	39.760	13.212	12.307	2.400	17.721	336.1	4.850	2.483
81	Villa Hidalgo	46.470	45.255	17.271	15.510	3.369	17.486	391.1	4.011	2.232
Minimum value		28.848	27.843	8.674	6.740	1.962	16.719	196.5	3.018	1.059
Maximum value		61.652	60.117	21.496	19.667	4.622	18.327	507.0	5.736	3.587

Legend:

[1] standard deviation.

[2] frequency factyors (Km_o = maximum observed and Km = calculated).

[3] probable maximum precipitation.

[4] Po = maximum observed value for annual maximum daily precipitation.
P_{Tr} = maximum 24-hr precipitation with return period (Tr) of 10 000 years.

homogeneous, both cases located within the region or geographic area. In general, to generate these estimations in localities without data, certain statistical requirements must be met. To this end, the regional frequency analysis (RFA) first verifies that the records are in agreement, then the regional hydrological homogeneity is tested, and dimensionless predictions which are valid within the area are determined. The predictions sought are then obtained only by scaling. Since the later analyses are based on *L* moments and their ratios, Stedinger *et al*. (1993), Hosking and Wallis (1997) or Campos (2010) can be consulted for these equations.

Fourteen rain gauge stations were identified in the geographic region of the state of Zacatecas, through which the Juchipila River runs, in Partial Hydrological Region 12 (Santiago River). The L-moment ratios for these stations were calculated. Table 6 shows the values of the ratios cited, as well as the discordance (D_i) obtained from the respective statistical test (Hosking & Wallis, 1997; Campos, 2010). The García de la Cadena station was the only one found to be discordant with the others and was therefore eliminated from the RFA.

Next, the hydrological homogeneity in the region was tested using the Langbein Test (Fill & Stedinger, 1995; Campos, 2012). Only the La Villita and Nochistlán stations were outside this test's control curves; the former was above and the latter below the curves. Since that number of dispersed stations is permissible, the region is considered homogeneous. Then, the regional method for stations-years (Garros-Berthet, 1994; Campos, 2008) was applied to the 13 joined records, previously scaled according to the arithmetic mean. The new record of dimensionless values has 544 elements. Table 7 shows the dimensionless predictions obtained with the two probabilistic models already used and the minimum SEF.

Table 8 shows the *L* moments (Hosking & Wallis, 1997; Campos,2010) of the 13 records from the region of Juchipila which were processed to obtain the dimensionless values for l_1, and the weighted values based on the range of each record (n). After obtaining the weighted dimensionless *L* moments (le_i), the GEV distribution was applied to obtain the dimensionless predictions (Campos, 2008). The results are shown in the last row of Table 7. These dimensionless predictions are the largest and were the ones adopted, for safety.

Lastly, Table 9 shows the predictions estimated with the regional method for rain gauge stations García de la Cadena (which was eliminated by the discordance test), Tecomate (which was intentionally not included from the beginning) and Tepechitlan (which does not have a rain gauge stations but is an important city). In these three cases, the mean magnitude of the MDP was estimated based on the observed nearby values. The data can also be weighted according to the distance between each rain gauge station and the study site.

In order to compare historical (H) and regional (R) predictions, the relative error (RE) was estimated, defined as:

$$RE = \frac{\left(MDP_{Tr}\right)_{\text{regional}} - \left(MDP_{Tr}\right)_{\text{historical}}}{\left(MDP_{Tr}\right)_{\text{historical}}} 100 \qquad (3)$$

The relative error is expressed as a percentage and is negative when the rainfall estimated with regional dimensionless predictions is less than the rainfall probabilistically calculated or historically recorded. Conversely, a positive RE indicates that the estimated prediction is larger than the recorded data. For the discordant records from the García de la Cadena station, the RE was 20 to 60% higher than the historical predictions, which is of course considered erroneous. In Tecomate, the RE were only between 9 and 26% higher, and therefore the predictions from the regional methods are considered to be quite precise.

Regional Frequency Analysis in Hydrological Region Number 37

The other RFA included 20 rain gauge stations in the state of Zacatecas belonging

Table 6. *L* moments ratios and discordances for *MDP* records in two geographic regions in the state of Zacatecas, Mexico.

Stations in the region of Juchipilaa	t	t_3	t_4	D_i	Stations in Hydrological Region No. 37	t	t_3	t_4	D_i
1. Excamé	0.15277	0.12216	0.04587	0.63	1. Agua Nueva	0.18368	0.13450	0.16887	0.44
2. García de la Cadena	0.13455	0.01033	0.16733	**3.11**	2. Calera de Víctor R.	0.16385	0.15786	0.16759	0.97
3. Huanusco	0.14845	0.06257	0.00533	1.28	3. Camacho	0.16171	0.20173	0.12884	1.27
4. Huitzila	0.15598	0.12714	0.06746	0.35	4. Cañitas de Felipe P.	0.22715	0.21471	0.13823	0.85
5. Jalpa	0.11391	0.16296	0.21525	1.19	5. Coapas	0.15869	0.13002	0.13348	0.63
6. Juchipila	0.15428	0.20720	0.16859	0.25	6. Concepción del O.	0.23536	0.15926	0.10614	1.67
7. La Villita	0.11611	0.11242	0.13096	0.72	7. El Salvador	0.19906	0.21614	0.18622	0.80
8. Los Campos	0.19337	0.22281	0.21185	1.68	8. Fresnillo	0.19482	0.12217	0.16558	0.47
9. Mezquital del Oro	0.13810	0.27106	0.21152	1.39	9. Gral. Guadalupe V.	0.19497	0.20525	0.20923	1.35
10. Moyahua de Estrada.	0.13615	0.16536	0.10380	0.41	10. Guadalupe	0.20361	0.06694	0.17305	1.82
11. Nochistlán	0.20191	0.13691	0.09829	1.66	11. Nuevo Mercurio	0.22853	0.26452	0.14582	1.43
12. Teúl de González O.	0.16853	0.15395	0.16774	0.41	12. Pinos	0.18295	0.15597	0.10857	0.16
13. Tlachichila	0.14511	0.21936	0.20266	0.50	13. San Antonio del C.	0.17838	0.10181	0.07163	0.73
14. Tlaltenango	0.14496	0.13778	0.06988	0.43	14. San Benito	0.24664	0.18817	0.06252	1.81
					15. San Jerónimo	0.17574	0.11915	0.09293	0.32
					16. San Tiburcio	0.21435	0.18565	0.11888	0.47
					17. Trancoso	0.15971	-0.03596	0.09517	**3.05**
					18. Villa de Cos	0.20161	0.15431	0.12490	0.10
					19. Villa González O.	0.18662	0.13979	0.05099	1.37
					20. Villa Hidalgo	0.20729	0.15366	0.15673	0.29

Table 7. Dimensionless predictions obtained with the regional methods indicated for the geographical region of Juchipila, state of Zacatecas, Mexico.

Regional method, probabilities distribution and method of fit	Return period in years				
	100	500	1 000	5 000	10 000
Stations-years. LP3. True domain Mo	1.797	2.078	2.196	2.469	2.586
Stations-years, GEV, Sextiles.	1.820	2.101	2.215	2.464	2.565
Weighted Mo. GEV. *L* moments.	1.843	2.170	2.309	2.625	2.760

to Hydrological Region 37 (El Salado). The procedure was identical to the one described above. Table 6 shows the *L* moment ratios and the respective discordances (D_i). Trancoso was the only station with discordant data. The corrected Langbein Test showed the region to be homogeneous, since all of its 19 rain gauge stations fell within the control curves.

Table 10 shows the dimensionless predictions obtained by the regional stations-years method, according to the probabilistic models LP3 and GEV with the lowest SEF, with a set of records containing 749 elements scaled according to the arithmetic mean. Table 11 shows the *L* moments of the 19 records from this region and the respective scaling and weighting.

The fitting of the GEV distribution using the weighted *L* moments method resulted in the dimensionless predictions shown in the last row of Table 10. These predictions were highest and the regional estimations were the ones adopted, for safety. Table 12 presents the regionally estimated predictions for the three

Table 8. Weighting of *L* moments for the 13 annual maximum daily precipitation records for the geographic region of the state of Zacatecas, Mexico.

Station	*n*	l_1	l_2	l_3	le_2	le_3	le_2	le_3
1. Excamé	66	52.759	8.060	0.985	0.1528	0.0187	0.0185	0.0023
2. Huanusco	36	48.131	7.145	0.447	0.1484	0.0093	0.0098	0.0006
3. Huitzila	25	61.652	9.617	1.223	0.1560	0.0198	0.0072	0.0009
4. Jalpa	34	50.335	5.734	0.934	0.1139	0.0186	0.0071	0.0012
5. Juchipila	59	46.547	7.181	1.488	0.1543	0.0320	0.0167	0.0035
6. La Villita	53	53.868	6.255	0.703	0.1161	0.0131	0.0113	0.0013
7. Los Campos	30	48.907	9.457	2.107	0.1934	0.0431	0.0107	0.0024
8. Mezquital del Oro	27	59.011	8.149	2.209	0.1381	0.0374	0.0069	0.0019
9. Moyahua de Estrada	31	50.884	6.928	1.146	0.1362	0.0225	0.0078	0.0013
10. Nochistlán	58	47.986	9.689	1.327	0.2019	0.0277	0.0215	0.0030
11. Teúl de González O.	44	51.566	8.691	1.338	0.1685	0.0259	0.0136	0.0021
12. Tlachichila	25	54.680	7.935	1.741	0.1451	0.0318	0.0067	0.0015
13. Tlaltenango	56	53.143	7.704	1.061	0.1450	0.0200	0.0149	0.0021
Sums and Averages	544	52.267	-	-	0.1493	0.0246	0.1493	0.0241

Table 9. Comparison between historical predictions and those from regional methods with two records from the region of Juchipila Zacatecas, Mexico.

Station	TP*	Return period in years				
		100	500	1 000	5 000	10 000
García de la Cadena	H	88.8	94.0	95.7	98.5	99.4
$\overline{X}_n$ = 57.700 mm	R	106.3	125.2	133.2	151.5	159.3
	RE	19.7	33.2	39.2	53.8	60.3
Tecomate	H	78.0	87.3	90.8	98.1	100.8
$\overline{X}_n$ = 45.962 mm	R	84.7	99.7	106.1	120.7	126.9
	RE	8.6	14.2	16.9	23.0	25.9
Tepechitlán $\overline{X}_n$ = 53 mm	R	97.7	115.0	122.4	139.1	146.3

* type of prediction; H = historical; R = regional; *RE* = relative error.

rain gauge stations in Hydrological Region 37, which were found to be non-homogeneous and discordant. For all these stations, the mean MDP was estimated according to the nearest observed values.

The values of the shape parameter (*k*) of the GEV distribution, calculated using stations-years and weighted *L* moments, were always near zero and positive for the two RFA in the geographic regions of Juchipila and Hydrological Region 37. This resulted in a Weibull distribution and, therefore, is not near the maximum global value of -0.150 found with Koutsoyiannis (2004), that is, a Frechet distribution, when jointly processing the 169 MDP records from Europe and the United States, with the number of data ranging from 100 to 154, for a total of 18 065 stations-years.

Conclusions

This study of annual maximum daily precipitation (MDP) for the state of Zacatecas, Mexico shows the importance of specific statistical tests that detect deterministic components in annual maximum series, given

that 17 of the 98 records containing more than 25 data (see Table 1) were not homogeneous and therefore not suitable for the probabilistic processing used to obtain the predictions required by the hydrological dimensioning.

This new probabilistic study of MDP for the state of Zacatecas was based on records or annual maximum series containing 30 to 39 more years, on average, than the records from the former Secretary of Hydraulic Resources (SHR), which contains data up to 1974. This resulted in higher predictions only in certain stations (Grande River, El Cazadero, Sain Alto, Nuevo Mercurio, Villa de Cos and Loreto). The majority of the predictions from other stations were nearly identical (El Arenal, Concepción del Oro, San Tiburcio, Cañitas de Felipe Pescador, Fresnillo, Boca del Tesorero and Presa Palomas). Nevertheless, most of the new predictions (Table 4) were significantly lower, and therefore it was concluded that the maximum isocontour maps published in 1976 by the SHR are still valid for the state of Zacatecas, Mexico (see Figures 5, 6 and 7).

The results from the Hershfield statistical method to estimate 24-hour point probable maximum precipitation (PMP) (Table 5) present a large range, from values of roughly 300 millimeters in hydrological regions 36 and 37 to over 400 millimeters in Hydrological Region 12. The ratios of *PMP* versus the *MDP* (P_0) observed from the records, and versus *MDP* for a 10 000-year return period (P_{Tr}) are quite stable, or similar, for each rain gauge station, as shown by the small variations. The central values are also very similar (Table 5), and therefore 4.20 is recommended for the first ratio and 2.20 for the second.

The regional frequency analyses make it possible to verify or reject predictions obtained with a small amount of *MDP* records, as well as to identify records that are not suitable for probabilistic processing because they are not homogeneous, and even more importantly to identify sites or localities that do not contain rain gauge information. Working by hydrological sub-region or geographic regions, it is most likely that regional homogeneity tests will verify the selection of rain gauge stations and that regional predictions will be very accurate, as shown by the two analyses performed in the state of Zacatecas —one in the region corresponding to the Juchipila River, in Partial Hydrological Region 12 (Santiago River) and the other in Hydrological Region 37 (El Salado).

Lastly, this type of *MDP* study is recommended for other hydrological regions or states in the country, now that a wide range of records exists and given that the usefulness of regional methods has been demonstrated. The purpose of this is to obtain reliable estimations or predictions in sites without rain gauge information, which are fundamental to hydrological methods used to obtain design floods in localities without hydrometric data.

Acknowledgements

Thank you to Humberto Abelardo Díaz Valdez, engineer, director of the Local Zacatecas Conagua Hydrometeorology Project, for providing the author with the Excel file for the 134 rain gauge stations with annual maximum daily precipitation records, as well as verifying and correcting all the values detected as anomalies, having exceeded 100 millimeters.

Thank you to Juan Antonio Araiza Rodríguez, Masters in Engineering and research professor with the Engineering School at the Autonomous University of San Luis Potosi, who performed the initial integration of the records to be processed, reviewing the data corresponding to the months available for each incomplete year and comparing them to the monthly means; when higher, they were selected as potential or probable values to be selected for the complete year. The potential values to be used for incomplete years were defined by examining the integrated records, and were usually higher than the minimums of the complete years.

References

Bobée, B. (1975). The Log-Pearson Type 3 Distribution and its Application to Hydrology. *Water Resources Research*, *11*(5), 681-689.

Table 10. Dimensionless predictions obtained with the regional methods indicated for Hydrological Region No. 37 (El Salado), state of Zacatecas, Mexico.

Regional method, probabilities distribution and method of fit	Return periods				
	100	500	1 000	5 000	10 000
Stations-years. LP3. Mo. Logarithmic domain.	2.050	2.430	2.591	2.961	3.120
Stations-years. GEV. Sextiles.	2.100	2.517	2.692	3.090	3.258
Weighted Mo. GEV. *L* moments.	2.108	2.542	2.726	3.148	3.327

Table 11. Weighting of L moments for 19 annual maximum daily precipitation records for Hydrological Region No. 37 (El Salado), state of Zacatecas, Mexico.

Station	n	l_1	l_2	l_3	le_2	le_3	le_2	le_3
1. Agua Nueva	43	36.316	6.671	0.897	0.1837	0.0247	0.0105	0.0014
2. Calera de Víctor R.	51	40.998	6.718	1.060	0.1639	0.0259	0.0112	0.0018
3. Camacho	31	28.848	4.665	0.941	0.1617	0.0326	0.0067	0.0013
4. Cañitas de Felipe P.	37	37.476	8.512	1.828	0.2271	0.0488	0.0112	0.0024
5. Coapas	41	41.634	6.607	0.859	0.1587	0.0206	0.0087	0.0011
6. Concepción del O.	47	37.300	8.779	1.398	0.2354	0.0375	0.0148	0.0024
7. El Salvador	25	46.812	9.318	2.014	0.1991	0.0430	0.0066	0.0014
8. Fresnillo	54	43.900	8.553	1.045	0.1948	0.0238	0.0140	0.0017
9. Gral. Guadalupe V.	45	43.460	8.473	1.739	0.1950	0.0400	0.0117	0.0024
10. Guadalupe	31	43.129	8.782	0.588	0.2036	0.0136	0.0084	0.0006
11. Nuevo Mercurio	38	35.263	8.059	2.132	0.2285	0.0605	0.0116	0.0031
12. Pinos	55	48.876	8.942	1.395	0.1830	0.0285	0.0134	0.0021
13. San Antonio del C.	37	44.905	8.010	0.816	0.1784	0.0182	0.0088	0.0009
14. San Benito	28	46.175	11.389	2.143	0.2466	0.0464	0.0092	0.0017
15. San Jerónimo	30	40.007	7.031	0.838	0.1757	0.0209	0.0070	0.0008
16. San Tiburcio	37	40.135	8.603	1.597	0.2144	0.0398	0.0106	0.0020
17. Villa de Cos	45	49.276	9.935	1.533	0.2016	0.0311	0.0121	0.0019
18. Villa González O.	31	40.713	7.598	1.062	0.1866	0.0261	0.0077	0.0011
19. Villa Hidalgo	43	46.470	9.633	1.480	0.2073	0.0318	0.0119	0.0018
Sums and averages	749	39.563	-	-	0.1971	0.0323	0.1961	0.0319

Table 12. Estimation of predictions for the rain gauge stations indicated in Hydrological Region No. 37 (El Salado), state of Zacatecas, Mexico

Station	Return period in years				
	100	500	1 000	5 000	10 000
Gruñidora ($\overline{X}_n$ = 38 mm)	80.1	96.6	103.6	119.6	126.4
El Rusio ($\overline{X}_n$ = 43 mm)	90.6	109.3	117.2	135.4	143.1
Zacatecas ($\overline{X}_n$ = 46 mm)	97.0	116.9	125.4	144.8	153.0
Trancoso ($\overline{X}_n$ = 44 mm)	92.8	111.8	119.9	138.5	146.4

Buishand, T. A. (1982). Some Methods for Testing the Homogeneity of Rainfall Records. *Journal of Hydrology*, *58*, 11-27.

Campos-Aranda, D. F. (1998). Estimación estadística de la precipitación máxima probable en San Luis Potosí. *Ingeniería Hidráulica en México*, *13*(3), 45-66.

Campos-Aranda, D. F. (2008). Ajuste regional de la distribución *GVE* en 34 estaciones pluviométricas de la zona Huasteca de San Luis Potosí. *Agrociencia*, *42*(1), 57-70.

Campos-Aranda, D. F. (2010). Verificación de la homogeneidad regional mediante tres pruebas estadísticas. *Tecnología y Ciencias del Agua*, *1*(4), 157-165.

Campos-Aranda, D. F. (2012). Descripción y aplicación de la versión corregida del Test de Langbein para verificar homogeneidad regional. *Ingeniería. Investigación y Tecnología*, *13*(4), 411-416.

Clarke, R. T. (1973). *Mathematical Models in Hydrology*. Chapter 5: The Estimation of Floods with Given Return Period (pp. 130-146). Irrigation and Drainage Paper 19. Rome: FAO.

Fill, H. D., & Stedinger, J. R. (1995). Homogeneity Test Based Upon Gumbel Distribution and a Critical Appraisal of Dalrymple's Test. *Journal of Hydrology*, *166*, pp. 81-105.

Garros-Berthet, H. (1994). Station-Year Approach: Tool for Estimation of Design Floods. *Journal of Water Resources Planning and Management*, *120*(2), 135-160.

Gupta, R. S. (2008). *Hydrology and Hydraulic Systems*. Chapter 8: Computation of Extreme Flows (pp. 427-482). Illinois: Waveland Press, Inc.

Hershfield, D. M. (1961). Estimating the Probable Maximum Precipitation. *Journal of Hydraulics Division*, *87*(HY5), pp. 99-106.

Hershfield, D. M. (1965). Method for Estimating Probable Maximum Rainfall. *Journal of American Water Works Association*, *57*, 965-972.

Hosking, J. R., & Wallis, J. R. (1997). *Regional Frequency Analysis. An Approach Based on L-Moments*. Chapter 3: Screening the Data (pp. 44-53) and Appendix: *L*-moments for some specific distributions (pp. 191-209). Cambridge: Cambridge University Press.

Kite, G. W. (1977). *Frequency and Risk Analyses in Hydrology*. Chapter 12: Comparison of Frequency Distributions (pp. 156-168). Fort Collins, USA: Water Resources Publications.

Kottegoda, N. T. (1980). *Stochastic Water Resources Technology*. Chapter 2: Analysis of Hydrologic Time Series (pp. 20-66). London: The MacMillan Press, Ltd.

Koutsoyiannis, D. (2004). Statistics of Extremes and Estimation of Extremes Rainfall: II. Empirical Investigation of Long Rainfall Records. *Hydrological Sciences Journal*, *49*(4), 591-610.

Linsley, R. K., Kohler, M. A., & Paulhus, J. L. (1988). *Hydrology for Engineers*. Chapter 3: Precipitation (pp. 46-93) and Chapter 14: Stochastic Hydrology (pp. 374-397). London: McGraw-Hill Book Co., SI Metric Edition.

Mansell, M. G. (2003). *Rural and Urban Hydrology*. Chapter 8: Analysis and Prediction of Flows (pp. 319-354). London: Thomas Telford Publishing.

Ostle, B., & Mensing, R. W. (1975). *Statistics in Research*. Chapter 7: Regression Analysis (pp. 165-236). Third edition. Ames, USA: Iowa State University Press.

Ruiz-Maya, L. (1977). *Métodos estadísticos de investigación*. Capítulo 9: Condiciones paramétricas del análisis de varianza (pp. 233-249). Madrid: Instituto Nacional de Estadística.

Schulz, E. F. (1976). *Problems in Applied Hydrology*. Section Ten: Applications to Engineering Problems (pp. 459-491). Fort Collins, USA: Water Resources Publications.

SRH (1976). *Boletín de Tormentas Máximas Observadas y Probables en México en 24 horas (hasta 1974)*. México, DF: Secretaría de Recursos Hidráulicos, Subsecretaría de Planeación. Dirección general de Estudios. Subdirección de Hidrología.

Shaw, E. M., Beven, K. J., Chappell, N. A., & Lamb, R. (2011). *Hydrology in Practice*. Chapter 9: Precipitation Analysis (pp. 155-194) and Chapter 13: Estimating Floods and Low Flows in the UK (pp. 322-350). Fourth edition. London: Spon Press.

Smith, J. A. (1993). Precipitation. Chapter 3. In D. R. Maidment (Ed.). *Handbook of Hydrology* (pp. 3.1-3.47). New York: McGraw-Hill, Inc.

Stedinger, J. R., Vogel, R. M., & Foufoula-Georgiou, E. (1993). Frequency Analysis of Extreme Events. Chapter 18. In D. R. Maidment (Ed.). *Handbook of Hydrology* (pp. 18.1-18.66). New York: McGraw-Hill, Inc.

WRC (1977). *Guidelines for Determining Flood Flow Frequency*. Bulletin # 17 A of the Hydrology Committee. Revised Edition. Washington, DC: Water Resources Council.

Weiss, L. L. (1964). Ratio of True to Fixed-Interval Maximum Rainfall. *Journal of Hydraulics Divisio*n, 90(HY1), 77-82.

WMO (1971). *Climatic Change*. Annexed III: Standard Tests of Significance to be Recommended in Routine Analysis of Climatic Fluctuations (pp. 58-71). Technical Note No. 79, WMO-No. 195. Geneva: World Meteorological Organization, Secretariat of the WMO.

WMO (1973). *Manual for Estimation of Probable Maximum Precipitation*. Chapter 4: Statistical Estimates (pp. 95-107). Operational Hydrology Report No. 1. WMO-332. Geneva: World Meteorological Organization.

Corresponding Author

Dr. Daniel Francisco Campos-Aranda

Profesor jubilado de la Universidad Autónoma de San Luis Potosí, México
Genaro Codina 240
Colonia Jardines del Estadio
78280 San Luis Potosí, San Luis Potosí, México
Teléfono: +52 (444) 8151 431
campos_aranda@hotmail.com

Click here to write the autor

Discussion

Technical notes and technical articles are open to discussion according to the following guidelines:

- The discussion will be written in the third person.
- The writer of the discussion shall use the term "commentator" when referring to oneself and the term "author" when referring to the one responsible for the technical note or article.
- The discussion shall be sent within 12 months of the last day of the quarter in which the a technical article or note was published.
- The length of the discussion may be extended by written request from the commentator.
- The discussion is to be presented according to the Guide for Collaborators published in this journal (omitting data referring to the length and abstract). In addition, the bibliographical citation of the technical notes or articles to which the discussion refers shall be included.
- The maximum length of the discussion is 4 journal pages (approximately 10 cuartillas, including figures and tables).
- The figures and tables presented by the commentator shall be progressively marked with Roman numbers and when citing those generated by the author the original numeration should be respected.
- The editors will suppress data that does not pertain to the subject of the discussion.
- The discussion will be rejected if it contains topics addressed by other sources, promotes personal interests, is carelessly prepared, raises controversy involving already established facts, is purely speculative or falls outside the purpose of the journal.
- The discussion will be published along with commentaries from the author or authors to which it refers.
- The discussion will be directed by the editor in chief.

Huayacan, Juitepec, Morelos, Mexico.

Photo: Raúl Flores Berrones.

Guide for Collaborators

The journal ***Tecnología and Ciencias del Agua*** invites specialists to collaborate with original, unpublished technical articles or notes **related to water, resulting from investigations and provide original contributions**, based on the disciplines of hydrology, hydraulics, water management, water and energy, water quality, and physical, biological and chemical sciences as well as political and social sciences, among other disciplines, according to the guidelines stated below.

PREPARATION OF THE ARTICLE

FORMAT

Font: Palatino throughout the entire document (body of text, tables and figures).

Font Size: Use 8, 9, 10 and 20 points, according to the following table:

8 points (Palatino)	9 points (Palatino)
• Tables. • Figures. • Acknowledgements.	• Name of authors. • Institution of authors. • Abstract. • *Abstract* and *keywords*. • Institutional address of the authors.
10 points (Palatino)	**20 points capital letters (Palatino)**
• Body of the text. • Title of the work in Spanish.	• Title of the work in English.

Line Spacing: double-spaced.

Page Numbers: all pages shall be numbered.

Length

Technical article: **30 pages** (numbered), including figures and tables.

Technical note: **10 pages** (numbered), including figures and tables.

CONTENS

Title

The article shall present significant contributions to scientific and technological knowledge pertaining to the specialty. It shall be based on finished works or those that have completed a development cycle. It shall show results from a series of experiences over 1 year or more of investigations and be supported by an adequate bibliographical review. **The basic structure of the text shall contain an introduction, the development and the conclusions**. The classic layout is preferable: abstract, introduction, methodology, results, discussion, conclusion and references.

Title

The title, **written in Spanish and English**, shall be informative and not exceed 12 words.

Abstract

The abstract, **written in Spanish and English**, shall be concise and provide a broad overview of the investigation (objective, method, results and conclusions) without exceeding 250 words.

Key Words

Eight words or key phrases (maximum) shall be provided **in Spanish and English** that facilitate the identification of the information.

Footnotes

Not admitted. The information is to be incorporated into the text.

Acknowledgements

To be included after the text and before the references.

Tables

- One page for each table.
- A list of all the tables cited shall be presented after the references.

Figures

- One page for each figure.
- All the names of the figures shall be included after the tables.
- They should be high-resolution (300 dpi).

Note: When the article is approved by the publication, the author shall send each figure in JPG format with high-resolution (300 dpi).

References

- The entire bibliography must be referenced in the main body of the text.
- In the case of addressing scientific and technological topics that are common domain, works that denote the knowledge of the authors about the state-of-art shall be cited.
- Avoid self-citations to the extent possible
- APA format shall be used as a basis.

Some examples of references in APA format are:

Complete Books

Last name, A. A. (Year). Title of work. city published: Publisher.
Last name, A. A. (Year). Title of work. Consulted at http://www.xxxxx
Last name, A. A. (Year). Title of work. doi:xxxxx
Last name, A. A. (Ed.). (year).City published: Publisher.

Book Chapters

Last Name, A. A., & Last Name, B. B. (Year).. Title of chapter or entry. In A. Last Name, B. Last Name & C. Last Name (Eds.), Title of book (pp. xxx-xxx). Place: Publisher.
Last Name, A. A., & Last Name, B. B. (Year).. Title of chapter or entry. In A. Last Name, B. Last Name & C. Last Name (Eds.), Title of book (pp. xxx-xxx). Consulted at http://www.xxxxxxx

Newspaper Article or Note Consulted Online

Last Name, A. A., & Last Name, B. B. (Year). Title of article. Title of publication, issue (number), pp. Consulted at http://www.xxxxxxx

That is: Last Name, A. A., & Last Name, B. B. (Year). Title of article. Title of publication, 1(2), 5-17, pp. Consulted at http://www.xxxxxxx

Printed Newspaper Article or Note

Last Name, A. A., & Last Name, B. B. (Year). Article Title. Title of publication, 8(1), 73-82.

Newspaper Article Publication with DOI

Last Name, A. A., & Last Name, B. B. (Year). Article Title. Title of publication, 8(1), 73-82, doi:xxxxxx

Conferences or Symposiums

Collaborator, A. A., Collaborator, B. B., Collaborator, C. C., & Collaborator, D. D. (Month, year). Title of collaboration. In E. E. President (Presidency), Title of symposium. Symposium held at the conference by Name of Organization, Place.

Citations within the body of the text

Type of citation	First appearance in text	Subsequent appearances	Format in parenthesis, first citation in text	Format in parenthesis, subsequent citing in text
Work by one author	Last name (Year)	Last name (Year)	(Last name, year)	(Last name, year)
Work by two authors	Last name and Last name (Year)	Last name and Last name (Year)	(Last name & Last name, Year)	(Last name & Last name, Year)
Work by three authors	Last name, Last name and Last name (Year)	Last name *et al*. (Year)	(Last name, Last name, & Last name, year)	(Last name of first author *et al*., year)
Work by four authors	Last name, Last name, Last name and Last name (Year)	Last name *et al*. (Year)	(Last name, Last name, Last name, & Last name, year)	(Last name of first author *et al*., year)
Work by five authors	Last name, Last name, Last name, Last name and Last name (Year)	Last name *et al*. (Year)	(Last name, Last name, Last name, Last name, & Last name, year)	(Last name of first author *et al*., 2008)
Work by six or more authors	Last name of first author *et al*. (Year)	Last name of first author *et al*. (Year)	(Last name of first author *et al*., Year)	(Last name of first author *et al*., year)
Groups (easily identified with abbreviations) such as authors	Complete name of institution (Acronym, year)	Acronym (Year)	(Complete name of institution [acronym], year)	(Institution, year)
Groups (without abbreviations) such as authors	Complete name of institution (year)	Complete name of institution (year)	(Complete name of institution, year)	

Language

Spanish or English

Separation of numbers and use of decimal points

In *Tecnología and Ciencias del Agua*, the separation between thousands is denoted with a blank space. A decimal point is used to separate whole numbers from fractions. In this regard, refer to Diccionario panhispánico de dudas, edited by the Real Academia Espyearla and the Asociación de Academias de la Lengua Espyearla, in 2005, with respect to numeric expressions: "**the Anglo-Saxon use of the period is accepted, normal in some Hispano-American countries…: π = 3.1416.".**

Delivery of Article

Send the article in *Word* with the name of the authors and institutional address to **revista.tyca@gmail.com**, with copy to Elizabeth Peña Montiel, elipena@tlaloc.imta.mx.

General Information

The review process will begin once the material is received, during which time the manuscript could be rejected. If the text is suitable for review, having fulfilled the Editorial Policy and the Editorial Committee having determined so, it will proceed to the review stage.

Depending on the review process, the text may be accepted without changes, with minor changes, with extensive changes or rejected.

Once a work is published, the main author has the right to two journals and ten offprints free of charge.

In there are any questions, please write to Helena Rivas López, hrivas@tlaloc.imta.mx or Elizabeth Peña Montiel, elipena@tlaloc.imta.mx

Editorial Policy

Mission

Disseminate scientific and technical knowledge and advances related to water through the publication of previously unpublished articles and technical notes that provide original contributions.

Our Principles

- Impartiality
- Objectivity
- Honesty

Our Values

- Knowledge
- Experience
- Thematic expertise

Contents

Interdisciplinary, composed of previously unpublished articles and technical notes related to water, that result from research and provide original scientific and technological contributions or innovations, developed based on the fields of knowledge of diverse disciplines.

Topics Covered

Interdisciplinary, related to water, with priority topics in the following knowledge areas:

- Water and energy
- Water quality
- Physical, biological and chemical sciences
- Hydro-agricultural sciences
- Political and social sciences
- Scientific and technological development and innovation
- Water management
- Hydrology
- Hydraulics

Type of Contributions

Technical article: scientific document that addresses and communicates, for the first time, results from a successful investigation or innovation, whose contributions provide and increase current knowledge about the topic of water.

Technical note: text that addresses advances in the field of hydraulic engineering and professional practices in the field of water, while not necessarily making an original contribution in every case it must be a previously unpublished work.

Some of the articles submitted to the review process can result in being published as notes and vice versa. This will occur through a proposal and process of mutual agreement between the authors and the editor responsible for the topic. The article and the note have nearly the same structure (abstract, introduction, methodology, results, discussion, conclusion, references).

Review Process

The journal is governed by a rigorous review process which establishes that each article be analyzed separately by three reviewers who recommend its acceptance, acceptance with minor changes, acceptance with extensive changes, rejection or acceptance as a technical note with the required changes.

At least one of three reviewers will be sought from a foreign institution.

The reviewers may not belong to the same institution as the authors proposing the article for publication.

When the decisions are opposing or inconsistent, the involvement of other reviewers or the members of the Editorial Committee may be requested.

On occasion, the approval of an article will be decided by two reviewers in addition to the opinion of the editor of the corresponding topic or, the editor in chief.

A rejected article will not be accepted for a new review process.

The review process will be performed in such a way that neither the authors nor the reviewers know the names of the other party.

The review process is performed by high-level specialists and experts who are national and internationally renowned in their professional fields and have the ability to reliably evaluate, in a timely manner, the quality as well as the originality of contributions, in addition to the degree of scientific and technological innovation in the topic under which it is submitted for possible publication.

This participation is considered a professional contribution and will be performed as a courtesy.

The reviews have a "Guide for the Reviewer" provided by the journal's Editorial Department.

Final Ruling

The ruling resulting from the review process is not subject to appeal.

Authors

Works are published from authors of any nationality who present their contributions in Spanish; nevertheless, we all accept works in Spanish or English.

Responsibility of the Authors

Submitting a proposal for the publication of an article commits the author not to simultaneously submit it for consideration by other publications. In the event an article has been submitted to another media for eventual publication, the author agrees to do so with the knowledge of the Editorial Department, which will suspend the review process and inform the Editorial Committee of the decision by the authors.

Collaborators whose articles have been accepted will formally cede the copyright to ***Tecnología y Ciencias del Agua***.

The authors are responsible for the contents of the articles.

The author is responsible for the quality of the Spanish used. If the writing is deficient the work will be rejected. ***Water Technology and Sciences*** will only be responsible for the editorial management.

The author commits to making the changes indicated by the editor of the topic in the time frame establish by the editor. In the event these indications are not met, the article will be removed from the review process and be classified as rejected.

The author shall be attentive to resolving the questions and proposals presented by the editors and the editorial coordinator.

Each author shall approve the final printed proofs of their texts.

It is suggested that authors consult the "Guide for Collaborators."

Readers

Academics, investigators, specialists and professionals interested in the analysis, investigation and search for knowledge and solutions to problems related to water.

Reception of Articles

The reception of articles and notes is ongoing.

Time period

Bimonthly, appearing in the second month of the period.

Subscription and Distribution

The journal is distributed through paid and courtesy subscriptions.

Open Access

Water Technology and Sciences, previously ***Hydraulic Engineering in Mexico***, provides a digital version of all the material published since 1985.

Special editions and issues

Water Technology and Sciences will publish special numbers independently or in collaboration with other journals, professional associations or editorial houses with renowned prestige and related to water resources.

In addition, it will publish articles by invitation, acknowledging the professional advances of prominent investigators.

In both cases, the quality of the technical continents and scientific contributions will be reviewed.

Water Technology and Sciences is registered in the following national and international indices and abstracts:

• Thomson Reuters Science Citation Index® (ISI) • Expanded Thomson Reuters Research Alert® (ISI) • Índice de revistas mexicanas de investigación científica y tecnológica del Consejo Nacional de Ciencia y Tecnología (Conacyt) (2013-2018) • Sistema de Información Científica Redalyc (Red de Revistas Científicas de América Latina y El Caribe, España y Portugal), Universidad Autónoma del Estado de México • EBSCO (Fuente Académica Premier NISC; Geosystems, como Marine, Oceanographic and Freshwater Resources) • ProQuest (Cambridge Scientific Abstracts) • Elsevier (Fluid Abstracts: Process Engineering; Fluid Abstracts: Civil Engineering) • CAB Abstracts, CAB International • Latindex (Sistema Regional de Información en Línea para Revistas Científicas de América Latina, el Caribe, España y Portugal), Universidad Nacional Autónoma de México • Periódica (Índice de Revistas Latinoamericanas en Ciencias), Universidad Nacional Autónoma de México • Catálogo Hela (Hemeroteca Latinoamericana), Universidad Nacional Autónoma de México • Actualidad Iberoamericana, CIT-III, Instituto Iberoamericano de Información en Ciencia y Tecnología.

Other Sources

The journal can also be found archived in Google scholar.